-Stability of steady states of meta-food webs on discrete spatial networks-

Vom Fachbereich Physik
der Technischen Universität Darmstadt

zu Erlangung des Grades
eines Doktors der Naturwissenschaften (Dr.rer.nat.)

genehmigte Dissertation von M.Sc. Philipp Fabian Gramlich aus Schweinfurt

Referent: Prof. Dr. Barbara Drossel
Korreferent: Prof. Dr. Kay Hamacher

Tag der Einreichung: 13.11.2017
Tag der Prüfung: 6.12.2017

Darmstadt 2018
D17

Stability of steady states of meta-food webs on discrete spatial networks

Stabilität stationärer Zustände von Meta-Nahrungsnetzen auf diskreten räumlichen Netzwerken

Zur Erlangung des Grades eines Doktors der Naturwissenschaften (Dr. rer. nat.)
genehmigte Dissertation von Philipp Gramlich aus Schweinfurt
Tag der Einreichung: 13.11.2017, Tag der Prüfung: 6.12.2017
Darmstadt — D 17

1. Gutachten: Barbara Drossel
2. Gutachten: Kay Hamacher

TECHNISCHE UNIVERSITÄT DARMSTADT

Fachbereich Physik
Institut für Festkörperphysik

Stability of steady states of meta-food webs on discrete spatial networks
Stabilität stationärer Zustände von Meta-Nahrungsnetzen auf diskreten räumlichen Netzwerken

Genehmigte Dissertation von Philipp Gramlich aus Schweinfurt

1. Gutachten: Barbara Drossel
2. Gutachten: Kay Hamacher

Tag der Einreichung: 13.11.2017
Tag der Prüfung: 6.12.2017

Darmstadt — D 17

Erklärung zur Dissertation

Hiermit versichere ich, die vorliegende Dissertation ohne Hilfe Dritter nur mit den angegebenen Quellen und Hilfsmitteln angefertigt zu haben. Alle Stellen, die aus Quellen entnommen wurden, sind als solche kenntlich gemacht. Diese Arbeit hat in gleicher oder ähnlicher Form noch keiner Prüfungsbehörde vorgelegen.

Darmstadt, den 27. Dezember 2017

(P.Gramlich)

Contents

Zusammenfassung

Das Konzept eines Nahrungsnetzes ist trügerisch einfach: Ein einfacher Graph der Interaktionsverbindungen von Spezies. Auch ein räumliches Netzwerk ist kein sonderlich abschreckendes Konstrukt. Dennoch gibt es nach fast einhundert Jahren der Forschung noch viele unbeantwortete Fragen was Nahrungsnetze und ihre raümlichen Erweiterungen, die Meta-Nahrungsnetze, angeht. Die vielleicht drängendste Frage, in den Worten des "Vaters der modernen Ökologie" (Slack, 2010), George Evelyn Hutchinson, lautet:

"Warum gibt es so viele Tiere?"(Hutchinson, 1959)

Man hat immer noch nicht ausreichend gut verstanden, warum komplexe Nahrungsnetze relativ stabil und robust sind. Die überwältigende Komplexität von echten Speziesbeziehungen und die Schwierigkeiten für Biologen und Ökologen sowohl genaue als auch umfangreiche Felddaten zu sammeln, machen es fast unmöglich alle Nuancen eines echten Nahrungsnetzes genau nachzubauen. Das macht dieses Thema besonders reizvoll für Physiker, die sich am Abstrahieren von Problemen zum bloßlegen tiefgreifender Prinzipien erfreuen. Der zentrale Fokus dieser Thesis ist daher zusätzliche Werkzeuge und Einblicke zur Thematik der Stabilität von Meta-Nahrungsnetzen bereit zu stellen.

Die generalisierte Methode der Modellierung ist besonders geeignet für diese Aufgabe, da sie um die Idee der Normalisierung auf stationäre Zustände und der Analyse ihrer Stabilität herum aufgebaut ist.

Wir bieten eine Einführung in diese Methode anhand des einfachsten möglichen Nahrungsnetzes: Ein Prädator mit einer Beute. Das gibt uns einen Einblick in die fundamentalen Begriffe und Möglichkeiten des generalisierten Modellierungsansatzes und die grundlegenden Trends für die Stabilität von Nahrungsnetzwerken, die überraschend weitreichend sind in ihrer Anwendbarkeit, zum Beispiel das höhere Exponenten in der Primärproduktion von Biomasse destabilisierend wirken.

Wir fügen im weiteren ein räumliches Element durch ein zweites Patch hinzu , so dass wir es nun mit einem Meta-Nahrungsnetz zu tun haben. Die Nahrungsnetze auf jedem Patch sind homogen und wir fokussieren uns auf den Effekt der Migration zwischen den Patches. Die Ausbreitung von Spezies ist im allgemeinen destabilisierend; kann aber weniger destabilisierend sein für adaptive Migration in bestimmten Parameterbereichen. Wir stellen auch die Frage, welche Dynamik beim Wechsel vom stabilen zum instabilen System entsteht, was uns zu den Phänomenen führt, die unter den Überbegriff Bifurkation fallen. Diese einfachen Systeme zeigen die volle Bandbreite an Bifurkationen inklusive einfacher Musterbildung.

Im Weiteren erhöhen wir die Komplexität, indem wir heterogene Nahrungsnetze auf jedem Patch einführen. Diese Asymmetrie erlaubt ein breiteres Spektrum an Verhalten am Punkt der Bifurkation und nun muss man das zusätzliche Element der Synchronisation zwischen Patches und Spezies in Betracht ziehen. Der Anteil der oszillatorischen Reaktionen auf Störung erhöht sich und die Oszillationen werden mehr antiphasisch im Vergleich zu homogenen Nahrungsnetzen; Indikatoren für eine höhere Robustheit. Der Einfluss auf die lineare Stabilität lässt sich aber leider nicht einfach vorhersagen.

Wir erweitern nun das Meta-Nahrungsnetz von zwei Patches mit je zwei Spezies auf viele Spezies auf räumlich verteilten Patchnetzwerken, aber mit homogenen lokalen Nahrungsnetzen. Wir zeigen die Analogie zwischen Reaktions-Diffusions Systemen im kontinuierlichen Raum und auf Netzwerken und wie dieser Formalismus auf Meta-Nahrungsnetze angewandt werden kann. Indem wir die inherente Struktur ausnutzen, können wir eine Master Stability Function formulieren, die eine Trennung der topologischen Einflüsse von den Einflüssen aus der Nahrungsnetzdynamik erlaubt. Meta-Gemeinschaften werden allgemein weniger stabil für größere Nahrungsnetze und können je nach räumlicher Konfiguration stabil oder instabil sein. Sie zeigen hauptsächlich oszillatorische und für Random Geometric Graphs relativ lokalisierte Reaktionen auf Störungen, was Argumente für die Robustheit solcher Meta-Gemeinschaften sind.

Abschließend fassen wir die Ergebnisse der einzelnen Kapitel zusammen. Die stationären Zustände der Nahrungsnetze auf räumlichen Netzwerken werden instabiler mit steigender Komplexität, zeigen aber simultan Zeichen von steigender Robustheit.

Abstract

The concept of a food web is deceivingly simple. A simple map of interaction links between species. Nor is a spatially discrete network a particular daunting construct. Yet, even after almost a century of research there are still many unanswered questions about food webs and their spatial extensions, meta-food webs, and the perhaps most urgent one is, in the words of "father of modern ecology" (Slack, 2010), George Evelyn Hutchinson:

"Why are there so many kinds of animals?" (Hutchinson, 1959)

It has yet to be satisfyingly understood how complex food webs remain relatively stable and robust. The overwhelming complexity of real species relations and the difficulty for biologists and ecologists in gathering both precise and extensive field data makes it nearly impossible to faithfully recreate all nuances of actual food webs. This makes the topic particular appealing to the physicist who delights in abstracting problems to reveal underlying principles. The central focus of this thesis is thus to provide additional tools and insights to the topic of stability in meta-food webs.

The generalized modelling method is particularly suited to this task as it is built around the idea of normalization to steady states which can be analysed concerning their stability.

We offer an introduction to this method by examining the most simple food web possible consisting of a single predator and a single prey species. This provides a look at the fundamental terms and possibilities of the generalized modelling approach and gives some basic trends for the stability of food webs that are surprisingly sturdy in their applicability, e.g. the notion that large exponents for the primary production of biomass are destabilizing.

We then add a spatial factor with a second patch so that we are dealing with a meta-food web. The food webs on each patch are homogeneous and we focus on the effect of migration between the two patches. Dispersal is overall destabilizing but can become less destabilizing for adaptive migration in certain parameter ranges. We also ask the question what dynamics occur during the transition from a stable to an unstable system which leads us to the phenomena that fall under the umbrella term of bifurcation. These simple systems show the full range of bifurcations including simple pattern building.

From there we increase the complexity by incorporating heterogeneous food webs on each of the patches. This asymmetry allows for a wider range of behaviour at the point of bifurcation and now the additional element of synchrony between patches and species has to be taken into account. The ratio of oscillatory behaviour in case of perturbation increases and the oscillations becomes more anti-phasic compared to the homogeneous food webs; indicators of a higher robustness. The impact on linear stability cannot be easily predicted.

We then extend the meta-food web from two patches and two species to many species on spatially distributed networks of patches though only with homogeneous local food webs. We show the analogy between reaction-diffusion systems on continuous space and on networks and how this can be applied to meta-food webs. Exploiting the inherent structure we can formulate a master stability function that allows for a separation of topological influences and those that stem from food web dynamics. Meta-communities become in general less stable for larger food webs and can be stable or unstable depending on the spatial configuration. They show primarily oscillatory and most likely rather localized responses to disturbances which are arguments for the robustness of the meta-communities.

Finally, we summarize the results from the different sections. The steady states of food webs on spatial networks become less and less stable for increasing complexity but at the same time show signs of increasing robustness.

1 Introduction

Understanding the processes that allow our environment to sustain conditions that are suitable for the continued existence of a certain biodiversity, including the human species, is obviously of great importance. The environment as the interaction of every conceivable factor is far too vast to be captured by a single academic field and has inspired research in probably all scientific disciplines and countless combined efforts. Biology as the study of living things comes perhaps first to mind when one thinks about environment in the sense of nature but complex systems of all kinds have always piqued the interest of physicists. Statistical physics offers the tools for the description of many biological systems (Drossel, 2001) and abstract concepts like the master stability function (Pecora and Carroll, 1998) have been successfully applied to ecological research (Yeakel et al., 2014a; Singh and Gakkhar, 2010; Chavez et al., 2007).

Ecological species connected by feeding relationships are called food webs. Food webs are one of the essential building blocks to describe the interaction of species (Cohen et al., 2012; Drossel and McKane, 2006; Pimm, 1982; Dunne, 2006). Simple food web models have been in use for about a century, pioneered by Alfred Lotka (Lotka, 1910; Lotka et al., 1925) and Vito Volterra (Volterra, 1927) who derived identical models of predator-prey interaction independently. Even these straightforward attempts are able to describe real species interactions to a surprisingly accurate degree on several occasions. The famous case of the lynx and snow hare population cycles comes to mind (Gilpin, 1973) but there have been other examples; e.g. moose populations (Jost et al., 2005).

One of the major questions of ecology is how complex systems as food webs can possibly be (relatively) stable in nature. They are at least stable to most small perturbations (Kitano, 2004). Models for vastly different time and spatial scales are in use, ranging from models that try to regard every individual as unique entity (Grimm, 1999; Lauridsen et al., 2010) to so called colonization-extinction models which simplify population dynamics to a binary question of existence or absence of species on habitats (Lafferty and Dunne, 2010; Levins, 1969a). First analytical attempts by Robert May to describe complex systems placed links at random between nodes and predicted a decline in stability for large systems (May, 1972b) yet biological reality defies this hypothesis. It is obvious that random connections between species are not realistic and a number of alternative ways to describe the basic structure of species communities has been developed (Williams and Martinez, 2000; Cohen et al., 2012; Cattin et al., 2004; Rossberg et al., 2005) though these models do not answer the famous “Why?” of (Hutchinson, 1959) but rather the “How?”. Evolutionary food web models try to find the principles that result in the creation of food webs like we see in nature (Drossel et al., 2004; Thompson, 1998; Rossberg et al., 2005; McKane and Drossel, 2006). Other research focuses on the reason why distinct food web structures seem to be stable, e.g. Anje Neutel presented the idea of trophic loops and their influence on stability as one of the reasons for real link patterns in food webs (Neutel et al., 2002, 2007) and based it upon extensive research of field data (de Ruiter et al., 1995).

The body mass of species has revealed itself to be a key property in modelling realistic food web structures and species interactions. Predator body mass is consistently one to two orders of magnitude larger than that of prey species (Brose et al., 2005, 2006; Cohen et al., 1993) and the metabolism of all species tends to scale allometrically (Kleiber, 1932).

The feeding relationships between predators and prey species are governed by the functional response - the ability of the predator to consume prey in dependence of the prey density. The first models (Lotka et al., 1925; Volterra, 1927) use a simple linear relationship but more advanced attempts take satiation (Rosenzweig and MacArthur, 1963) and potential competition or interference between predators into account (Beddington, 1975; DeAngelis et al., 1975).

Most forms of networks on networks like for instance the prime example of complex networks – the internet – are strongly influenced by the topology of the underlying structure (Barrat et al., 2008) and the spatial dimension is an integral and often critical component of many complex systems, e.g. for

disease-vector models (Keeling, 1999; Riley et al., 2015), forest fires (Schertzer et al., 2015) or neuronal networks (Hütt et al., 2014).

Food webs have no inherent spatial component in their description (Holt, 1996) but it is obvious that most species in nature participate in some form of movement; be it to gather food or to find shelter or to find new living space and so on. The range for the gathering/hunting of food and regular activity is called home range (Burt, 1943) and travel to other habitats is called dispersal. Migration is often used interchangeably with dispersal (as in this thesis) but technically is a particular form of reoccurring seasonal travel. If the ranges of travel and everyday activity are significantly different we have little direct interaction between populations in different habitats and it becomes sensible to consider them as separate communities on habitat patches that are connected by dispersal links. Such spatially distributed networks of food webs are called meta-communities.

An extensive part of the biological world can in a good approximation be described as meta-communities (Murray, 2002). The exact definition of meta-community is up to debate (Leibold et al., 2004) but all formulations incorporate food webs to describe the interaction of species as communities, and place these food webs in a spatial dimension, be it in continuous or discretized space. The simplest form of meta-communities are meta-populations which only feature one spatially distributed species (Bascompte and Solé, 1994) though this stretches the definition of food web. Meta-populations have been investigated quite thoroughly (Tromeur et al., 2013; Holland and Hastings, 2008; Hanski and Gaggiotti, 2004) and have in turn helped in the research of other complex systems like disease models (Grenfell and Harwood, 1997).

The overwhelming complexity of real meta-communities can be daunting. Most attempts at understanding underlying processes use minimalistic meta-communities with only a single predator-prey pair on a patch and usually only two patches, for example (Abrams, 2000; Jansen and Lloyd, 2000; Abdllaoui et al., 2007; Jansen, 1995; Abrams and Ruokolainen, 2011) and many more. Thankfully large systems seem to have the same qualitative tendencies as small systems (Jansen and de Roos, 2000).

To connect multiple patches we need dispersal. Research on the dynamics of food webs in space is fragmented in its methods and assumptions (Amarasekare, 2008a) but there are a number of generally observed but seemingly paradoxical properties for meta-communities. On one hand, dispersal frequently induces synchrony between spatially separated populations (Goldwyn and Hastings, 2008; Liebhold et al., 2004; Bjørnstad et al., 1999), in particular for random dispersal (Goldwyn and Hastings, 2008; Jansen, 2001). One the other hand, there are many forms of dispersal induced stability (Abbott, 2011). This is a conflict as a high level of synchrony is considered to be destabilizing as it can create large fluctuations in total biomass which might lead to extinction events on a global level (see for example (Heino et al., 1997)). These are obviously simplified statements as the effects of dispersal depend on the exact nature and intensity of the dispersal (Kisdi, 2010; Briggs and Hoopes, 2004), similarity of the food webs or species that disperse (Esa Ranta and Lundberg, 1998) and the exact topology of spatially extended systems (Bascompte and Solé, 1994). Synchrony can also be potentially stabilizing if the amplitudes are weakly correlated, creating travelling wave phenomena (Blasius et al., 1999) or in combination with environmental factors (Vasseur and Fox, 2007).

The synchronisation of dynamics is not limited to patches couples by dispersal. It is found in many ecological systems (Satake and Koizumi, 2008) and is often driven by environmental factors like periodic seasons (Sæther et al., 2007; Koenig and Knops, 2013; Rosenstock et al., 2011). This is called Moran's effect after Pat Moran (Moran, 1953) and, similar to synchrony induced by dispersal, is usually destabilizing. It can have persistence enhancing qualities, e.g. for plants that produce seeds simultaneously to overwhelm the feeding capacity of seed predators and thus increase the chance of survival (Janzen, 1971).

There is a number of other factors to keep in mind. Real populations are obviously discrete as populations consist of individuals and dynamics must be stochastic but are usually assumed as continuous in most models. This can change the effect of dispersal (Thiel and Drossel, 2017) or reveal new phenomena (Black and McKane, 2012; Grima, 2010) if population sizes or dispersal rates are relatively small. For

sufficiently large populations and migration rates it is reasonable to assume continuous functions for the dynamics.

We will use discrete patches in space which is fitting for e.g. island chains or lakes. The questions of interest in meta-communities are in many ways the same ones as for local communities but topology and dispersal behaviour can now additionally affect the system properties. We are foremost interested in the linear stability of (meta-)communities in steady states in case of perturbation but will also consider robustness.

The definition of stability is often used in a rather confusing manner and multiple distinct features can be used as a measurement (Jen, 2003; Grimm and Wissel, 1997). Robustness as the ratio of surviving species is frequently used (Dunne et al., 2002, 2004; Kartascheff et al., 2010), as the exact species make-up in terms of abundance or type is usually of less importance than the existence of a certain amount of biodiversity. Another definition of stability is whether a system returns to the original/previous state if disturbed. The later interpretation is of primary importance in this thesis, though we will make indirect statements about the former. It should be noted that the different measures of stability in the form of linear stability, robustness, invasibility or persistence show surprisingly often similar trends (Ives and Carpenter, 2007).

The interest in the stability of meta-communities is not just an academic fancy but has deep roots in necessity. Humanity has on innumerable occasions shown that it can affect meta-communities on any scale to any degree. From eradicating megafauna across a continent (Miller et al., 1999) to hunting incredibly abundant prey species to or near extinction (Taylor, 2011) to changing environmental conditions themselves on local (Mieth and Bork, 2010) or even global scale (Pongratz et al., 2011). Understanding the impact of our actions on nature is imperative as it directly affects our lives in numerous ways. These could be financial, e.g. how much biomass can be harvested without driving a population to extinction (Guill et al., 2011), or ethical, e.g. what measures must be taken to ensure biodiversity is preserved for future generations. The safety and well-being of humankind is not exempt from this list. Anthropogenic climate change has been a focal point of research for decades now (Oreskes, 2004; Rosenzweig et al., 2008; Walther, 2010) and with tangible effects adding up interest has not ebbed.

Global warming and climate change in general affects meta-communities. The influence of changing distributions of natural resources and rising temperature as well as a higher variance in climate has an impact on flora and fauna across the world (Pecl et al., 2017; Hoegh-Guldberg and Bruno, 2010). We know of the importance of temperature for the metabolism of living beings (Gillooly et al., 2001) and that resource distribution influences biodiversity and dynamics (Hamm and Drossel, 2017; Amarasekare and Nisbet, 2001). Scarcity or even overabundance (Hammock, 1971) of resources can be damaging to populations.

Higher temperatures are often associated with higher respiration rates but most research has been done on marine species and thus might not apply in general (Clarke and Fraser, 2004; Ehnes et al., 2011). There has been at least one study that found a negative trend for metabolism rates with higher temperatures for insects (Addo-Bediako et al., 2002). The effects on whole food webs can be conflicting and depend on carrying capacity and trophic structure (Binzer et al., 2012).

Understanding how and to what extend meta-communities will react to the ongoing changes would be invaluable. This means we need tools to analyse complex systems.

A rather recently developed method to analyse the stability of meta-communities is the generalized method. It was introduced by Thilo Gross and Ulrike Feudel (Gross and Feudel, 2006) and has proven its worth as a versatile tool that can describe a wide range of systems, from lasers to ecological food webs to (very simplified) chinese history. This approach has already been applied to numerous meta-food webs. It has been used for large but localized food webs (Gross et al., 2009) and for spatially distributed meta-populations (Tromeur et al., 2016). Even the stability of ancient Egyptian food webs has been analysed (Yeakel et al., 2014c). It focuses on the steady states of such systems and forgoes any interpretation of dynamics away from the steady state. While fixed points are the concern of this thesis, the generalized model can be applied to periodic solutions as well (Kuehn and Gross, 2011). One of the

main benefits of the generalized modelling approach is that, due to the normalization to a steady state and the subsequent linear stability analysis, all remaining parameters have ecologically interpretable meaning. The *scale parameters* describe the relative importance of different processes like respiration, primary production, etc to the total biomass turnover. The *exponent parameters*, which originally were used in economic models (Marshall, 1920), describe sensitivities of processes to population changes.

We use the generalized modelling approach to analyse increasingly complex meta-communities in regards to their stability. Special attention is given to the effects of dispersal and the behaviour of the system at the point of diffusion-driven bifurcations.

A list of common abbreviations and terms can be found at the end of the thesis.

2 Theoretical Basis

To investigate meta-communities, we need some prior knowledge. For one, we need to know how food webs, the local components of meta-communities that are found on every patch, are structured and what kind of dynamics between species are to be expected. We then introduce simple spatial constructs, random geometric graphs, so we can build actual meta-food webs with these two distinct elements. After establishing the basic structure for meta-communities we define how to measure stability and comment on some helpful tools for the computation of stability and what happens for the transition between stable and unstable regions (bifurcations). Finally, we introduce the generalized method which we use to describe food web dynamics and some auxiliary concepts.

2.1 Food Webs

We need to establish what we consider as a food web. We also need a way to construct food webs that have similar properties to food webs found in nature if we do not want to be limited to pathological examples. An excellent introduction to food webs can be found in (Drossel and McKane, 2006). We introduce the designations commonly used for food webs and the niche model which is used to create food webs in section 6.

2.1.1 Food Web Properties

Food webs are, as far as this thesis is concerned, communities of species that are linked by feeding relationships. If a species has no feeding link to any other species in that community, it is not part of that food web. While this seems obvious one could argue that parasites or symbionts are part of a food web as they influence other species even if they do not necessarily participate in predator-prey dynamics. Since there is still a biomass flow from one species to another species, parasitic behaviour can often be modelled as a form of predation and ignoring parasites is potentially a significant oversight (Lafferty et al., 2008, 2006).

Also, there have to be arbitrary limits to what is still considered a feeding link and thus what species are included. If a feeding link is rarely in use or provides a insignificant portion of biomass it is usually not included. E.g. bull sharks are known as opportunistic feeders and there is at least one recorded attack on a horse (Weier, 2005) but the frequency of this interaction would be considered negligible for most food web modelling. Another limiting factor is the resolution. The diet of any macroscopic species involves, at least by accident, a number of microorganisms which are often not included as they would be impossible to record. So far we have avoided to define what we mean by “species” as it conjures a simple picture of clearly identifiable animals like mice, eagles and lions. But biological taxonomy is not trivial and it can be very hard to differ between species. At times it is reasonable to group a number of taxonomically different species into a vague term to acknowledge an interaction without getting bogged down by specifics; e.g. the term plankton refers to many aquatic species that are often the bottom layer of marine food webs. As a matter of fact, species in food webs are more often than not so called trophic species. This means that rather than using the biological definition of species we combine species that share the same prey species and thus have similar functions in a community. For abstract food webs this differentiation between biological and trophic species is of no particular importance but if one wants to apply insights to research of real food webs it is vital to keep this in mind.

To define food webs, we need some quantitative measures. A food web can be regarded as a graph with nodes and edges. The species are nodes and the feeding links are the directed edges between the vertices. The direction of the links is the same as the direction of the biomass flow; the links goes from the prey species to the predator. If a species has no prey species it is considered a basal species. If a species has no predator it is called a top species. All other species are considered intermediate species. The size of food webs is measured in the number of species of the community, here denoted as S. The links give the interactions between species. The number of links is L. The connectance or connectivity C is the total number of realised links compared to the number of possible links. If any species can be

linked to any other species we get $C = L/S^2$. If there is no cannibalism we get $C = \frac{L}{S(S-1)}$. The trophic level assigns a hierarchy between species. For a food chain, where each species feeds on a maximum of one species and in turn is at most fed upon by one species, the trophic level of a species is simply the number of steps it takes to get from the basal species to the species in question. For a food web where the number of steps from the basal species to other species varies there is a number of definitions for the trophic level. Since the trophic level is not an important topic in this thesis, we don't go into further detail.

At this point, we defined food webs as a construct of S species connected by L links with certain properties and how it can be interpreted as a graph. Field data provides ample examples for food webs but does not answer how the observed structures emerge which begs the question how to create realistic food webs from scratch. This could be approached in a number of ways. The more ambitious and insightful way is to create food webs based upon dynamic models and then compare the resulting food webs to real ones. If the food webs are comparable, one can assume that the dynamic models entail essential principles found in nature. This can be done by using models that start with one species and introduce new species over time and let some go extinct, similar to evolution in nature, or with models that start with some interacting species that form into a stable food web by extinction of species that are not fit for survival.

A much quicker way is to built food webs as static graph objects based upon rules that do not take any dynamics into account. We will discuss this in the following subsection.

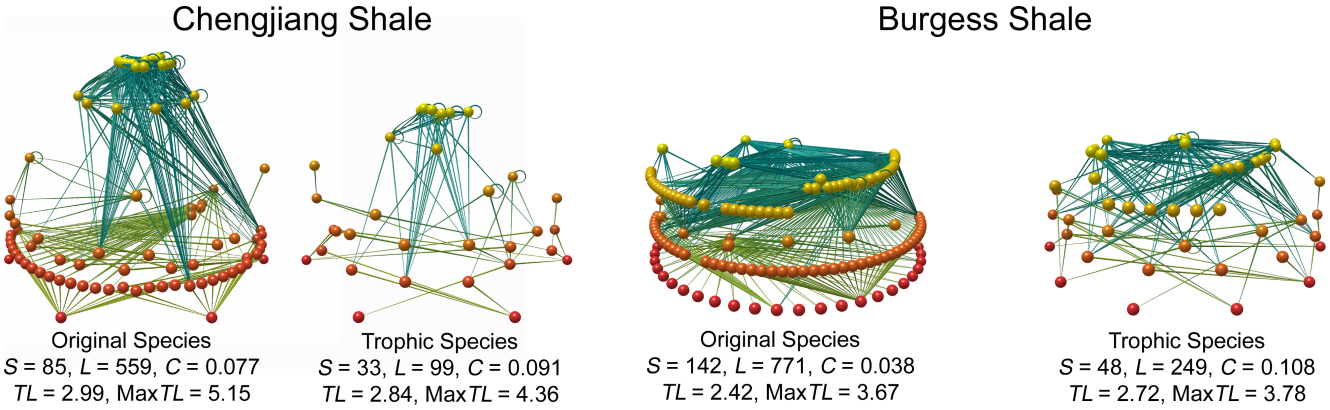

Figure 1: To illustrate the complexity of food webs that are encountered by biologist, here are a couple of examples taken from (Dunne et al., 2008) under creative commons. The red spheres are basal species, the yellow spheres top predators. The hues inbetween signify species of different trophic levels with a color gradient from red to yellow for higher trophic levels. The food webs with the subtitle "Original Species" use the biological species and the food webs with "Trophic Species" aggregate species with identical sets of prey species into trophic species. The data sets these food webs are based on from the Cambrian Period but food webs today have very similar forms which indicates strong underlying principles in the formation of food webs.

2.1.2 Niche Model

There are a number of static models; models that create food web graphs without any dynamics; that have been used in research (Cohen et al., 2012; Solow and Beet, 1998). First models used Erdős-Rényi-graphs, i.e. random graphs, that assigned links between species without any particular biological reasoning. This did not reproduce any properties of any real food web in a satisfying manner. Some form of biological guideline for the creation of links was needed.

The cascade model assigns a value to each species from 1 to S and only allows species to feed on species with a lower value. Additionally, the probability to feed on any such species is $\frac{d}{S}$. The parameter d can be

fitted to real food web data and governs the link density. The cascade model reproduces key properties of food webs significantly better than the models based on random graphs (Cohen et al., 2012) but has still issues. For one, the random nature of assigning feeding links does not mirror the observation that species of comparable body size often have the same predators. The hard upper limit for feeding links is also problematic as it imposes the name-giving cascade structure without any possibility for deviation.

Other models like the nested hierarchy model (Cattin et al., 2004) or the matching model (Rossberg et al., 2005) try to include the observation that species that share some attributes frequently also share sets of predators and preys.

This is also the case for the niche model which we will use for food web construction in this thesis. The niche model was introduced by (Williams and Martinez, 2000). It creates food webs that fit field research data quite well despite a very simple premise. In this model, each species i is assigned at random a niche value $n_i \in [0,1]$, a feeding range r_i and a feeding center c_i. A species $j \neq i$ is a prey of species i if its niche value n_j is within the interval $[c_i - r_i/2, c_i + r_i/2]$. The niche value is uniformly distributed and the feeding range is drawn from a beta distribution:

$$r_i = \left\{1-(1-x)^{\frac{2C}{1-2C}}\right\} \cdot n_i, \tag{1}$$

with C as the desired connectance of the food web and $x \in [0,1]$ as a random number. The connectance of a graph under the assumption of no self-loops is defined as

$$C = \frac{L}{N(N-1)} \tag{2}$$

with L as the number of links between nodes and N as the number of nodes. Species without any prey are basal species. The feeding center c_i is chosen uniformly and at random from an interval which can be defined depending on the desired food web structure but is always smaller than the niche value of species i. In the original model of Martinez and Williams an interval of $c_i \in [\frac{r_i}{2}, n_i]$ was used. For a graphic explanation see Fig. 2 and for an example of a resulting food web see Fig. 3.

Since this creates a food web structure where species with a high niche value are rarely fed upon and most feed on smaller niche values the niche value is often associated with body size as in nature predators are ordinarily significantly larger than their prey (Brose et al., 2005). The feeding range gives an estimate of how specialized a predator is on average. Larger ranges mean more prey species and thus offer a measure of redundancy for the predator as it is not solely dependent on a single species. If a prey species goes extinct or is just hard to find a generalist predator could potentially make up the lost prey biomass by focusing its foraging efforts, i.e. the time spent on each particular prey, on alternate prey; for details on distributing foraging efforts see (Heckmann et al., 2012). A highly specialized predator would have no such option. Predators with multiple prey species are thus usually less affected if a single prey population is removed.

The model is often modified so that the feeding relationships are not binary questions. A species on the outskirts of the feeding range is then usually considered less desirable than a species near the feeding center and species with a smaller feeding range are able to form stronger feeding links. This allows to integrate specialist and generalist predators into the food web.

The niche model, though certainly not perfect (see (W Fox, 2006)) outperforms the cascade model in predicting most properties of food webs and will be used to construct food webs in Sec. 6 of this thesis.

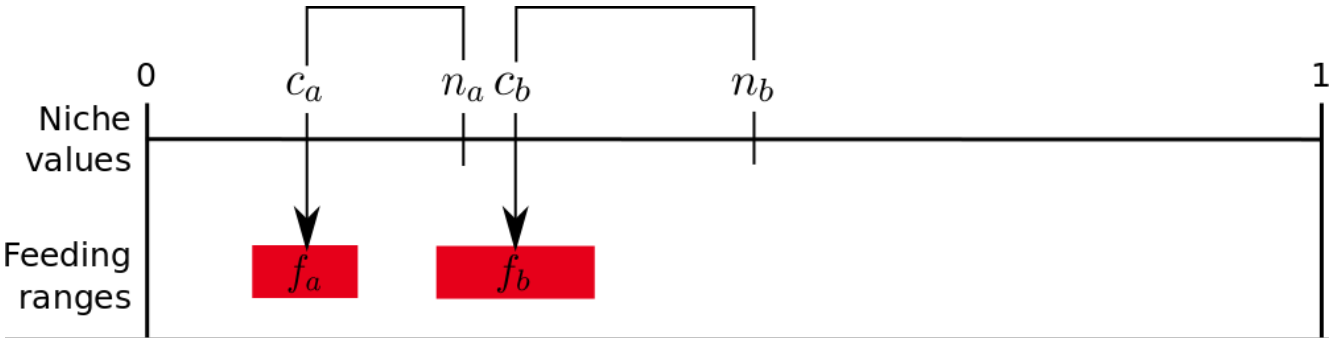

Figure 2: The basic concept of the niche model. We have two species a and b with assigned niche values of n_a and n_b. They have feeding centres at c_a and c_b and can feed on any species within a range of f_a and f_b around their respective feeding centres. Niche value n_a lies within the feeding range of species b, so species a is preyed upon by species b. Picture used with kind permission of and created by Tatjana Thiel and Michaela Hamm.

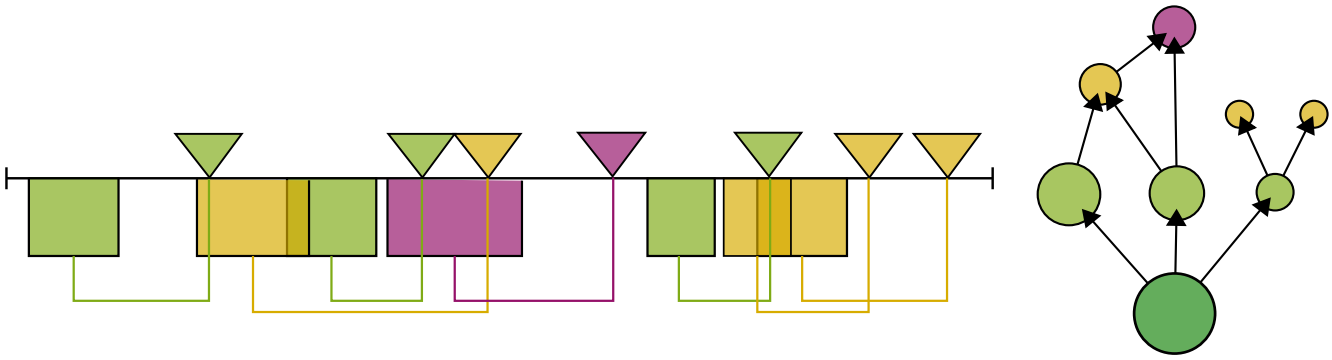

Figure 3: A more complicated example of the niche model. The coloured triangles represent the niche values and the coloured boxes connected to the triangles the feeding ranges around the respective feeding centres. Species that have no prey species feed on the resource. The resulting food web can be seen on the right. The circles are analogously coloured to the niche values used on the left and the resource is at the bottom of the food web. Picture used with kind permission of and created by Tatjana Thiel and Michaela Hamm.

2.2 Common Models for Predator-Prey Interaction

In the following subsections we present several ways to model the dynamics of species interactions. We present these models in some detail to allow the reader to get an impression of explicit population dynamics and how relatively small changes affect the dynamics. We will use these approaches in their generalized forms in the sections 3, 4 and 5 to describe species interactions.

2.2.1 Lotka-Volterra Predator-Prey Equations

One of the first and one of the simplest attempts at describing predator-prey interaction are the Lotka-Volterra equations and we go into a little more detail than necessary to give the reader an idea of how predator-prey models are usually analysed. Originally intended for simple chemical reactions (Lotka, 1910) they have been applied to predator-prey systems as early as 1925 (Lotka et al., 1925). Vito Volterra and Alfred Lotka arrived at the equations independently at almost the same time. Volterra applied them first to fluctuations in fish populations (Volterra, 1926) while Lotka had primarily oscillations of concentrations due to chemical reactions in mind. Applied to a predator-prey system the equations are

$$\dot{X} = \alpha X - \beta XY = (\alpha - \beta Y)X\,, \tag{3}$$

$$\dot{Y} = \delta XY - \gamma Y = (\delta X - \gamma)Y \tag{4}$$

with X and Y as prey and predator populations in units of density. The different Greek letters are constants that define the interaction strengths.

The different terms have intuitive interpretations. Parameter α is the growth rate of the prey species without any correction due to predation and is assumed to be proportional to the prey population size. The loss rate by predation β depends both linearly on the prey and the predator population. The rate of gain by predation δ for the predator species is also dependent on prey and predator population size. Since the predator cannot grow more in biomass than biomass of prey consumed, we have $\delta \leq \beta$. The mortality rate of the predator is defined by the γ parameter and proportional only to the predator.

We can find a conservation quantity for the Lotka-Volterra model. If we integrate the equations we get an identity of the form

$$C = \alpha \ln(X(t)) - \beta Y(t) - \delta X(t) + \gamma \ln(X(t)) \tag{5}$$

which is fulfilled for all times t. The constant C is

$$C = \alpha \ln(X(0)) - \beta Y(0) - \delta X(0) + \gamma \ln(X(0)) \tag{6}$$

and thus is defined by the starting conditions of the system. Fig. 4 shows how such a conservation law leads to closed curves or points for any solution of the model. If we assume a positive growth rate α for the prey there are always two equilibria at $X = 0, Y = 0$, which means extinction of both species, and $X = \frac{\gamma}{\delta}, Y = \frac{\alpha}{\beta}$, which represents coexistence of predator and prey. For a negative growth rate there is obviously only extinction.

Despite the simplicity of the Lotka-Volterra equations they can produce closed curves, meaning population oscillations, which are a common occurrence in real food webs (May, 1972a). Famous examples for population oscillations include lynx and snowshoe hare (Gilpin, 1973) and moose and wolf (Jost et al., 2005) populations.

This model is kept intentionally simple and lacks several essential components of species interaction, e.g. neither predator nor prey have any intra-specific competition. We discuss a slight expansion of this model in the next section.

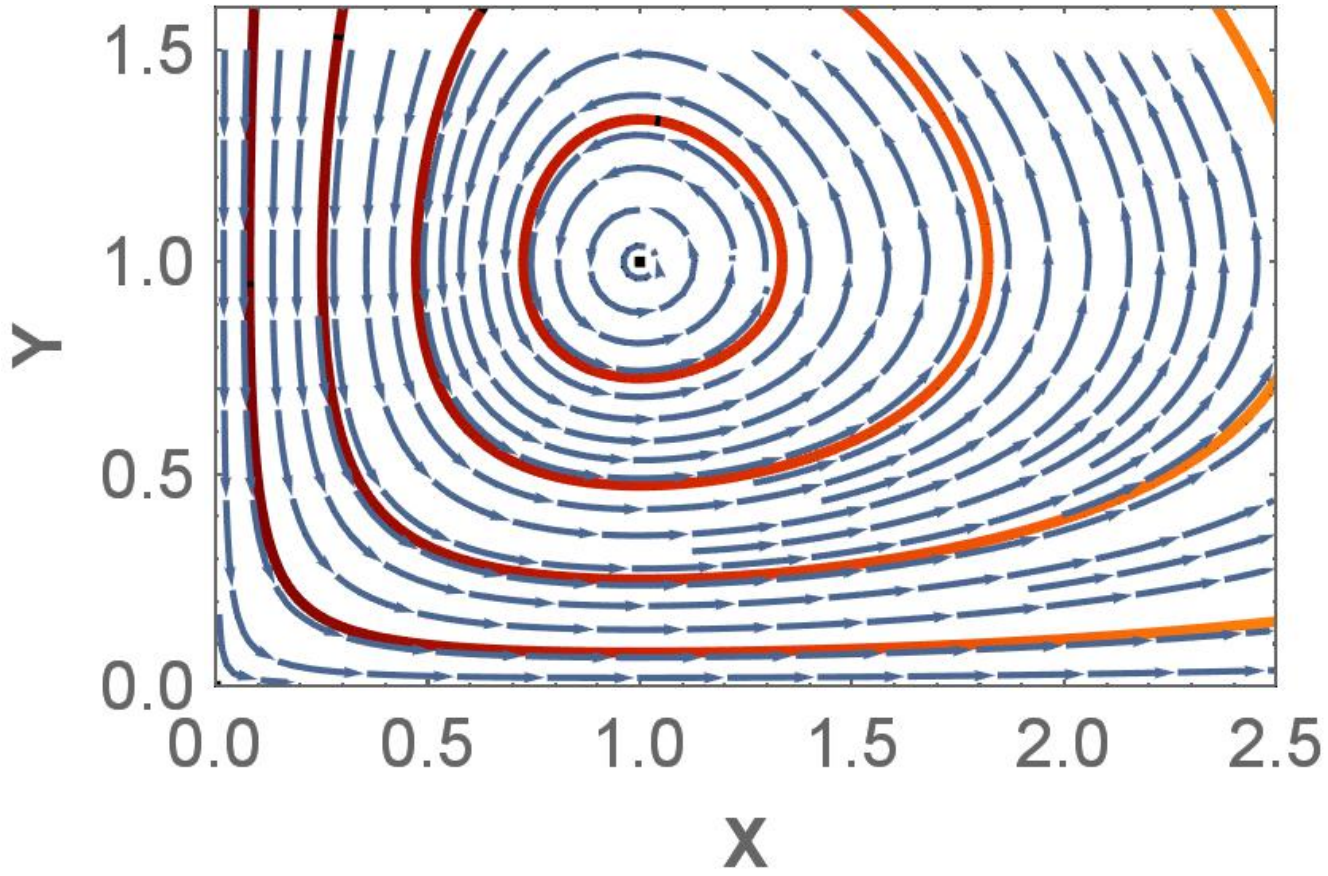

Figure 4: Prey-predator dynamics for a Lotka-Volterra system as described by the level curves of the conserved quantity C. The arrows describe the velocity and direction of solutions. There are equilibria at X=1,Y=1 and at X=0,Y=0. For any point not at the equilibrium we are within a limit cycle. Any perturbation simply results in different limit cycle for the population or extinction. We used $\alpha = \beta = \delta = \gamma = 1$ in this simulation.

2.2.2 Rosenzweig-MacArthur

The Rosenzweig-MacArthur model is perhaps the most commonly used predator-prey interaction model. It is usually attributed to a paper from 1963 from Rosenzweig and MacArthur (Rosenzweig and MacArthur, 1963). An excellent explanation of the model (and many other food web models) can be found in (Turchin, 2003). The Rosenzweig-MacArthur model expands the formula of Lotka-Volterra by two assumptions: The predator is limited in his consumption of prey and the prey growth is self-limiting. The equations are usually given as

$$\dot{X} = rX\left(1-\frac{X}{K}\right) - Yh(X), \tag{7}$$

$$\dot{Y} = \xi Yh(X) - \delta Y, \tag{8}$$

with

$$h(X) = \frac{cX}{d+X}. \tag{9}$$

The variables X and Y are prey and predator populations. The function $h(X)$ is the so called functional response; the consumption rate per predator in dependence of the prey density. The form of the functional response will be explained in more detail in Sec. 2.2.4. The parameter K is the carrying capacity; a measure of how much prey biomass could be supported without predator interference. The biomass conversion efficiency of prey-to-predator biomass is given by ξ. The rate of growth for the prey without any losses factored in is given by r and the combined mortality and respiration rate of the predator is given by δ. This expands the basic Lotka-Volterra model by two significant parts: For one, the growth rate of the prey species is now limited by a *carrying capacity* K; introducing in essence a density dependent mortality rate for the prey. This kind of growth is called *logistic growth*. Without any predation pressure the prey grows asymptotically towards $X = K$:

$$\lim_{t\to\infty} X(t) = K.$$

The self-limiting behaviour of the prey species can be caused by e.g. a lack of or limited regrowth of resources or intra-species competition. Additionally, the functional response of the predator to the prey density is no longer linear but hyperbolic, i.e. goes towards an asymptotic limit for prey consumed per predator for large numbers of prey. The reasoning behind this is explained below in section 2.2.4 but can be summarized to the ultimately limited digestive capabilities of a single predator. In contrast to the Lotka-Volterra model this allows for new behaviour depending on the parameter values. The Lotka-Volterra model predicts population cycles but these are not stable to perturbation. A disturbance to the species populations would create a new cycle with a new period and amplitudes. In nature cycles are often robust to slight changes, i.e. they return to a (nearly) identical cycle if perturbed. The Rosenzweig-MacArthur model allows for such stable limit cycles and for stable equilibria of coexistence as shown in Fig. 5.

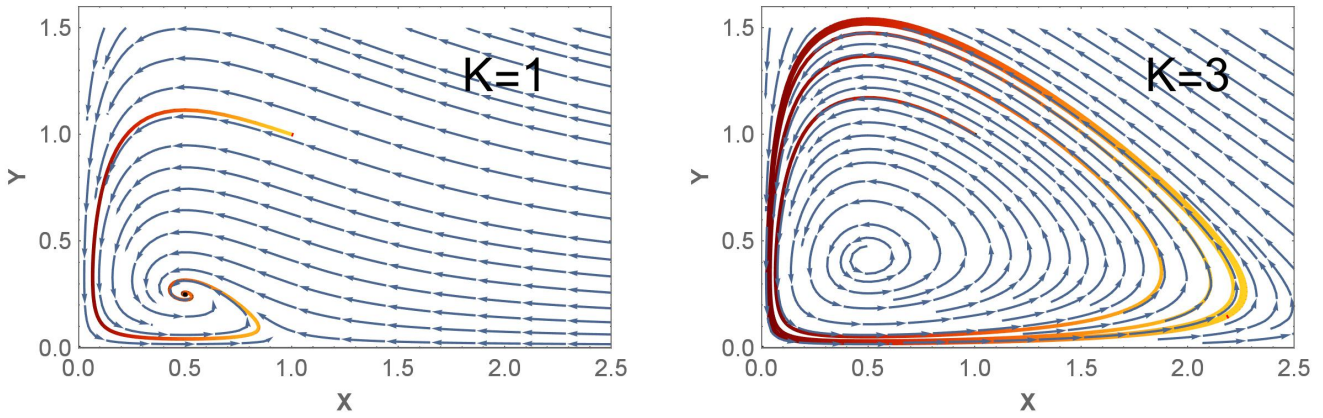

Figure 5: Phase plots of the Rosenzweig-MacArthur model for different carrying capacities. The arrows describe the velocity and direction of solutions. The coloured line is an exemplary solution, the color scheme itself has no particular meaning. In the left graph we see that we have an equilibrium point. On the right we have an attracting limit cycle. The graphs differ only in carrying capacity K.

2.2.3 Beddington-DeAngelis

John Beddington (Beddington, 1975) and Donald DeAngelis (DeAngelis et al., 1975) proposed a predator-prey dynamics with a function response that satiates not only with prey but also predator density. The simplest form of such dynamics is

$$\dot{X} = rX\left(1-\frac{X}{K}\right) - Yh(X), \tag{10}$$

$$\dot{Y} = \xi Yh(X) - \delta Y, \tag{11}$$

with

$$h(X,Y) = \frac{cX}{1+d\cdot X+e\cdot Y}. \tag{12}$$

The variables X and Y are prey and predator populations and the functional response h depends now on both the predator and the prey population in contrast to the Rosenzweig-MacArthur model. The satiation of the functional response for high predator density can be interpreted as competition or interference between predators. Energy that could be spent hunting is invested in e.g. defence of hunting grounds or search for now frequently occupied resting spots. Alternatively, the prey might be more cautious due to high number of visible predators or simultaneous predation attempts inhibit each other. Models that incorporate a functional response that is dependent on the predator population, like the Beddington-DeAngelis model, are quite under-represented despite performing well in fits to real data (Skalski and Gilliam, 2001). The most commonly used approach is the Rosenzweig-MacArthur model and most models discussed in the later sections of this thesis are based upon it, simply because there is abundance of literature.

2.2.4 Functional Response

One of the key features of food web models is the interaction form of predator and prey and the core element of the predator-prey relationship is the consumption of the prey by the predator. The functional

response is the consumption rate per predator in dependence of the prey density. It is usually classified in accordance to C.S. Holling (Holling, 1959) in type I, II and III. It can be written as

$$\text{Type I}: \qquad h(X) = aX\,, \tag{13}$$

$$\text{Type II}: \qquad h(X) = \frac{aX}{1+acX}\,, \tag{14}$$

$$\text{Type III}: \qquad h(X) = \frac{aX^k}{1+acX^k}\,, \tag{15}$$

with X as the prey population density and the constant 1 given in same units as rest of the divisor. We have already seen type I in the Lotka-Volterra equations and type II in the Rosenzweig-MacArthur model. While type I grows without bounds, meaning predators presented with more prey will always consume proportionally more prey, both type II and III set a limit to the amount of food a predator can consume. The limit in prey consumption is due to the handling time for the predator for each prey encounter. An apt if slightly humorous description of the handling time can be found in (Smith, 2008) as "for the predator to handle (stalk, catch, eat, burp, clean teeth, sleep) ". It bundles the limits of prey consumption like digestion, hunting time, grooming, etc. into one variable; here called c. The parameter a can be interpreted as an attack rate. If there is no time needed to digest prey it is equal to the biomass consumption rate of the predator. The exponent k in type III gives a measure for the non-linearity of the functional response. For large k we approach a step-function like functional response; the predator could only consume prey at high prey populations and at a constant value. The most commonly used value for type III is $k = 2$ which means the prey consumption rises slower with increasing prey density at first but approaches the limit value of prey consumed faster than type II. Type III functional responses are usually associated with learning curves for the predator. For low prey densities the predator is not actively hunting for the prey or does not yet recognize it as prey and only consumes it by chance. With higher prey densities the predator becomes more proficient at recognizing and hunting the prey and thus approaches the limit consumption value faster.

Most food webs have more than a single predator and a single prey. This means we have to take into account how a predator reacts to density changes in prey if there are multiple option available. As an example we start with a Holling type II response. Assume we have a predator denoted by the index i and $\mathcal{G}$ is the set of species i preys upon. There are N species in $\mathcal{G}$. We introduce a functional response of the form

$$h_i(X_1,\ldots,X_N) = \sum_{j\in\mathcal{G}} \frac{a_{ij} f_{ij} X_j}{1+\sum_{l\in\mathcal{G}} a_{il} f_{il} c_{il} X_l}\,, \tag{16}$$

$$\tag{17}$$

where we introduce f_{ij} as the fractional foraging effort: The relative amount of time the predator invests in foraging for an individual prey species compared to its total time and effort expenditure. We also introduce the index ij to the attack rate and the handling time as they could change from prey to prey. It is easy to see that the equation reduces to the basic form of the Holling type II functional response if there is only one prey species. We have essentially substituted the individual population expressions like aX and ahX with sums of fractional contributions. This can be applied analogously to other functional responses.

The functional response is not limited to the three Holling types though these are the most commonly used. The Holling type functional responses for instance do not consider the predator density as a factor for the consumption rate.

2.3 Dispersal between Patches

Meta-communities are connected food webs on patches distributed in space. Each patch is home to a number of species that form a local food web. These local food webs are connected to other patches and food webs by dispersal. Assume we have a meta-community with N species per patch and M patches. The population dynamics of species n on patch m can be written as

$$\dot{X}_n^m(\mathbf{X^1},\ldots,\mathbf{x^M}) = F_m + \sum_k^M E_n^{kl}(\mathbf{X}^k,\mathbf{X}^l) - \sum E_n^{lk}(\mathbf{X}^k,\mathbf{X}^l) \tag{18}$$

where interactions within a patch m that do not depend on other patches are summarized by the term F_m and the migration from patch l to patch k is defined by the term E^{kl}. All populations densities within a patch k are represented by $\mathbf{X}^k = \left[X_1^k,\ldots,X_N^k\right]$. The form of the term E^{kl} is highly variable. A common version is the simple diffusive migration (used for instance by (Jansen, 1995)) where the dispersal is proportional to X_n

$$E_n^k l = d_n^l X_n^l - d_n^k X_n^k \tag{19}$$

with d_n^k as a diffusion coefficient. In this case, migration of a population only depends on the population itself. The assumption is that there is constant ratio of curious specimens that happen to travel to another patch. Biological species often have other incentives than mere curiosity. Prey species might flee from predators, predators might look actively for patches with high prey density, etc. Dispersal that depends on other species populations or different patch conditions is called adaptive dispersal or cross-diffusion and has been the focus of a number of ecological and mathematical papers, e.g. (Shigesada et al., 1979; Holmes et al., 1994; Lou and Ni, 1996; Ruiz-Baier and Tian, 2013).

For an example of cross-diffusion we look at (Huang and Diekmann, 2001). We look at a simple two patches two species model with a population of the predator and a population of the prey on each patch. The predator is limited in his movement during the handling time of the prey. For sufficiently large prey density there is no movement. The dispersal is given by

$$E_p^k l = \frac{1+\theta h X_n^l}{1+hX_n^l} X_p^l - \frac{1+\theta h X_n^k}{1+hX_n^k} X_p^k \tag{20}$$

with the index p for the predator and the index n for the prey species. The parameter θ sets the movement ability of the predator and h is the handling time. For $\theta = 0$ we have simple diffusive migration. For $\theta = 1$ the predator is either searching for prey within his patch or incapable of movement as he is handling prey; effectively isolating the patches from one another.

2.4 Laplace Matrix

The Laplacian matrix will be of importance in section 6 to define the spatial network and its influence on the meta-food web.

2.4.1 Definition and Properties

The Laplace matrix is used in graph representation. For a simple graph we can use the definition

$$\mathbf{L} = \mathbf{D} - \mathbf{A}, \tag{21}$$

with $\mathbf{D} = [d_{i,j}]$ as the degree matrix that contains the degrees of the vertices v_i on the diagonal

$$d_{i,j} := \begin{cases} \deg(v_i) & \text{if } i = j \\ 0 & \text{if } i \neq j \end{cases},$$

and the adjacency matrix $\mathbf{A} = [a_{i,j}]$ that has entries for all vertices that share an edge

$$a_{i,j} := \begin{cases} 1 & \text{if } (i,j) \in E \\ 0 & \text{otherwise} \end{cases}$$

with E being the set of edges between vertices.
The Laplacian matrix $\mathbf{L}$ has several attributes we will be using later on:

- $\mathbf{L}$ is positive-semidefinite. This means all eigenvalues are zero or larger.
- The smallest eigenvalue is always $\lambda = 0$.
- The second smallest eigenvalue, the Fiedler eigenvalue, is $\lambda_F = \frac{4}{n \cdot D}$ with n as the number of vertices and D as the maximal distance in steps between vertices
- The largest eigenvalue is limited by the number of vertices n : $\lambda \leq n$.

An additional important relationship between eigenvalues and graph properties is much harder to quantify and still a topic of research. The maximum eigenvalue of the Laplacian matrix is connected to the degrees of the vertices. This means that a graph can have an ever increasing number of vertices but the associated eigenvalues of the Laplacian matrix do not necessarily increase in the same manner. Graphs with comparable largest degree values have usually similar eigenvalue limits. Using the Gershgorin circle theorem (which will be explained in detail in Sec. 2.6.1) we can easily give a rough limit for the eigenvalues depending on the largest degree

$$\lambda_{\max} \leq 2 \cdot \deg_{\max}(v). \tag{22}$$

More elaborate upper bounds have been established (for example by (Guo, 2005), (Shu et al., 2002), (Liu et al., 2004) and many more) but this estimate is precise enough for this thesis.

2.4.2 Random Geometric Graphs

Random geometric graphs are arguably the simplest form of spatial networks. Nodes are placed randomly within a space with a defined metric and if nodes are within a certain range r, an undirected link is established. The connections between the nodes can be easily summarized in an adjacency or Laplace matrix. The ease of construction and the very limited number of assumptions make them ideal starting points for spatial networks and we will use them in Sec. 6 to infer properties we expect in real spatial networks.

2.5 Linear Stability Analysis

Linear stability analysis is used to define the stability of a steady state for a system of linear differential equations. We will use it to define the stability of meta-communities as their dynamics can be written in ordinary differential equations. We write a system of ordinary differential equations (ODEs) as

$$\frac{\mathrm{d}}{\mathrm{d}t}\vec{x}(t) = \dot{\vec{x}}(t) = \vec{f}(\vec{x}(t)); \; x \in \mathbb{R} \tag{23}$$

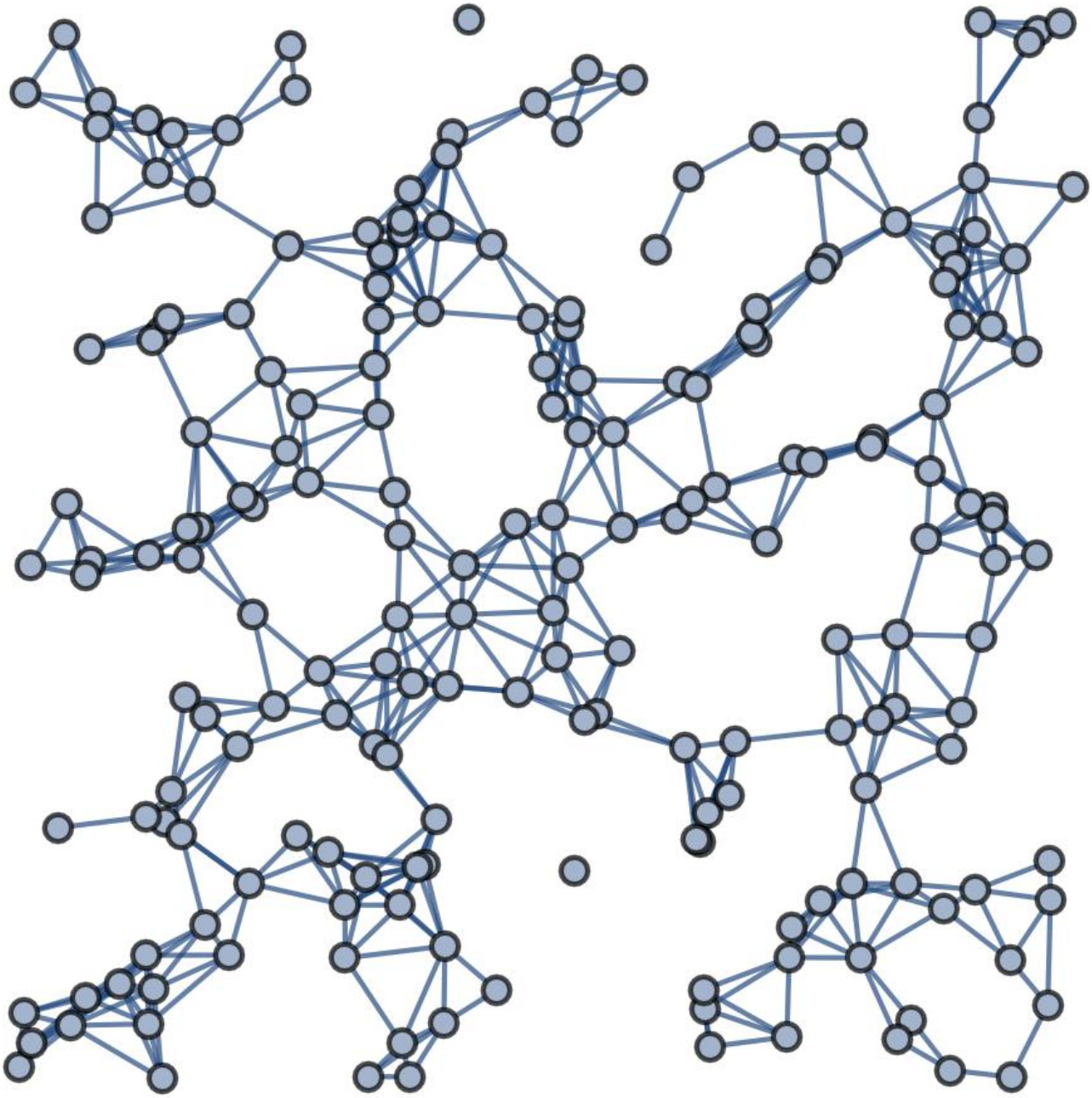

Figure 6: An RGG plot of 200 nodes with a range of $r = 0.1$. The nodes are placed in 1×1 area of arbitrary units.

The vector $\vec{x}$ consists of functions $\vec{x}(t) = (x_1(t), ..., x_n(t))$ with an equilibrium at $\vec{x}^* = (x_1^*(t), ..., x_n^*(t))$.
In proximity of the equilibrium we can write $\vec{x}$ as

$$\vec{x}(t) = \vec{x}^* + \vec{\zeta}(t) \; ; \; \vec{\zeta}(t) = (\zeta_1, ..., \zeta_n) \tag{24}$$

where ζ is a small disturbance of the equilibrium. We write a Taylor-expansion around the steady state

$$\dot{\vec{x}}^* + \dot{\vec{\zeta}} = \vec{f}(\vec{x}^* + \vec{\zeta}) = \vec{f}(x^*) + D\vec{f}(x^*)\vec{\zeta} + \mathcal{O}(|\vec{\zeta}|^2) \tag{25}$$

with $D\vec{f}(\vec{x}^*)$ as the Jacobian matrix of the function $\vec{f}$ at the equilibrium $\vec{x}^*$.
For sufficiently small deviations from the steady state $\mathcal{O}(|\vec{\zeta}|^2)$ can be neglected. We remind us that at the equilibrium $\dot{x} = f(x) = 0$ and we get

$$\dot{\vec{\zeta}} = D\vec{f}(x^*)\vec{\zeta} \tag{26}$$

We want to know whether a deviation ζ grows or vanishes for $t \to \infty$. Assuming the Jacobian matrix $D\vec{f}(x^*)$ has only real entries, we can write potential solutions in the form

$$\zeta(t) = c\, v e^{\lambda t} \tag{27}$$

if the eigenvalue λ is purely real and has an eigenvector $\vec{v}$. If the eigenvalue is part of a pair of complex conjugated eigenvalues $\lambda = \alpha \pm i\beta$ and the associated eigenvectors are $v = u \pm iw$ then we have two types of solutions

$$\zeta_1(t) = e^{\alpha t}(u\cos(\beta t) - w\sin(\beta t)),$$
$$\zeta_2(t) = e^{\alpha t}(u\sin(\beta t) - w\cos(\beta t)).$$

In any case we find that the real part of the eigenvalue is crucial for the amplitude.

- If all eigenvalues fulfil $\mathrm{Re}(\lambda) < 0$ then the amplitude for ζ goes towards 0 for $t \to \infty$.
- If any eigenvalue has $\mathrm{Re}(\lambda) > 0$ then the amplitude for that solution $|\zeta|$ goes towards infinity for $t \to \infty$.
- If an eigenvalue has $\mathrm{Re}(\lambda) = 0$ but non-zero imaginary parts the amplitude of the solution oscillates.

This means if all eigenvalues of a system of differential equations have negative real parts at the steady state we have a stable steady state as all amplitudes of small disturbances vanish over time. If any eigenvalue has a positive real part the amplitude for that disturbance grows larger and the steady state is unstable. If the largest real part is the zero we have an oscillating amplitude for the linear approximation of the disturbance. The higher order terms that we have neglected for small deviations need to be analysed to make a statement about stability.

2.6 Eigenvalue Approximation

The study of steady states and their stability is a major subject of this thesis. As mentioned in the previous section, stability is based upon eigenvalues. In section 6 we need to establish bounds for the eigenvalues that determine the stability of a meta-food web. Here we present two ways to compute such eigenvalue limits.

2.6.1 Gershgorin Circle

An approximation for eigenvalues can be made with the Gershorgin circle theorem.

Theorem: Let **A** be a complex $n \times n$ matrix with the entries $a_{i,j}$. For $i \in 1,\ldots,n$ let $R_i = \sum_{j\neq i} |a_{ij}|$ be the sum of the absolute values of the non-diagonal entries in the i-th row. Let $D(a_{ii},R_i)$ be the closed disk centred at a_{ii} with radius R_i. Such a disk is called a Gershgorin disk (Gershgorin, 1931). Every eigenvalue of **A** lies within at least one of the Gershgorin discs.

The same theorem holds true if we use the column sum instead of the row sum. As a simple example we look at the matrix

$$\mathbf{A} = \begin{pmatrix} 10 & -1 & 0 & 1 \\ 0.2 & 8 & 0.2 & 0.2 \\ 1 & 1 & 2 & 3 \\ -1 & -1 & -1 & -9 \end{pmatrix}. \tag{28}$$

Note that since we do not have a symmetrical matrix we are able to choose between row and column sum for the radius of the disk; e.g. for the first eigenvalue we can define both the disk D(10,2) and D(10,2.2). With this in mind we get the discs D(10,2), D(8,0.6), D(2,1.2) and D(-9,3). We can see the Geshgorin discs and their actual eigenvalues in Fig. 7.

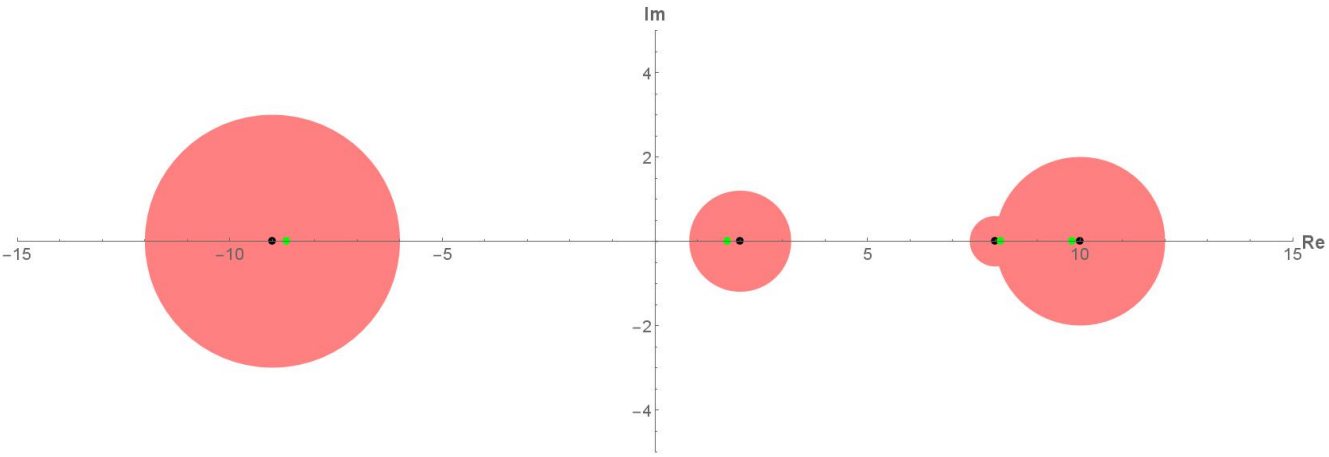

Figure 7: The Gershgorin discs for the matrix A. The centres of the discs are shown as black dots. We note that we can easily define minimal and maximal real parts for all discs. The actual eigenvalues are $\lambda = \{9.81878, -8.6624, 8.13942, 1.7042\}$. They are displayed as green dots.

We can use this theorem to define the regions in which potential eigenvalues can be and thus make statements about the linear stability of a system with the help of the Jacobian matrix.

2.6.2 Brauer-Cassini Ovals

An alternative way to approximate the position of the eigenvalues of a square matrix is the use of Brauer-Cassini ovals (Brauer, 1947).

Theorem: Let **A** be a complex $n \times n$ matrix with the entries $a_{i,j}$. Let

$$R_i(A) := \sum_{j\neq i}^{n} |a_{i,j}| \tag{29}$$

denote the deleted row sums of the matrix A and define the (i,j)-th row oval of Cassini for the matrix $\mathbf{A}$ as

$$K^r_{i,j}(\mathbf{A}) := \left\{ z \in \mathbb{C} : |z - a_{i,i}| \cdot |z - a_{j,j}| \leq R_i \cdot R_j \right\}, \qquad i \neq j; (1 \leq i, j \leq n). \tag{30}$$

Further, set

$$K^r(\mathbf{A}) := \bigcup_{i \neq j}^{n} K^r_{i,j}(\mathbf{A}), \tag{31}$$

and let $\sigma(\mathbf{A})$ denote the eigenvalues of $\mathbf{A}$, i.e.,

$$\sigma(\mathbf{A}) = \{ \lambda \in \mathbb{C} : \det(\lambda \cdot \mathbf{I} - \mathbf{A}) = 0 \}. \tag{32}$$

Using these definitions we can say that

$$\sigma(\mathbf{A}) \subset K^r(\mathbf{A}). \tag{33}$$

Let us consider a sample matrix $\mathbf{A}$:

$$\mathbf{A} = \begin{pmatrix} 4-4i & -2-2i & 1+2i \\ 3 & 0 & 1+3i \\ 3-1i & 1 & -5-10i \end{pmatrix}.$$

If we look at Fig. 8 we see that the eigenvalues of matrix $\mathbf{A}$ are within both the Gershgorin discs as well as the Cassini ovals.

The Cassini ovals are always at least as precise as the Gershgorin discs as the ovals are a subset of the Gershgorin discs. A potential downside of the Cassini ovals compared to the Gershgorin discs is the number of necessary objects to define the boundaries of the eigenvalues. For a $n \times n$ matrix we need n Gershgorin discs but $\binom{n}{2} = \frac{n(n-1)}{2}$ Cassini ovals. It is interesting to note that while the combination of two columns or rows to estimate eigenvalues, as is the method for the Cassini ovals, improves accuracy for the eigenvalue bounds using more columns/rows provides no additional benefit and is frequently less precise.

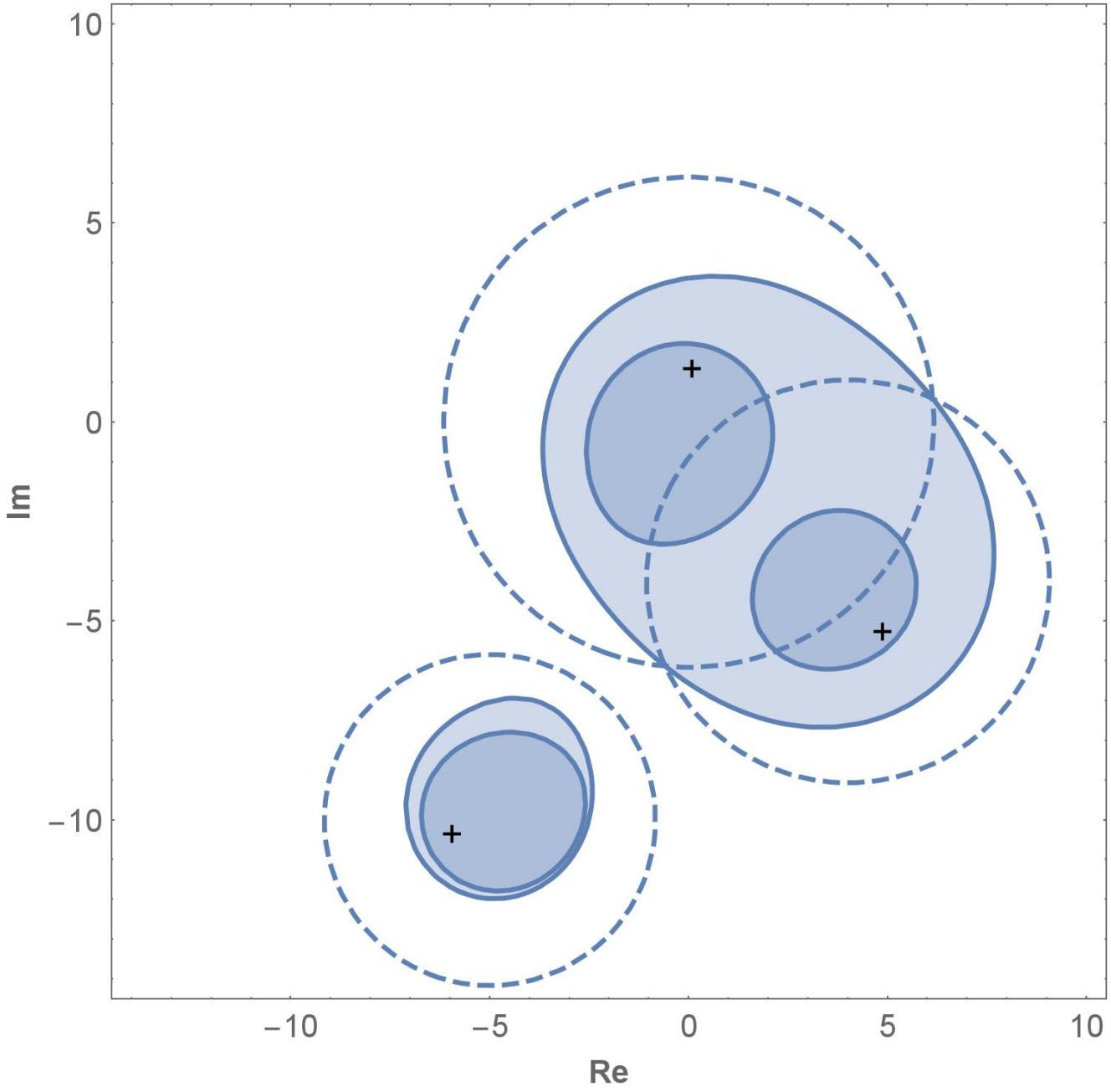

Figure 8: The Gershgorin discs and Cassini ovals for the sample matrix $\mathbf{A}$. The Gershgorin disc boundaries are dashed and the Cassini ovals tinged blue. The eigenvalues are marked by the crosses. The Cassini ovals are subsets of the Gershgorin discs and thus always provide at least the same accuracy.

2.7 Master Stability Function

The master stability function is used to describe systems of identical coupled oscillators. By separating the terms for the behaviour of the isolated local oscillator from the coupling to others, the behaviour of the total system can be described in a succinct manner (Pecora and Carroll, 1998).

We consider a system of N oscillators, each of them with identical dynamics if not coupled. These local dynamics can be captured by the equation

$$\dot{x}_i = f(x_i) \tag{34}$$

with x_i as a measure of the state of oscillator i which could be for example an amplitude. We set the vector of all oscillator states as $\vec{x} = \{x_1, x_2, \ldots, x_N\}$ and for all functions as $\vec{F}(x) = \{f(x_1), f(x_2), \ldots, f(x_N)\}$. We now introduce a coupling between the oscillators. The coupling is defined by several parameters. First, we define a matrix $\mathbf{G} = [g_{i,j}]$ which contains all information regarding between which oscillators there is a link. The elements $g_{i,j}$ are called coupling coefficients. Second, we define a general coupling strength σ. At last, we take a function $\vec{H} = \{H(x_1), H(x_2), \ldots, H(x_N)\}$ that modifies the interaction of each oscillators based upon its state. The dynamics of an individual node can now be written as

$$\dot{x}_i = F(x_i) + \sigma \sum_j G_{i,j} H(x_j) \tag{35}$$

and for all nodes as

$$\dot{\vec{x}} = \vec{F}(x) + \sigma \mathbf{G} \otimes \mathbf{H}(x) \tag{36}$$

$$\dot{\vec{x}} = \vec{F}(x) + \sigma \mathbf{G} \otimes \mathbf{H}(x) \tag{37}$$

with x now modified by the coupling interaction and $\otimes$ as the direct product.

The master stability equation (MSE), a single equation that governs the stability of the system, can now be derived. For details we refer to (Pecora and Carroll, 1998). We define it as

$$\dot{\zeta} = [D\mathbf{F} + \sigma\gamma D\mathbf{H}]\zeta \tag{38}$$

with γ as an eigenvalue of $\mathbf{G}$, and $D\mathbf{H}$ and $D\mathbf{F}$ as the Jacobian matrices for $\mathbf{H}$ and $\mathbf{F}$. The eigenvalues of this matrix equation can be used to define the stability of the system (hence the name master stability equation). We compute the eigenvalues of the combined matrices on the right-hand side of the equation and define the largest real part as $\lambda_{\max}$. If for all combinations of γ with the MSE we have $\lambda_{\max} < 0$, then the entire system is stable. The function describing the largest real part of the matrix equation is the *master stability function* (MSF).

2.8 Bifurcations

Bifurcations describe the change of the number or the stability of steady states. As we are interested in stability of meta-communities and how, when and why they become unstable we introduce some basic concepts and types of bifurcations. We will use this in Sec. 4, Sec. 5 and Sec. 6 to describe the behaviour of the meta-communities near the steady state in case of a bifurcation and the implications of these dynamics.

2.8.1 Definition

The term bifurcation was coined by the famous Henri Poincaré (Poincaré, 1885). The basic definition of a bifurcation is:

"A *sudden* change in behaviour for a system with a *smooth* change of a parameter."

The parameter in that scenario is called the *bifurcation parameter*. A bifurcation differs from other changes in two aspects:

- The change in behaviour has to be *sudden*, otherwise any function that is not constant would be in a constant state of bifurcation.
- The change of the parameter in question has to be *smooth*, otherwise random large jumps that lead to different behaviour would qualify as bifurcation.

This might sound like rather imprecise terms but attempts at making a clear mathematical definition do not offer much more immediate insight (Guckenheimer, 2007):

Consider an autonomous system of ordinary differential equations (ODEs)

$$\dot{x} = f(x, \mu); \quad x \in \mathbb{R}^n,\ \mu \in \mathbb{R}^m \tag{39}$$

where f is smooth. A bifurcation occurs at parameter μ_0 if there are parameter values μ_1 arbitrarily close to μ_0 with dynamics *topologically inequivalent* from those at μ_0.

Bifurcations can be classified by their normal form. The normal form is a simplified equation which describes the topological behaviour near the equilibrium for a given type of bifurcation. There are two types of bifurcations, local and global. Local bifurcations can be described by analysis of small neighbourhoods of the equilibria. Global bifurcations create changes that are not confined to such small neighbourhoods. We are solely interested in the former in this thesis.

Another way of phrasing the definition of (local) bifurcations is that the fixed points of a system change their stability at the point of bifurcation. How a system behaves at a fixed point can usually be quantified by looking at the Jacobian (assuming a linear stability analysis is feasible) at the fixed point. We will discuss this in detail later on.

A mechanical example for a bifurcation is a stiff rod under pressure. Assume a rod set into and perpendicular to the ground. There is weight placed onto the top and we measure the mechanical deflection of the rod. With increasing weight the rod bends but returns to the vertical position (a stable fixed point) until it buckles. This is the bifurcation point, the changing weight the bifurcation parameter. The previously stable vertical position becomes unstable. Two new fixed points emerge. The rod has

now stable positions bent to the left or right (or more directions and fixed points if we assume a three dimensional problem) and an unstable fixed point in the vertical position.

The sudden nature of the change is what makes bifurcations so intriguing for many fields. While there is research into early warning signs for bifurcations in multiple fields (Lenton, 2011) with different methods (generalized modelling among them (Lade and Gross, 2012)), in climate change (Scheffer et al., 2009) and ecology (Guttal and Jayaprakash, 2008), they are very hard to predict and potentially catastrophic. A firm understanding of the underlying principles is necessary to predict bifurcations and how they will affect the system. In the following subsections we will discuss several types of bifurcations.

2.8.2 Saddle-node Bifurcation

A saddle-node bifurcation has a simple zero eigenvalue $\lambda = 0$ for the Jacobian at the fixed point. This happens if two equilibria merge and disappear (Kuznetsov, 2006b; Andronov et al., 1971).

The normal form for the one dimensional case (see Fig. 9) is given by

$$\frac{\mathrm{d}}{\mathrm{d}t} y = \beta + \sigma y^2; \qquad y \in \mathbb{R}, \beta \in \mathbb{R}, \sigma = \pm 1. \tag{40}$$

For values of $\sigma\beta$ below zero we have two fixed points $\frac{\mathrm{d}}{\mathrm{d}t} y = 0$ at $y_{1,2} = \pm\sqrt{-\sigma\beta}$. For $\sigma\beta = 0$ there is an equilibrium at $y = 0$. For $\sigma\beta < 0$ we find that the point $y = \sqrt{-\sigma\beta}$ is stable since $\frac{d}{dt} y > 0$ for values lower than $y = \sqrt{-\sigma\beta}$ and $\frac{\mathrm{d}}{\mathrm{d}t} y < 0$ for values greater than $y = \sqrt{-\sigma\beta}$; i.e. the function returns to the fixed point for any small perturbation. The point $y = \sqrt{+\sigma\beta}$ is unstable because any perturbation grows in size. If we increase $\sigma\beta$ towards zero the two fixed points decrease their distance. At $\sigma\beta = 0$ the fixed points merge and their attributes as well: For any value $y < 0$ we are moving towards the fixed point, for any value $y > 0$ we are moving away from the fixed point. The combined point is unstable but still has a stable direction. This change from two fixed points to one fixed point is called saddle-node bifurcation.

Increasing β further makes any fixed point vanish. The behaviour in higher dimensions is obviously more complex but analogous (see Fig. 10 for a two dimensional example). As fixed points are merged we see a new point that carries attributes of both points (though being partially unstable is still unstable) and then vanishes. One of the points is a saddle point and the other a node which gives the saddle-node bifurcations its name. The reverse process (the emergence of fixed points as a bifurcation parameter is varied) is called a saddle-node bifurcation as well.

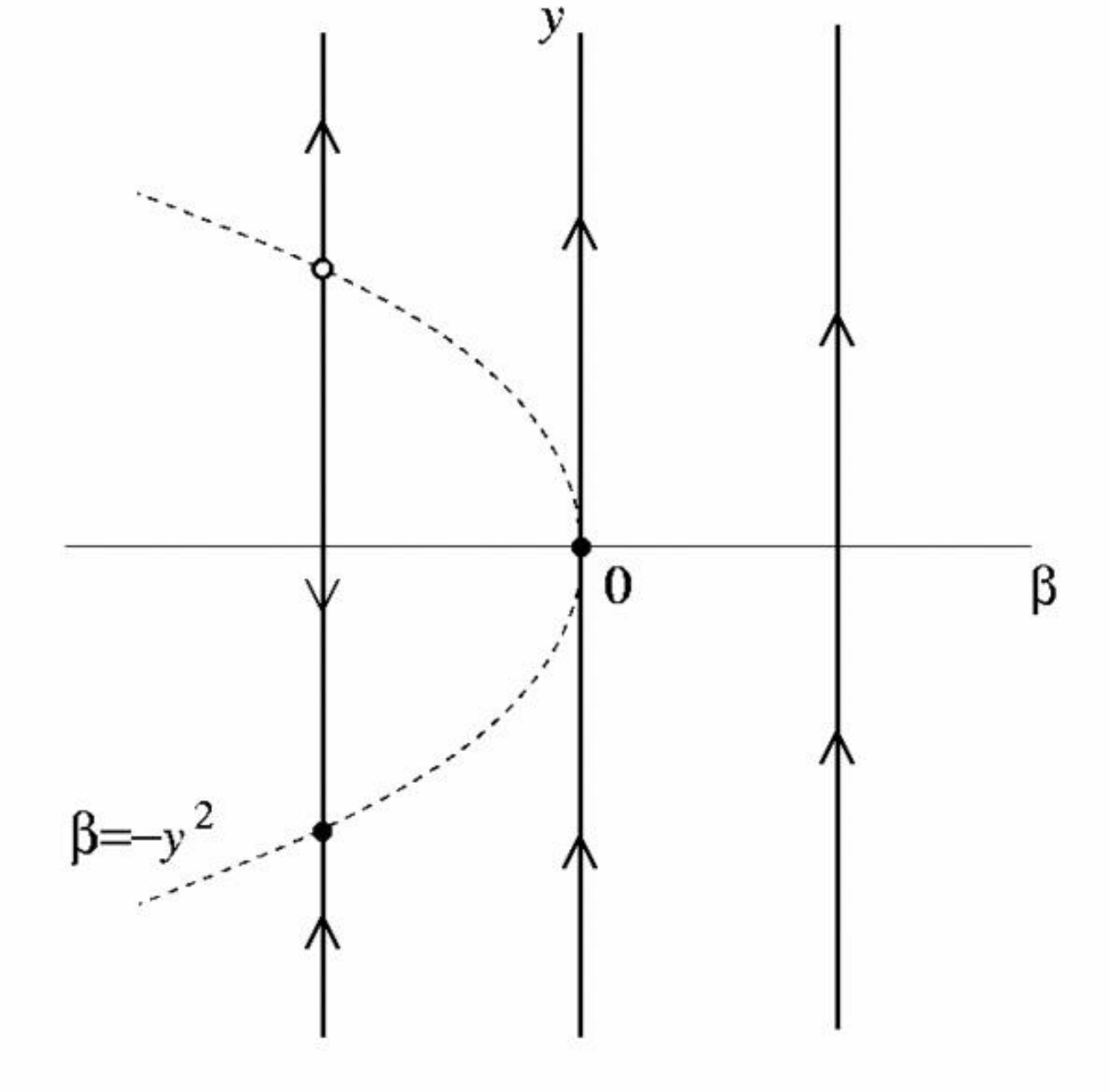

Figure 9: Saddle-node bifurcation for a one dimensional system with $\dot{y} = \beta + y^2$. The arrows indicate the sign of the derivative. The black disk indicates a stable fixed point, the empty circle an unstable fixed point. The half-filled circle indicates the point of the saddle-node bifurcation.The blue dashed line indicates $\beta = -y^2$. We increase the value of β from the left to the right; starting at negative values and going to positive ones. At the middle line we have $\beta = 0$. We see how, as we increase β we go from two fixed points to a single point with intermediate semi-stable properties to no fixed point at all.

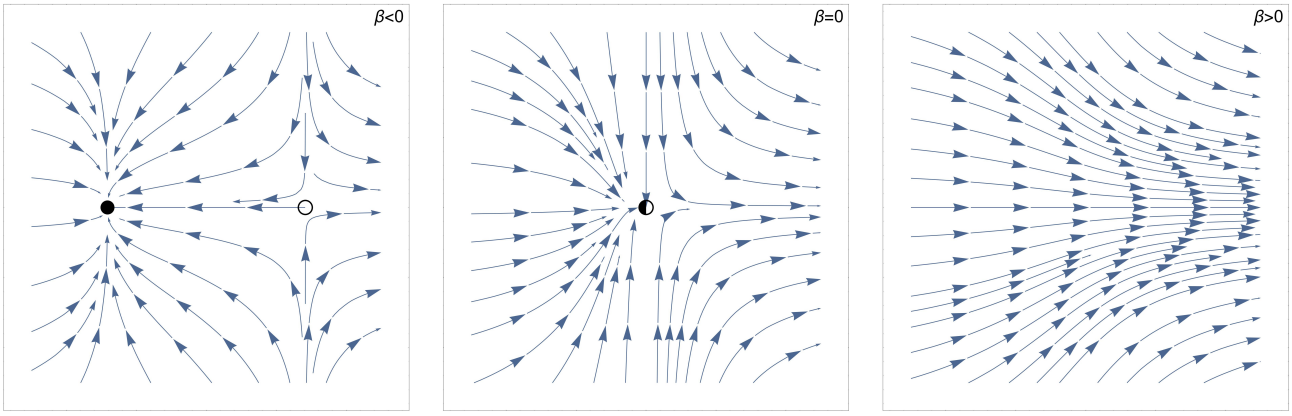

Figure 10: Saddle-node bifurcation for the two dimensional case. As we see the principle remains the same. Circle and disk have the same meaning as in picture Fig. 9. The blue arrows indicate the amplitude and direction of the derivative $\vec{\dot{y}} = (\dot{y}_1, \dot{y}_2)$. The fixed points get closer till they merge, which forms a unique point, and then disappear.

2.8.3 Hopf Bifurcation

The Poincaré-Andronov-Hopf-bifuraction, usually shortened to Hopf bifurcation, is defined as a bifurcation where a pair of distinct complex conjugated eigenvalues of the Jacobian of the system cross the imaginary axis in the complex plane (Marsden and McCracken, 2012; Andronov et al., 1971) (which means that they become purely imaginary) at the point of bifurcation:

$$\lambda_{1,2} = \pm i \cdot c; \qquad c \in \mathbb{R}. \tag{41}$$

The main contribution of Hopf was the extension of the definition from two dimensions to many (Hopf, 1942). A Hopf bifurcation creates a limit cycle around the previous equilibrium. Limit cycles are closed trajectories in phase space. They are called limit cycles as all other trajectories converge to them either in infinity or negative infinity time steps. If all trajectories reach the limit cycle in positive infinity the limit cycle is called stable; if some or all trajectories reach it in negative infinity it is called unstable.

The normal form for the two-dimensional case of the Hopf bifurcation (which the author of this thesis considers the most intuitive) is given by

$$\dot{y}_1 = \beta y_1 - y_2 + \sigma y_1 (y_1^2 + y_2^2), \tag{42}$$
$$\dot{y}_2 = y_1 + \beta y_2 + \sigma y_2 (y_1^2 + y_2^2). \tag{43}$$

We use β as the bifurcation parameter. The parameter σ is either -1 or 1 and changes the behaviour of the bifurcation.

- For $\sigma = -1$ we have a supercritical Andronov-Hopf bifurcation (see Fig. 11). For $\beta \leq 0$ there is a stable fixed point. For $\beta > 0$ this fixed point becomes unstable and a stable limit cycle forms.

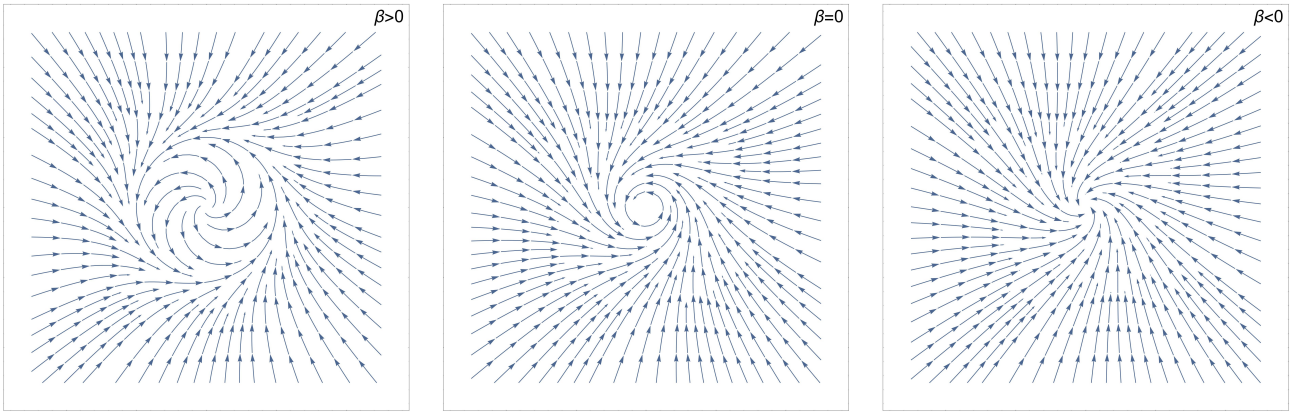

Figure 11: Supercritical Andronov-Hopf bifurcation in the plane. The arrows indicate the direction and amplitude of $\dot{\vec{y}} = (\dot{y}_1, \dot{y}_2)^\top$. If we increase β we see how from a stable fixed point a stable limit cycle emerges and the fixed point becomes unstable.

- For $\sigma = +1$ we have a subcritical Andronov-Hopf bifurcation (see Fig. 12). The fixed point is stable for negative β and becomes unstable for $\beta \geq 0$. An unstable limit cycle with the fixed point as center exists for $\beta < 0$.

For higher dimensions the principles remain the same (see Fig. 13).

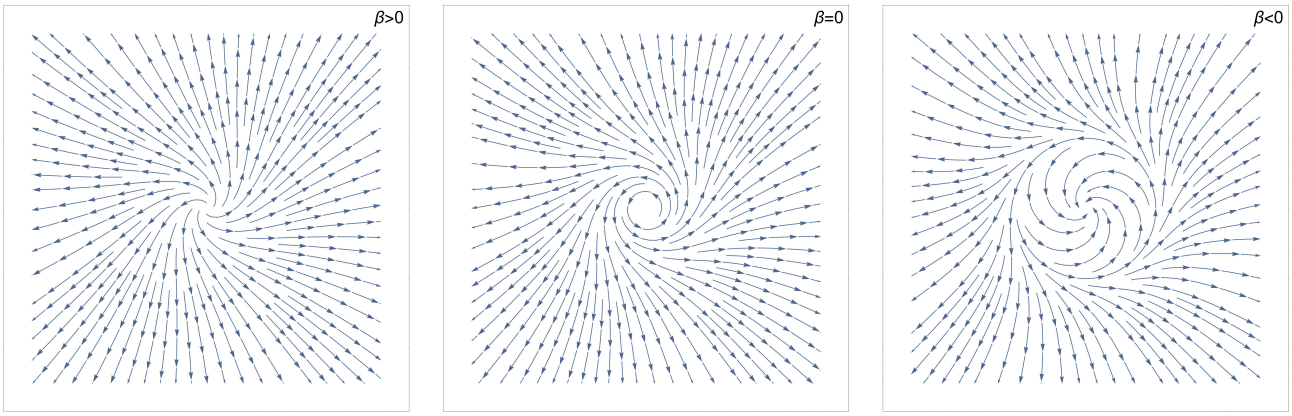

Figure 12: Subcritical Andronov-Hopf bifurcation in the plane. The arrows indicate the direction and amplitude of $\dot{\vec{y}} = (\dot{y}_1, \dot{y}_2)^\top$. For β below zero we have a stable fixed point surrounded by an unstable limit cycle. The limit cycle becomes smaller in diameter for larger β and finally vanishes. The stable fixed point becomes unstable at the same time.

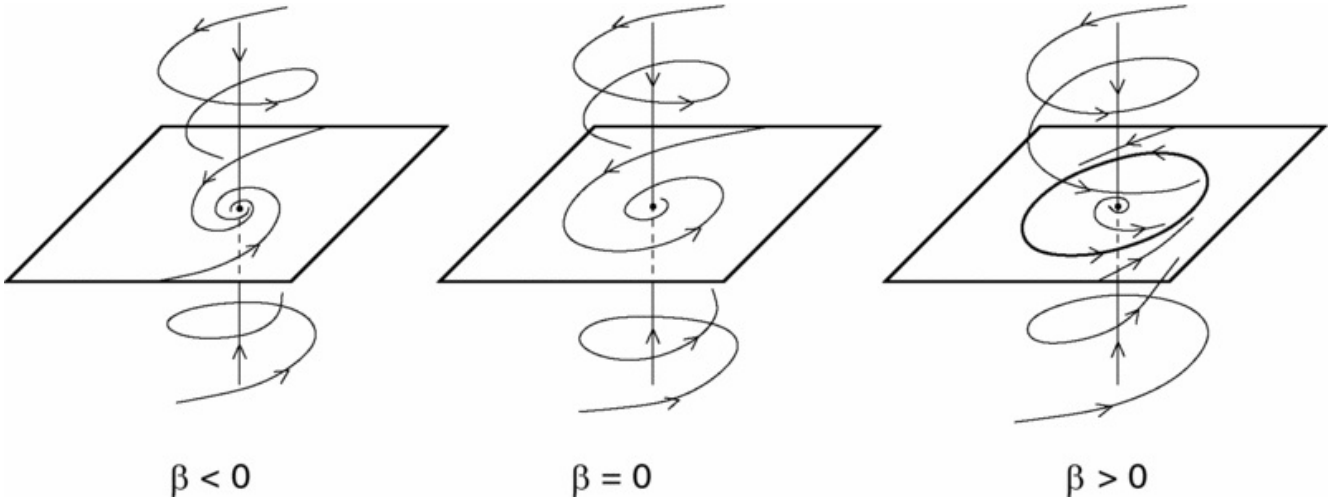

Figure 13: Supercritical Hopf bifurcation in three dimensions (Kuznetsov, 2006a). The arrows indicate the direction and amplitude of $\dot{\vec{y}} = (\dot{y}_1, \dot{y}_2, \dot{y}_3)^\top$ which is analogously defined to (43). The same principles as in two dimensions (Fig. 11) apply.

2.8.4 Turing Instabilities

The famous mathematician Alan Turing described how diffusion can destabilize a locally stable system (Turing, 1952). The original paper focused on chemical reactions trying to explain the formation of structures like e.g. organs within a living body. The basic setting requires two types of interaction partners: An activator and an inhibitor. The inhibitor limits the growth of the activator. The activator facilitates the growth of the inhibitor. We assume that activator and inhibitor are in a steady state if there is no diffusion. We introduce diffusion and write the dynamics as a partial differential equation (Murray, 2011):

$$\left.\begin{aligned} \dot{u} &= \Delta u + \gamma f(u,v) \\ \dot{v} &= d\Delta v + \gamma g(u,v) \end{aligned}\right\} \text{ on } B \subseteq \mathbb{R}^n . \tag{44}$$

The variable u is the local abundance of the inhibitor and v is the local abundance of the activator. Parameter d is the ratio of the diffusion coefficients $d = \frac{d_v}{d_u}$. Parameter γ is the relative importance of local reaction strength to diffusion. The dot indicates the derivative by time. We assume the boundary conditions $\vec{n} \cdot \nabla u = \vec{n} \cdot \nabla v = 0$ on ∂B and denote partial derivation of a function f in regard to a variable u as f_u. If the system is stable with no diffusion; $(\Delta u = 0, \Delta v = 0)$; then the inequalities

$$f_u + g_v < 0 \tag{45}$$

and

$$f_u g_v - f_v g_u > 0 \tag{46}$$

have to hold. On the other hand, if diffusion is to destabilize the system, then inequalities

$$d f_u + g_v > 0 \tag{47}$$

and

$$(d f_u + g_v)^2 - 4d(f_u g_v - f_v g_u) > 0 \tag{48}$$

have to be satisfied as well. For Eq. (48) we see that $d > 1$ and thus the activator has to diffuse faster than the inhibitor to be destabilizing.

A solution for partial differential equation of the form (44) is

$$w(r,t) = \sum_k c_k \exp^{\lambda(k)t} W_k(r) \tag{49}$$

which is a wave form. The wave numbers k that fulfil the inequalities necessary for instability with diffusion are limited to an interval dependent on the boundary conditions. Only modes with wave numbers within that interval do not vanish after sufficient time. The surviving modes shape the emerging patterns. The striking patterns created by this relatively simple mechanism can be seen in Fig. 14 as a simulation. Turing instabilities are often assumed as the probable cause behind many types of patterns occurring in biology, e.g. stripes and dots on fur or vegetation distribution (see Fig. 16 and Fig. 15).

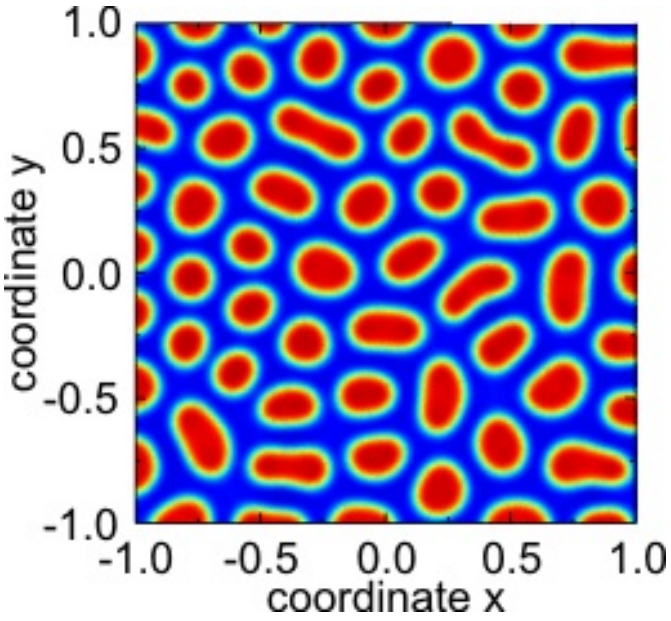

Figure 14: The result of a simulation of reaction-diffusion system with a Turing bifurcation. The x- and y-axis give spatial coordinates in arbitrary units. The picture shows the state of the system near the converged state when patterns have fully established themselves. The different colours mark different densities for one of the components (Bödeker, 2007).

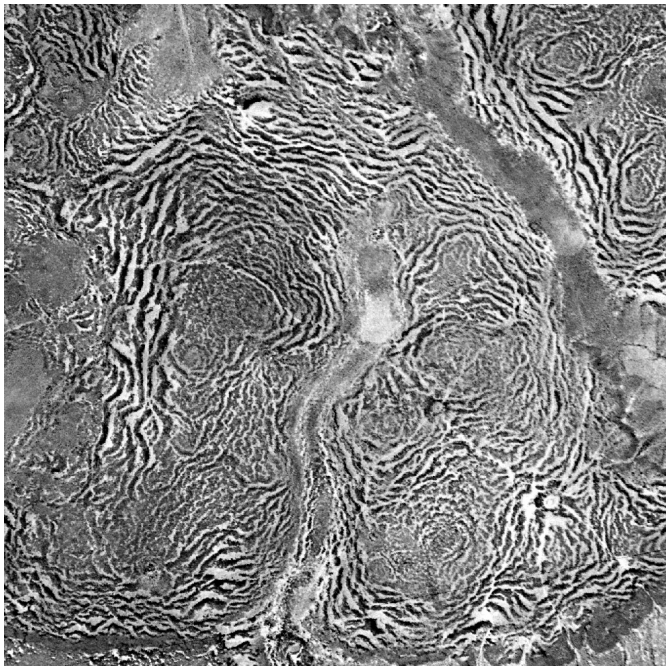

Figure 15: Aerial view of bush growth. The "prey" in this case is water that is consumed by the plants (the darker shades) (Agency, 1965). We can clearly see the stripe patterns.

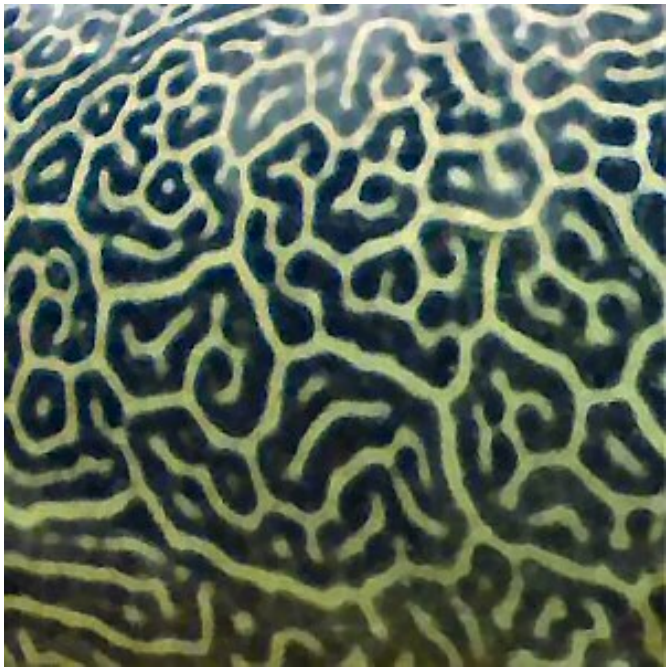

Figure 16: Patterns on the scales of a giant pufferfish (Chiswick, 2012). Different diffusion speeds of biological agents are the likely cause of this maze patterns.

2.9 The Generalized Method

In the following we will explain the generalized modelling approach which is the core method for the analysis of steady states in this thesis. We derive in detail the generalized expressions for population dynamics at the steady state for meta-communities of varying sizes. These terms are the mathematical basis for the sections 4, 5 and 6.

2.9.1 Basic Principle

The generalized method was first applied to food webs by (Gross and Feudel, 2006). The basic principles are deceivingly simple.

Assume there is some dynamic system represented by a set of equations

$$\dot{X}_i(t) = F_1(X_1, X_2, ..., X_N) + F_2(X_1, X_2, ..., X_N) + ... \ , \tag{50}$$

with F_i being arbitrary functions and there exists a steady state at which

$$\forall i \quad \dot{X}_i(t) = 0 \, . \tag{51}$$

The value of X_i at the steady state be X_i^*. We can now express all X_i and F_i in terms relative to the steady state value (which we will do in detail for some scenarios later on).

$$\dot{x}_i(t) = f_1(x_1, x_2, ..., x_N) + f_2(x_1, x_2, ..., x_N) + ... \ , \tag{52}$$

with x_i and $f_i, i \in \mathbb{N}$ being expressions normalized to the steady state value. We are now capable of doing a linear stability analysis with these normalized parameters and make statements about the steady

state without actually computing the absolute values. This means we get insight into all steady states with these ratios and are not bound by absolute numbers.

2.9.2 Localised Predator-Prey System

We start with a simple system of a single predator feeding on a single prey to introduce the concept of generalized modelling for food webs. The dynamics of food webs can be described by differential equations. A commonly used form is

$$\begin{aligned} \dot{X}(t) &= G(X) - F(X,Y) - K(X), \\ \dot{Y}(t) &= \epsilon F(X,Y) - D(Y). \end{aligned} \tag{53}$$

X and Y represent the biomass densities of the prey and predator population; $G(X)$ is the primary production rate; $K(X)$ and $D(Y)$ are the prey and predatory respiration and mortality rates and $F(X,Y)$ is the prey consumption rate of the predator with ϵ being the efficiency of consumed-prey-to-biomass conversion. These different functions can have a multitude of forms, some of which we will discuss in more detail later on. In the generalized method we are particularly interested in the stability of potential steady states and not as much in the dynamics previous to reaching the steady state. We would like to express our population densities and functions in terms of the values at the steady state and thus normalize the biomass densities and functions to the steady state values.

The normalized biomasses are

$$x = \frac{X}{X^*}, \quad y = \frac{Y}{Y^*}, \tag{54}$$

and the normalized functions are

$$h(x,y) = \frac{H(X,Y)}{H(X^*,Y^*)} \equiv \frac{H(X,Y)}{H^*}, \tag{55}$$

with $H = \{F,G,K\}$ and the asterisk (*) is used to denote the values of variables and functions in this steady state under consideration. We rewrite the equations in (53) in normalized terms:

$$\begin{aligned} \dot{x} &= \frac{G^*}{X^*} g(x) - \frac{K^*}{X^*} k(x) - \frac{F^*}{X^*} f(x,y) \\ \dot{y} &= \frac{\epsilon F^*}{Y^*} f(x,y) - \frac{D^*}{Y^*} d(y). \end{aligned} \tag{56}$$

While the steady state is per definition unchanging without disturbance this does not mean – setting aside pathological cases – that the individual processes of population dynamics have vanished. Biomass is still processed but gain and loss terms are matching. It is therefore useful to define the biomass turnover rate $\alpha^U, U \in [X,Y]$ at the steady state. We know the value of the functions $h(x,y)$ is 1 at the steady state and thus get

$$\alpha^X = \frac{G^*}{X^*} = \frac{K^*}{X^*} + \frac{F^*}{X^*} \tag{57}$$

$$\alpha^Y = \frac{\epsilon F^*}{Y^*} = \frac{D^*}{Y^*}. \tag{58}$$

The biomass turnover rate gives a good approximation of the average inverse lifespan of an individual. Assuming we have e.g. a biomass turnover of about one creature biomass per year, then this indicates that an average individual has about a year before it dies or gets eaten. For the sake of comparison and brevity the turnover rate of the predator is expressed in terms of the prey turnover

$$\alpha = \frac{a^X}{a^Y}. \tag{59}$$

If we look at the prey we notice that the turnover depends both on mortality and predation. To quantify the relative contribution of each process to the total biomass turnover we introduce *scale parameters*. In our very simple example we only need one scale parameter to describe the aforementioned relationship of mortality and predation:

$$\delta = \frac{1}{\alpha^X}\frac{F^*}{X^*}, \qquad \tilde{\delta} = (1-\delta) = \frac{1}{\alpha^X}\frac{K^*}{X^*}. \tag{60}$$

The scale parameter δ gives the proportion of total biomass flow at the steady state due to predation while its complement $\tilde{\delta}$ is the relative contribution of prey mortality.

With the addition of α and scale parameters we can again rewrite the differential equations Eq. (56) to

$$\begin{aligned} \dot{x} &= \alpha^X[g(x) - \tilde{\delta}k(x) - \delta f(x,y)], \\ \dot{y} &= \alpha^Y[f(x,y) - d(y)]. \end{aligned} \tag{61}$$

We now have a form that describes the dynamics of the system purely in terms relative to a steady state. The primary interest remains the stability of this steady state. To determine the behaviour near the steady state we use linear stability analysis and need the Jacobian **J** of the system defined as

$$J_{i,j} = \left.\frac{\partial \dot{V}_i}{\partial V_j}\right|_*, \tag{62}$$

with $V = \{x, y\}$ as the set of state variables and $|_*$ indicating that the derivatives are evaluated in the steady state (1,1). We get a Jacobian of the form

$$\mathbf{J} = \begin{pmatrix} 1 & 0 \\ 0 & \alpha \end{pmatrix} \cdot \begin{pmatrix} \phi - \tilde{\delta}\mu^X - \delta\gamma & -\delta\psi \\ \gamma & \psi - \mu^Y \end{pmatrix}, \tag{63}$$

which includes several new parameters called *exponent parameters*. They are the partial derivatives of the population dynamic functions with respect to the prey or predator populations. The definitions of the exponent parameters are

$$\phi := \left.\frac{\partial g(x)}{\partial x}\right|_*, \quad \mu^X := \left.\frac{\partial k(x)}{\partial x_i}\right|_*, \quad \mu^Y := \left.\frac{\partial d(y)}{\partial y}\right|_*, \quad \gamma := \left.\frac{\partial f(x,y)}{\partial x}\right|_*, \quad \psi := \left.\frac{\partial f(x,y)}{\partial y}\right|_*. \tag{64}$$

The exponent parameters are so-called elasticities, i.e. they are logarithmic derivatives of the original functions. For example

$$\phi = \left.\frac{\partial g(x)}{\partial x}\right|_* = \left.\frac{\partial \log(G(X))}{\partial \log(X)}\right|_* . \tag{65}$$

Such logarithmic derivatives have a number of advantageous properties. Elasticities as a measure of nonlinearity where first introduced in the 1920s (Marshall, 1920) in economic theory, because of their statistical properties which allows them to be estimated precisely based on limited noisy data. For the same reason these parameters are now commonly used in metabolic control theory.

In generalized models we use elasticities mainly because they allow for an intuitive interpretation: For any linear function, say $G(X) = AX$, the corresponding elasticity $\partial \log(G(X))/\partial \log(X)|_*$ is 1, regardless of the slope A. More generally, for any power law $G(X) = A \cdot X^p$ the elasticity is the power law exponent p. For more complex functions the elasticity provides an intuitive measure of the saturation of the underlying process. For example for the Holling type-II kinetics the corresponding elasticity is close to 1 in the linear regime at low prey density, but becomes 0 in the limit of predator saturation at high prey density.

The exponent parameters in Eq. (64) are briefly explained in Tab. 1. We go into more detail to give insight into how different models would lead to different parameter values.

The parameter ϕ describes the sensitivity of the primary production to changes in the population of the primary producer. The exponent parameter is usually set somewhere between zero and one which mirrors basic assumptions about the system. For growth rates proportional to population size we have a linear relationship and thus an exponent parameter of 1. If the growth rates cannot grow in the same manner as the population size because of e.g. limited and/or increasingly hard to find resources, then we have an exponent parameter lower than one but larger than zero. If the rates are fixed we have constant growth function and thus ϕ equals to zero. The parameter μ describes the change of mortality and respiration rates depending on the own population size. The rate is usually proportional to the population size ($\mu = 1$) but if we consider factors like intra-specific competition or disease that spread with population densities we can get quadratic dependencies ($\mu = 2$). A mortality rate of zero is sometimes used for prey species as they seldom die of natural causes but instead feed the predator though this neglects respiration to some degree. The case $0 < \mu < 1$ is seldom considered but could describe situations in which respiration decreases for larger groups as e.g. maintaining body heat at night becomes easier in a huddle or other tasks like keeping guard for predators can be achieved in a more efficient manner. The sensitivity of the predation gain to the prey population is called γ. If the population of predators can consume a constant proportion of an increasing prey population we have a linear relationship. This is the case if the digestive ability of the individual predator is not fully taxed and the prey can be caught proportional to its abundance which means low prey densities. For comparatively large prey populations the predator is simply not capable of eating more and thus the sensitivity to an increase becomes zero. Values of $\gamma > 1$ are assuming that the increasing prey population increases the predation success disproportionally which can be the case if e.g. hiding places are limited or hunters become more adept due to practice. Finally, the parameter ψ is the elasticity of the gain by predation in relation to the predator population itself. An increase in predator density can lead to competition between individuals which decreases the total amount of prey consumed. If predators are not interfering with each other it is reasonable to assume a linear increase in the consumption of prey with the number of predators. Therefore parameter values are somewhere between zero and one, depending on the amount of intra-specific competition. Higher values than one could be considered if there is a certain number of predators necessary to implement advantageous hunting strategies or if the increased competition would lead to feeding frenzies beyond usual food consumption.

Table 1: The five exponent parameters, their meaning, and the range of their values in our computations.

Parameter	Interpretation	Range	Examples
ϕ	Elasticity of the gain function	$[0,1]$	0: growth independent of population size, e.g. due to nutrient limitation, 1: growth prop. to population density
μ^X	Sensitivity of prey mortality to prey population	$[1,2]$	1: constant mortality 2: mortality proportional to density, e.g. due to diseases
μ^Y	Sensitivity of predator mortality to predator population	$[1,2]$	Same as for prey
γ	Sensitivity of predation gain to prey population	$[0,2]$	Holling type functions: value close to 1 for small prey population, low value for large pop. due to saturation
ψ	Sensitivity of predation gain to predator population	$[0,1]$	1: No predator competition, lower values are due to predator interference

We can now compute the eigenvalues of the Jacobian to determine the stability of the steady state. For a simple 2×2 Jacobian matrix as needed for the predator-prey system

$$\mathbf{J} = \begin{pmatrix} J_{1,1} & J_{1,2} \\ J_{2,1} & J_{2,2} \end{pmatrix}, \tag{66}$$

we find that we can write the eigenvalue in terms of the trace and the determinant

$$\begin{aligned} \Delta(J - \lambda I) &= (J_{1,1} - \lambda) \cdot (J_{2,2} - \lambda) - J_{2,1} \cdot J_{1,2} && (67) \\ &= \Delta(\mathbf{J}) - \lambda \cdot \mathrm{Tr}(\mathbf{J}) + \lambda^2 = 0 && (68) \\ \lambda_{1,2} &= \frac{\mathrm{Tr}(\mathbf{J})}{2} \pm \sqrt{\left(\frac{\mathrm{Tr}(\mathbf{J})}{2}\right)^2 - \Delta(\mathbf{J})} && (69) \end{aligned}$$

with Δ as the determinant and Tr as the trace:

$$\begin{aligned} \Delta(\mathbf{J}) &= (\phi - \tilde{\delta}\mu^X - \delta\gamma)(\psi - \mu^Y) + \delta\psi\gamma\,, && (70) \\ \mathrm{Tr}(\mathbf{J}) &= \phi - \tilde{\delta}\mu^X - \delta\gamma + \psi - \mu^Y\,. && (71) \end{aligned}$$

For a stable steady state we need eigenvalues below zero. For a saddle-node bifurcation we need to have one eigenvalue that is exactly zero. For a Hopf bifurcation we need a pair of complex conjugated eigenvalues with real part zero. The necessary conditions can be found in Tab. 2.

Table 2: The necessary conditions for stable and unstable steady states as well as saddle-node and Hopf bifurcations.

Steady State	Eigenvalues	Conditions
Stable	All $\mathrm{Re}(\lambda) < 0$	$\mathrm{Tr}(\mathbf{J}) < 0$ and $\Delta(\mathbf{J}) > 0$
Unstable	$\mathrm{Re}(\lambda_1) > 0 \vee \mathrm{Re}(\lambda_2) > 0$	$\mathrm{Tr}(\mathbf{J}) > 0$ or $\Delta(\mathbf{J}) < 0$
Saddle-Node bifurcation	$\mathrm{Re}(\lambda_1) = 0 \vee \mathrm{Re}(\lambda_2) = 0$	$\mathrm{Tr}(\mathbf{J}) < 0$ and $\Delta(\mathbf{J}) = 0$
Hopf bifurcation	$\lambda = \pm i \cdot c;\ c \in \mathbb{R}$	$\mathrm{Tr}(\mathbf{J}) = 0$ and $\Delta(\mathbf{J}) > 0$

Using linear stability analysis we can now analyse any potential steady state using no absolute population sizes, abundances or densities and bypassing any population dynamics. We simply need the functional dependencies of a population model to compute the stability of any steady state.

This is the smallest food web with predator-prey interaction. In the next section we add a spatial element by introducing a second patch.

2.9.3 Two Patches Predator-Prey Systems

We consider a system consisting of two habitat patches, where each patch i can potentially sustain a prey population X_i and a predator population Y_i. The population dynamics are described by

$$\begin{aligned}
\dot{X}_1 &= G_1(X_1) - K_1(X_1) - F_1(X_1,Y_1) \\
&\quad + \eta^X_{1,2} E^X_{1,2}(X_2,Y_2,X_1,Y_1) - E^X_{2,1}(X_1,Y_1,X_2,Y_2) \\
\dot{Y}_2 &= \lambda F_1(X_1,Y_1) - D_1(Y_1) \\
&\quad + \eta^Y_{1,2} E^Y_{1,2}(X_2,Y_2,X_1,Y_1) - E^Y_{2,1}(X_1,Y_1,X_2,Y_2) \\
\dot{X}_2 &= G_2(X_2) - M_2(X_2) - F_2(X_2,Y_2) \\
&\quad + \eta^X_{2,1} E^X_{2,1}(X_1,Y_1,X_2,Y_2) - E^X_{1,2}(X_2,Y_2,X_1,Y_1) \\
\dot{Y}_2 &= \lambda F_2(X_2,Y_2) - D_2(Y_2) \\
&\quad + \eta^Y_{2,1} E^Y_{2,1}(X_1,Y_1,X_2,Y_2) - E^Y_{1,2}(X_2,Y_2,X_1,Y_1),
\end{aligned} \tag{72}$$

where the dot over a variable indicates the temporal derivative. The variables are in arbitrary units. For the purpose of this thesis we will assume that they describe the system in terms of carbon biomass density. However, the same equations also apply to other measures of population, such as abundance. The prey population density changes due to a growth rate $G(X_i)$, a combined respiration and mortality rate $K(X_i)$, and a rate of biomass loss by predation $F(X_i,Y_i)$. Predator populations have a growth term $\lambda F(X_i,Y_i)$, with the prefactor λ describing the efficiency of the energy conversion. The respiration/mortality rate of the predator is given by $D(Y_i)$. The rate of emigration from patch j to patch i is $E^U_{i,j}(\mathbf{X},\mathbf{Y})$ for both species $U = X, Y$ and the migration loss factor is $\eta^U_{i,j}$. In the most general case, emigration rates depend on all four populations. The case where the emigration rate of population U_i is proportional to E_i and independent of other variables corresponds to diffusive migration, otherwise we get different versions of adaptive migration. Models of the form of Eqs. (72) can have multiple feasible steady states, depending on the choice of functional forms and parameter values.

We consider an arbitrary feasible, but not necessarily stable state. The normalized biomasses are

$$x_i = \frac{X_i}{X^*}, \quad y_i = \frac{Y_i}{Y^*}, \tag{73}$$

and the normalized functions are

$$h(\mathbf{x},\mathbf{y}) = \frac{H(\mathbf{X},\mathbf{Y})}{H(\mathbf{X}^*,\mathbf{Y}^*)} \equiv \frac{H(\mathbf{X},\mathbf{Y})}{H^*} \tag{74}$$

with $H = \{E, F, G, K\}$ and $\mathbf{X} = \{X_1, X_2\}$. The asterisk (*) is used to denote the values of variables and functions in the steady state under consideration.

In terms of these normalized quantities, Eqs. (72) take the form

$$\begin{aligned}
\dot{x}_1 &= \frac{G^*_1}{X^*_1} g(x_1) - \frac{K^*_1}{X^*_1} k(x_1) - \frac{F^*_1}{X^*_1} f_1(x_1,y_1) + \frac{E^{X*}_{1,2}\eta^X_{1,2}}{X^*_1} e^X_{1,2}(\mathbf{x},\mathbf{y}) - \frac{E^{X*}_{2,1}}{X^*_1} e^X_{2,1}(\mathbf{x},\mathbf{y}), \\
\dot{y}_1 &= \frac{\lambda F^*_1}{Y^*_1} f_1(x_1,y_1) - \frac{D^*}{Y^*_1} d_1(y_1) + \frac{E^{Y*}_{1,2}\eta^Y_{1,2}}{Y^*_1} e^Y_{1,2}(\mathbf{x},\mathbf{y}) - \frac{E^{Y*}_{2,1}}{Y^*_1} e^Y_{2,1}(\mathbf{x},\mathbf{y}), \\
\dot{x}_2 &= \frac{G^*_2}{X^*_2} g_2(x_2) - \frac{K^*_2}{X^*_2} k_2(x_2) - \frac{F^*_2}{X^*_2} f_2(x_2,y_2) + \frac{E^{X*}_{2,1}\eta^X_{2,1}}{X^*_2} e^X_{2,1}(\mathbf{x},\mathbf{y}) - \frac{E^{X*}_{1,2}}{X^*_2} e^X_{1,2}(\mathbf{x},\mathbf{y}), \\
\dot{y}_2 &= \frac{\lambda F^*_2}{Y^*_2} f_2(x_2,y_2) - \frac{D^*_2}{Y^*_2} d_2(y_2) + \frac{E^{Y*}_{2,1}\eta^Y_{2,1}}{Y^*_2} e^Y_{2,1}(\mathbf{x},\mathbf{y}) - \frac{E^{Y*}_{1,2}}{Y^*_2} e^Y_{1,2}(\mathbf{x},\mathbf{y}).
\end{aligned} \tag{75}$$

The total biomass turnover rate of the each species is

$$\alpha_i^X = \frac{G_i^*}{X_i^*} + \frac{E_{i,j}^{X_i*}\eta_{i,j}^X}{X_i^*} = \frac{K_i^*}{X_i^*} + \frac{F_i^*}{X_i^*} + \frac{E_{j,i}^{X_i*}}{X_i^*}, \tag{76}$$

$$\alpha_i^Y = \frac{\lambda F_i^*}{Y_i^*} + \frac{E_{i,j}^{Y*}\eta_{i,j}^Y}{Y_i^*} = \frac{D_i^*}{Y_i^*} + \frac{E_{j,i}^{Y*}}{Y_i^*}. \tag{77}$$

We have already established that the parameter α^U describes the inverse average lifespan for species U in a non-spatial system. If we add migration this definition must be adapted to average lifespan *within a patch*. A value of 0.25/year would indicate that an individual spends on average 4 years in the patch before either dying or emigrating.

We scale the turnover rates to the prey turnover. The turnover rate of the prey is set to 1 in arbitrary time units and the turnover rate of the predator is

$$\alpha_i = \frac{\alpha_i^Y}{\alpha_i^X}. \tag{78}$$

Furthermore, we define the scale parameters δ, ν and ρ and their complements

$$\delta_i = \frac{1}{\alpha_i^X \rho_i^X}\frac{F_i^*}{X_i^*}, \qquad \tilde{\delta}_i = (1-\delta_i) = \frac{1}{\alpha_i^X \rho_i^X}\frac{K_i^*}{X_i^*}, \tag{79}$$

$$\nu_i^U = \frac{1}{\alpha_i^U}\frac{E_{j,i}^{U*}\eta_{j,i}^U}{U_i^*}, \qquad \tilde{\nu}_i^U = (1-\nu_i^U) = \frac{1}{\alpha_i^U}\frac{\{G_i^*;\lambda F_i^*\}}{U_i^*}, \tag{80}$$

$$\rho_i^U = \frac{1}{\alpha_i^U}\frac{E_{i,j}^{U*}}{U_i^*}, \qquad \tilde{\rho}^U = (1-\rho_i^U) = \frac{1}{\alpha_i^U}\frac{\{K_i^*+F_i^*;D_i^*\}}{U_i^*}. \tag{81}$$

All of these parameters describe the branching of the biomass flow which is now considerably more complex than for an isolated patch. The parameter δ denotes the proportion of energy intake of the prey that is eventually lost again due to respiration or mortality, whereas the complement $\tilde{\delta}$ is the proportion of the energy intake that is eventually lost due to predation. The parameters ν and $\tilde{\nu}$ denote the relative contributions of migration and feeding to the total gain, respectively. The parameters ρ and $\tilde{\rho}$ are the counterpart to ν and $\tilde{\nu}$ and denote the relative loss by emigration and by the within-patch processes (respiration/mortality and predation).

Using the definitions above we can write Eqs. (75) as

$$\begin{aligned}
\dot{x}_1 &= \alpha_1^X[\tilde{\nu}_1^X g_1(x_1) - \tilde{\rho}_1^X\tilde{\delta}k_1(x_1) - \tilde{\rho}_1^X\delta f_1(x_1,y_1) + \nu_1^X e_{2,1}^X(\mathbf{x},\mathbf{y}) - \rho_1^X e_{1,2}^X(\mathbf{x},\mathbf{y})] \\
\dot{y}_1 &= \alpha_1^Y[\tilde{\nu}_1^Y f_1(x_1,y_1) - \tilde{\rho}_1^Y d_1(y_1) + \nu_1^Y e_{2,1}^Y(\mathbf{x},\mathbf{y}) - \rho_1^Y e_{1,2}^Y(\mathbf{x},\mathbf{y})] \\
\dot{x}_2 &= \alpha_2^X[\tilde{\nu}_2^X g_2(x_2) - \tilde{\rho}_2^X\tilde{\delta}_2 k_2(x_2) - \tilde{\rho}_2^X\delta_2 f_2(x_2,y_2) + \nu_2^X e_{1,2}^X(\mathbf{x},\mathbf{y}) - \rho_2^X e_{2,1}^X(\mathbf{x},\mathbf{y})] \\
\dot{y}_2 &= \alpha_2^Y[\tilde{\nu}_2^Y f_2(x_2,y_2) - \tilde{\rho}_2^Y d_2(y_2) + \nu_2^Y e_{1,2}^Y(\mathbf{x},\mathbf{y}) - \rho^Y e_{2,1}^Y(\mathbf{x},\mathbf{y})].
\end{aligned} \tag{82}$$

For the linear stability analysis of the system it is expressed in terms of the Jacobian matrix. For a system of four dynamical variables this is a 4×4 matrix defined by

$$J_{i,j} = \left.\frac{\partial \dot{V}_i}{\partial V_j}\right|_*, \tag{83}$$

where $V = (x_1, y_1, x_2, y_2)$ is the set of state variables and $|_*$ indicating that the derivatives are evaluated in the steady state (1,1,1,1).

For the case of a system with two heterogeneous patches the Jacobian matrix can be written as the block matrix

$$\mathbf{J} = \begin{pmatrix} P_1 & M_{1,2} \\ M_{2,1} & P_2 \end{pmatrix}, \tag{84}$$

with

$$\mathbf{P}_i = \begin{pmatrix} 1 & 0 \\ 0 & \alpha_i \end{pmatrix} \cdot \begin{pmatrix} \tilde{\nu}_i^X \phi_i - \tilde{\rho}_i^X \tilde{\delta}_i \mu_i^X - \tilde{\rho}_i^X \delta_i \gamma_i + \nu_i^X \hat{\omega}_{i,j}^X - \rho_i^X \omega_{j,i}^X & -\tilde{\rho}_i^X \delta_i \psi_i + \nu_i^X \hat{\kappa}_{i,j}^X - \rho_i^X \kappa_{j,i}^X \\ \tilde{\nu}_i^Y \gamma_i + \nu_i^Y \hat{\kappa}_{i,j}^Y - \rho_i^Y \kappa_{j,i}^Y & \tilde{\nu}_i^Y \psi_i - \tilde{\rho}_i^Y \mu_i^Y + \nu_i^Y \hat{\omega}_{i,j}^Y - \rho_i^Y \omega_{j,i}^Y \end{pmatrix} \tag{85}$$

and

$$\mathbf{M}_{i,j} = \begin{pmatrix} 1 & 0 \\ 0 & \alpha_i \end{pmatrix} \cdot \begin{pmatrix} \nu_i^X \omega_{i,j}^X - \rho_i^X \hat{\omega}_{j,i}^X & \nu_i^X \kappa_{i,j}^X - \rho_i^X \hat{\kappa}_{j,i}^X \\ \nu_i^Y \kappa_{i,j}^Y - \rho_i^Y \hat{\kappa}_{j,i}^Y & \nu_i^Y \omega_{i,j}^Y - \rho_i^Y \hat{\omega}_{j,i}^Y \end{pmatrix}. \tag{86}$$

We note that the matrix $\mathbf{P}_i$ captures the effects of in-patch dynamics of patch i whereas the matrix $\mathbf{M}_{i,j}$ captures between-patch dynamics for migration from patch j to patch i. The definitions of the exponent parameters are

$$\begin{aligned}
\phi_i &:= \left.\frac{\partial g_i(x_i)}{\partial x_i}\right|_*, & \mu_i^X &:= \left.\frac{\partial k(x_i)}{\partial x_i}\right|_*, & \mu_i^Y &:= \left.\frac{\partial d(y_i)}{\partial y_i}\right|_*, \\
\gamma_i &:= \left.\frac{\partial f(x_i, y_i)}{\partial x_i}\right|_*, & \psi_i &:= \left.\frac{\partial f(x_i, y_i)}{\partial y}\right|_*, \\
\hat{\omega}_{i,j}^X &:= \left.\frac{\partial e_{i,j}^X(\mathbf{x},\mathbf{y})}{\partial x_i}\right|_*, & \omega_{i,j}^X &:= \left.\frac{\partial e_{i,j}^X(\mathbf{x},\mathbf{y})}{\partial x_j}\right|_*, \\
\hat{\kappa}_{i,j}^X &:= \left.\frac{\partial e_{i,j}^X(\mathbf{x},\mathbf{y})}{\partial y_i}\right|_*, & \kappa_{i,j}^X &:= \left.\frac{\partial e_{i,j}^X(\mathbf{x},\mathbf{y})}{\partial y_j}\right|_*, \\
\hat{\omega}_{i,j}^Y &:= \left.\frac{\partial e_{i,j}^Y(\mathbf{x},\mathbf{y})}{\partial y_i}\right|_*, & \omega_{i,j}^Y &:= \left.\frac{\partial e_{i,j}^Y(\mathbf{x},\mathbf{y})}{\partial y_j}\right|_*, \\
\hat{\kappa}_{i,j}^Y &:= \left.\frac{\partial e_{i,j}^Y(\mathbf{x},\mathbf{y})}{\partial x_i}\right|_*, & \kappa_{i,j}^Y &:= \left.\frac{\partial e_{i,j}^Y(\mathbf{x},\mathbf{y})}{\partial x_j}\right|_*.
\end{aligned} \tag{87}$$

The parameters $\omega_{i,j}$ and $\kappa_{i,j}$ are the migration exponent parameters, where $\omega_{i,j}$ describes the dependence of the emigration on the density of species of the emigrating individuals, whereas $\kappa_{i,j}$ describes the dependence of emigration on the density of the other species in the patch, respectively. The parameters with a hat ($\hat{\omega}_{i,j}, \hat{\kappa}_{i,j}$) are defined analogously but describe the dependence on the densities in

the destination patch. Different types of adaptive migration imply different parameter ranges for these exponent parameters. Simple diffusive migration for species U means $\omega^U_{i,j} = 1$ and when the emigration rate increases with population size we get an exponent $\omega^U_{i,j} > 1$. In predator evasion, prey emigration is increased with predator density, which means a value $\kappa^X_{i,j} > 0$. In predator pursuit, predator emigration is decreased with prey density, which means $\kappa^Y_{i,j} < 0$.

The remaining five parameters (first five in Eq. (87)) describe the elasticity of the local (within-patch) processes. They are discussed in detail in the previous section and short definitions, parameter ranges and examples are given in Tab. 1.

2.9.4 Homogeneous Two Patches Predator-Prey Model

As a special case of the previously discussed two patches predator-prey model we discuss the case of two homogeneous patches. This means in the context of the generalized model that we assume identical exponent and scale parameter for both patches.

For the case of a system with two identical patches the 4×4 matrix can be written as a block matrix

$$\mathbf{J} = \begin{pmatrix} \mathbf{P} & \mathbf{M} \\ \mathbf{M} & \mathbf{P} \end{pmatrix} \tag{88}$$

with

$$\mathbf{P} = \begin{pmatrix} 1 & 0 \\ 0 & \alpha \end{pmatrix} \begin{pmatrix} \tilde{\nu}^X \phi - \tilde{\rho}^X \tilde{\delta} \mu^X - \tilde{\rho}^X \delta \gamma + \nu^X \hat{\omega}^X - \rho^X \omega^X & -\tilde{\rho}^X \delta \psi + \nu^X \hat{\kappa}^X - \rho^X \kappa^X \\ \tilde{\nu}^Y \gamma + \nu^Y \hat{\kappa}^Y - \rho^Y \kappa^Y & \tilde{\nu}^Y \psi - \tilde{\rho}^Y \mu^Y + \nu^Y \hat{\omega}^Y - \rho^Y \omega^Y \end{pmatrix} \tag{89}$$

and

$$\mathbf{M} = \begin{pmatrix} 1 & 0 \\ 0 & \alpha \end{pmatrix} \begin{pmatrix} \nu^X \omega^X - \rho^X \hat{\omega}^X & \nu^X \kappa^X - \rho^X \hat{\kappa}^X \\ \nu^Y \kappa^Y - \rho^Y \hat{\kappa}^Y & \nu^Y \omega^Y - \rho^Y \hat{\omega}^Y \end{pmatrix}. \tag{90}$$

Due to the symmetric block structure of the Jacobian, the eigenvalue equation can be solved with the ansatz (MacArthur et al., 2008)

$$\begin{pmatrix} P_1 & P_2 & M_1 & M_2 \\ P_3 & P_4 & M_3 & M_3 \\ M_1 & M_2 & P_1 & P_2 \\ M_3 & M_4 & P_3 & P_4 \end{pmatrix} \begin{pmatrix} \xi_1 \\ \xi_2 \\ \pm\xi_1 \\ \pm\xi_2 \end{pmatrix} = \lambda \begin{pmatrix} \xi_1 \\ \xi_2 \\ \pm\xi_1 \\ \pm\xi_2 \end{pmatrix},$$

with P_i and M_i denoting the matrix elements of P and M. This is equivalent to solving the 2×2 problem

$$\mathbf{J}_\pm = \begin{pmatrix} P_1 \pm M_1 & P_2 \pm M_2 \\ P_3 \pm M_3 & P_4 \pm M_4 \end{pmatrix} \begin{pmatrix} \xi_1^\pm \\ \xi_2^\pm \end{pmatrix} = \lambda \begin{pmatrix} \xi_1^\pm \\ \xi_2^\pm \end{pmatrix}.$$

Every solution of the eigenvalue equation describes an eigenmode of the system, i.e., a specific perturbation that retains its shape while it grows or declines in time. For the plus sign, the eigenvector components relating to the two patches are identical, for the minus sign, they point in opposite directions.

The steady state is stable if the real parts of all eigenvalues are negative. The eigenvalues for a 2×2 matrix J' can be written in the same terms as already seen in Eq. (69):

$$\lambda_{1,2} = \frac{1}{2}\mathrm{Tr}(J') \pm \sqrt{\frac{1}{4}\mathrm{Tr}(J')^2 - \Delta(J')}\,.$$

In order to obtain a stable steady state, the real part of both eigenvalues must be negative, which is the case when the trace is negative and the determinant is positive. These criteria must be satisfied for both matrices $P \pm M$ (below denoted by the index "+" for "$P + M$" and "−" for "$P - M$").
As parameters are changed, a stable steady state can become unstable when the parameter change causes an eigenvalue to cross the imaginary axis and acquire a positive real part. For our system, there are four different types of such local bifurcations.

Let us first consider the "$J_+ = P + M$" case. Instabilities that are detected by the analysis of this matrix affect both patches equally and in synchrony. First, stability of the steady state can be lost in a saddle-node bifurcation, which occurs when $\Delta(J_+) = 0$ and $\mathrm{Tr}(J_+) < 0$ while both eigenvalues of J_- have a negative real part. In this bifurcation a sudden change in the population densities occurs, which most likely results in the collapse of one or both populations in both patches simultaneously. The second fundamental bifurcation in which stability can be lost is the Hopf bifurcation. This bifurcation occurs when $\mathrm{Tr}(J_+) = 0$ and $\Delta(J_+) > 0$ while the eigenvalues of J_- have a negative real part. The Hopf bifurcations detected in the $L + M$ matrix gives rise to synchronous oscillations. From the study on non-spatial predator-prey systems it is well known that oscillation amplitudes can grow rapidly after the bifurcation, leading to subsequent extinctions (Rosenzweig and MacArthur, 1963).

Let us now consider the $J_- = P - M$ matrix. Bifurcations detected in this matrix affect the two patches in such a way that they develop in opposite directions. Again, stability can be lost either in a saddle-node or in a Hopf bifurcation. However, now the saddle-node bifurcation leads to a shift where each population increases in one patch and decreases in the other. This occurs when $\Delta(J_-) = 0$ and $\mathrm{Tr}(J_-) < 0$ and both eigenvalues of J_+ have a negative real part. A Hopf bifurcation detected in the $L - M$ matrix leads to anti-synchronous oscillations. While this can lead to large-amplitude oscillations in both individual patches, the overall biomass in the system will stay nearly constant as the loss in one patch is compensated by gains in the other. This type of bifurcation occurs at $\mathrm{Tr}(J_-) = 0$ and $\Delta(J_-) > 0$ with both eigenvalues of J_+ having a negative real part.

Both bifurcations occurring in the $P - M$ matrix can be considered as *pattern-forming* bifurcations that create spatial heterogeneity. In fact, the saddle-node bifurcation in the $P - M$ matrix is closely reminiscent of the Turing bifurcation in systems of partial differential equations, which gives rise to stationary patterns. The Hopf bifurcation in the $P - M$ matrix is reminiscent of the wave instability bifurcation in partial differential equations, which leads to travelling waves.

In the following we will use the terms Hopf and saddle-node bifurcation only for the corresponding bifurcations from the $P+M$ matrix in the homogeneous two patches model. For simplicity we will denote the respective bifurcations in the $P - M$ system as Turing and wave instability. We emphasize that this is a rather liberal usage of the bifurcation names that we adopt here as it leads to the right ecological intuition although it is not strictly mathematically justified[1].

The question of the type of bifurcation becomes more complicated if we consider heterogeneous patches or a spatial network. We will discuss the details in the relevant sections.

[1] Strictly, a bifurcation is of a given type only if it can be reduced to the type's normal form. For instance the saddle-node bifurcation observed in the $P - M$ system can be reduced to the saddle-node normal form but not to the Turing normal form. So strictly it is a saddle-node and not a Turing bifurcation. Still one can justify denoting this bifurcation as "Turing" as follows: The bifurcation would not change fundamentally when we considered a system with more than two patches. The bifurcation would then be governed by a matrix that is closely reminiscent of the network Laplacian, which in turn can be seen as a discretization of the real space laplacian on a complex network. In this sense even the 2-patch system can be interpreted as a discretization of an underlying continuous space in which the bifurcation would be a true Turing bifurcation

2.9.5 Homogeneous Many Patches Many Species Models

For a unlimited number of connected species and patches we have to expand the notation of the generalized model. We define a species i in habitat k by its biomass density on that particular patch X_i^k. The different functions like e.g. the primary growth rate G_i^k get assigned patch and species indices as well. The set of ODEs describing such a system is given by

$$\begin{aligned}\dot{X}_i^k &= G_i^k(X_i^k) - M_i^k(X_i^k) \\ &\quad + \epsilon_i F_i^k(X_1^k,\ldots,X_S^k) - \sum_j D_{ji}^k(X_1^k,\ldots,X_S^k) \\ &\quad + \sum_l \Big[E_i^{kl}(X_1^k,\ldots,X_S^k,X_1^l,\ldots,X_S^l) \\ &\qquad - E_i^{lk}(X_1^l,\ldots,X_S^l,X_1^k,\ldots,X_S^k) \Big] ,\end{aligned} \tag{91}$$

where G_i^k is the growth by primary production, M_i^k is the loss by respiration and mortality, F_i^k is the growth due to predation, D_{ji}^k is the loss of biomass due to predation by species j, E_i^{kl} is the migration from habitat l to k. Furthermore we used ϵ_i to denote the conversion efficiency of prey biomass.

We now have potentially multiple prey species per predator and vice versa. To accommodate for this, we proceed analogous to (Gross and Feudel, 2006) and introduce an new auxiliary variable T_j^k which represents all the prey biomass available to predator j in patch k if all prey species of predator j are summed. This allows us to rewrite both the gain by predation F_j^k and the loss due to predation D_{ji}^k in terms of individual importance of different predator and prey species. We write

$$T_j^k(X_1^k,\ldots,X_S^k) = \sum_i R_{ji}^k(X_i^k) , \tag{92}$$

where $R_{ji}^k(X_i^k)$ is the relative contribution of species i in patch k to the total amount of food available to the population of species j in that habitat.

We can now write the amount of prey consumed by population j as

$$F_j^k(X_1^k,\ldots,X_N^k) = F_j^k(T_j^k,X_j^k) , \tag{93}$$

and the loss of species i due to predation by species j in habitat k as

$$D_{ji}^k(X_1^k,\ldots,X_S^k) = \frac{R_{ji}^k(X_i^k)}{T_j^k(X_1^k,\ldots,X_S^k)} F_j^k(T_j^k,X_j^k) . \tag{94}$$

We now normalize Eq. (91) to the potential steady state. We then denote the (unknown) steady-state population densities by X_i^{k*}. Likewise we use the asterisk to denote functions evaluated in the steady state, e.g $F_i^{k*} = F_i^k(X_1^{k*},\ldots,X_S^{k*})$. We then normalize all dynamical variables and functions to their steady-state values. The results of this normalization are denoted by lowercase symbols For instance $x_i^k = \frac{X_i^k}{X_i^{k*}}$.

Using these definitions we obtain the normalized equations

$$\begin{aligned}\dot{x}_i^k = &\frac{G_i^{k*}}{X_i^{k*}} g_i^k(x_i^k) - \frac{M_i^{k*}}{X_i^{k*}} m_i^k(x_i^k) \\ &+ \frac{\epsilon_i F_i^{k*}}{X_i^{k*}} f_i^k(t_i^k, x_i^k) \\ &- \sum_j \frac{D_{ji}^{k*}}{X_i^{k*}} d_{ji}^k(x_1^k, \ldots, x_S^k) \\ &+ \sum_l \left[\frac{E_i^{kl*}}{X_i^{k*}} e_i^{kl}(x_1^k, \ldots, x_S^k, x_1^l, \ldots, x_S^l) \right. \\ &\left. - \frac{E_i^{lk*}}{X_i^{k*}} e_i^{lk}(x_1^l, \ldots, x_S^l, x_1^k, \ldots, x_S^k) \right]. \end{aligned} \tag{95}$$

We can now identify the biomass turnover rates α_i^k and scale parameters in the steady state under consideration. We start with the time scales

$$\begin{aligned}\alpha_i^k &= \frac{G_i^{k*}}{X_i^{k*}} + \frac{\epsilon_i F_i^{k*}}{X_i^{k*}} + \sum_l \frac{E_i^{kl*}}{X_i^{k*}} \\ &= \frac{M_i^{k*}}{X_i^{k*}} + \sum_j \frac{D_{ji}^{k*}}{X_i^{k*}} + \sum_l \frac{E_i^{lk*}}{X_i^{k*}} . \end{aligned} \tag{96}$$

These scale parameters quantify the rate of biomass flow in the steady state. The relative contributions to the biomass gain by the different processes are

$$\nu_i^k = \sum_l \nu_i^{kl} = \frac{1}{\alpha_i^k} \sum_l \frac{E_i^{kl*}}{X_i^*} , \tag{97}$$

$$\tilde{\nu}_i^k = 1 - \nu_i^k = \frac{1}{\alpha_i^k} \frac{\epsilon_i F_i^{k*}}{X_i^{k*}} + \frac{1}{\alpha_i^k} \frac{G_i^{k*}}{X_i^{k*}} , \tag{98}$$

$$\tilde{\nu}_i^k \delta_i^k = \frac{1}{\alpha_i^k} \frac{\epsilon_i F_i^{k*}}{X_i^{k*}} , \tag{99}$$

$$\tilde{\nu}_i^k \tilde{\delta}_i^k = \tilde{\nu}_i^k (1 - \delta_i^k) = \frac{1}{\alpha_i^k} \frac{G_i^{k*}}{X_i^{k*}} . \tag{100}$$

The relative contributions of the different processes to the biomass loss are given by

$$\rho_i^k = \sum_l \rho_i^{lk} = \frac{1}{\alpha_i^k} \sum_l \frac{E_i^{lk*}}{X_i^*} , \tag{101}$$

$$\tilde{\rho}_i^k = 1 - \rho_i^k = \frac{1}{\alpha_i^k} \frac{M_i^{k*}}{X_i^{k*}} + \frac{1}{\alpha_i^k} \sum_j \frac{D_{ji}^{k*}}{X_i^{k*}} , \tag{102}$$

$$\tilde{\rho}_i^k \sigma_i^k = \frac{1}{\alpha_i^k} \sum_j \frac{D_{ji}^{k*}}{X_i^{k*}} , \tag{103}$$

$$\tilde{\rho}_i^k \tilde{\sigma}_i^k = \tilde{\rho}_i^k (1 - \sigma_i^k) = \frac{1}{\alpha_i^k} \frac{M_i^{k*}}{X_i^{k*}} . \tag{104}$$

It is necessary to resolve the contribution of different species to the loss by additionally defining the parameters

$$\beta_{ji}^{k} = \frac{1}{\alpha_i^k \tilde{\rho}_i^k \sigma_i^k} \frac{D_{ji}^{k*}}{X_i^{k*}} \,. \tag{105}$$

Using Eq. (94) the normalized function for the loss due to predation can be written as

$$\begin{aligned} d_{ji}(x_1^k, \ldots, x_S^k) &= \frac{R_{ji}^{k*} F_j^{k*}}{T_j^{k*} D_{ji}^{k*}} \frac{r_{ji}^k}{t_j^k} f_j(t_j^k, x_j^k) \\ &= \frac{r_{ji}^k}{t_j^k} f_j(t_j^k, x_j^k) \,, \end{aligned} \tag{106}$$

where the normalized total available biomass for predation by species j is given by

$$t_j^k = \sum_i \frac{R_{ji}^{k*}}{T_j^{k*}} r_{ji}^k \,. \tag{107}$$

Using the parameters

$$\chi_{ji}^k = \frac{R_{ji}^{k*}}{T_j^{k*}}, \tag{108}$$

we can write

$$t_j^k = \sum_i \chi_{ji}^k r_{ji} \,. \tag{109}$$

In summary this yields the normalized meta-food web model

$$\begin{aligned} \dot{x}_i^k = \alpha_i^k \Big[& \quad \tilde{\nu}_i^k \tilde{\delta}_i^k g_i^k(x_i^k) \\ & + \tilde{\nu}_i^k \delta_i^k f_i^k(t_i^k, x_i^k) \\ & - \tilde{\rho}_i^k \tilde{\sigma}_i^k m_i^k(x_i^k) \\ & - \tilde{\rho}_i^k \sigma_i^k \sum_j \beta_{ji}^k d_{ji}^k(x_1^k, \ldots, x_S^k) \\ & + \sum_l \nu_i^{kl} e_i^{kl}(x_1^k, \ldots, x_S^k, x_1^l, \ldots, x_S^l) \\ & - \sum_l \rho_i^{lk} e_i^{lk}(x_1^l, \ldots, x_S^l, x_1^k, \ldots, x_S^k) \Big] , \end{aligned} \tag{110}$$

where $i = 1, \ldots, S$ and $k = 1, \ldots, N$.

We proceed with the definition of the *exponent parameters*. For the local processes we define

$$\phi_i^k = \frac{\partial}{\partial x_i^k} g_i^k(x_i^k)\Big|_{x=x^*}, \tag{111}$$

$$\mu_i^k = \frac{\partial}{\partial x_i^k} m_i^k(x_i^k)\Big|_{x=x^*}, \tag{112}$$

$$\lambda_{ji}^k = \frac{\partial}{\partial x_i^k} r_{ji}^k(x_i^k)\Big|_{x=x^*}, \tag{113}$$

$$\gamma_i^k = \frac{\partial}{\partial t_i^k} f_i^k(t_i^k, x_i^k)\Big|_{x=x^*}, \tag{114}$$

$$\psi_i^k = \frac{\partial}{\partial x_i^k} f_i^k(t_i^k, x_i^k)\Big|_{x=x^*}, \tag{115}$$

and for migration

$$\hat{\omega}_i^{kl} = \frac{\partial}{\partial x_i^k} e_i^{kl}(x_1^k, \ldots, x_S^k, x_1^l, \ldots, x_S^l)\Big|_{x=x^*}, \tag{116}$$

$$\omega_i^{kl} = \frac{\partial}{\partial x_i^l} e_i^{kl}(x_1^k, \ldots, x_S^k, x_1^l, \ldots, x_S^l)\Big|_{x=x^*}, \tag{117}$$

$$\hat{\kappa}_{ij}^{kl} = \frac{\partial}{\partial x_j^k} e_i^{kl}(x_1^k, \ldots, x_S^k, x_1^l, \ldots, x_S^l)\Big|_{x=x^*} \quad \text{with } i \neq j\,, \tag{118}$$

$$\kappa_{ij}^{kl} = \frac{\partial}{\partial x_j^l} e_i^{kl}(x_1^k, \ldots, x_S^k, x_1^l, \ldots, x_S^l)\Big|_{x=x^*} \quad \text{with } i \neq j\,. \tag{119}$$

We use two types of matrices to construct the Jacobian. The matrices $\mathbf{P}^k$ capture the local biology within a patch, whereas the matrices $\mathbf{C}^{kl}$ capture the dependencies of the dynamics for migration from patch l to k. From the GM above we find the diagonal elements of $\mathbf{P}^k$

$$\begin{aligned} P_{ii}^k = & \\ \alpha_i^k \Big[& \tilde{\nu}_i^k \tilde{\delta}_i^k \phi_i^k \\ & + \tilde{\nu}_i^k \delta_i^k \left(\gamma_i^k \chi_{ii}^k \lambda_{ii}^k + \psi_i^k\right) \\ & - \tilde{\rho}_i^k \tilde{\sigma}_i^k \mu_i^k \\ & - \tilde{\rho}_i^k \sigma_i^k \left(\beta_{ii}^k \psi_i^k + \sum_n \beta_{ni} \lambda_{ni} \left[\left(\gamma_n^k - 1\right) \chi_{ni}^k + 1\right]\right)\Big], \end{aligned} \tag{120}$$

and the non-diagonal elements

$$\begin{aligned} P_{ij}^k = & \\ \alpha_i^k \Big[& \tilde{\nu}_i^k \delta_i^k \gamma_i^k \chi_{ij}^k \lambda_{ij}^k \\ & - \tilde{\rho}_i^k \sigma_i^k \left(\beta_{ji}^k \psi_j^k + \sum_n \beta_{ni}^k \lambda_{nj}^k \left(\gamma_n^k - 1\right) \chi_{nj}\right)\Big]. \end{aligned} \tag{121}$$

The matrices $\mathbf{C}^{kl}$ have diagonal elements

$$C_{ii}^{kl} = \alpha_i^k \left[-\nu_i^{kl} \hat{\omega}_i^{kl} + \rho_i^{lk} \omega_i^{lk} \right] \tag{122}$$

and non-diagonal elements

$$C_{ij}^{kl} = \alpha_i^k \left[-\nu_i^{kl} \hat{\kappa}_{ij}^{kl} + \rho_i^{kl} \kappa_{ij}^{lk} \right] . \tag{123}$$

The Jacobian is then constructed as

$$\mathbf{J} = \begin{pmatrix} \ddots & & & & \\ & \mathbf{P}^k - \sum_m \mathbf{C}^{km} & \cdots & +\mathbf{C}^{kl} & \\ & \vdots & \ddots & \vdots & \\ & +\mathbf{C}^{lk} & \cdots & \mathbf{P}^l - \sum_m \mathbf{C}^{lm} & \\ & & & & \ddots \end{pmatrix} . \tag{124}$$

The unknown stable steady state under consideration is stable if all eigenvalues have negative real parts.

Although the functions and the steady states are unknown, the exponent and scale parameters that enter the Jacobian are directly interpretable in the context of the system and can therefore be measured directly in nature or can be chosen based on theoretical considerations (see (Gross and Feudel, 2006; Gross et al., 2009) for details and table 3 for the interpretation of the parameters).

Note that different steady states are characterized by different values of the scale and exponent parameters and thus can have different stability properties.

In the context of section 6 we consider the stability of homogeneous steady states, i.e. states in which all patches are characterized by the same parameters and have the same biomass density. We then speak of diffusion-driven instabilities (DDI) if such a state is stable without diffusion, but loses stability under non-zero diffusive coupling. In such a case it has benefits to identify the biomass turnover of dispersal and local dynamics separately.

Parameter	Interpretation	Parameter	Interpretation
Elasticities		Turnover & Scale	
ϕ_i^k	Sensitivity of primary production of i in k to itself	${\alpha_P}_i^k$	Intra-habitat biomass flow of i in k
γ_i^k	Sensitivity of predation of i in k to prey density	${\alpha_C}_i^k$	Biomass flow by migration of i in k
λ_i^k	Exponent of prey switching of i in k	β_{ji}^k	Contribution of predation by i to local biomass loss of j
ψ_i^k	Sensitivity of predation of i to density of itself	σ_i^k	Fraction of local biomass loss of i in k due to predation
μ_i^k	Exponent of closure of i in k	$\tilde{\sigma}_i^k$	Fraction of local biomass loss of i in k due to respiration
ω_i^{kl}	Sensitivity of migration of i from l to k to itself	δ_i^k	Fraction of local growth by predation of i in k
$\tilde{\omega}_i^{kl}$	Sensitivity of migration of i from l to k to itself	$\tilde{\delta}_i^k$	Fraction of local growth by primary production of i in k
κ_{ij}^{kl}	Sensitivity of migration of i from l to k to j	χ_i	Contribution of i to prey of j on k
$\tilde{\kappa}_{ij}^{kl}$	Sensitivity of migration of i from l to k to j		
		ν_i^k	Fraction of total biomass gain of i in k due to migration
		$\tilde{\nu}_i^k$	Fraction of total biomass gain of i in k due to predation
		ρ_i^k	Fraction of total biomass loss of i in k due to migration
		$\tilde{\rho}_i^k$	Fraction of total biomass loss of i in k due to predation

Table 3: Generalized parameters used to describe the meta-foodweb. The indices i and j denote different species and k and l different habitats.

2.9.6 Separation of Biomass Turnover Rates

In some settings it is not possible to give easy or sensible scale parameters and it might be more advisable to separate the biomass turnover rates α for different processes. In particular migration and local dynamics can be entangled in numerous ways which make such a separation of turnover rates helpful. We consider a case where we have a homogeneous equilibrium across a meta-community. This means that we have identical exponent parameters on each patch. In an equilibrium there is no change, so we have the same output and input for each patch as all biomass flows have to cancel each other out. We can therefore say

$$\tilde{\nu}_i^k \alpha_i^k = \tilde{\rho}_i^k \alpha_i^k \tag{125}$$

which means the local dynamics are in equilibrium and furthermore

$$\nu_i^k \alpha_i^k = \rho_i^k \alpha_i^k \,. \tag{126}$$

which means the dispersal influx is equal to the outflux.

Therefore we obtain

$$\tilde{\nu}_i^k = \tilde{\rho}_i^k \tag{127}$$

and

$$\nu_i^k = \rho_i^k \,. \tag{128}$$

We can now define the biomass flow within a patch excluding all dispersal as

$$\alpha_{P_i}{}^k = \tilde{\nu}_i^k \alpha_i^k = \tilde{\rho}_i^k \alpha_i^k \tag{129}$$

and the biomass flow due to migration as

$$\alpha_{C_i}{}^k = \nu_i^k \alpha_i^k = \rho_i^k \alpha_i^k \,. \tag{130}$$

Using these definitions we can rewrite the matrices $\mathbf{P}^k$ and $\mathbf{C}^{kl} = \hat{\mathbf{C}}^{kl}$. The matrix for local dynamics is given by

$$\begin{aligned} P_{ii}^k = & \\ \alpha_{P_i}{}^k \Big[& \quad \tilde{\delta}_i^k \phi_i^k \\ & + \delta_i^k \left(\gamma_i^k \chi_{ii}^k \lambda_{ii}^k + \psi_i^k \right) \\ & - \tilde{\sigma}_i^k \mu_i^k \\ & - \sigma_i^k \left(\beta_{ii}^k \psi_i^k + \sum_n \beta_{ni} \lambda_{ni} \left[\left(\gamma_n^k - 1 \right) \chi_{ni}^k + 1 \right] \right) \Big] \end{aligned} \tag{131}$$

and

$$P_{ij}^{k} = \alpha_{P_i}{}^{k}\Big[\quad \delta_i^k \gamma_i^k \chi_{ij}^k \lambda_{ij}^k - \sigma_i^k \left(\beta_{ji}^k \psi_j^k + \sum_n \beta_{ni}^k \lambda_{nj}^k \left(\gamma_n^k - 1\right) \chi_{nj}\right)\Big]. \tag{132}$$

The matrix for migration dynamics is given by

$$C_{ii}^{kl} = \alpha_{C_i}{}^{k}\left[-\hat{\omega}_i^{kl} + \omega_i^{lk}\right], \tag{133}$$

and

$$C_{ij}^{kl} = \alpha_{C_i}{}^{k}\left[-\hat{\kappa}_{ij}^{kl} + \kappa_{ij}^{lk}\right]. \tag{134}$$

2.10 Auxiliary Definitions

There are concepts that are used in the later sections that many readers might not be familiar with. The order parameter is a measure of synchrony that is used in section 6. It assesses how in synch the reactions of multiple species are in case of a perturbation. The sections 4 and 5 also consider how in-phase or out of phase dynamics are but since there are only a small number of patches and species other less complex and more intuitive terms can be used. The Pearson correlation coefficient gives - as the name implies - the degree of correlation between two parameters. We use it to a quantify the influence of a parameter on stability in section 4 and 5 though we are well aware that it only implies correlation and not causation.

2.10.1 Order Parameter

The eigenvectors of the Jacobian show us the relationships between the population amplitudes. We define an order parameter to quantify these relationships. We write

$$r \cdot e^{i\psi} = \frac{1}{N}\sum_{j=1}^{N} e^{i\theta_j} \tag{135}$$

and define r as the order parameter, N as number of species, ψ as average phase and θ_j as the phase of species j. We look at the eigenvector entries to get the values of θ_j. These are the arguments of the complex number entries of the eigenvector.

The order parameter gives us a measure of synchronisation between populations. A perfectly synchronized system would have $r = 1$, a completely desynchronized one $r = 0$.

The average phase of an eigenvector is arbitrary as any multiplication of an eigenvector's basis with $e^{i\theta}$ would create another eigenvector basis. The relationship between the elements though is distinct and thus the variance of the eigenvector elements. We concentrate on the relationship of the arguments Arg() of the elements as these tell us the phase between population reactions.

$$\mathrm{Var}(v_i) = \frac{1}{N}\sum_{j}^{N}(\mathrm{Arg}(v_i^j) - \overline{\mathrm{Arg}(v_i)})^2. \tag{136}$$

The information gathered by looking at the variance $\mathrm{Var}(v_i)$ might seem redundant if one already knows the order parameter. But there are multiple ways to achieve the same order parameter with different variances (see Fig. 17).

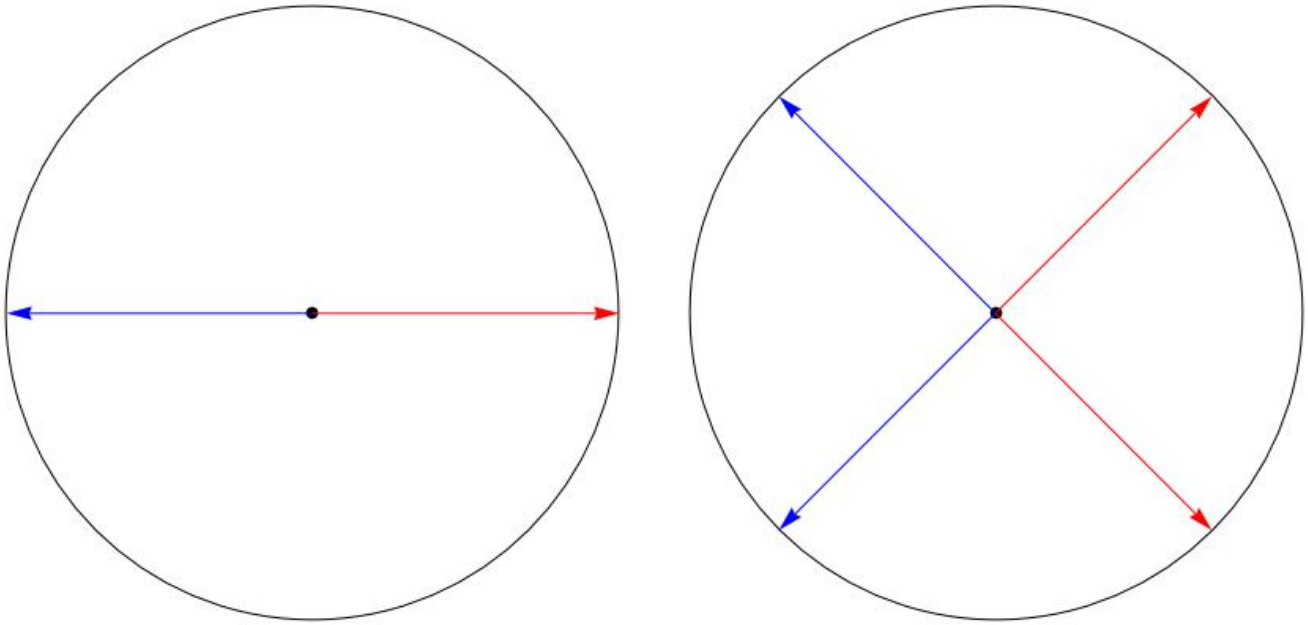

Figure 17: Example for two combinations of eigenvector entries with identical order parameters but different variances.

2.10.2 Pearson Correlation Coefficient

The Pearson correlation coefficient, created by Karl Pearson (Pearson, 1895) and Francis Galton (Stigler, 1989), is a measure of linear correlation between two variables. For a sample data set of two variables $x = [x_1, x_2, \ldots, x_n]$ and $y = [y_1, y_2, \ldots, y_n]$ we define the sample correlation coefficient r, in the following sections commonly referred to as the correlation value, as

$$r = \frac{\sum_{i=1}^{n}(x_i - \overline{x})(y_i - \overline{y})}{\sqrt{\sum_{i=1}^{n}(x_i - \overline{x})^2}\sqrt{\sum_{i=1}^{n}(y_i - \overline{y})^2}}. \tag{137}$$

In case of perfect positive linear correlation we have a value of $r = 1$, in case of perfect negative linear correlation we have $r = -1$. If there is no linear correlation we get $r = 0$. One must always keep in mind that the Pearson correlation coefficient is only intended to measure linear correlation. Nonlinear relationships are not properly captured and the correlation coefficient is thus best seen as a rough guideline.

The following sections progress through several levels of complexity for meta-communities and how to present them in a generalized form. We start with predator-prey interaction with no spatial component in section 3. We will use Sec. 3 as an introduction to the different properties and problems we encounter in the study of meta-communities.

In Sec. 4 we add another patch but with the restriction that the steady state is homogeneous on both patches. This allows for dispersal and some analytical insights but is limited in comparability to many previous publications on similar systems.

This is alleviated by another layer of complexity in the next section, Sec. 5. We include heterogeneous steady states and while there are still some inherent assumptions to the generalized method it is now formulated in a way that any classic formulation of the two patches two species problem is a special case.

In the final section 6 we go back to homogeneous steady states to expand the spatial network and the size of the food webs. We show how the stability of such a system can be expressed in the form of a master stability function. We try to establish a definition for stability that is meaningful without explicit topology. We also consider the impact of different niche web parameters on the local scale on the bifurcation distribution and the synchrony of the system at the bifurcation point.

We add a conclusion for each individual section and then summarize all findings across all sections at the very end.

3 Single Patch Predator-Prey System

The simplest possible food-web with inter-species interaction is a system with a single prey and a single predator species. Such systems have been well researched with a near infinite amount of additional factors (for example (Xiao and Chen, 2001) introduces a disease to the prey population and (Cushing and Saleem, 1982) differentiates age classes of the predator) but the basic premise of a predator feeding on a prey species remains the same. For an in-depth discussion of several (simple) variations we recommend (Hassell and May, 1974). We have introduced basic forms of species interaction in the theoretical sections: The Rosenzweig-MacArthur model, the different definitions of a functional response by Holling, the Lotka-Volterra model and the Beddington-DeAngelis model. We add to this the standard class which we introduce in the next subsection.

To demonstrate the practical application of the generalized method we take a look at this relatively uncomplicated case and how it can be expressed and analysed in generalized terms. We compare the stability across the parameter space for the different classes and compute the correlation of the individual parameters with stability.

3.1 Generalized Modelling Formulation

A detailed derivation of the generalized modelling formulation for localized predator-prey interaction is given in section 2.9.2 but we reiterate a couple of the key points and equations. We consider a system of one predator population X and one prey population Y. A general description of the dynamics can be given as

$$\begin{aligned} \dot{X}(t) &= G(X) - F(X,Y) - K(X), \\ \dot{Y}(t) &= \epsilon F(X,Y) - D(Y). \end{aligned} \tag{138}$$

Each of the functions G, F, K, Y stands for some process like feeding on prey or respiration. We normalize all functions and populations to their value at a potential steady state, denoted by lowercase

letters, and introduce a scale parameter δ and biomass turnover α to give the relative importance of each process and a gauge for the average lifetime of the species

$$\begin{aligned} \dot{x} &= \alpha^X[g(x)-\tilde{\delta}k(x)-\delta f(x,y)], \\ \dot{y} &= \alpha^Y[f(x,y)-d(y)]. \end{aligned} \tag{139}$$

We can now use linear stability analysis for the steady state used for normalization. For this we need the Jacobian of the system and we express the derivatives in the Jacobian as exponent parameters which are. The Jacobian can be written as

$$J = \begin{pmatrix} 1 & 0 \\ 0 & \alpha \end{pmatrix} \cdot \begin{pmatrix} \phi - \tilde{\delta}\mu^X - \delta\gamma & -\delta\psi \\ \gamma & \psi - \mu^Y \end{pmatrix}, \tag{140}$$

with the exponent parameters as greek letters. We can use this Jacobian to make statements about the stability and the dynamics at the steady state.

3.2 Classes

We consider several classes based upon commonly used models (see Tab. 4) which are defined by the intervals of the exponent and scale parameters.

Generalized modelling has the additional benefit that due to the normalization to the steady state the description with exponent and scale parameters fits to *any* underlying model that would produce such normalized parameters. This means that e.g. if a system with Holling type I and another system with Holling type III have the same exponent parameters for their respective steady states, they have the same Jacobian and thus properties at the steady state. This means that each class describes all models that fall within a particular interval range. It should be noted that the generalized parameters are not necessarily independent of another. The intervals represent the maximum range of any individual parameter and some parameter combinations are not possible with the underlying explicit dynamics; e.g. the value of the exponent parameter γ depends usually on the prey population which in turn might be related to the mortality of the prey μ_x. We do not take these potential relationships into account as this would weigh the results in favour of a particular interpretation or model. The parameters are considered independent if not otherwise noted.

The models upon which the different classes are based are the Lotka-Volterra model (we will abbreviate the associated class as *LV*), which we use primarily to demonstrate the limits of the generalized model, and the Rosenzweig-MacArthur model (*RM*), which is a combination of the Holling type II functional response and a logistic growth term. We also combine the Holling type I and III (*H.III*) functional responses with logistic growth. The former is Lotka-Volterra with self-limiting growth (*LG*). We add a class based upon the Beddington-DeAngelis functional response (*DeAngelis*). It was derived separately by Beddington (Beddington, 1975) and DeAngelis (DeAngelis et al., 1975) and adds predator interference to the Holling type II functional response. This means that a relatively large number of predators hinders itself from catching prey at maximum efficiency.

We also use a class not based upon any particular model. The class *Stand* (short for “Standard”) is supposed to exhaust the maximum range of any reasonable predator-prey interaction and thus has a large range for all parameters. These ranges represent the limits of most common models. While there are certainly publications about models which would require larger ranges, they are rare.

Table 4: The different classes used for the single patch predator-prey system and the models they are based upon. The parameters are not dependent on each other if not otherwise noted. For more details on the models see Sec. 2.2.

Model	Class	ϕ	δ	γ	ψ	μ^X	μ^Y	α
n.a.	Stand	$[0;1]$	$[0;1]$	$[0;2]$	$[0;1]$	$[1;2]$	$[1;2]$	$[10^{-3};10^{1}]$
Lotka-Volterra	LV	1	1	1	1	0	1	$[10^{-3};10^{1}]$
Rosenzweig-MacArthur	RM	1	$[0;1]$	$[0;1]$	1	2	1	$[10^{-3};10^{1}]$
Logistic Growth	LG	1	$[0;1]$	1	1	2	1	$[10^{-3};10^{1}]$
Holling Type III	H.III	1	$[0;1]$	$[0;2]$	1	2	1	$[10^{-3};10^{1}]$
Beddington-DeAngelis	DeAngelis	1	$[0;1]$	$[0;1]$	$[0;1]$	2	1	$[10^{-3};10^{1}]$

3.3 Proportion of Stable Webs

We computed 10^7 runs for each type of predator-prey dynamics (see Tab. 4) and took the percentage of stable webs (PSW) of the given ensemble as defined by the linear stability analysis of the Jacobian given in by Eq. (140). The parameter values were chosen uniformly from within the parameter intervals with the exception of α. The biomass turnover α was logarithmically distributed within the given range. This is concession to roughly log-normal distribution of actual body sizes in species (Blackburn and Gaston, 1994) to which biomass turnover is correlated. The percentage of stable webs gives us an idea on how stable a class is across the parameter space. The relationships between parameters depending on the explicit model and/or the starting conditions limit the accessible parameter space for models within a generalized class. We therefore cannot infer the stability of a specific model based upon the class for non-pathological cases.

We see that *RM* has the lowest average stability. Class *H.III* is stabler than *RM* but less than the *Stand* class and less than *LG*, which is always stable. The difference between the three types of functional response (Holling I in *LG*, Holling III in *H.III* and Holling II for *RM*) is a good example that simple extrapolation for a parameter does not work since the only parameter that changes is γ but the models cannot be sorted in stability by the size of γ. For the Lotka-Volterra class we cannot make a valid statement about stability. We do know that there are only neutrally stable limit cycles and a fixed point at extinction but this cannot be properly assessed with the generalized approach. The *DeAngelis* class is stabler than the *RM* class. This must be caused by the additional intra-species interference of the predator. The *Stand* class has the highest percentage of stable webs despite a wide range for each parameter. The probable reason for this is the introduction of parameter ranges that are limiting gain terms and facilitating loss terms. We have potentially higher mortality terms μ_X and μ_Y and lower increases by predation ψ and intrinsic growth ϕ. This is associated with higher stability of the steady state (see (Gross et al., 2009)).

Table 5: The percentages of stable webs (PSW) for the ensemble of runs for each class. LV has no value as it is always neutrally stable and linear stability analysis cannot give conclusive answers for this case.

Class	Stand	LV	RM	H.III	LG	DeAngelis
PSW	0.94	n.a.	0.69	0.85	1.00	0.74

3.4 Correlations

We took the Parson-Moment correlation (see Sec. 2.10.2) of each parameter with the stability of the system for all generalized parameters for 10^7 runs per class. For such simple systems one can usually determine analytically if a parameter is more stabilizing or destabilizing compared to another model. The analytical comparison can be cumbersome though – even for this simple case – and for more complex food webs become nearly impossible. The correlation value is a good measurement to capture the overall influence of a parameter if an in-detail analysis is not possible or required. The drawback is a lack of detail. A parameter could vary wildly in his influence on stability depending on its value but average out in its total correlation with stability. We see the correlation values for δ and γ in Fig. 18 as these vary for most systems. In all cases we see that γ is stabilizing and δ is destabilizing. We see that the stability differences between *RM*, *DeAngelis* and *H.III* can be explained by a progressively less destabilizing influence of δ. Other parameters that were varied are ψ for *DeAngelis* and every parameter for *Stand*. The correlations for *Stand* can be seen in Fig. 19. We see that δ and γ have the largest correlation values with only ϕ in comparable regions. The correlation value for ψ in the *DeAngelis* class is very low at roughly 0.01 yet still has measurable effect on the percentage of stable webs compared to the *RM* class. This might be counter-intuitive but a parameter does not need to be correlated with stability to change stability. In this instance the overall influence of ψ averages nearly out but the new mean has an inherently higher stability.

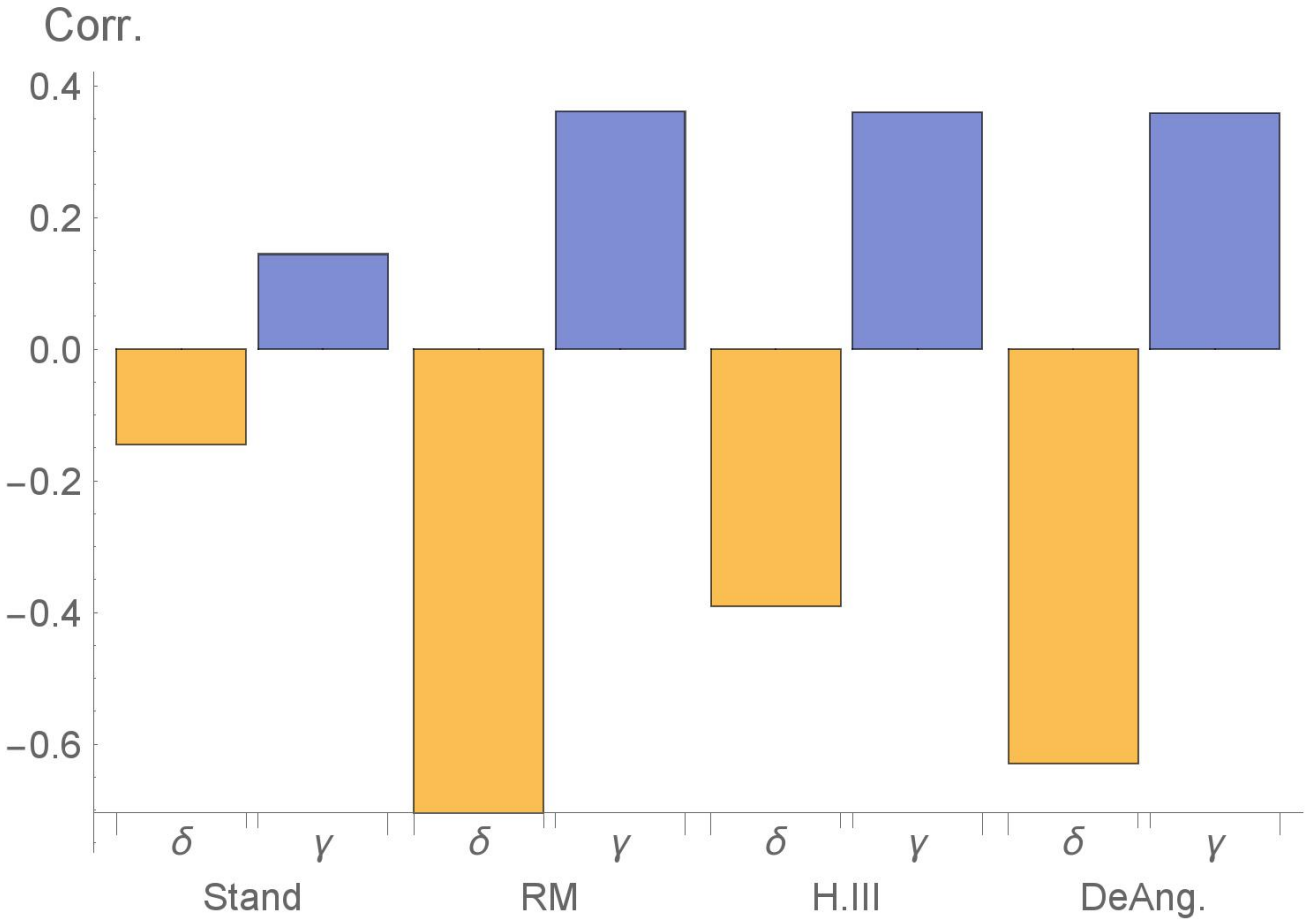

Figure 18: Correlations of parameters δ and γ for all classes that vary these parameters. On the x-axis we have the different classes and parameters and on the y-axis the correlation value. The parameter δ is always negatively correlated with stability and the parameter γ is always positively correlated with stability.

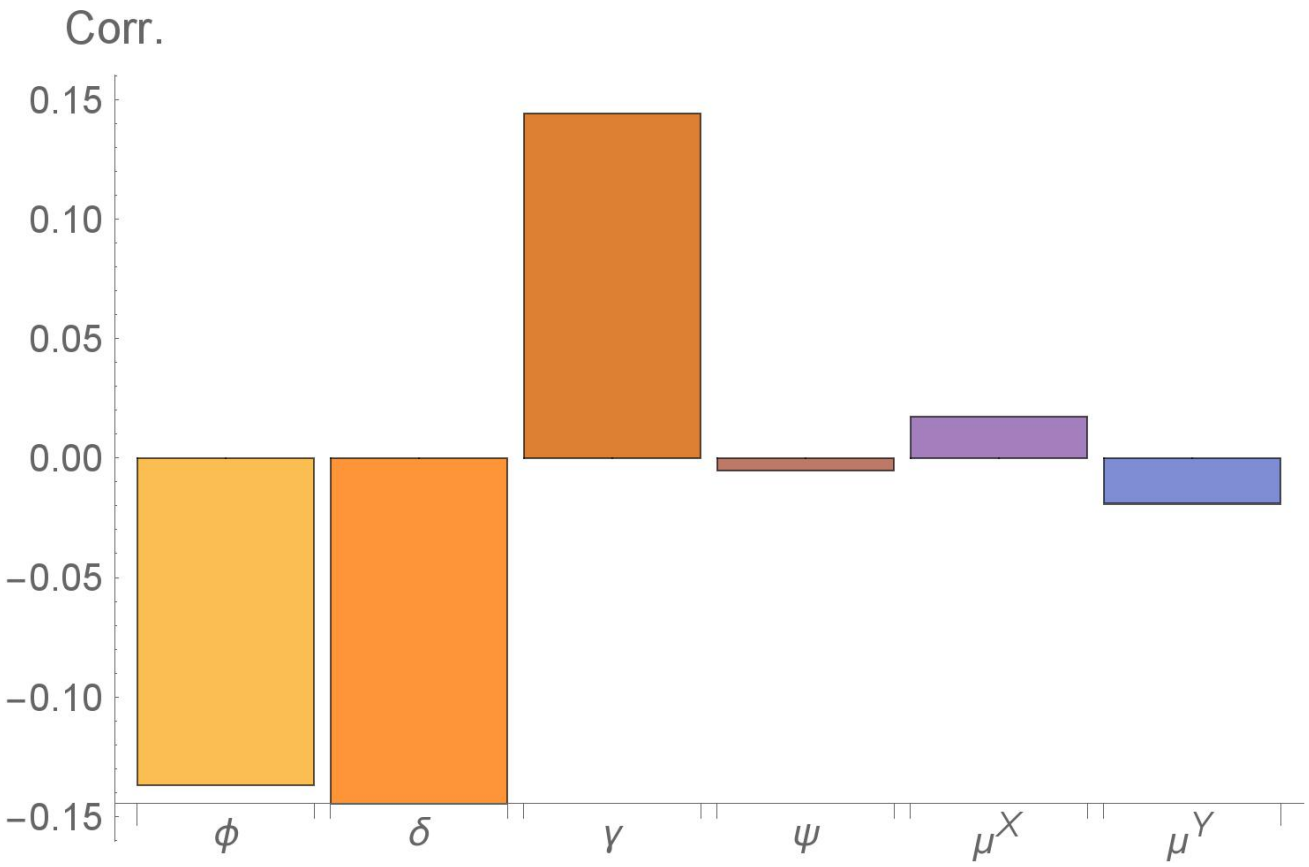

Figure 19: Correlations of all parameters except α for the *Stand* class. On the x-axis we have the different parameters and on the y-axis the correlation value. The *Stand* model allows for a wide range of values for all parameters. The parameters δ, γ and ϕ provide the strongest influences and all other parameters are relatively unimportant.

3.5 Analytical Description of Stability

For a small and relatively simple system as the single patch predator-prey system we can write down reasonably straightforward analytic expressions for the stability of the steady state. In the following we demonstrate this for the different classes. The figures from Fig. 20 to 24 contain all the numerically computed relationships between parameters and the percentage of stable webs to which we can compare the analytical results.

The stability of the system is given by the Jacobian. The Jacobian of the predator-prey system is given by

$$J = \begin{pmatrix} 1 & 0 \\ 0 & \alpha \end{pmatrix} \cdot \begin{pmatrix} \phi - \tilde{\delta}\mu^X - \delta\gamma & -\delta\psi \\ \gamma & \psi - \mu^Y \end{pmatrix}. \tag{141}$$

The eigenvalues of the 2×2-matrix can be given in analytical form:

$$\lambda_{1,2} = \frac{1}{2}\mathrm{Tr}(J) \pm \sqrt{\frac{1}{4}\mathrm{Tr}(J)^2 - \Delta(J)}, \tag{142}$$

with

$$\begin{aligned} \mathrm{Tr}(J) &= \phi - \tilde{\delta}\mu^X - \delta\gamma + \alpha(\psi - \mu^Y), \\ \Delta(J) &= \alpha((\phi - \tilde{\delta}\mu^X - \delta\gamma) \cdot (\psi - \mu^Y) + \delta\psi\gamma). \end{aligned}$$

Depending on the assumptions of the system all parameters can vary within certain intervals (as seen in the *Stand* model) and this can make case differentiation tedious. Fortunately, most common predator-prey models have only two generalized parameters, δ and γ, that have non-fixed values. The parameter δ gives the relative contribution of predation to the biomass loss of the prey species and γ the sensitivity of the predation term to changes in the prey population.

For the *RM* class (see Fig. 20) we get

$$\begin{aligned} \mathrm{Tr}(J) &= -1 + (2-\gamma)\delta, \\ \Delta(J) &= \alpha\delta\gamma, \end{aligned}$$

and thus

$$\lambda_{1,2} = \frac{1}{2}(-1 + (2-\gamma)\delta) \pm \sqrt{\frac{1}{4}(-1 + (2-\gamma)\delta)^2 - \alpha\delta\gamma}. \tag{143}$$

For a stable web we need $\mathrm{Tr}(J) < 0$ and $\Delta(J) > 0$. Since the determinant is always larger than or equal to zero, we can focus on the trace. For $\delta < 0.5$ the trace is negative regardless of the value of γ. We can also see that for $\delta = 1$ we get the inequation

$$\mathrm{Tr}(J) > 0\,, \tag{144}$$

and thus no stable web is possible. The higher γ is the more likely we are to have a stable web.

For a Holling type I functional response (see Fig. 21) in combination with logistic growth in the *LG* class we get

$$\begin{aligned}\mathrm{Tr}(J) &= -1+\delta\,,\\ \Delta(J) &= \alpha\delta\,,\end{aligned}$$

and thus all eigenvalues are always below zero and any steady state would be stable.

For the Holling type III functional response in *H.III* (see Fig. 22) it is slightly more complicated. We have

$$\begin{aligned}\mathrm{Tr}(J) &= -1+(2-\gamma)\delta\,,\\ \Delta(J) &= \alpha\delta\gamma\,,\end{aligned}$$

just like in the *RM* class but the γ range is between $[0;2]$. For $\delta < 0.5$ the system is still always stable but due to the potentially larger values of γ we have a higher likelihood that the system remains stable.

The Lotka-Volterra model shows us one of the limitations of the generalized model. If we look at the trace and the determinant we get

$$\begin{aligned}\mathrm{Tr}(J) &= 0\,,\\ \Delta(J) &= \alpha\,,\end{aligned}$$

which means that our eigenvalues are always of the form

$$\lambda_{1,2} = \pm\sqrt{-\alpha} = \pm i\cdot\sqrt{\alpha}\,. \tag{145}$$

The largest real part is thus always zero and we cannot use simple linear stability analysis to make meaningful statements about the stability. The non-zero imaginary value indicates that we have a population oscillation of some sorts and we know from explicit computation of the model that we indeed have neutrally stable limit cycles expect for the fixed point at $X = Y = 0$. Such a fixed point cannot be correctly described by the generalized method in this form as it would require a normalization to zero. This means that the Lotka-Volterra model is not accessible to linear stability analysis despite being arguably the simplest form of the dynamics.

The Beddington-DeAngelis functional response (see Fig. 24) is comparable to the Holling type II functional response but with an additional saturation term for the predator, i.e. the predator is self limiting in its rate of prey consumption. This is expressed in the interval for the parameter ψ which describes the sensitivity of the functional response to the predator population. Trace and determinant are

$$\mathrm{Tr}(J) = 1 - \tilde{\delta}2 - \delta\gamma + \alpha(\psi - 1), \tag{146}$$

$$\Delta(J) = \alpha((1 - \tilde{\delta}2 - \delta\gamma) \cdot (\psi - 1) + \delta\psi\gamma). \tag{147}$$

The form is identical to Holling type II with exception of the ψ parameter. For the trace we now have the potential for an additional negative term and thus a trend to higher average stability. For the determinant we can have both a negative or positive influence of ψ. If we have a ψ value close to one we are approaching the same conclusions as for Holling type II. If we have a small ψ value the stability depends on the relationship of δ and γ. High γ values are stabilizing while δ values larger than 0.5 are destabilizing. If γ is low enough and δ is large enough the first half of the term for the determinant can outweigh the second half of the determinant which is always positive. A large ψ is therefore destabilizing for the determinant but stabilizing in the trace. Intermediate ψ values thus produce the highest percentage of stable webs.

The most general and complicated case we consider is the *Stand* class which is created to encompass all dynamics that lie within reasonable ranges. Obviously the choice of sensible ranges is up to debate but very few dynamics that have been researched go beyond these parameter ranges.

The trace and determinant for the most general case are

$$\mathrm{Tr}(J) = \phi - \tilde{\delta}\mu^X - \delta\gamma + \alpha(\psi - \mu^Y), \tag{148}$$

$$\Delta(J) = \alpha((\phi - \tilde{\delta}\mu^X - \delta\gamma) \cdot (\psi - \mu^Y) + \delta\psi\gamma). \tag{149}$$

For this class a case differentiation is significantly more time consuming than a simple simulation yet still doable. We limit ourselves to a short discussion of some trends of the parameters.

For the trace, we can see that both large ϕ and ψ could lead to potentially positive contributions and thus are destabilizing. The parameters μ_X, μ_Y and γ have a stabilizing effect in the trace.

For the determinant we can see that the latter half is always positive and thus stabilizing. The former half is more complex. The factor $(\psi - \mu^Y)$ is always negative or zero as μ^Y is larger or equal to ψ. The factor $(\phi - \tilde{\delta}\mu^X - \delta\gamma)$ can only be positive and thus - in combination with the previous factor - destabilizing if the positive ϕ is larger than $|-(1-\delta)\mu^X - \delta\gamma|$. Since μ^X is in the range $[1,2]$ and always larger than ϕ but γ is in the range $[0,2]$, the parameter ϕ can only outweigh the combination of γ and ϕ if δ is large and γ is small. Therefore large δ are destabilizing. Following this, we also find that large μ^Y are destabilizing for the determinant as it acts as a factor for the first half of the determinant.

To establish whether a parameter is in total stabilizing or destabilizing or has any effect at all we would have to take into account the effect on both trace and determinant in combination with all other parameters. We could go into further detail but it becomes clear that a full analysis would be cumbersome. Instead, we look at the results of the simulation (Fig. 23) and see our analytical findings confirmed or at the very least find nothing contrary. The parameter δ still decreases the percentage of stable webs for higher values and γ stabilizes the system for larger values. Both the predator mortality μ_y and the sensitivity of the functional response to the predator population ψ have no impact on stability. A higher exponent for the prey mortality μ_X has a slight stabilizing effect, while larger values for the intrinsic growth of the prey ϕ are destabilizing. The fact that μ^Y has no noticeable impact despite adding a clearly negative term to the trace can be explained if one considers that μ^Y has contrary effects on trace and determinant. Taking all potential parameter combinations into account for a complex scenario can be overwhelming and the relative ease of the numerical computations makes it the preferred choice for many cases.

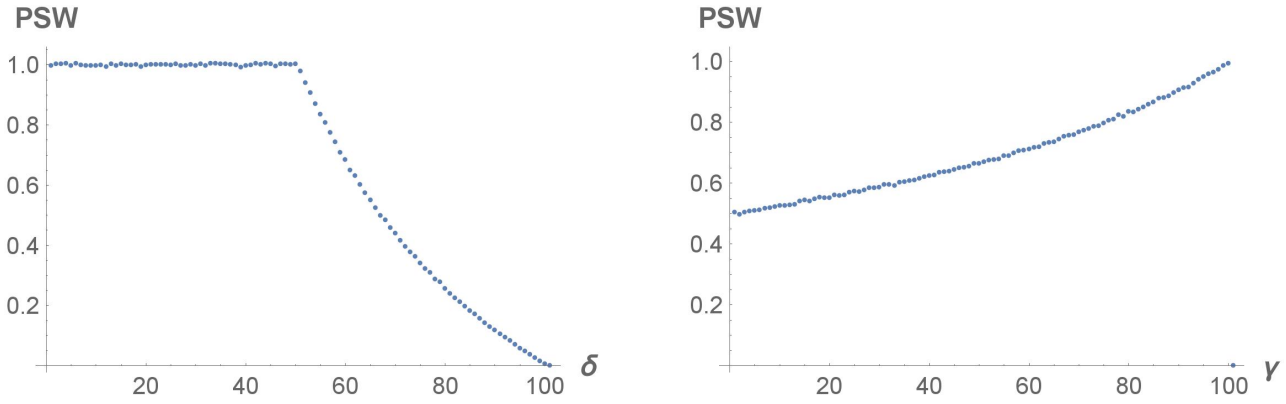

Figure 20: Histogram of the percentage of stable webs for the *RM* class over the parameters δ (left) and γ (right). The bin size for the parameters is the interval range divided by 100. We see the sharp drop-off at half the interval range of δ as predicted by the analytical analyses.

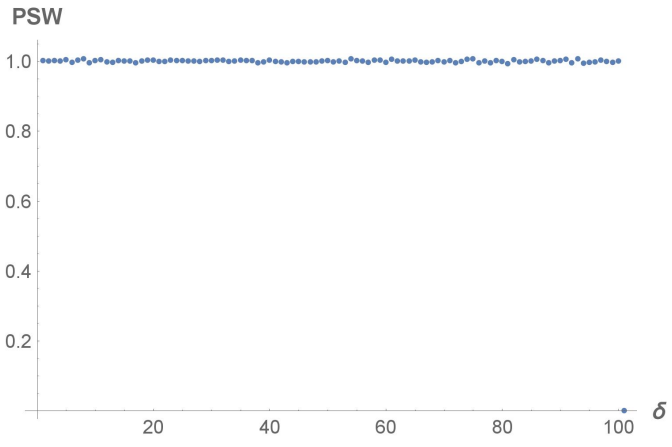

Figure 21: Histogram of the percentage of stable webs for the *LG* class over the parameters δ. The bin size for the parameters is the interval range divided by 100. There is no correlation with stability whatsoever.

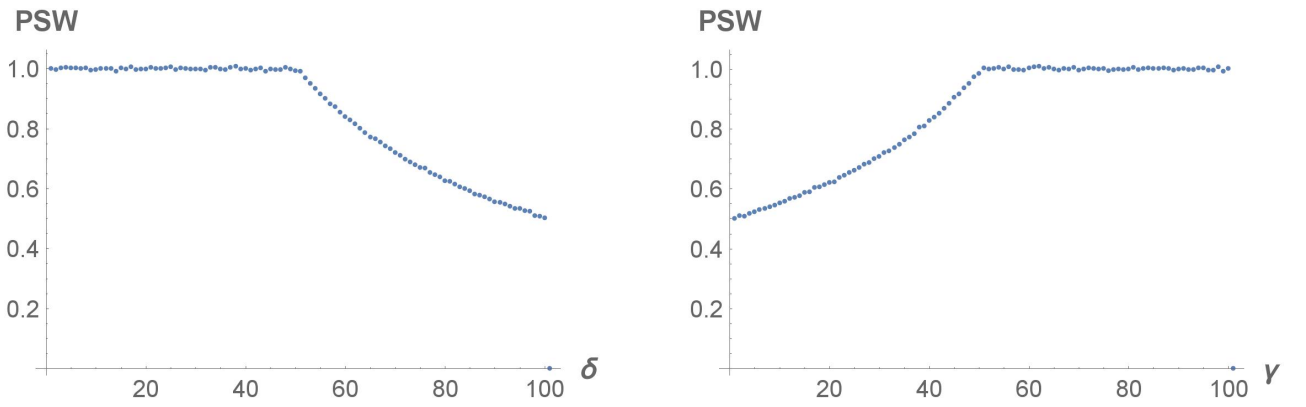

Figure 22: Histogram of the percentage of stable webs for the *H.III* class over the parameters δ (left) and γ (right). The bin size for the parameters is the interval range divided by 100. The γ range is double that of the *RM* class and we can see exactly the same curve for the first half of γ for *H.III* but the looking at the δ parameter we see how this changes the behaviour even though δ is not changed compared to *RM*.

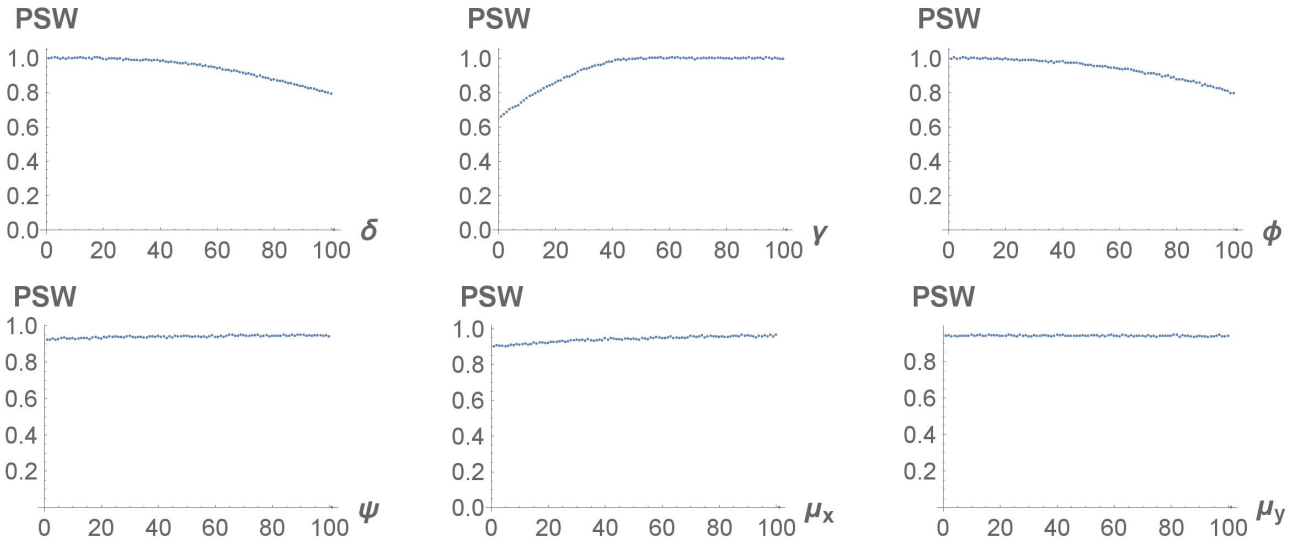

Figure 23: Histogram of the percentage of stable webs for the *Stand* model over all local parameters. The bin size for the parameters is the interval range divided by 100. The curves are much smoother than for the other models as more parameters can vary and we no longer have any "hard" sign changes for the eigenvalues that only depend on one parameter.

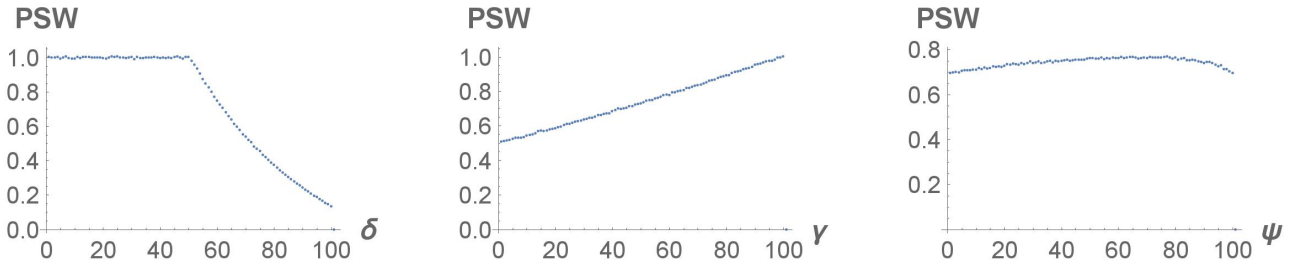

Figure 24: Histogram of the percentage of stable webs for the *DeAngelis* model over the parameters δ, γ and ψ. The bin size for the parameters is the interval range divided by 100. *DeAngelis* only differs in the ϕ parameter from *RM* and shows very similar behaviour.

3.6 Conclusion

The generalized model allows for an easy description of predator-prey dynamics if one is only concerned with the behaviour near or at the steady states. With little effort we can describe the behaviour of all potential steady states for the most commonly used classes. We show how we can potentially arrive analytically at the results and why this quickly becomes unreasonably difficult or even impossible for more complex systems. The concepts of parameter correlations and percentage of stable webs are introduced and their benefits and limitations are explained. We demonstrate the limits of the generalized method with the LG class that - despite being deceivingly simple - cannot be properly analysed. In the generalized form we see that there are only a few parameters that are usually varied while most parameters are kept fixed. In particular the exponent parameter γ, the dependence of the functional response to the prey populations, has almost always a range. The variable parameters have the same qualitative but not quantitative influence across several classes and a simple extrapolation of the influence is not necessarily possible. The generalized formulation proves to be a good tool to get general insight into a wide arrangement of systems with the least amount of preconceived notions about the exact nature of the systems and with minimal numerical effort.

4 Homogeneous Two Patches Predator-Prey Systems

Dispersal between different habitats influences the dynamics and stability of populations considerably. Furthermore, these effects depend on the local interactions of a population with other species. Here, we perform a general and comprehensive study of the simplest possible system that includes dispersal and local interactions, namely a two patches two species system. We evaluate the impact of dispersal on stability and on the occurrence of bifurcations, including pattern forming bifurcations that lead to spatial heterogeneity, in 19 different classes of models with the help of the generalized modelling approach. We find that dispersal in general destabilizes equilibria, but an increase of dispersal compared to little dispersal can stabilize them if it increases population losses. If dispersal is nonrandom, i.e. if emigration or immigration rates depend on population densities, the correlation of stability with dispersal rates is positive in part of the models. We also find that many systems show all four types of local bifurcations possible in homogeneous two patches two species models and that anti-synchronous oscillations occur mostly with nonrandom dispersal.

4.1 Motivation

In ecology both the exploration of dynamical models of food webs (Pascual and Dunne, 2005; Thompson et al., 2012; Rooney and McCann, 2012) and the study of spatial metapopulations (Holland and Hastings, 2008; Hanski and Gaggiotti, 2004; Tromeur et al., 2013) are well established lines of research. The two modelling approaches emphasize different aspects of ecological dynamics that are both relevant for most species: the dispersal between different habitat patches and trophic interactions with other species. Yet, models that combine dispersal with trophic dynamics have only recently begun to appear. In the following we refer to such models that include both of these features as meta-food webs.

An elegant meta-food web model that is based on rates for colonization and extinction was proposed by Pillai (Pillai et al., 2011). More detailed dynamical models were proposed in (Abrams and Ruokolainen, 2011), (Abdllaoui et al., 2007) and (Jansen, 2001), to name a few. The different models draw their motivation from different biological systems and hence make different modelling choices regarding the nature of dispersal and local dynamics. For example (Jansen, 2001) assumes diffusive dispersal between patches which is appropriate for simple life forms such as bacteria, whereas (Abrams and Ruokolainen, 2011) make dispersal dependent on growth rate differences between patches, implying that individuals can actively choose the site with the best growth conditions. Though many of these studies only describe two patches, conclusions from multi-patch models are often consistent with those from two patches models (Jansen and de Roos, 2000), and therefore the insights gained from two patches systems have wider applications.

The two mentioned examples for implementing dispersal are only a small subset of the large space of possibilities. In the literature different assumptions are made regarding the functional forms of the number of emigrants from a given habitat patch, the choice of destination, the proportion of survivors that arrive as immigrants in the destination patch and the settlement success (Amarasekare, 2008b; Armsworth and Roughgarden, 2008; Rowell, 2010). In the simplest case a fixed proportion of the population emigrates per unit time and instantaneously and losslessly settles in a randomly chosen neighbouring patch (Leibold et al., 2004). This type of migration is usually called “random dispersal” or “diffusive migration”, and often leads to a synchronisation of the population dynamics of the two patches (Goldwyn and Hastings, 2008; Jansen, 2001). Examples for non-random dispersal are predator evasion and predator pursuit (Li et al., 2005), or a migration rate that is proportional to the difference in growth rates between two patches (Abrams and Ruokolainen, 2011).

The type of dispersal strongly affects the stability and the dynamics of the system. In general, more rapid dispersal is more likely to synchronize populations, although synchronisation does not necessarily require strong dispersal (Liebhold et al., 2004). With adaptive dispersal, anti-synchronous oscillations of

the two patches are observed, which increase metapopulation persistence. The less similar populations are the less likely it is that dispersal is synchronizing (Esa Ranta and Lundberg, 1998). Other authors find that increased dispersal can decrease synchrony in population dynamics depending on the interactions between migrating species (Koelle and Vandermeer, 2005). A general investigation of metapopulations based on a linear stability analysis (Tromeur et al., 2013) found that costly dispersal and social fencing are stabilizing, while positive density dependence and settlement facilitation reduce stability. Other papers have shown that costly dispersal might be destabilizing to a metapopulation with homogeneous patches (Kisdi, 2010) so the specific mechanisms appear to be of importance. The effects of dispersal on stability can depend not only on the type but also on the intensity of the dispersal (Briggs and Hoopes, 2004).

While much progress has been made for metapopulations and for specific example systems for meta-food webs, a broad and general understanding of how different factors impact the stability of meta-food webs is still lacking. For instance is it unclear under which conditions dispersal has a stabilizing impact. Furthermore, meta-food webs can potentially undergo various types of instabilities. The study of food webs has provided abundant examples of two basic mechanisms of instability. The saddle-node bifurcation, which can lead to the relatively sudden collapse of populations, and the Hopf bifurcation, which gives rise to (at least transient) oscillations. In meta-food webs both of these instabilities can occur in two variants. The first of these affects all patches equally and is thus closely related to the bifurcations in non-spatial food web models. In the second type different patches are affected differently. They are thus reminiscent of pattern-forming instabilities such as the Turing and wave-instabilities, which are known from systems of partial differential equations (Segel and Jackson, 1972). While also these bifurcations lead to instability, their impact on the overall population density is less pronounced, and they act as drivers of heterogeneity, which, in the long run, might benefit the system. In addition to these four types of instabilities, meta-food webs show further instabilities that occur out of the attractors created by these basic bifurcations, such as bifurcations involving heterogeneous fixed points, and nonlocal bifurcations involving limit cycles or strange attractors.

In order to gain an overview of the possible dynamical patterns of a system and their requirements, the generalized modelling approach (Gross and Feudel, 2006; Yeakel et al., 2011; Gross et al., 2009), which is based on a linear stability analysis of steady states, is particularly powerful. The idea behind this approach is to consider models where the kinetics of some processes have not been restricted to specific functional forms. Considering a model with a specific structure, but containing general functions, allows capturing well-known insights into the structure of the system, without requiring often questionable assumptions on the exact form of kinetics. Further advantages are a short computation time and ease of biological interpretation. We will confine our study to bifurcations out of homogeneous equilibria. This means that instabilities of heterogeneous systems and nonlocal bifurcations are not considered.

In this section we investigate the dynamics of two species on two identical patches using the generalized modelling approach. We are able to analyse a broad class of models that includes several previously studied systems as special cases. We focus on the effect of the type and strength of migration on the stability and the dynamics of the system. We find migration in most cases to be either destabilizing or to have a marginal effect on stability. However, complex migration rules allow for a stabilizing influence of dispersal and can produce saddle-node and Hopf bifurcations and spatial-pattern forming bifurcations.

This section is based upon a collaboration (Gramlich et al., 2016) with Sebastian. J. Plitzko, Lars Rudolf, Barbara Drossel and Thilo Gross. Sebastian Plitzko provided the first version of the code used for the numerical simulations and, together with Barbarba Drossel, scouted for publications that might be translated to and compared with the generalized modelling findings. Both Thilo Gross and Barbara Drossel provided value insights to the nature of bifurcations and the current state of research. Lars Rudolf provided help with coding problems. Everything else (figures, simulations, interpretation, etc) was done by the author of this thesis.

4.2 Generalized Modelling Formulation

We consider a system consisting of two habitat patches, where each patch i can potentially sustain a prey population X_i and a predator population Y_i. We assume a homogeneous system, such that both patches are described by identical parameter values. The population dynamics are described by

$$\begin{aligned}
\dot{X}_1 &= G(X_1) - K(X_1) - F(X_1, Y_1) \\
&\quad + \eta^X E^X(X_2, Y_2, X_1, Y_1) - E^X(X_1, Y_1, X_2, Y_2), \\
\dot{Y}_1 &= \lambda F(X_1, Y_1) - D(Y_1) \\
&\quad + \eta^Y E^Y(X_2, Y_2, X_1, Y_1) - E^Y(X_1, Y_1, X_2, Y_2), \\
\dot{X}_2 &= G(X_2) - K(X_2) - F(X_2, Y_2) \\
&\quad + \eta^X E^X(X_1, Y_1, X_2, Y_2) - E^X(X_2, Y_2, X_1, Y_1), \\
\dot{Y}_2 &= \lambda F(X_2, Y_2) - D(Y_2) \\
&\quad + \eta^Y E^Y(X_1, Y_1, X_2, Y_2) - E^Y(X_2, Y_2, X_1, Y_1),
\end{aligned} \tag{150}$$

where we used the dot over a variable to indicate the temporal derivative. We have already shown the derivation of the more general heterogeneous two patches two species system in Sec. 2.9. For the homogeneous case we can reduce the number of variables and indices. We assume that the exponent and scale parameters are identical on both patches, meaning the proportions of biomass flows due to different processes are the same. This does not implicitly mean we have identical steady state values on both patches since any constant off-sets in the process rates are lost in the normalization process. But, given that the patches are coupled and in a combined steady state this would mean that all differences due to heterogeneity must be compensated by constants. This would be a possible but highly artificial case and we simply assume that the steady state values on each patch are identical.

For this assumption we can give the normalized biomasses as

$$x_i = \frac{X_i}{X^*}, \quad y_i = \frac{Y_i}{Y^*}, \tag{151}$$

and the normalized functions are

$$h(\mathbf{x},\mathbf{y}) = \frac{H(\mathbf{X},\mathbf{Y})}{H(\mathbf{X}^*,\mathbf{Y}^*)} \equiv \frac{H(\mathbf{X},\mathbf{Y})}{H^*} \tag{152}$$

with $H = \{E, F, G, K\}$, $\mathbf{U} = \{U_1, U_2,\}$ for $U = \{X, Y, x, y\}$ and the asterisk (*) is used to denote the values of variables and functions in this steady state under consideration.

The Eqs. (150) can now be expressed in the normalized terms

$$\begin{aligned}
\dot{x}_1 &= \frac{G^*}{X^*} g(x_1) - \frac{K^*}{X^*} k(x_1) - \frac{F^*}{X^*} f(x_1, y_1) + \frac{E^{X*}\eta^X}{X^*} e^X(\mathbf{x},\mathbf{y}) - \frac{E^{X*}}{X^*} e^X(\mathbf{x},\mathbf{y}), \\
\dot{y}_1 &= \frac{\lambda F^*}{Y^*} f(x_1, y_1) - \frac{D^*}{Y^*} d(y_1) + \frac{E^{Y*}\eta^Y}{Y^*} e^Y(\mathbf{x},\mathbf{y}) - \frac{E^{Y*}}{Y^*} e^Y(\mathbf{x},\mathbf{y}), \\
\dot{x}_2 &= \frac{G^*}{X^*} g(x_2) - \frac{K^*}{X^*} k(x_2) - \frac{F^*}{X^*} f(x_2, y_2) + \frac{E^{X*}\eta^X}{X^*} e^X(\mathbf{x},\mathbf{y}) - \frac{E^{X*}}{X^*} e^X(\mathbf{x},\mathbf{y}), \\
\dot{y}_2 &= \frac{\lambda F^*}{Y^*} f(x_2, y_2) - \frac{D^*}{Y^*} d(y_2) + \frac{E^{Y*}\eta^Y}{Y^*} e^Y(\mathbf{x},\mathbf{y}) - \frac{E^{Y*}}{Y^*} e^Y(\mathbf{x},\mathbf{y}).
\end{aligned} \tag{153}$$

The total biomass turnover rate of the populations on each patch at their steady state can be identified as

$$\alpha^X = \frac{G^*}{X^*} + \frac{E^{X*}\eta^X}{X^*} = \frac{K^*}{X^*} + \frac{F^*}{X^*} + \frac{E^{X*}}{X^*}, \tag{154}$$

$$\alpha^Y = \frac{\lambda F^*}{Y^*} + \frac{E^{Y*}\eta^Y}{Y^*} = \frac{D^*}{Y^*} + \frac{E^{Y*}}{Y^*}. \tag{155}$$

It is convenient to measure time in terms of the inverse of the prey turnover rate α^X. In these rescaled time units the turnover rate of the prey is 1 and the turnover rate of the predator is

$$\alpha = \frac{\alpha^Y}{\alpha^X}. \tag{156}$$

We now define the *scale parameters* δ, ν and ρ and their complements. As they are identical on each patch we can drop any patch indicators.

$$\delta = \frac{1}{\alpha^X \tilde{\rho}^X} \frac{F^*}{X^*}, \qquad \tilde{\delta} = (1-\delta) = \frac{1}{\alpha^X \tilde{\rho}^X} \frac{K^*}{X^*}, \tag{157}$$

$$\nu^U = \frac{1}{\alpha^U} \frac{E^{U*}\eta^U}{U^*}, \qquad \tilde{\nu}^U = (1-\nu^U) = \frac{1}{\alpha^U} \frac{\{G^*; \lambda F^*\}}{U^*}, \tag{158}$$

$$\rho^U = \frac{1}{\alpha^U} \frac{E^{U*}}{U^*}, \qquad \tilde{\rho}^U = (1-\rho^U) = \frac{1}{\alpha^U} \frac{\{K^* + F^*; D^*\}}{U^*}. \tag{159}$$

The meaning of the parameters is explained in detail in the theoretical basis but to reiterate: Scale parameters give the relative contribution of a process to the total biomass turnover at the steady state.

With help of the turnover rates and the scale parameters, we can now write Eq. (153) as

$$\begin{aligned}
\dot{x}_1 &= \alpha^X[\tilde{\nu}^X g(x_1) - \tilde{\rho}_1^X \tilde{\delta} k(x_1) - \tilde{\rho}^X \delta f(x_1, y_1) + \nu^X e^X(\mathbf{x},\mathbf{y}) - \rho^X e^X(\mathbf{x},\mathbf{y})], \\
\dot{y}_1 &= \alpha^Y[\tilde{\nu}^Y f(x_1, y_1) - \tilde{\rho}^Y d(y_1) + \nu^Y e^Y(\mathbf{x},\mathbf{y}) - \rho^Y e^Y(\mathbf{x},\mathbf{y})], \\
\dot{x}_2 &= \alpha^X[\tilde{\nu}^X g(x_2) - \tilde{\rho}^X \tilde{\delta} k(x_2) - \tilde{\rho}^X \delta f(x_2, y_2) + \nu^X e^X(\mathbf{x},\mathbf{y}) - \rho^X e^X(\mathbf{x},\mathbf{y})], \\
\dot{y}_2 &= \alpha^Y[\tilde{\nu}^Y f(x_2, y_2) - \tilde{\rho}^Y d(y_2) + \nu^Y e^Y(\mathbf{x},\mathbf{y}) - \rho^Y e^Y(\mathbf{x},\mathbf{y})].
\end{aligned} \tag{160}$$

To analyse the stability we linearise the system around the steady state under consideration which is at $x = y = 1$ in the normalized system. The linearisation can then be expressed in terms of the Jacobian matrix. For a system of four dynamical variables this is a 4×4 matrix defined by

$$J_{i,j} = \left. \frac{\partial \dot{V}_i}{\partial V_j} \right|_*, \tag{161}$$

where $V = (x_1, y_1, x_2, y_2)$ is the set of state variables, and $|_*$ indicating that the derivatives are evaluated in the steady state (1,1,1,1).

For the case of a system with two identical patches the 4×4 matrix can be written as a block matrix

$$J = \begin{pmatrix} P & M \\ M & P \end{pmatrix} \tag{162}$$

with a matrix P that describes the in-patch dynamics,

$$P = \begin{pmatrix} 1 & 0 \\ 0 & \alpha \end{pmatrix} \begin{pmatrix} \tilde{\nu}^X \phi - \tilde{\rho}^X \tilde{\delta} \mu^X - \tilde{\rho}^X \delta \gamma + \nu^X \hat{\omega}^X - \rho^X \omega^X & -\tilde{\rho}^X \delta \psi + \nu^X \hat{\kappa}^X - \rho^X \kappa^X \\ \tilde{\nu}^Y \gamma + \nu^Y \hat{\kappa}^Y - \rho^Y \kappa^Y & \tilde{\nu}^Y \psi - \tilde{\rho}^Y \mu^Y + \nu^Y \hat{\omega}^Y - \rho^Y \omega^Y \end{pmatrix} \tag{163}$$

and a matrix M that captures between-patch dynamics,

$$M = \begin{pmatrix} 1 & 0 \\ 0 & \alpha \end{pmatrix} \begin{pmatrix} \nu^X \omega^X - \rho^X \hat{\omega}^X & \nu^X \kappa^X - \rho^X \hat{\kappa}^X \\ \nu^Y \kappa^Y - \rho^Y \hat{\kappa}^Y & \nu^Y \omega^Y - \rho^Y \hat{\omega}^Y \end{pmatrix}. \tag{164}$$

The definitions of the exponent parameters are

$$\begin{aligned}
\phi &:= \left.\frac{\partial g(x)}{\partial x}\right|_*, & \mu^X &:= \left.\frac{\partial k(x)}{\partial x}\right|_*, & \mu^Y &:= \left.\frac{\partial d(y)}{\partial y}\right|_*, \\
\gamma &:= \left.\frac{\partial f(x,y)}{\partial x}\right|_*, & \psi &:= \left.\frac{\partial f(x,y)}{\partial y}\right|_*, & & \\
\hat{\omega}^X &:= \left.\frac{\partial e^X(\mathbf{x},\mathbf{y})}{\partial x_f}\right|_*, & \omega^X &:= \left.\frac{\partial e^X(\mathbf{x},\mathbf{y})}{\partial x_i}\right|_*, & & \\
\hat{\kappa}^X &:= \left.\frac{\partial e^X(\mathbf{x},\mathbf{y})}{\partial y_f}\right|_*, & \kappa^X &:= \left.\frac{\partial e^X(\mathbf{x},\mathbf{y})}{\partial y_i}\right|_*, & & \\
\hat{\omega}^Y &:= \left.\frac{\partial e^Y(\mathbf{x},\mathbf{y})}{\partial y_f}\right|_*, & \omega^Y &:= \left.\frac{\partial e^Y(\mathbf{x},\mathbf{y})}{\partial y_i}\right|_*, & & \\
\hat{\kappa}^Y &:= \left.\frac{\partial e^Y(\mathbf{x},\mathbf{y})}{\partial x_f}\right|_*, & \kappa^Y &:= \left.\frac{\partial e^Y(\mathbf{x},\mathbf{y})}{\partial x_i}\right|_*. &&
\end{aligned} \tag{165}$$

We use the indices i and f to indicate whether the derivation is by the population on the patch from which the migration starts (i) or on the target patch (f). We can drop all other patch indices as the exponent parameters are the same on both patches.

4.3 Classes of Models Studied in the Following

In order to evaluate the proportion of stable systems and the frequency of the different types of bifurcations, we need to specify intervals for the exponent parameters and the scale parameters. Different classes of models are characterized by different choices for these intervals. We use several models from the existing literature as well as more general models. All these models are listed in Tab. 6.

Scen.	ϕ	δ	γ	ψ	μ^X	μ^Y	α	ν^X	ν^Y	ρ^X	ρ^Y	ω^X	ω^Y	$\hat{\omega}^X$	$\hat{\omega}^Y$	κ^X	κ^Y	$\hat{\kappa}^X$	$\hat{\kappa}^Y$
(1) Stand.	$[0;1]$	$[0;1]$	$[0;2]$	$[0;1]$	$[1;2]$	$[1;2]$	$[10^{-3};10^1]$	$[0;1]$	$[0;1]$	$[0;1]$	$[0;1]$	$[-2;2]$	$[-2;2]$	$[-2;2]$	$[-2;2]$	$[-2;2]$	$[-2;2]$	$[-2;2]$	$[-2;2]$
(1x) Stand.	$[0;1]$	$[0;1]$	$[0;2]$	$[0;1]$	$[1;2]$	$[1;2]$	$[10^{-3};10^1]$	$[0;1]$	$[0;1]$	0	0	$[-2;2]$	$[-2;2]$	$[-2;2]$	$[-2;2]$	$[-2;2]$	$[-2;2]$	$[-2;2]$	$[-2;2]$
(1z) Stand.	$[0;1]$	$[0;1]$	$[0;2]$	$[0;1]$	$[1;2]$	$[1;2]$	$[10^{-3};10^1]$	$[0;1]$	$[0;1]$	ν^X	ν^Y	$[-2;2]$	$[-2;2]$	$[-2;2]$	$[-2;2]$	$[-2;2]$	$[-2;2]$	$[-2;2]$	$[-2;2]$
(2) Diff	$[0;1]$	$[0;1]$	$[0;2]$	$[0;1]$	$[1;2]$	$[1;2]$	$[10^{-3};10^1]$	$[0;1]$	$[0;1]$	$[0;1]$	$[0;1]$	1	1	0	0	0	0	0	0
(2x) Diff	$[0;1]$	$[0;1]$	$[0;2]$	$[0;1]$	$[1;2]$	$[1;2]$	$[10^{-3};10^1]$	$[0;1]$	$[0;1]$	0	0	1	1	0	0	0	0	0	0
(2z) Diff	$[0;1]$	$[0;1]$	$[0;2]$	$[0;1]$	$[1;2]$	$[1;2]$	$[10^{-3};10^1]$	$[0;1]$	$[0;1]$	ν^X	ν^Y	1	1	0	0	0	0	0	0
(2y) Diff	$[0;1]$	$[0;1]$	$[0;2]$	$[0;1]$	$[1;2]$	$[1;2]$	$[10^{-3};10^1]$	$[0;1]$	0	ν^X	0	1	1	0	0	0	0	0	0
(3) Mchich	1	1	1	1	0	1	$[10^{-3};10^1]$	$[0;1]$	$[0;1]$	$[0;1]$	$[0;1]$	1	1	0	0	$[0;1]$	0	0	0
(3x) Mchich	1	1	1	1	0	1	$[10^{-3};10^1]$	$[0;1]$	$[0;1]$	0	0	1	1	0	0	$[0;1]$	0	0	0
(4) Jans95	1	$[0;1]$	$[0;1]$	1	2	1	$[10^{-3};10^1]$	$[0;1]$	$[0;1]$	$[0;1]$	$[0;1]$	1	1	0	0	0	0	0	0
(4x) Jans95	1	$[0;1]$	$[0;1]$	1	2	1	$[10^{-3};10^1]$	$[0;1]$	$[0;1]$	0	0	1	1	0	0	0	0	0	0
(4z) Jans95	1	$[0;1]$	$[0;1]$	1	2	1	$[10^{-3};10^1]$	$[0;1]$	$[0;1]$	ν^X	ν^Y	1	1	0	0	0	0	0	0
(5) Jans01	1	$[0;1]$	$[0;1]$	1	2	1	$[10^{-3};10^1]$	0	$[0;1]$	0	$[0;1]$	0	1	0	0	0	0	0	0
(5z) Jans01	1	$[0;1]$	$[0;1]$	1	2	1	$[10^{-3};10^1]$	0	$[0;1]$	0	ν^Y	0	1	0	0	0	0	0	0
(6) Huang	1	$[0;1]$	$[0;1]$	1	2	1	$[10^{-3};10^1]$	0	$[0;1]$	0	$[0;1]$	0	1	0	0	0	$[-1;0]$	0	0
(6R) Huang	1	$[0;1]$	$[0;1]$	1	2	1	$[10^{-3};10^1]$	0	$[0;1]$	0	$[0;1]$	0	1	0	0	0	$[0;1]$	0	0
(7) Abrams11	1	$[0;1]$	$[0;1]$	1	2	1	$[10^{-3};10^1]$	0	$[0;1]$	0	$[0;1]$	0	1	0	0	0	$-\hat{\kappa}^Y$	0	$[0;\frac{\lambda b}{4h}]$
(8) El Abdl.	1	$[0;1]$	1	1	2	1	$[10^{-3};10^1]$	$[0;1]$	$[0;1]$	$[0;1]$	$[0;1]$	1	1	0	0	1	-1	0	0
(9) Growth	$[0;1]$	$[0;1]$	$[0;2]$	$[0;1]$	$[1;2]$	$[1;2]$	$[10^{-3};10^1]$	$[0;1]$	$[0;1]$	$[0;1]$	$[0;1]$	ϕ	ψ	ϕ	ψ	γ	0	γ	0
(10) Growth2	1	$[0;1]$	$[0;1]$	1	2	1	$[10^{-3};10^1]$	$[0;1]$	$[0;1]$	$[0;1]$	$[0;1]$	ϕ	ψ	ϕ	ψ	γ	0	γ	0

Table 6: The different classes analysed in this thesis, together with the intervals from which the parameters were chosen randomly. The models *Jan95*, *Jan01*, *Abrams11*, *Mchich*, *ElAbdl*, *Huang* can be found in (Jansen, 1995), (Abdllaoui et al., 2007), (Abrams and Ruokolainen, 2011), (Jansen, 2001), (Mchich et al., 2007) and (Huang and Diekmann, 2001). *Stand* represents the most general scenario where all parameters take the biologically plausible range. *Diff* combines general local dynamics with diffusive migration. *Growth* couples growth rates and feeding terms to migration terms. *Jans95*, *Jans01*, *Huang* and *Abrams11* share the same local dynamics but have different migration mechanisms. *Mchich* and *ElAbdll.* do not share local dynamics with any other class and have to be treated separately. In the text and the figures, the labels in the left column (number plus letter, or name) are used to name the classes. The letters x, y or z after the number indicate a migration rule where there is no migration loss (x), or where gain and loss are identical, $\nu_x = \rho_x$, which means that all migrating individuals arrive at their destination (y if this applies only to the prey and z if this applies to both species).

Group (1) represents the most general models, for which all exponent parameters have their maximum meaningful range. In group (2), migration is diffusive for both species, but the local exponent parameters are still in the maximum meaningful range. Models (4) to (7) have a Holling type 2 functional response with logistic growth and no predator interference, the Rosenzweig-MacArthur model (Rosenzweig and MacArthur, 1963) for predator-prey interaction, and they differ with respect to the migration term. Model (4) *Jans95* has simple diffusive migration. Model (5) is the same as model (4) but with no prey migration. Model (6R) *Huang* adds that over-abundance of prey facilitates predator migration while model (6) incites predators to stay if there is plenty of food available. Model (7) *Abrams11* implements predator pursuit, which means that predators migrate towards the patch with larger prey abundance.

Models (9) and (10) establish a relation between consumption rate and migration: the migration rate of the predator scales in the same way as its feeding rate (i.e. the biomass production), and the migration rate of the prey scales with its own growth rate as well as with the predator feeding rate and with predation on the other patch.

We group all these models into two classes, with class I comprising the models with general intervals for the five in-patch scale parameters (models (1), (2), (9)) and class II comprising models (4) to (7) and (10), which are based on the Rosenzweig-MacArthur model.

Models (3) *Mchich* and (8) *ElAbdllaoui* fix more parameters for the in-patch dynamics. *Mchich* reduces to Lotka-Volterra dynamics and *ElAbdllaoui* has a Holling type I functional response in combination with logistic growth. They have interesting migration rules: *Mchich* lets the prey flee if there are many predators in the own patch. *ElAbdllaoui* additionally makes the predator sedentary if there is plenty of food available.

4.4 Proportion of Stable Systems

We evaluated the proportion of stable states in an ensemble where the scale and exponent parameters were chosen at random from the intervals indicated in Tab. 6. We generated 10^7 random sets of parameters for each model where each parameter was drawn uniformly from the respective intervals. We define the proportion of stable webs (PSW) as the number of parameter sets which produce a stable steady state, divided by the total number of sets sampled. We use a random distribution of values for exponent and scale parameters as we do not assume any relationship between parameters. A specific scenario will have most likely dependencies between functions (e.g. predator feeding rate and prey mortality share common variables) but these are subsets of our parameter space. Weights for the parameter distribution would skew the results towards particular assumptions which we want to avoid. In the absence of migration (i.e., for single patches), we obtained PSW=0.939 for class I, PSW=0.639 for class II and PSW=0 for model *Mchich* and PSW=1 for model *ElAbdllaoui*. These results are a measure of the stability of the within-patch dynamics alone. We have shown in the previous section for non-spatial predator-prey dynamics how these particular dynamics can be explained analytically. Other research (Levins, 1974; Gross et al., 2009) has shown that in general mortality and feeding terms tend to be positively correlated with stability and growth terms are negatively correlated with stability for local dynamics. This means that high values for γ and $\mu^{x,y}$ and low values for ϕ and ψ enhance stability. Based on this knowledge we expect model *Mchich* to be less stable than model *ElAdbllaoui*, and systems with class I local dynamics to be more stable than systems with class II local dynamics. This is confirmed by our results. Model *Mchich* is a special case as the particular parameter choices of (Mchich et al., 2007) create a pair of purely imaginary eigenvalues, both for the case with and without migration. This does not allow for a conclusive linear stability analysis, and higher order terms are needed to judge the stability of a steady state.

The percentages of stable webs obtained in the presence of migration are given in Tab. 7. In all cases, stability with migration is smaller than or roughly equal to stability without migration. It can be proven that for homogeneous steady states stability cannot be larger than the stability for the isolated patch.

The slightly higher values are numerical errors of the eigenvalue solver. The principle for the proof will be explained in the section Sec. 6.

The proportion of stable webs ranges from 0.05 for model (10), which has a complex migration rule, to 0.94 for class I with diffusive, conservative migration, i.e., models (2y) and (2z). In fact, the models (1), (9), (10) have the largest drop in stability due to migration. These models have in common that $\hat{\omega}$ and/or $\hat{\kappa}$ are nonzero, which means that dispersal of a population depends on the population of the other species on the other patch. This can be understood by applying the qualitative stability considerations established by (Levins, 1974): Including an element in the Jacobian that connects different species on different patches creates a positive feedback loop of length 3, which has a strong destabilizing effect.

It is interesting to note that the class II systems are less stable than the models with diffusive migration, (2) to (2z), despite the high exponent of closure $\mu_x = 2$. A high exponent of closure is well known to be stabilizing since it implies a strong density limitation of the predator (Levins, 1974; Gross et al., 2009; Plitzko et al., 2012). In order to investigate the effect of the exponent of closure, we run the class II systems also with $\mu_x = 1$ instead of 2. In this case all systems become unstable. When μ_x is chosen at random from the interval $[1, 2]$, the average stability was lower than for the isolated patches (around 0.50), but with trends similar to those for $\mu_x = 2$. This is particular interesting if one compares it to the findings for *Stand* without any migration as seen in the section Sec. 3. Here we see that μ_x has relatively little influence for the parameter range $[1, 2]$.

Scenario	PSW without migration	PSW with migration
(1)Stand	0.939	0.227
(1x)Stand	0.939	0.570
(1z)Stand	0.939	0.394
(2)Diff	0.939	0.924
(2x)Diff	0.939	0.876
(2y)Diff	0.939	0.942
(2z)Diff	0.939	0.939
(9)Growth	0.939	0.450
(4)Jans95	0.693	0.693
(4x)Jans95	0.693	0.693
(4z)Jans95	0.693	0.693
(5)Jans01	0.693	0.693
(5z)Jans01	0.693	0.693
(6)Huang	0.693	0.552
(6R)Huang	0.693	0.530
(7)Abrams11	0.693	0.693
(10)Growth2	0.693	0.051
(3)Mchich	0.000	0.00
(3x)Mchich	0.000	0.00
(8)ElAbdllaoui	1.000	0.625

Table 7: The different classes and the proportion of stable webs with and without migration. The double horizontal lines separate the classes I, II, and the exceptions model *Mchich* and model *ElAbdllaoui*. The parameter values for the different classes were drawn uniformly from the intervals given in Tab. 6.

In order to obtain more detailed information about the effect of migration on stability, we evaluated the correlation of stability with the scale parameters of migration. We used the Pearson product-moment correlation coefficient to compute the correlation between stability and the migration scale parameters. The result is shown in Fig. 25.

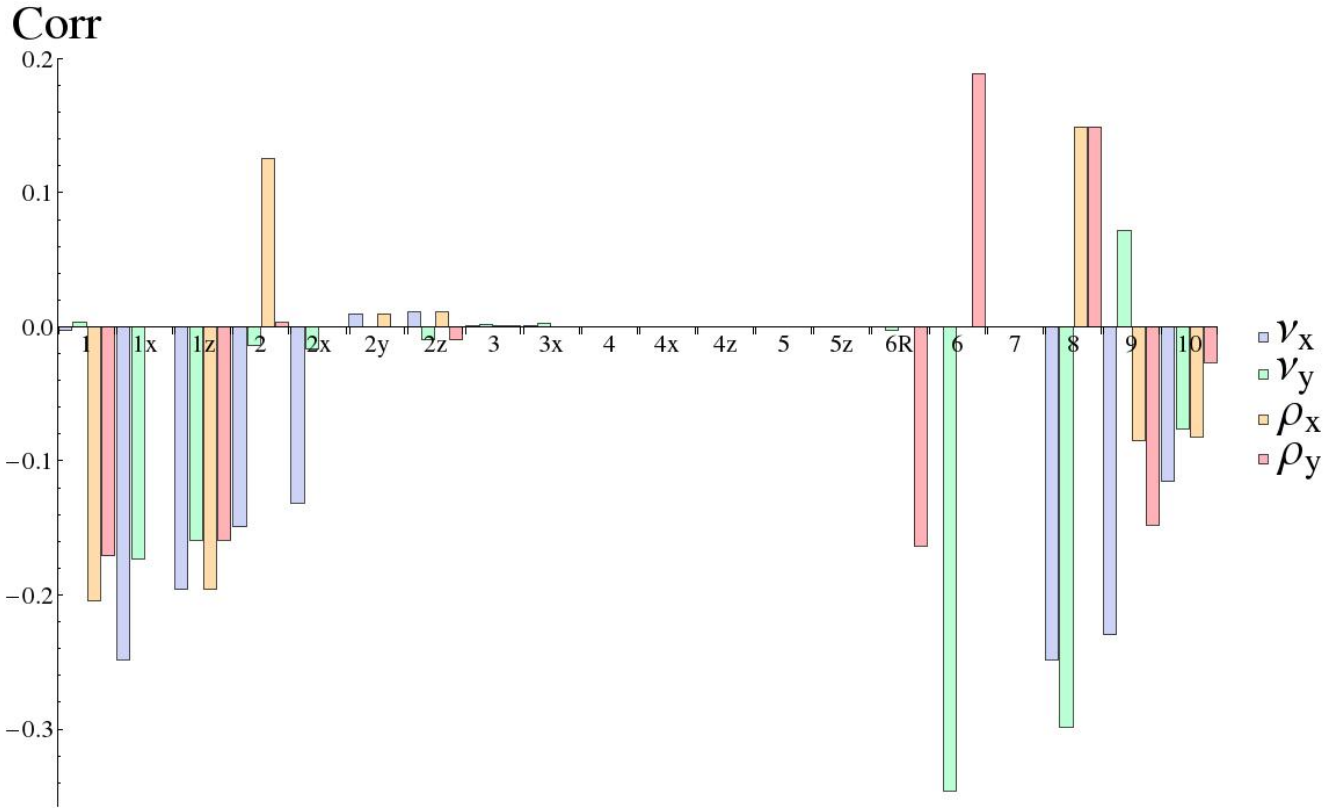

Figure 25: The correlation of the four scale parameters of migration ($\nu_x, \nu_y, \rho_x, \rho_y$) with stability for 10^7 randomly chosen parameter sets for each model. The different models are arranged along the x-axis, the correlation value is given along the y-axis. The different scale parameters are coded by colour. Most models show a negative correlation of the migration parameters with stability.

In most cases, the correlation is zero or negative, and there are only four instances of a significant positive correlation with migration. Positive correlation values mean that higher relative migration rates make the steady state more stable, negative correlation values indicate that the steady state becomes less stable. It is interesting to note that out of the five instances with positive correlations four are loss terms $\rho_{x,y}$. This fits together with the observation that loss terms are comparable to death terms, which are known to be stabilizing for local dynamics (Gross et al., 2009).

To summarize, the results in Fig. 25 imply that most models become less stable when the contribution of migration to the total gain and loss terms increases. However, several models become more stable with increasing migration losses, *ElAbdllaoui*, *Huang* and *Diff*, and only model *Growth* becomes more stable with increasing migration gains. The models *ElAbdllaoui*, *Huang* and *Growth* all show types of adaptive migration. The model *Diff* has simple diffusion as a dispersal mechanism, though both *Diff* and *Growth* have wide parameter interval ranges for local parameters.

In addition to evaluating the correlation of the scale parameters with stability, we also evaluated how average stability changes as a scale parameter is varied. Example curves that represent the qualitatively different types of behaviour found are shown in Fig. 26.

The top left graph shows a monotonous decrease, which is most often obtained and applies to most scenarios that have a negative correlation of the scale parameter with stability. The bottom right graph shows a monotonous increase, which is seen in the cases of positive correlation of the scale parameters with stability. The bottom left graph shows an instance of a non-monotonous curve, found for the scenarios *Stand*, *Growth* and *Growth2*, which have complex migration rules, where more than two of the eight migration exponent parameters (ω, κ) are different from zero. This shows that cross-patch cross-species interactions as seen in these three classes can create positive correlation of migration scale parameters with stability within certain ranges even if the overall correlation remains negative. The top right graph is an instance where migration has no effect on stability.

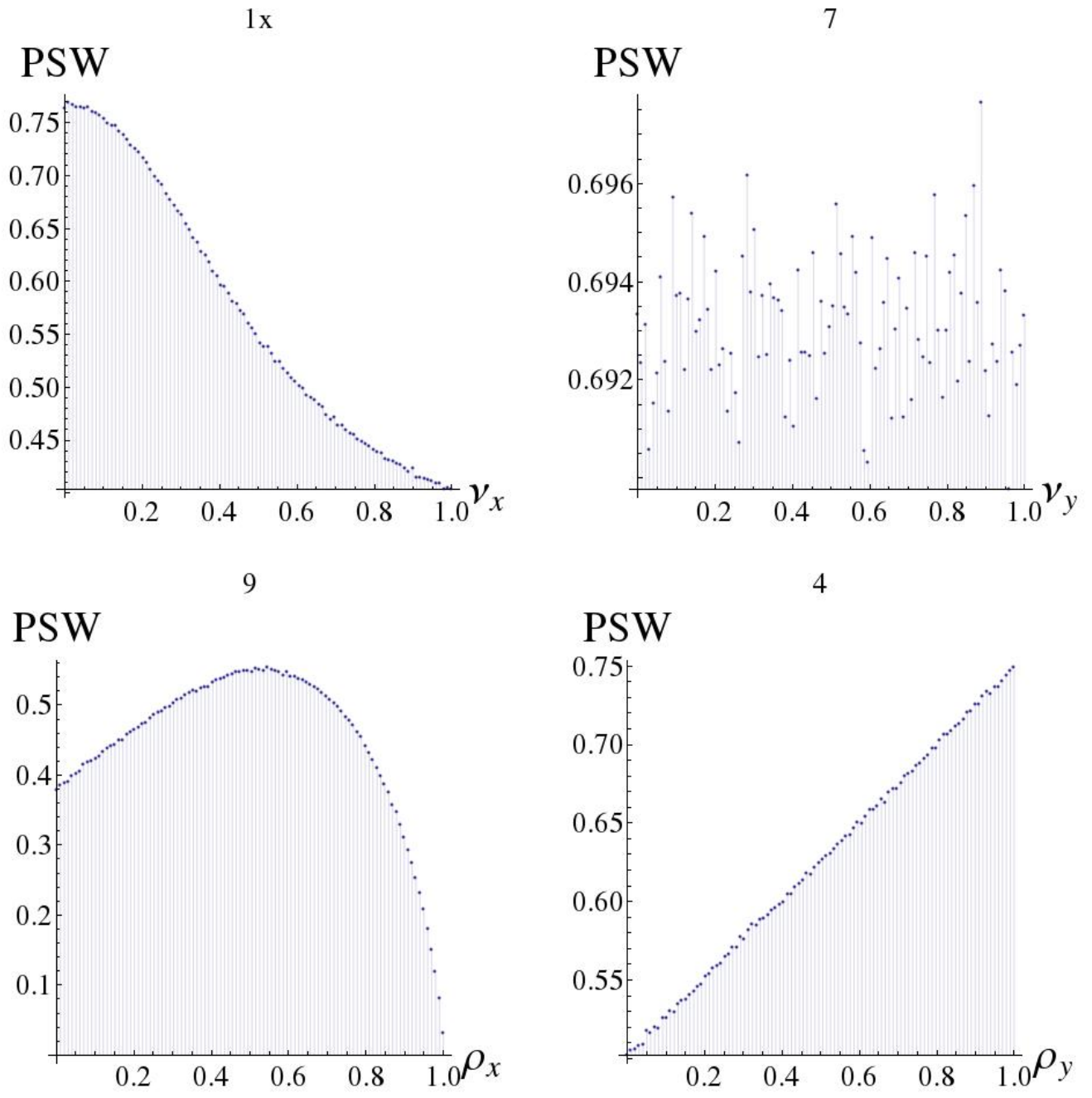

Figure 26: Examples of the different types of functional relation between scale parameters and average stability. The graphs show the proportion of stable systems as function of a migration scale parameter. The numbers above each plot denote the model (see Tab. 6) which is defined by the intervals of the exponent parameters and the relationship between scale parameters used to create the data. Apart from a monotonous decrease or increase, there are also models with a constant proportion of stable systems and those with maxima at intermediate values of the scale parameter.

Inspired by these findings, we investigated additional cases: Instead of linear relationships for the sensitivity of the migration on the respective population ($\omega_{x,y}=1$, as used in class II), we used quadratic relationships ($\omega_{x,y}=2$) for the scenarios of class II. This caused clear trends, with the average stability decreasing with increasing values of the scale parameters $\nu_{x,y}$ and increasing with $\rho_{x,y}$. Even though slope and absolute values vary, this effect dominates over every other influence on stability and shapes the curves almost solely. This is understood by realizing that $\omega_{x,y}=2$ implies large loss terms at high values of ρ. The dependence on ν is more complicated as ν affects only the non-diagonal elements of the Jacobian matrix. High ν creates larger diagonal elements for the migration sub-matrix. This increases the trace $\mathrm{Tr}(J_+)$ and thus decreases the likelihood of a stable steady state even though $\mathrm{Tr}(J_-)$ becomes more stable as the total stability is limited by the stability of each sub-matrix.

4.5 Example of Analytical Computation

In most cases, the stability curves are not easily understood. The stability condition comprises four inequalities, two for each matrix $P\pm M$ (see paragraph after Eq. (2.9.4)). Each of these inequalities contains several parameters, and checking whether they are satisfied requires the consideration of a multitude of cases. In the following we demonstrate for the model with the smallest number of free parameters, which is the model *ElAbdllaoui*, how the shape of the stability curve results from the inequalities. As an example we use the average stability versus the scale parameter ν_y, as it has a distinct shape of two linear sections with different slopes which can be seen in Fig. 27.

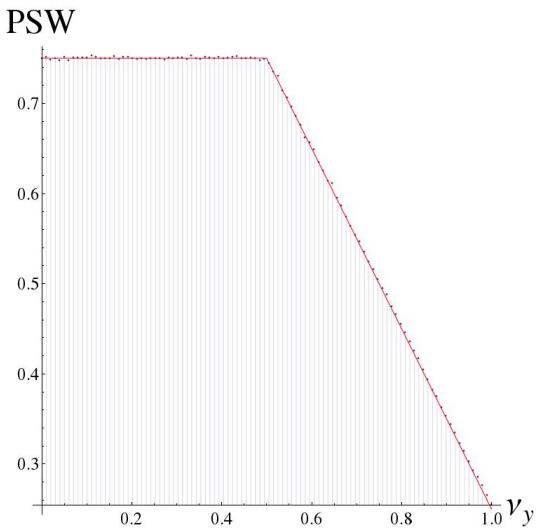

Figure 27: The average stability as a function of ν_y for the scenario *ElAbdllaoui*. The solid red line shows the analytical result.

The traces and determinants for this model are

$$\begin{aligned}
\mathrm{Tr}(J_+) &= 1-2(1-\delta)(1-\rho_x)-\delta(1-\rho_x)-\rho_x\,,\\
\mathrm{Tr}(J_-) &= 1-2(1-\delta)(1-\rho_x)-\delta(1-\rho_x)-\rho_x-2\nu_x-2\alpha_y\nu_y\,,\\
\Delta(J_+) &= -[\delta(-1+\rho_x)-\rho_x+\nu_x][\alpha_y(1+\rho_y-\nu_y)-\alpha_y\nu_y]\,,\\
\Delta(J_-) &= -2\alpha_y[1-2(1-\delta)(1-\rho_x)-\delta(1-\rho_x)-\rho_x-2\nu_x]\nu_y\,,\\
&\quad -[\delta(-1+\rho_x)-\rho_x-\nu_x)(\alpha_y(1+\rho_y-\nu_y)+\alpha\nu_y]\,.
\end{aligned}$$

The steady state is stable if both traces are negative and both determinants are positive. The values of δ, $\rho_{x,y}$ and $\nu_{x,y}$ are in the interval $[0,1]$. This means that $\mathrm{Tr}(J_{+,-}) < 0$ and $\Delta(J_-) > 0$. The stability is thus solely dependent on $\Delta(J_-)$. Rewriting $\Delta(J_+)$ as

$$\Delta(J_+) = -\alpha_y f_1 \cdot f_2$$

with $f_1 = \delta(\rho_x - 1) - \rho_x + \nu_x$ and $f_2 = 1 + \rho_y - 2\nu_y$, the stability condition becomes $f_1 f_2 < 0$, which means that f_1 and f_2 must have opposite signs. The term f_1 is independent of ν_y and thus cannot change sign as ν_y is changed. With all parameters in f_1 being random numbers in $[0,1]$, $f_1 < 0$ in 75% of the cases, and $f_1 > 0$ in 25% of the cases. f_2 is always larger than zero as long as $\nu_y < 0.5$. This means that the steady state is stable in 75% of the cases. As ν_y increases from 0.5 to 1, the probability that $f_2 > 0$ drops linearly from 1 to 0. For $\nu_y = 1$, only 25% of the systems are stable because now f_1 must be positive. This explains the linear drop of the stability curve from 0.75 to 0.25.

4.6 Bifurcations

We evaluated how often each of the four different types of local bifurcations occurs as a migration scale parameter is increased from 0 to 1, averaging over 10^7 parameter sets and over the four different migration scale parameters. Varying the migration scale parameter means varying the relative contribution of migration to the population growth and loss terms. This approach is different from merely increasing a migration rate in an explicit model and therefore leads to somewhat different statistics of bifurcations. The comparison with explicit models will be provided in the next section. The result is shown in Fig. 28.

The dominant bifurcation is always the saddle-node bifurcation. We see all four different types of bifurcations in models *Stand* and *Standx* as well as models *Growth* and *Growth2*. These are the only models in which migration responds to population changes differently for predators and prey. The models with diffusive migration (*Diff* and *Jans*) do not show wave instabilities. For the scenarios of class II we see barely any bifurcations, with the exception of the models *Huang*, *HuangR* and *Growth2*, though model *Huang* only exhibits saddle-node and model *HuangR* saddle-node and Turing bifurcations. This is consistent with the earlier analysis of stability. If migration does not cause a change in stability, there can be no bifurcations that are induced by migration. Comparing these results with Tab. 7, we see that there is some correlation between the amount by which migration decreases stability and the number of bifurcations that occur.

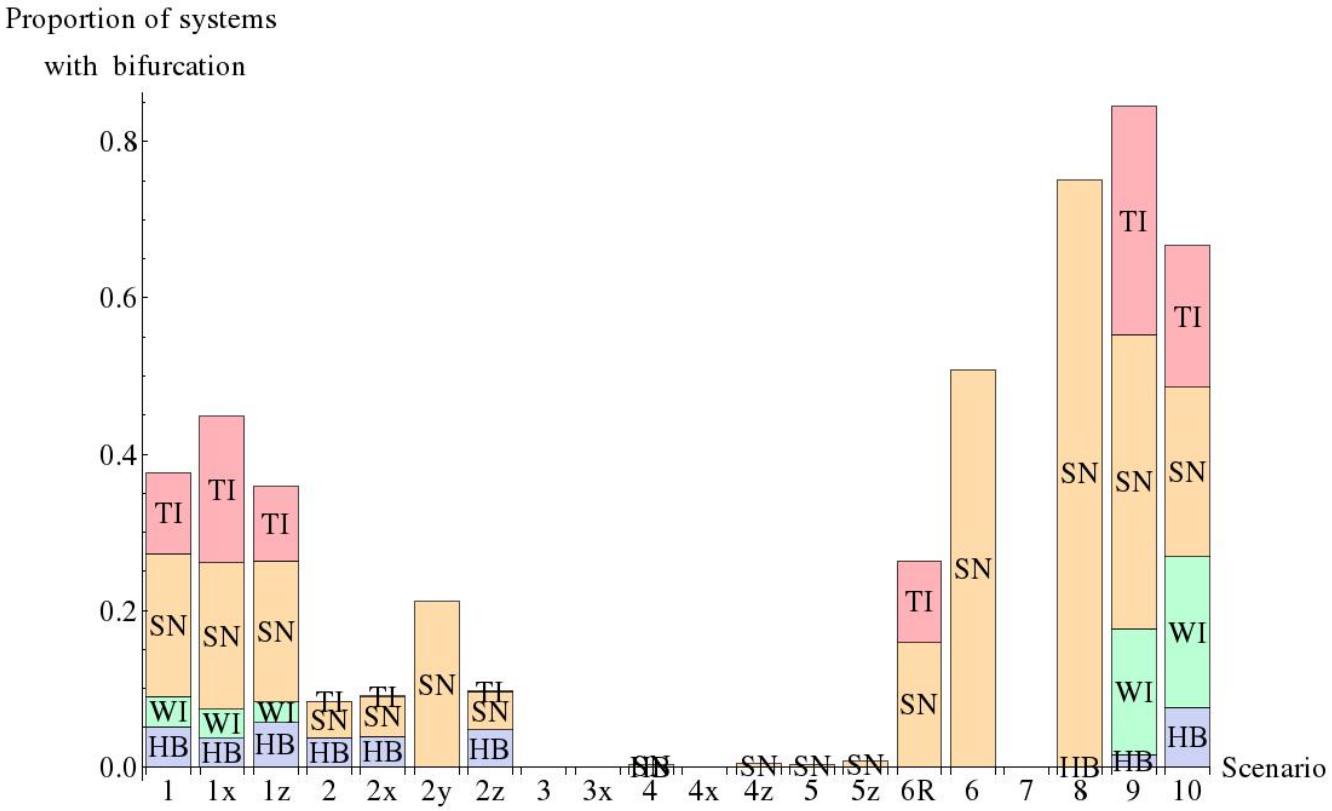

Figure 28: The statistics of the four types of bifurcations for all considered models for 10^5 random parameter sets. The numbers on the x-axis denote the model (see Tab. 6). Since more than one type of bifurcation can occur as a scale parameter is increased from 0 to 1, the maximum total height of each bar is 4. The symbols are SN for saddle-node bifurcation, HB for Hopf bifurcation, TI for Turing instability and WI for wave instability. (See Section 2.9.4 for the definition of the bifurcations.)

By evaluating the bifurcation statistics separately for different intervals of the migration scale parameters, we found that generally Hopf bifurcations and wave instabilities occur more often for intermediate values of the scale parameters, while saddle-node bifurcations and Turing instabilities occur more often for large and small values. Figs. 29 and 30 show the corresponding histograms for selected models. For these figures, we evaluated additionally the information whether the used parameter set would produce a stable steady state without migration, i.e. with all migration scale parameters set to zero. This subset of the total number of bifurcations is marked by the violet colour.

Saddle-node bifurcations are more likely to occur at high migration values, whereas Turing-bifurcations tend to low and mid values. The steep increase of the number of saddle-node bifurcations for ρ close to 1 is expected since large loss terms can lead to predator extinction, i.e., to a transcritical bifurcation, which is identical to a saddle-node bifurcation in the generalized modelling approach. Synchronous Hopf bifurcations are usually found at mid-to-high levels of migration while wave-instabilities prefer mid-to-low migration. Intermediate values of the migration scale parameters imply that the interactions between populations within and between patches are equally important for the dynamics, which in turn means that the phase space in which the dynamical trajectories of the system evolve is four-dimensional. Without migration or with very fast migration the phase space is only two-dimensional, with less complex dynamics and less oscillations.

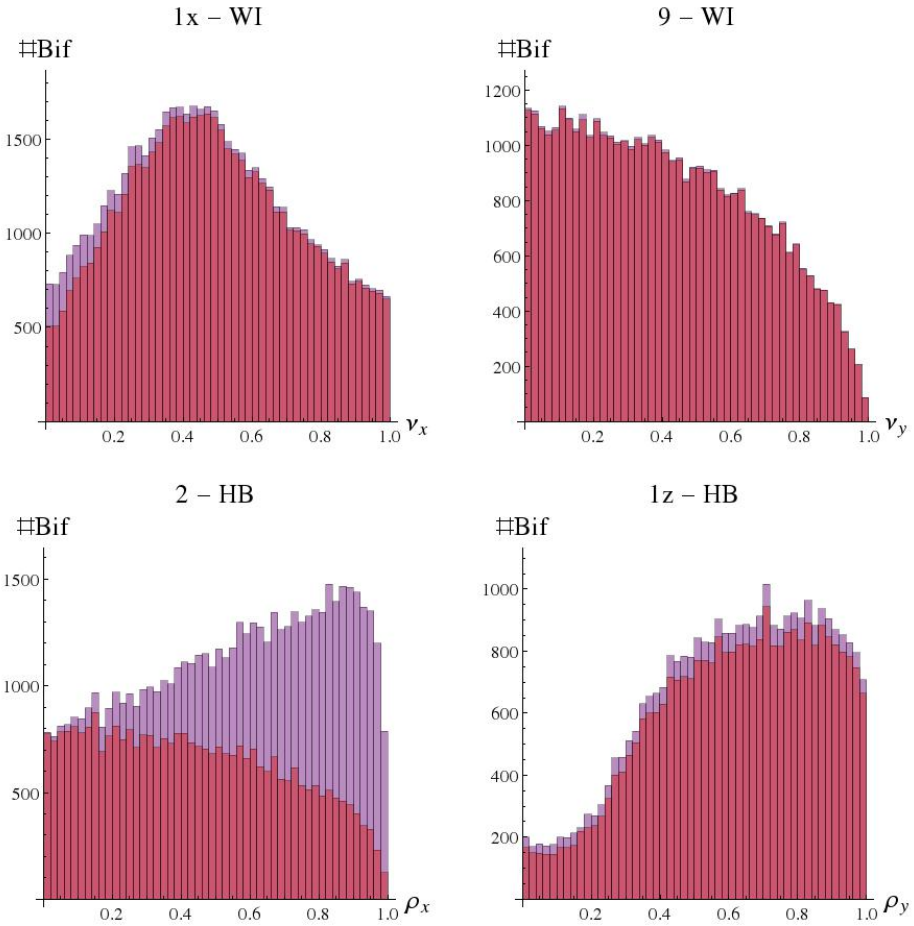

Figure 29: The number of bifurcations into oscillating states in dependence of the migration scale parameters, in a sample of 10^6 random parameter sets. The symbols above each graph denote the model (see Tab. 6) and type of bifurcation("HB" stands for synchronous Hopf bifurcation and "WI" stands for wave instability). The shape in the top left graph with most bifurcations at mid-range values is found for 38 percent of cases. Other forms that are seen less often (predominantly in models with complex migration dynamics) are shown in the other histograms. The darker bars indicate the part of parameter sets with a bifurcation that would have been stable without any migration.

It has been noted that prey pursuit or predator evasion can decrease synchrony (Li et al., 2005). The scenarios *ElAbdllaoui*, *Growth* and *Growth2* implement such types of migration. Model *ElAbdllaoui* shows more synchronous Hopf bifurcations at high values of the migration scale parameters. Models *Growth* and *Growth2* have no clear trend.

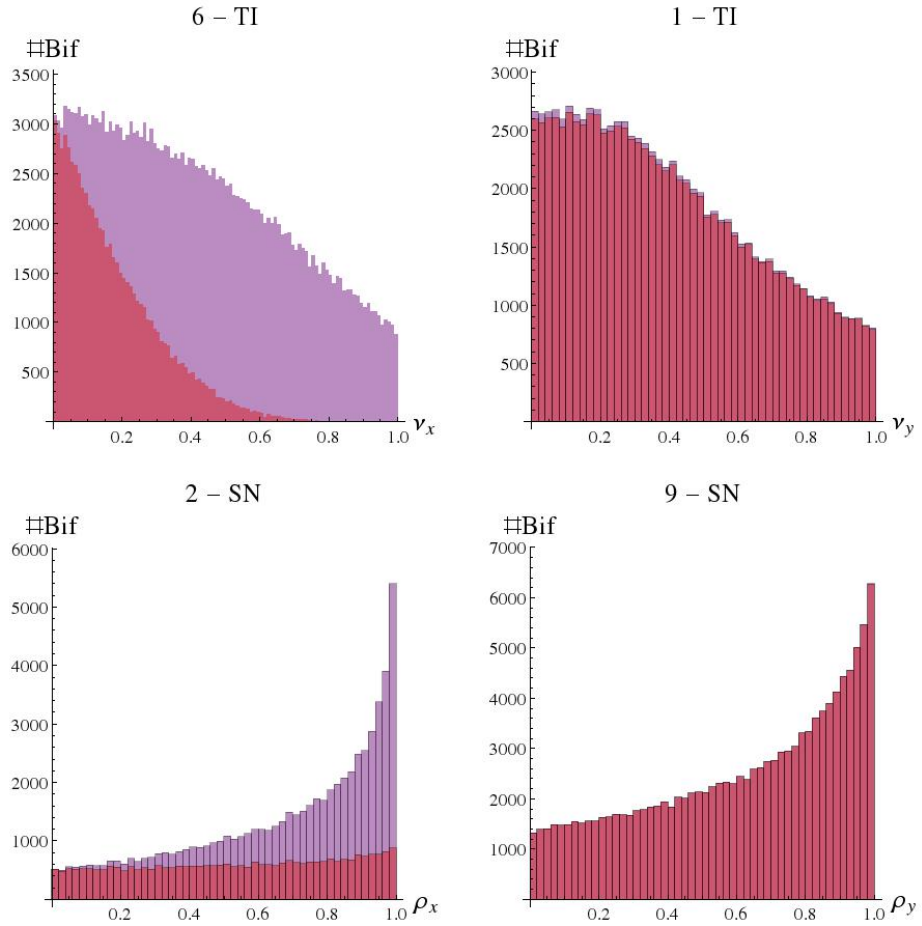

Figure 30: Histograms of the number of saddle-node and Turing bifurcations over migrations scale parameters. The majority of bifurcations occur for scale parameters close to zero or 1. We sampled 10^5 random sets of parameters per model. The symbols above each graph denote the model (see Tab. 6) and type of bifurcation ("SN" stands for saddle-node bifurcation and "TI" stands for Turing instability). The majority of bifurcations, 67 percent of total cases, occur for scale parameters close to zero or 1. The darker bars indicate the part of parameter sets with a bifurcation that would have been stable without any migration.

4.7 Comparison with Results from Explicit Models

Many of the models listed in Table 6 were investigated earlier using explicit population dynamics models. These are the models by (Mchich et al., 2007), (Jansen, 2001, 1995), (Abdllaoui et al., 2007), (Abrams and Ruokolainen, 2011) and (Huang and Diekmann, 2001). Our approach provides a different perspective and gives general insights. It thus complements the findings of models that use specific functional forms for the different gain and loss terms. In order to illustrate the respective strengths of the different approaches, we compare in the following our results with those publications. We have to keep in mind that our study was confined to homogeneous systems with identical patches and to local bifurcations of steady states, while the cited publications often include heterogeneous systems and global bifurcations as well.

(Jansen, 1995) sees no dependence of the bifurcation condition on migration for the homogeneous steady state with both species present on both patches. In our study, we found (few) saddle-node and Hopf bifurcations in this model when the migration scale parameters are changed. Such bifurcations are also present in the model by (Jansen, 1995) and are crossed when the parameters that characterize

the in-patch dynamics are changed. This holds also for the follow-up paper from 2001 (Jansen, 2001). This nicely illustrates the fact that changing one parameter in the generalized approach is not equivalent to changing one parameter in a compatible explicit model, but to changing several parameters simultaneously, and vice versa. For instance, increasing the migration scale parameter ν in our approach means that a larger proportion of biomass increase is due to immigration, and that the biomass increase due to resource consumption decreases. In contrast, increasing the migration rate in an explicit model while keeping all other parameters fixed means that migration rate increases without a change in other processes. Varying scale parameters provides more generic insights as they refer to relative and not to absolute quantities. It is of course possible to change the parameters in an explicit model in a fixed relation and thus to obtain the same kind of insight.

(Mchich et al., 2007) find a stabilizing effect of migration for a situation where the prey migrates with a rate that depends on predator density. This study uses a Lotka-Volterra model, for which a linear stability analysis is exact, and evaluates it in the limit of rapid migration. Our study always gives eigenvalues with a real part of zero for the Jacobian, since we look at homogeneous systems. The Hopf bifurcations observed by (Mchich et al., 2007) are due to the fact that they investigate the inhomogeneous case where the parameters on the two patches are different. The study by (Abdllaoui et al., 2007) is similar to that by (Mchich et al., 2007), but uses a type II functional response and finds that migration can create limit cycles. We see a large percentage of stable webs, with Hopf bifurcations occurring only rarely. This leads to the conclusion that the majority of Hopf bifurcations seen by (Abdllaoui et al., 2007) is due to the fact that they study an inhomogeneous system.

(Abrams and Ruokolainen, 2011) state that adaptive migration produces frequent anti-synchronous limit cycles. Our study generally shows wave instabilities for scenarios with adaptive migration (models *Stand*, *Growth*), and such wave instabilities lead to anti-synchronous limit cycles. However, we did not find wave instabilities for model *Abrams*. Since (Abrams and Ruokolainen, 2011) do not show bifurcation diagrams, there is no contradiction between their findings and ours. They focussed on parameter ranges where local patch dynamics is oscillatory. It is well possible that in this model anti-synchronous oscillations result only (or almost always) out of inhomogeneous fixed points or by non-local bifurcations.

(Huang and Diekmann, 2001) investigate the case that predators cannot migrate while handling prey, which means that predators migrate at low prey densities but become immobile for large prey densities. By performing a linear stability analysis, the authors found a stable steady state for a wide range of parameters, which can become unstable by Hopf bifurcations and saddle-node bifurcations. We only find saddle-node bifurcations when we vary the migration scale parameters. However, we find also Hopf bifurcations when we vary additionally one of the local parameters. This again illustrates the fact that changing one parameter in an explicit model corresponds to changing several parameters in the generalized model, and vice versa. Furthermore, (Huang and Diekmann, 2001) state that anti-synchronous oscillations are always unstable if they exist, in agreement with our result that a stable steady state cannot become unstable by a wave instability.

To conclude this section, we would like to point out that a model with explicit population dynamics explores only a small subspace of the general class of models that are compatible with what is known from empirical systems. In particular, it introduces functional dependencies between the parameters used in the generalized modelling approach and thus limits the space that can be explored. Other explicit models would lead to somewhat different functional relations between the corresponding generalized parameters and would thus explore a different region of the space of possibilities. For instance, the model by (Abrams and Ruokolainen, 2011) does not show wave instabilities, which do however occur in models that belong to the same overall class of systems that have a growth-rate dependent migration.

4.8 Conclusions

In this section we studied the impact of dispersal on a general class of two patches two species predator-prey system. We used the approach of generalized modelling, which allows to investigate the stability of the system without restricting the kinetics to specific functional forms. In comparison to previous studies we are thus able to provide a broader overarching perspective.

Our analysis confirms that dispersal generally decreases the local stability of the system. Although, dispersal creates benefits, such as the rescue effect (Brown and Kodric-Brown, 1977), not studied here, it does not generally promote the dynamical stability of the system. Thus dispersal may lead to undesirable dynamics, causing for instance increased spatial, temporal, or spatio-temporal variability. However, we found also large parameter regions in which dispersal increases the stability and may thus help avoiding such undesirable dynamics.

For the case of identical patches we were able to compute the thresholds at which destabilization occurs analytically. Furthermore, we used a numerical sampling procedure for a broad survey of the impact of parameters of the generalized model. By restricting the parameters of the generalized model to appropriate ranges we were able to analyse 19 different scenarios.

In a number of scenarios the impact of dispersal is very weak. For instance if dispersal occurs completely randomly it does not have a notable effect on stability. Moreover, density independent dispersal only affects stability if the growth of the prey shows effects of saturation. Finally, superlinear mortality rates, such as quadratic mortality, have a stabilizing effect that can be much stronger than the effect of dispersal, to an extent that dispersal does not generally lead to a destabilization of such systems. These findings are consistent with (Tromeur et al., 2013), who studied the dynamics of a single population in a system with many patches. In contrast to this previous study we found that dispersal can in certain cases be stabilizing in the two species system. The parameter regions in which a positive effect of dispersal on stability are observed are much wider when dispersal of a given species depends on the densities of other species in the system.

While we studied only two patches, our results allow for some extrapolation to larger systems. We need to distinguish between pattern forming (Turing, wave) and non-pattern forming (Hopf, saddle-node) instabilities. In agreement with (Abrams and Ruokolainen, 2011) we find that pattern forming instabilities can only occur in systems with non-random dispersal, a result that should hold also in systems with more patches.

Using general insights into the dynamics of networks (Do et al., 2012; MacArthur et al., 2008) we can say that non-pattern-forming instabilities cannot depend on network structure. If dispersal affects these instabilities then it does so only because it shifts the operating point of the system and introduces new nonlinearities, e.g. from losses during migration. Both of these effects can be captured faithfully in single patch models, where migration effects are modelled as additional terms.

By contrast, pattern forming instabilities depend sensitively on network structure and thus can only be analysed if the spatial structure at hand is captured in the model. Previous results (Do et al., 2012) suggest that the symmetric pair of patches studied here is a particularly unstable configuration that promotes pattern-forming instabilities, while larger, less symmetric systems should be tentatively more stable.

Perhaps most importantly our findings illustrate the complex nature of dispersal effects. In the simplest scenarios dispersal is neither stabilizing nor destabilizing, but the interplay of dispersal with other nonlinearities in the system can increase or reduce stability. To fully understand dispersal effects in complex food webs, and in particular pattern forming instabilities, we will eventually have to study large, many patches, many species systems. For addressing this challenge, the generalized modelling approach, used here, could be a valuable tool.

5 Heterogeneous Two Patches Predator-Prey Systems

The dynamics and stability of ecological networks are strongly influenced by spatial effects. In particular, dispersal and habitat heterogeneity are generally believed to have positive effects on the survival of populations, however, the multitude of possible mathematical models hampers a systematic investigation. Here, we address this topic by using a generalized modelling approach that is capable of exploring many different types of models within the same framework. We include trophic interactions and spatial structure in the most basic form by using a predator-prey system on two habitats, and study the stability of steady states as well as the types of bifurcations and the extent of synchrony of the two habitats, comparing a spatially heterogeneous with the homogeneous model that has been introduced in the previous section. We find that while overall stability can differ drastically between homogeneous and heterogeneous systems, the influence of model parameters on stability is qualitatively similar. Heterogeneity has the strongest effect on stability when migration is adaptive. Furthermore, heterogeneous systems are more likely to show oscillating dynamics, and oscillations are more likely to be anti-synchronous compared to homogeneous systems.

5.1 Motivation

In this part of the thesis, we will use the generalized modelling approach to study the simplest possible class of models that include trophic interactions, dispersal, and heterogeneity, namely a predator-prey system on two habitats (which we will call "patches" in the following). In the previous section Sec. 4, which is based on (Gramlich et al., 2016), we investigated the homogeneous case where both patches are in the same steady state and have the same parameter values. However, empirical systems as well as many models with explicit population dynamics show steady states that are heterogeneous. We will study how heterogeneity affects the stability of equilibria, their correlation with the type and strength of migration, and the synchrony between the patches. The latter will be studied by considering Hopf and saddle-node bifurcations that are caused by migration. We will find in particular that heterogeneity has the strongest effect on stability when migration is adaptive, that heterogeneous systems are more likely to show oscillating dynamics, and that oscillations are more likely to be anti-synchronous compared to homogeneous systems. This demonstrates that similar findings obtained with explicit and specific models are generic, as they occur in the majority of the 23 models investigated by us. We expect that the general message of our study will also apply to systems with more patches, as the general effect of including dispersal is taken into account as soon as there are two patches, see also (Jansen and de Roos, 2000).

This section is based upon (Gramlich, 2017) which was created in collaboration with Barbara Drossel who provided general feedback and advice.

5.2 Generalized Modelling

The derivation of the generalized formulation is explained in detail in the theoretical basis (see Sec. 5). The fundamental difference between the homogeneous system in the previous section is that, for a homogeneous system, the scale parameters and elasticities are the same on both patches but for a heterogeneous system, they are different. This means we have to keep indices for the different patches for both scale and exponent parameters. The Jacobian has the form

$$\mathbf{J} = \begin{pmatrix} P_{1,1} & M_{1,2} \\ M_{2,1} & P_{2,2} \end{pmatrix} \tag{166}$$

with the matrix for the in-patch dynamics

$$\mathbf{P_i} = \begin{pmatrix} 1 & 0 \\ 0 & \alpha_i \end{pmatrix} \cdot \begin{pmatrix} \tilde{\nu}_i^X \phi_i - \tilde{\rho}_i^X \tilde{\delta}_i \mu_i^X - \tilde{\rho}_i^X \delta_i \gamma_i + \nu_i^X \hat{\omega}_{i,j}^X - \rho_i^X \omega_{j,i}^X & -\tilde{\rho}_i^X \delta_i \psi_i + \nu_i^X \hat{\kappa}_{i,j}^X - \rho_i^X \kappa_{j,i}^X \\ \tilde{\nu}_i^Y \gamma_i + \nu_i^Y \hat{\kappa}_{i,j}^Y - \rho_i^Y \kappa_{j,i}^Y & \tilde{\nu}_i^Y \psi_i - \tilde{\rho}_i^Y \mu_i^Y + \nu_i^Y \hat{\omega}_{i,j}^Y - \rho_i^Y \omega_{j,i}^Y \end{pmatrix} \tag{167}$$

and matrix for the dynamics for migration between patches

$$\mathbf{M_{i,j}} = \begin{pmatrix} 1 & 0 \\ 0 & \alpha_i \end{pmatrix} \cdot \begin{pmatrix} \nu_i^X \omega_{i,j}^X - \rho_i^X \hat{\omega}_{j,i}^X & \nu_i^X \kappa_{i,j}^X - \rho_i^X \hat{\kappa}_{j,i}^X \\ \nu_i^Y \kappa_{i,j}^Y - \rho_i^Y \hat{\kappa}_{j,i}^Y & \nu_i^Y \omega_{i,j}^Y - \rho_i^Y \hat{\omega}_{j,i}^Y \end{pmatrix}. \tag{168}$$

This does not necessarily mean that the original population dynamics equations contain different functions or different coefficients for different patches. It can also mean that an originally homogeneous system has settled on a steady state that is heterogeneous, i.e., has different population sizes on the two patches. We assume that the dynamics on both patches can be expressed by the same parameter intervals and therefore need only one interval for a parameter on both patches. The different models used in the following can be found in Tab. 8.

5.3 Proportion of Stable Systems

We created an ensemble of 10^7 systems for each of the classes presented in Tab. 8 implementing the heterogeneous case as well as the homogeneous case. For each realization of the ensemble the parameters were drawn uniformly from the respective interval ranges. For the homogeneous case the parameter values were identical on both patches, for the heterogeneous case they were independently chosen. The proportion of stable webs (PSW) is the ratio of parameter sets within an ensemble that have a stable steady state to the total number of sets within the ensemble. Our results for the first two groups of classes in Tab. 8 are shown in Fig. 31.

For homogeneous systems, stability of the two patches system is smaller than or roughly equal to stability without migration (i.e., for isolated patches). It can in fact be proven analytically that stability is limited by that of isolated patches (Brechtel et al., 2016).

For heterogeneous systems there are several classes for which the percentage of stable webs is higher with migration than without migration. These belong to the model classes *Diff* (with exception of *Diffx*) and *Jansen95*, all of which have diffusive dispersal. Otherwise, there are no systematic trends for the difference in stability between homogeneous and heterogeneous patches, and the difference between them as well as to the case without migration varies widely between the classes. Generally, classes with adaptive migration are less stable than those with diffusive migration.

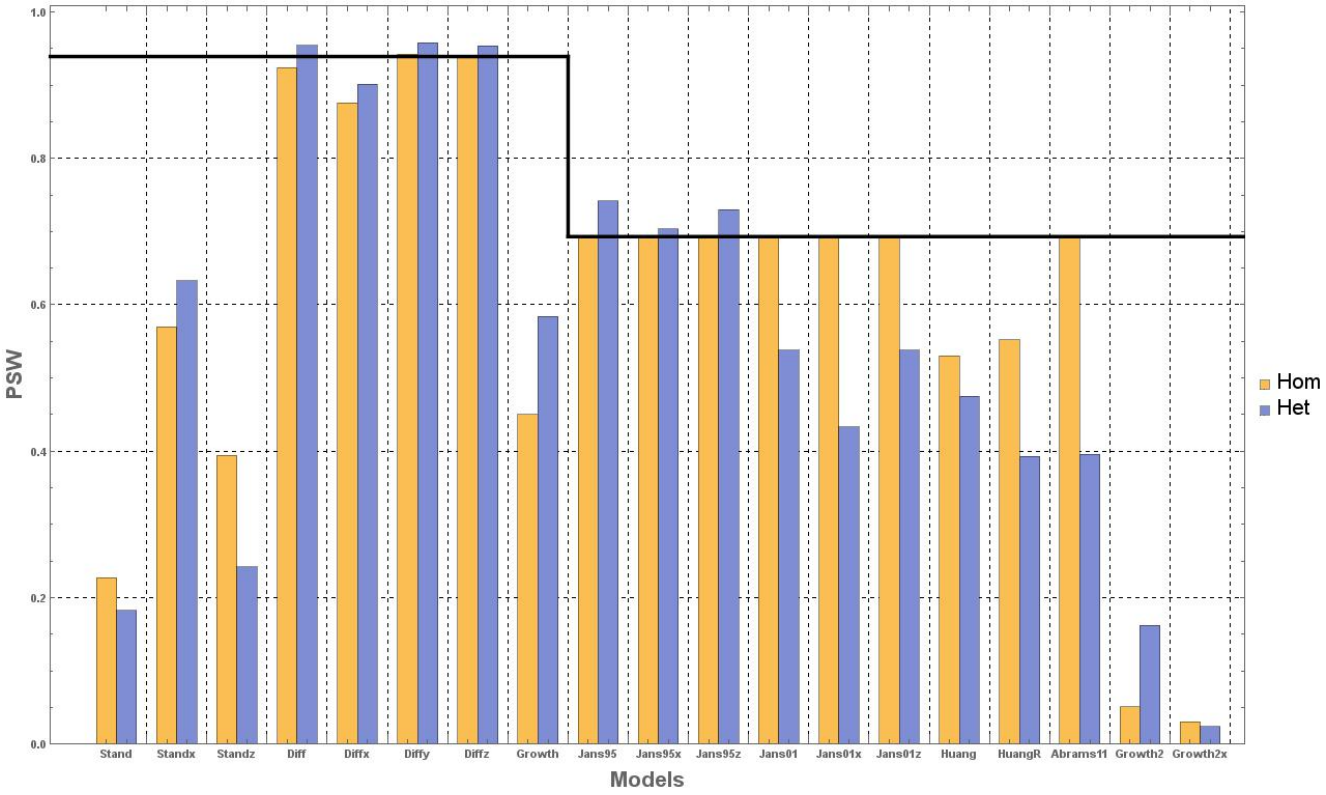

Figure 31: Comparison of the average stability of steady states for systems with and without migration. The percentage of stable webs (PSW) for homogeneous (yellow) and heterogeneous (violet) systems for group I (left of the vertical black line, from *Stand* to *Growth*) and II (right of the vertical black line, from *Jans95* to *Growth2*) are shown. The class names are on the x-axis and the PSW values are on the y-axis. The horizontal line indicates the PSW for isolated patches for groups I and II, showing that the PSW of homogeneous systems is never larger than that of isolated patches, and that the PSW of heterogeneous systems can exceed that of isolated patches only for classes with diffusive migration.

Scen.	ϕ	δ	γ	ψ	μ^X	μ^Y	α	ν^X	ν^Y	ρ^X	ρ^Y	ω^X	ω^Y	$\hat{\omega}^X$	$\hat{\omega}^Y$	κ^X	κ^Y	$\hat{\kappa}^X$	$\hat{\kappa}^Y$
(1) Stand.	$[0;1]$	$[0;1]$	$[0;2]$	$[0;1]$	$[1;2]$	$[1;2]$	$[10^{-3};10^{1}]$	$[0;1]$	$[0;1]$	$[0;1]$	$[0;1]$	$[-2;2]$	$[-2;2]$	$[-2;2]$	$[-2;2]$	$[-2;2]$	$[-2;2]$	$[-2;2]$	$[-2;2]$
(1x) Stand.	$[0;1]$	$[0;1]$	$[0;2]$	$[0;1]$	$[1;2]$	$[1;2]$	$[10^{-3};10^{1}]$	$[0;1]$	$[0;1]$	0	0	$[-2;2]$	$[-2;2]$	$[-2;2]$	$[-2;2]$	$[-2;2]$	$[-2;2]$	$[-2;2]$	$[-2;2]$
(1z) Stand.	$[0;1]$	$[0;1]$	$[0;2]$	$[0;1]$	$[1;2]$	$[1;2]$	$[10^{-3};10^{1}]$	$[0;1]$	$[0;1]$	ν^X	ν^Y	$[-2;2]$	$[-2;2]$	$[-2;2]$	$[-2;2]$	$[-2;2]$	$[-2;2]$	$[-2;2]$	$[-2;2]$
(2) Diff	$[0;1]$	$[0;1]$	$[0;2]$	$[0;1]$	$[1;2]$	$[1;2]$	$[10^{-3};10^{1}]$	$[0;1]$	$[0;1]$	$[0;1]$	$[0;1]$	1	1	0	0	0	0	0	0
(2x) Diff	$[0;1]$	$[0;1]$	$[0;2]$	$[0;1]$	$[1;2]$	$[1;2]$	$[10^{-3};10^{1}]$	$[0;1]$	$[0;1]$	0	0	1	1	0	0	0	0	0	0
(2z) Diff	$[0;1]$	$[0;1]$	$[0;2]$	$[0;1]$	$[1;2]$	$[1;2]$	$[10^{-3};10^{1}]$	$[0;1]$	$[0;1]$	ν^X	ν^Y	1	1	0	0	0	0	0	0
(2y) Diff	$[0;1]$	$[0;1]$	$[0;2]$	$[0;1]$	$[1;2]$	$[1;2]$	$[10^{-3};10^{1}]$	$[0;1]$	0	ν^X	0	1	1	0	0	0	0	0	0
(9) Growth	$[0;1]$	$[0;1]$	$[0;2]$	$[0;1]$	$[1;2]$	$[1;2]$	$[10^{-3};10^{1}]$	$[0;1]$	$[0;1]$	$[0;1]$	$[0;1]$	ϕ	ψ	ϕ	ψ	γ	0	γ	0
(4) Jans95	1	$[0;1]$	$[0;1]$	1	2	1	$[10^{-3};10^{1}]$	$[0;1]$	$[0;1]$	$[0;1]$	$[0;1]$	1	1	0	0	0	0	0	0
(4x) Jans95	1	$[0;1]$	$[0;1]$	1	2	1	$[10^{-3};10^{1}]$	$[0;1]$	$[0;1]$	0	0	1	1	0	0	0	0	0	0
(4z) Jans95	1	$[0;1]$	$[0;1]$	1	2	1	$[10^{-3};10^{1}]$	$[0;1]$	$[0;1]$	ν^X	ν^Y	1	1	0	0	0	0	0	0
(5) Jans01	1	$[0;1]$	$[0;1]$	1	2	1	$[10^{-3};10^{1}]$	0	$[0;1]$	0	$[0;1]$	0	1	0	0	0	0	0	0
(5x) Jans01	1	$[0;1]$	$[0;1]$	1	2	1	$[10^{-3};10^{1}]$	0	$[0;1]$	0	0	0	1	0	0	0	0	0	0
(5z) Jans01	1	$[0;1]$	$[0;1]$	1	2	1	$[10^{-3};10^{1}]$	0	$[0;1]$	0	ν^Y	0	1	0	0	0	0	0	0
(6) Huang	1	$[0;1]$	$[0;1]$	1	2	1	$[10^{-3};10^{1}]$	0	$[0;1]$	0	$[0;1]$	0	1	0	0	0	$-[0;1]$	0	0
(6R) Huang	1	$[0;1]$	$[0;1]$	1	2	1	$[10^{-3};10^{1}]$	0	$[0;1]$	0	$[0;1]$	0	1	0	0	0	$[0;1]$	0	0
(7) Abrams11	1	$[0;1]$	$[0;1]$	1	2	1	$[10^{-3};10^{1}]$	0	$[0;1]$	0	$[0;1]$	0	1	0	0	0	$-\hat{\kappa}^Y$	0	$[0;\frac{\lambda b}{4\pi}]$
(10x) Growth2	1	$[0;1]$	$[0;1]$	1	2	1	$[10^{-3};10^{1}]$	$[0;1]$	$[0;1]$	0	0	ϕ	ψ	ϕ	ψ	γ	0	γ	0
(8) El Abdl.	1	$[0;1]$	1	1	2	1	$[10^{-3};10^{1}]$	$[0;1]$	$[0;1]$	$[0;1]$	$[0;1]$	1	1	0	0	1	-1	0	0
(8x) El Abdl.	1	$[0;1]$	1	1	2	1	$[10^{-3};10^{1}]$	$[0;1]$	$[0;1]$	0	0	1	1	0	0	1	-1	0	0
(3) Mchich	1	1	1	1	0	1	$[10^{-3};10^{1}]$	$[0;1]$	$[0;1]$	$[0;1]$	$[0;1]$	1	1	0	0	$[0;1]$	0	0	0
(3x) Mchich	1	1	1	1	0	1	$[10^{-3};10^{1}]$	$[0;1]$	$[0;1]$	0	0	1	1	0	0	$[0;1]$	0	0	0

Table 8: The different models ("scenarios") analysed for in the section Sec. 5. The nomenclature is identical to the analogous table (Tab. 6) in section Sec. 4. We have added several subcases of existing classes. The nomenclature is as follows: In the text and the figures, the labels in the left column (number plus letter, or name) are used to name the scenarios. The letters x, y or z after the number indicate a migration rule where there is no migration loss (x), or where gain and loss are identical, $\nu_x = \rho_x$, which means that all migrating individuals arrive at their destination (y if this applies only to the prey and z if this applies to both species).

5.4 Correlation of Parameters with Stability

In order to study the influence of the different parameters on stability, we evaluated the Pearson product-moment correlation coefficient between each non-fixed parameter and stability for each class. The result for the migration scale parameters is shown in Fig. 32 for selected classes. The subclasses of type x, y, z show comparable trends to the more general classes.

In general, the correlation between a parameter and stability is qualitatively the same between most classes and between the homogeneous and heterogeneous case, and has the sign shown in Tab. 9. The local parameters behave qualitatively as in the isolated case. The most interesting observations that are not shown in the table are (i) For group I both μ_X and μ_Y have surprisingly little or no correlation with stability for isolated patches despite being usually associated with stabilizing effects; (ii) Usually heterogeneous systems have smaller absolute correlation values than homogeneous systems as can be expected due to the larger degree of randomness in the parameter values; (iii) The classes, where the correlation of migration scale or exponent parameters with stability differs most between the homogeneous and heterogeneous case, have adaptive migration.

Parameter	ν_x	ν_y	ρ_x	ρ_y	δ	γ	ϕ	ψ	μ_x	μ_y	α_y
Mostly stabilizing						×			×	×	
Mostly destabilizing	×	×	×	×	×		×	×			×

Parameter	ω_x	ω_y	κ_x	κ_y	$\hat{\omega}_x$	$\hat{\omega}_y$	$\hat{\kappa}_x$	$\hat{\kappa}_y$
Mostly stabilizing	×	×						
Mostly destabilizing			×	×	×	×	×	×

Table 9: The parameters and their primary influence on stability. A positive correlation with stability occurs for the exponent parameter γ of the functional response, the exponent of closure μ, and the exponent parameter associated with diffusive migration ω. These results are similar for homogeneous and heterogeneous systems.

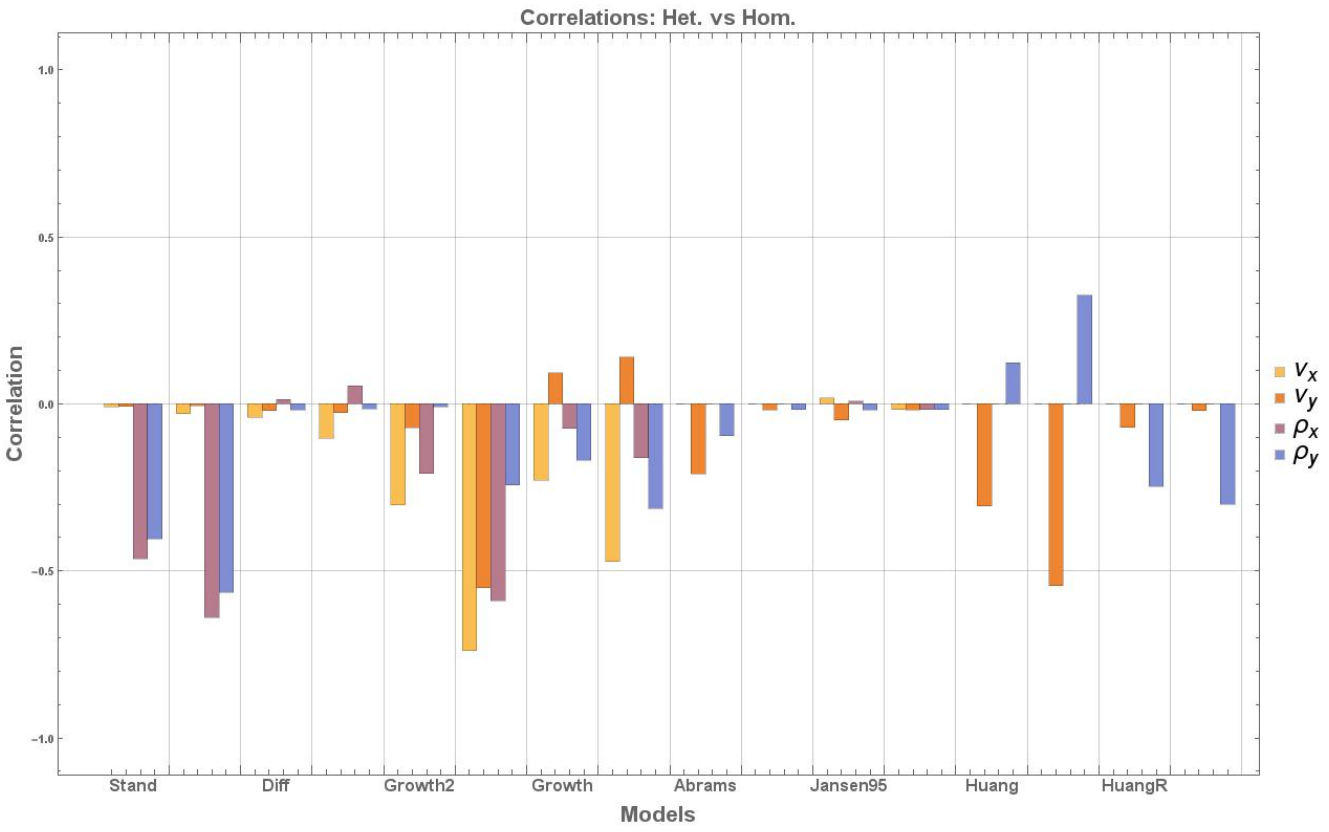

Figure 32: The correlation of the migration scale parameters with stability for selected classes. The set of bars directly above the class name is for heterogeneous patches, the following for homogeneous patches. On the y-axis are the correlation values and on the x-axis are the classes. The correlation of stability with migration is usually negative.

5.5 Bifurcations

In the following, we will not only evaluate the stability of fixed points (as given by the real part of the largest eigenvalue λ of the Jacobian), but also the types of bifurcations that occur when an equilibrium becomes unstable as a parameter is changed. There are two basic types of bifurcations, depending on whether the eigenvalue that becomes positive is real ($\lambda = 0$) at the bifurcation or complex ($\lambda = \pm i \cdot c$; $c \in \mathbb{R}$). The first case describes saddle-node bifurcations, where steady states are created or destroyed, causing sudden changes in population densities. The second case describes a Hopf bifurcation, which creates oscillations. Correspondingly, the eigenvector associated with the leading eigenvalue

$$v = \begin{pmatrix} v_1^x \\ v_1^y \\ v_2^x \\ v_2^y \end{pmatrix}$$

has real entries for a saddle-node bifurcation and has complex entries for a Hopf bifurcation. In the homogeneous case, the eigenvector entries corresponding to the two patches are either identical ($v_1^x = v_2^x$ and $v_1^y = v_2^y$) or have opposite signs ($v_1^x = -v_2^x$ and $v_1^y = -v_2^y$), while in the heterogeneous case the four entries of the eigenvector can in principle take any combination of real (for saddle-node bifurcations) or complex (for Hopf bifurcations) values.

When the entries for the two patches have opposite signs, the resulting bifurcations are analogous to pattern-forming bifurcations (Turing in the case of saddle-node bifurcations and wave instabilities in the case of Hopf bifurcations) known from continuous space. Since the biomass changes on the two patches compensate each other after such a bifurcation, the robustness of the system is higher than for a bifurcation where the biomass changes have the same sign on both patches. For heterogeneous systems, the phase difference between the two patches is not exactly 0 or π at a Hopf bifurcation, but we will nevertheless classify systems according to whether the phase difference is smaller or larger than $\pi/2$. If the phase difference between patches is smaller than $\phi/2$ we describe the dynamics of a system as in-phase; if it is larger we describe the dynamics as anti-phase.

5.6 Frequency of Bifurcations

Fig. 33 shows the number of Hopf and saddle-node bifurcations divided by the total number of bifurcations, for variation of the scale parameter ν_x. For the heterogeneous case there is a higher proportion of Hopf bifurcations across all scenarios compared to the homogeneous case. Nonetheless, saddle-node bifurcations are in general more abundant.

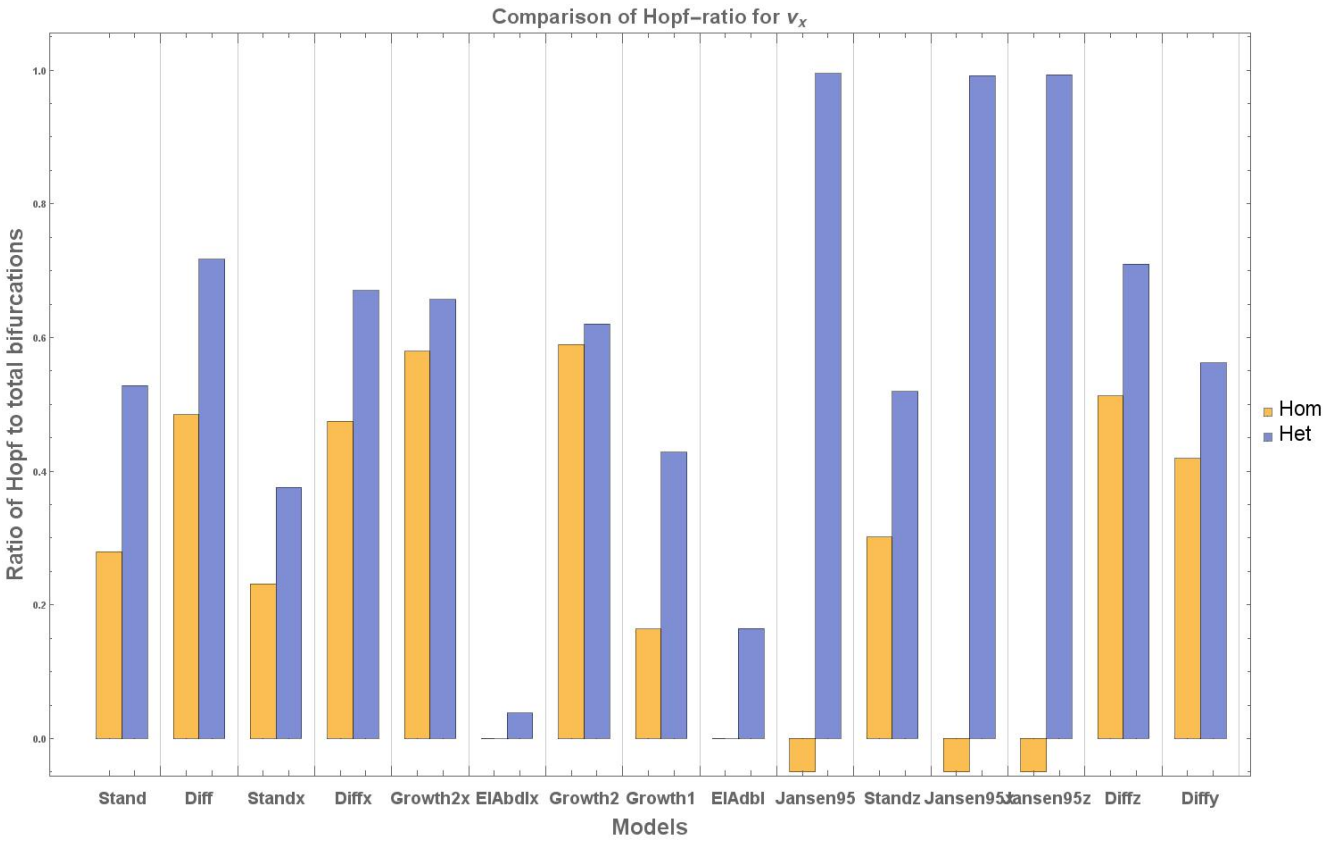

Figure 33: The ratio of Hopf bifurcations to total bifurcations for ν_x displayed over the different classes. A value -0.05 means that no bifurcations at all occurred for that parameter.

5.7 Phase Difference between Patches

In order to evaluate the extent of synchrony of population dynamics at Hopf bifurcations, we measured the phase difference between the two patches at the bifurcation point. To this purpose, we averaged the eigenvector elements of predator and prey for each patch,

$$\overline{v}_j = \frac{v_j^x + v_j^y}{2} = |\bar{v}_j| e^{i\phi_j},$$

and evaluated the phase difference $|\phi_1 - \phi_2|$. Fig. 34 shows the resulting distribution for four selected classes. All phase differences occur, although they frequently cluster around $\frac{\pi}{2}$ and 0 and occasionally around π. This behaviour can be explained by a rough estimate of the relationships between eigenvector elements for Hopf bifurcations. If one assumes that all entries of the Jacobian are of the order c and one also takes into account that the leading eigenvalue at a Hopf bifurcation has the form $\lambda = \pm i \cdot x$, then the relationships between the summed eigenvector elements can be expressed as

$$\frac{v_1 + v_2}{v_3 + v_4} = \frac{-2}{c^2(-i \cdot x + c)}. \tag{169}$$

The clusters around 0 or π occur for small values of x as the Hopf bifurcation becomes increasingly similar to a saddle-node bifurcation. For comparatively large values of x we tend towards zero but the real part of (169) decreases faster than the imaginary part which creates a phase difference of nearly $\frac{\pi}{2}$. The asymmetry of the phase differences around $\frac{\pi}{2}$ results from class-specific conditions.

In order to compare these results to the homogeneous case (where only phase differences of 0 and π occur), we classify Hopf bifurcation as mostly synchronous or anti-synchronous depending on whether the phase difference between the two patches is smaller or larger than $\frac{\pi}{2}$. We find that heterogeneous conditions increase the number of bifurcations that are mostly anti-synchronous, see Fig. 35.

We did a similar evaluation for saddle-node bifurcations. Since eigenvectors are real in this case, all phase differences are 0 (“in-phase”) or π (“anti-phase”) also for heterogeneous systems. Fig. 35 shows that the proportion of anti-phase saddle-node bifurcations tends to be smaller in the heterogeneous case as in the homogeneous case.

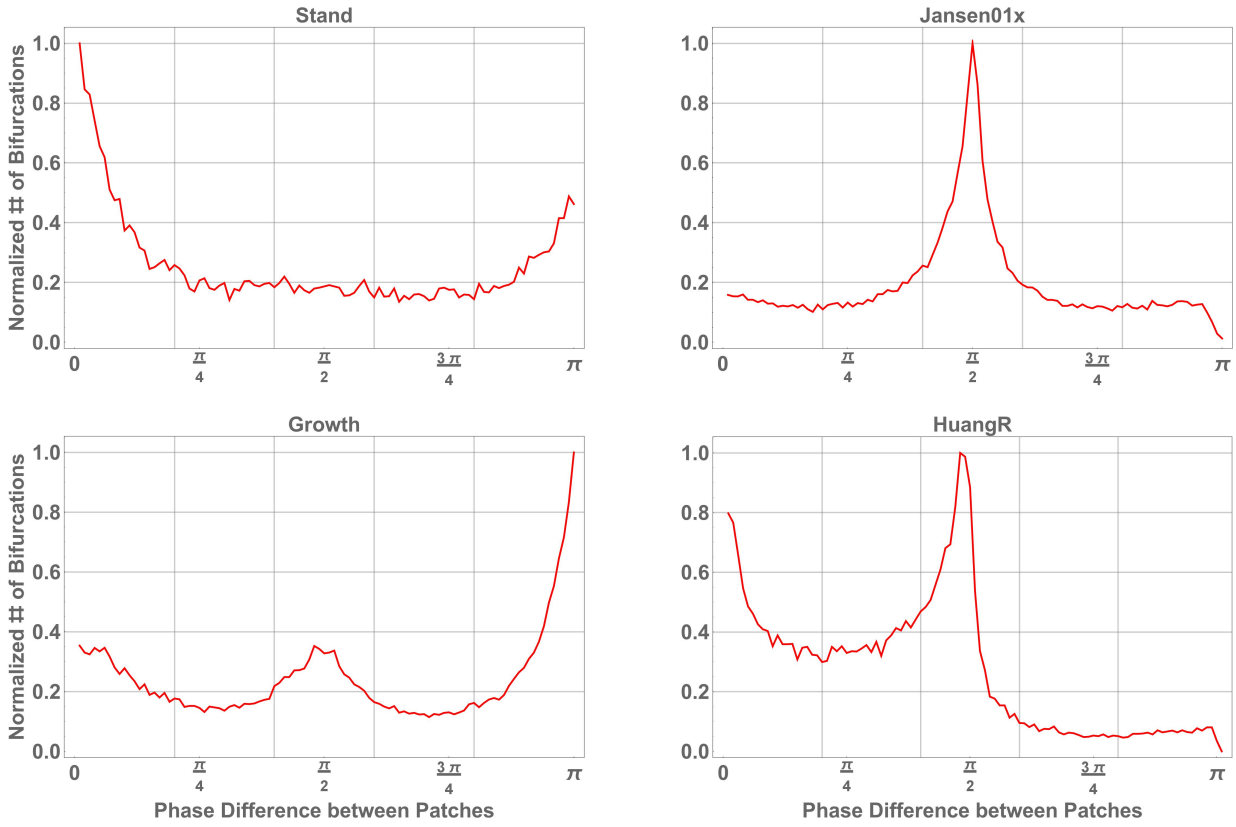

Figure 34: The distribution of the phase difference between patches for Hopf bifurcations for four selected classes. The x-axis shows the phase difference between patch dynamics and the y-axis the number of bifurcations normalized to the highest bin number. The classes are *Stand*, *Jansen01x*, *Growth* and *HuangR*. Each class has a distinct, characteristic distribution.

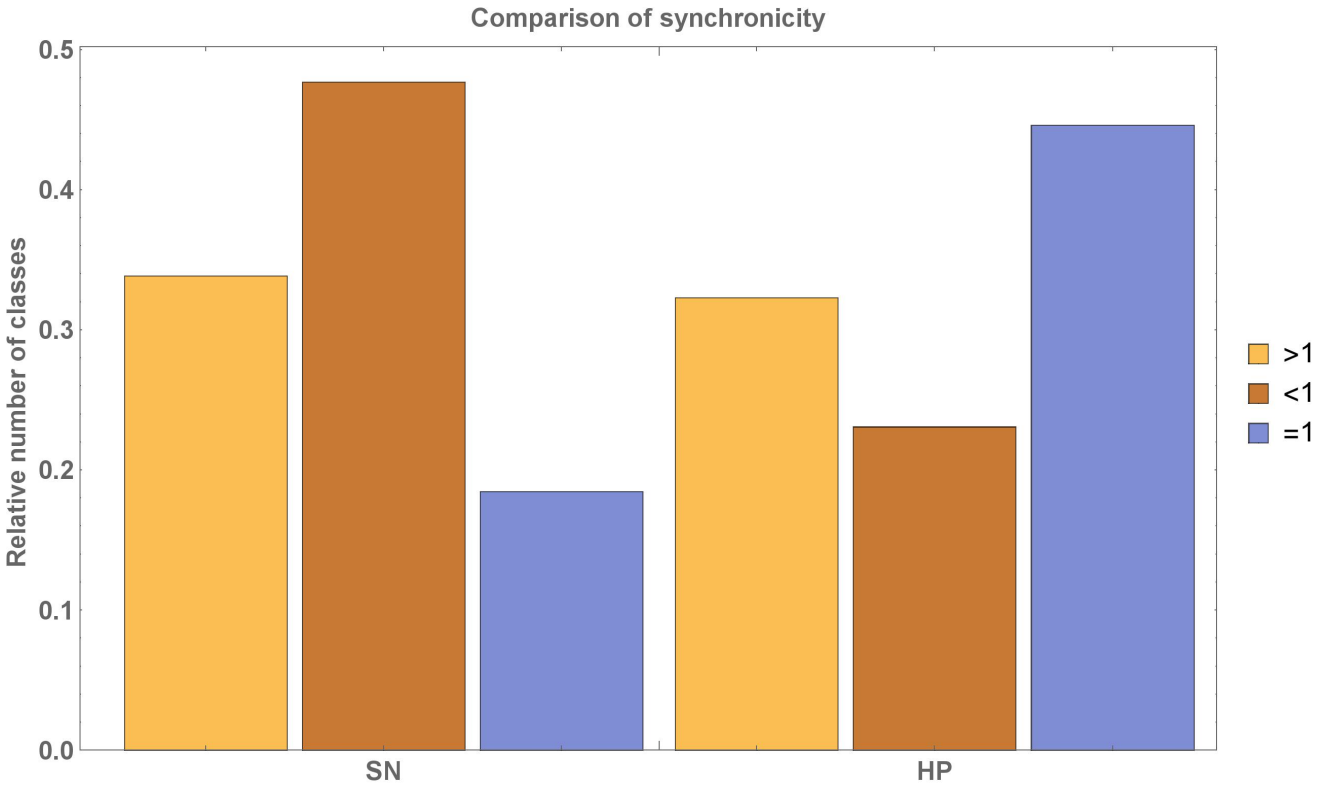

Figure 35: Proportion of classes for which the ratio of anti-synchronous to synchronous Hopf bifurcations (HP) and of in-phase and anti-phase saddle-node bifurcations (SN) increases from the homogeneous to the heterogeneous case. On the x-axis we have the saddle-node and Hopf bifurcations for the heterogeneous divided into more, less synchronous or equally synchronous compared to the homogeneous case and on the y-axis the ratio of models to which the description applies. ">1" means an increase of anti-synchronous or anti-phase behaviour compared to the homogeneous case, "<1" means a decrease and "$=1$" means no difference, which usually means that no anti-synchronous or anti-phase behaviour occurs. The data show that heterogeneous systems have more anti-synchronous oscillations and less anti-phase saddle-node instabilities.

5.8 Comparison with Results from Explicit Models

Many of the classes we studied with generalized modelling listed in Tab. 8 were investigated earlier using explicit population dynamics models. These are the models by (Mchich et al., 2007), (Jansen, 2001, 1995), (Abdllaoui et al., 2007), (Abrams and Ruokolainen, 2011) and (Huang and Diekmann, 2001). Our attempts to explain the finding of these authors with homogeneous classes in the previous section (the findings are published as (Gramlich et al., 2016)) failed in several instances as those studies included heterogeneous situations. We now revisit them with the understanding gained from the effect of heterogeneity on the stability of steady states. (Jansen, 1995) found limit cycles which are an indicator of the occurrence of Hopf bifurcations. We do indeed have a high percentage of Hopf bifurcations compared to saddle-node bifurcations. From the results in (Jansen, 1995), we expect asynchronous oscillations in our class *Jansen95*, and from (Jansen, 2001), where prey cannot migrate, synchronized behaviour for our class *Jansen01* for low migration rates and more asynchronous behaviour with intermediate levels of migration. We find asynchronous to synchronous oscillations for *Jansen95* which conforms qualitatively to the expectations.

For *Jansen01* bifurcation behaviour is most commonly either perfectly synchronized or in a wide range of asynchronous behaviour. This fits to the findings of (Jansen, 2001). (Abdllaoui et al., 2007) state that migration can create limit cycles in their model. We find that the number of Hopf bifurcations increases from negligible to single-digit percentages when we go from the homogeneous to the heterogeneous case, confirming that they can be caused by migration. (Abrams and Ruokolainen, 2011) state that adaptive migration produces frequently anti-synchronous limit cycles. We find for asymmetric parameters there are both saddle-node and Hopf bifurcations. While (nearly) synchronized dynamics are most frequent *Abrams* is one of the few classes that have a significant amount of bifurcations with anti-synchronous behaviour. (Huang and Diekmann, 2001) states that there is a stable equilibrium for a wide range of parameters and that there are Hopf bifurcations and wave instabilities, in addition to saddle-node bifurcations. In agreement with this, heterogeneity in the parameter sets of our investigations produces Hopf bifurcations as well as saddle-node bifurcations.

5.9 Conclusions

We have analysed the influence of heterogeneity on predator-prey systems on two patches that are coupled by migration and compare the results to the previous study on homogeneous systems (Gramlich et al., 2016). We used the generalized modelling approach that considers the dynamics near steady states without having to specify the explicit functional forms of the population dynamics or absolute parameter values. This permits the simultaneous investigation of many different general types of dynamics. Concordantly, we analysed 23 different classes of models, which are characterized by the ranges that the exponent parameters can take.

For the homogeneous case, dispersal exclusively leads to a decrease in overall stability compared to an isolated patch; for heterogeneous systems, we found a few classes where dispersal makes systems more stable, but only if it is diffusive.

Whether a parameter is positively or negatively correlated with stability is similar for homogeneous or heterogeneous systems. Nevertheless, going from a homogeneous to a heterogeneous system can lead to large changes in average stability. This illustrates that one can often extrapolate the qualitative but not the quantitative behaviour of a simplified system to a more complex system (Jansen and de Roos, 2000). For classes with adaptive migration, the extent of correlation between stability and migration parameters changes considerably between the homogeneous and the heterogeneous case. This does not happen in classes with diffusive migration. In this light, explicit models that want to explore the impact of heterogeneity on meta-food webs should consider using adaptive migration.

While our study suggests that dispersal seems to have a universal destabilizing effect on steady states, its influence on robustness, which is more relevant for species survival, is less clear. Going from homogeneous to heterogeneous systems increases the relative amount of Hopf bifurcations. The oscillations are more anti-synchronous for heterogeneous systems and there is a wider parameter interval of non-synchronous behaviour in general as most oscillations are not perfectly in-phase even if we count them as mostly in-phase. This can means that spatial heterogeneity probably increases robustness as total biomass fluctuations are dampened by non-synchronous dynamics. This fits together with expectations for natural systems, which always have some form of heterogeneity (due to local climate, geography, species composition, etc.) and are usually found to be robust to small perturbations (Kitano, 2004). Our finding that saddle-node bifurcations are more in-phase in heterogeneous systems may counter the stabilizing effect of heterogeneity, but since Hopf bifurcations become much more frequent in heterogeneous systems, their combined effect on robustness can be expected to be positive.

Finally, we want to point out that even when oscillations are synchronous they need not be destabilizing. Even though most research suggest a positive effect of less synchronization for species persistence, there is also some indication that synchronized behaviour can conceivably improve species persistence (Blasius et al., 1999). For phase-locked oscillations with weakly correlated and/or chaotic amplitudes there can be travelling-wave phenomena that ensure species survival on large spatial scales. Certainly, more research into the different ways in which oscillations in spatially extended food webs relate to stability is needed.

6 Food Webs on Many Patches

Diffusion-driven pattern formation, comparable to Turing instabilities, can be found in networks of networks systems; a subset of multilayer systems. One can show that pattern-formation in continuous space and in networks can be based on the same principles resulting in a master stability function which expresses the dynamics of the networks-of-networks system. We apply this insight to the example of a spatial distributed food web in terms of the generalized method. This meta-food web model incorporates many species with complex predator-prey interactions as well as dispersal across multiple habitats. Using the master stability function we show the impact of the underlying spatial network on the stability of the meta-food web and the capacity of this method for use in non-trivial settings in ecology and for comparable networks-on-networks scenarios. Furthermore we give reasonable boundaries for the interval of analysis of the master stability function based upon eigenvalue approximations and provide statistical insights on several properties like synchronization of species, stability and behaviour of spatial modes.

This section is based upon a collaboration with Andreas Brechtel, Daniel Ritterskamp, Barbara Drossel and Thilo Gross (Brechtel et al., 2016) and the pictures Fig. 37, 38, 39, 51 have been taken from that paper. The design of these pictures has been done primarily by Daniel Ritterskamp and Thilo Gross with significant contributions by Andreas Brechtel for figures 51 and 38. Thilo Gross and Barbara Drossel have done much work to properly place this work in context of other research. Thilo Gross has provided the didactic built from diffusion in continuous space to diffusion in discrete networks. Andreas Brechtel's research on grid networks has sparked the initial idea that a master stability equation could be found, Barbara Drossel proved that it applies to wide range of systems and Brechtel provided the final polished derivation of the master stability equation. Andreas Brechtel also performed the explicit simulation of non-steady state behaviour in Fig. 51. The author of this thesis provided the derivation for the eigenvalue limits, the food webs and coupling matrices used for the figures 37, 38, 39, all numerical simulations regarding stability and behaviour at the steady states and all interpretation, discussion and graphical representation regarding the eigenvalue approximations and numerical simulations.

6.1 Motivation

In this section we focus on the description of meta-food webs with multiple species and patches in varying spatial configurations. The spatial network made up by patches which host food webs represents a so called multi-layer network. We have two distinct networks: One which defines the dispersal links and one which defines species interaction. This type of multi-layer network is called networks-on-networks. We explain how one can apply the principles of diffusion in continuous space to the derivation of diffusion on networks-(on-networks) which is almost completely analogous. This allows for a formulation of a master stability function which gives us a powerful tool in the study of stability.

Master stability function approaches have historically been used on systems of coupled oscillators (Pecora and Carroll, 1998; Arenas et al., 2008) with primary focus on synchronization between oscillators (Pikovsky et al., 2001). The field of multi-layer networks is quite active (Parshani et al., 2010; Buldyrev et al., 2010; Bashan et al., 2013; De Domenico et al., 2015) and many recent research paper have shown interest in synchronization on multilayer networks (for example (Asllani et al., 2014; De Domenico et al., 2014; Zhang et al., 2015; Kouvaris et al., 2015; del Genio et al., 2016; Sevilla-Escoboza et al., 2016; Tang et al., 2016; Leyva et al., 2017)). It is not surprising that there were several attempts at using a master stability approach in multi-layer network research (De Domenico et al., 2014; Zhang et al., 2015; del Genio et al., 2016; Sevilla-Escoboza et al., 2016; Tang et al., 2016; Leyva et al., 2017). These papers focused on inter-layer dynamics and used the master stability function to describe coupled oscillators mostly in the form of limit cycles. We, in contrast, use the master stability function approach in combination with the generalized method which is explicitly used at and for steady states of a system.

The network-on-network systems in question are ecological multi-species multi-patch models. The central question of current and past research in ecology is how biodiversity is maintained, if complexity by itself destabilizes (random) food webs (May, 1972b)(McCann, 2000). Attempts to find an explanation for this apparent disjunction between simple mathematical assumptions and the obvious lushness of biological life usually take two forms. On the one hand there is the search for stabilizing properties of food webs that are clearly not simply random (McCann, 2000; Gross et al., 2009; Kartascheff et al., 2010). The complexity of species interaction makes analytical results hard to come by and simulations, while common (McCann, 2000), are limited by the differences in timescales between the trophics levels; making simulations for large food webs often nearly infeasible.

On the other hand there is the effect of spatial distribution on biodiversity. From meta-populations, a single species scattered across space(Levins, 1969b; Yeakel et al., 2014b; Tromeur et al., 2016), to simple meta-communities of competing species up to predator-prey interactions (Pillai et al., 2010, 2011; Ristl et al., 2014; Gramlich et al., 2016; Barter and Gross, 2016; Mougi and Kondoh, 2016) there has been a trend to more complex interaction but the combination of spatial effects with increasing complexity in species interaction is limiting either the number of habitats or species.

One of the essential benefits of the work presented here is the relative ease with which comparably large and interaction rich meta-food webs can be constructed and analysed for spatial networks of any size. This is possible in part thanks to the use of the generalized food web model (Gross and Feudel, 2006; Gross et al., 2009; Gramlich et al., 2016) which we extend to include dispersal on discrete spatial networks. By concentrating on the homogeneous steady states we can simplify the system in such a way that a single master stability function contains all information about potential stability of a meta-food web on any given spatial network configuration and at what parameter values bifurcations due to spatial factors could occur. Additionally we provide limits for the master stability function beyond which no change in stability can occur.

We begin with a comparison of diffusion in continuous space and discrete networks and then extend the analogy to diffusion-driven instabilities (see Sec. 6.2) and how meta-food webs with equal species densities on all patches can be described in a similar manner (see Sec. 6.3). We then show this results in a master stability function for networks of this particular structure (see Sec. 6.4) which gives us a single function that governs the stability of the entire meta-community. Using two types of approximations we provide limits for the interesting range of the master stability functions for different conditions (see Sec. 6.6, 6.7 and 6.8). We use the ecological model introduced in section 6.3 for numerical simulations and show exemplary results, e.g. diffusion-driven instabilities, as well as general statistical data.

6.2 Diffusion on Networks: Continuous to Discrete Domains

For didactic reasons we precede the main segments with a reminder of the relationship of the Laplace matrix and the Laplace operator and their roles in the description of diffusion on networks. If we consider a continuous space and $X(x,t)$ as the density of particles or agents we can write

$$\dot{X} = c\,\triangle X. \tag{170}$$

The parameter c is a diffusion constant and $\triangle$ is the Laplace operator. We can give the solution to Eq. 170 as

$$X(x,t) = \sum_n a_n \mathrm{e}^{c\kappa_n t}\, v_{\boldsymbol{n}} \tag{171}$$

with κ_n and $v_{\boldsymbol{n}}$ as the eigenvalues and eigenvectors of the Laplace operator. The coefficients a_n are based upon the initial conditions of the system and geometric form. If the domain in which the agents or

particles diffuse is connected, we find that if enough time passes we reach a constant state as expressed by

$$\lim_{t\to\infty} X(x,t) = \text{const}. \tag{172}$$

Diffusion in networks is a well established line of research (Newman et al., 2006) and there are multiple types of diffusion processes that can be and were considered. We focus on one type that is rather straightforward in its assumptions.

A network of N nodes can be described by an adjacency matrix $\mathbf{A}$ with $A_{ij} = 1$ if nodes i and j are connected and $A_{ij} = 0$ otherwise. Let there be a number of agents on node i whose time evolution can be described by $X_i(t)$. Agents perform a random walk in continuous time and thus have a constant probability density (per time) to use each link for travel that is incident to its current node. The more links a node has, the faster does an agent leave a node. This assumption is true for some cases of animal behaviour (Hirt et al., 2017) and is frequently applied in e.g. microfluidics. The adjacency matrix $\mathbf{A}$ can be weighted to represent different likelihoods for an agent to use different links; for instance if links are to represent tunnels between nodes a lower weight could mean a smaller diameter of the connection.

For large agent numbers we can describe the behaviour of the system as

$$\dot{\boldsymbol{X}} = -c\mathbf{L}\boldsymbol{X} \tag{173}$$

where $\boldsymbol{X} = (X_1, \ldots, X_N)^{\mathrm{T}}$ describes the concentrations of the agents on the different nodes and $\mathbf{L}$ is the Laplace matrix of the network of nodes. The construction of the Laplace matrix is explained in Sec. 2.4.1.

The analogy between Eq. (173) and Eq. (170) is quite obvious. We only need to change the sign for the Laplacian when we switch from operator to matrix and we have otherwise identical equations. This is not particularly surprising if one knows that the Laplace matrix can be seen as an approximation of $-\triangle$ for finite differences on a network (Merris, 1998). We can now – again – separate the solution into the contributions of the eigenvalues and eigenvectors and get

$$\boldsymbol{X}(t) = \sum_n a_n \mathrm{e}^{-c\kappa_n t}\, \boldsymbol{v_n} \tag{174}$$

with analogous meanings for the different components: κ_n and $\boldsymbol{v_n}$ are eigenvalues and eigenvectors of the Laplacian (matrix) and the coefficients a_n are determined by the starting state. Aside from the sign change in the exponent caused by the transition between Laplace operator matrix equations (174) and (171) are identical. Now we know from Sec. 2.4.1 that the Laplace matrix always has an eigenvalue of $\kappa_1 = 0$ with a multiplicity equal to the number of connected components of the graph. Looking at non-connected graphs in one equation is of questionable value and thus we only consider Laplace matrices with a singular eigenvalue of $\kappa_1 = 0$ and an associated eigenvector $\boldsymbol{v_n} = (1, 1, \ldots, 1)$. All elements with non-zero (and by definition positive) κ vanish in the sum of Eq. (174) for $t \to \infty$ and we approach a final state

$$\boldsymbol{X}(t \to \infty) = a_1 \boldsymbol{v_1}. \tag{175}$$

This means that for sufficiently large times we have identical agent concentrations on every node which is similar to the results of Eq. (172). Reasoning and results for simple diffusion are analogous

on continuous space and networks with changes in signs in parts because of the transition from Laplace operator to Laplace matrix.

We now look at systems with diffusion and some form of interaction between agents; similar to the ones that are used in Sec. 2.8.4 to showcase the principle of Turing bifurcations. For a system in a continuous space where different agents or particles interact in some way we can write

$$\dot{\boldsymbol{X}} = f(\boldsymbol{X}) + c\,\triangle\boldsymbol{X}\,, \tag{176}$$

where $\boldsymbol{X}$ is a vector that contains information for all agents' concentrations $\boldsymbol{X} = (X_1(x), \ldots, X_M(x))$ and c is a coupling constant for the relative strength of the interaction or reaction between agents compared to the diffusion. The local interaction/reaction is defined by the function f. This system can be split into a term for spatial contribution $c\,\triangle\boldsymbol{X}$ as already discussed above and a term for local contribution,

$$\dot{\boldsymbol{X}} = f(\boldsymbol{X}), \tag{177}$$

which contains the information about the interaction between agents. If the local component by itself has a potential stationary solution $\boldsymbol{X}^*$ we can define a steady state $\boldsymbol{X}^*(x)$ for the spatially extended system. This would mean that all agents have a constant value for each point in space.

We consider the stability of this steady state using linearisation around the steady state which gives us the equation

$$\boldsymbol{X} = \boldsymbol{X}^* + \delta \tag{178}$$

with δ being a small displacement from the steady state. In turn this gives us

$$\dot{\delta} = \mathbf{J}\delta\,, \tag{179}$$

where we use the Jacobian matrix $\mathbf{J}$ to define the changes near the steady state. The Jacobian matrix can be written as

$$J_{ab} = \frac{\partial}{\partial X_b}\dot{X}_a\bigg|_* = \frac{\partial}{\partial X_b}\left(f_a(\boldsymbol{X}) + c\,\triangle X_a\right)\bigg|_*\,, \tag{180}$$

but to avoid having to derive by the spatial variable x we write the Jacobian with $\boldsymbol{X}$ decomposed into the sum of the eigenvalues and eigenvectors of the Laplacian. While this allows us to circumvent the spatial derivative it requires us to compute a Jacobian for each of the eigenvalues κ_n of the Laplacian.

$$J^{(n)}_{ab} = \left(\frac{\partial}{\partial X_b} f_a(\boldsymbol{X})\right)_* + c\kappa_n\delta_{ab} = P_{ab} + c\kappa_n\delta_{ab}. \tag{181}$$

This way, we can put all non-spatial terms into the matrix $\mathbf{P}$ which is the Jacobian of the purely local system as seen in Eq. (177). The δ_{ab} in this context is the Kronecker delta operator and should not be confused with δ without index from Eq. (178). Each Jacobian of Eq. 181 now gives the stability of the n-th eigenmode which is associated with the eigenvalue κ_n of the Laplacian.

The stability of a system described by a Jacobian is determined by the real parts of the eigenvalues of the Jacobian. If all eigenvalues have real parts below zero, then the system is stable to small perturbations. If each eigenmode is stable, then the system consisting of these eigenmodes as a whole as defined by the Eq. 180 is stable. We can now say there is a diffusion-driven instability if a change of parameters results in the emergence of unstable eigenmodes with the exception of the eigenmode of the eigenvalue $\kappa_1 = 0$ as this would mean a local instability unrelated to diffusion.

As before, we now use analogous steps to describe a system consisting of a spatially extended network and a local network on each node of the spatial network. To avoid confusion between the two different networks we will call nodes of the spatial network patches and nodes of the local network species as we will ultimately apply the results to food webs on spatial distributed patches, though the concept is applicable to any combination of networks.

Let us take a system with agents of a species a that resides on a patch i and whose concentration is given by X_{ia}. The time evolution of the system is given by

$$\dot{X_{ia}} = \underbrace{f_a(\boldsymbol{X_i})}_{\text{reactions}} \underbrace{-\sum_j c_a L_{ij} X_{ja}}_{\text{diffusion}}, \tag{182}$$

where the function f_a gives the local interactions of species based only upon the concentrations of species within that patch $\boldsymbol{X_i} = (X_{i1}, \ldots, X_{iM})$. The parameter c_a is the diffusion constant of species a and $\mathbf{L}$ is the Laplacian matrix. We note the analogy to Eq. 176 for the continuous space. We would like to separate the local from the spatial components so we define the dynamics for the local system as

$$\dot{X_a} = f_a(\boldsymbol{X}), \tag{183}$$

for each species a. A steady state on the local level can be used to construct a homogeneous steady state on the spatial network as well:

$$X_{ia}{}^* = X_a{}^* \quad \forall i. \tag{184}$$

We can analyse the stability of these steady states just as we did for the steady states of Eq. 183. This would require a Jacobian of size $N \times M$ for N patches and M nodes. While this is certainly possible we would like to simplify it as much as possible and therefore introduce a particular ordering of the elements of the Jacobian

$$\boldsymbol{Y} = (X_{1,1}, \ldots, X_{1,M}, X_{2,1}, \ldots), \tag{185}$$

which keeps all variables for species in a particular patch together. This creates a very simple block structure for the new Jacobian

$$J_{lm} = \frac{\partial}{\partial Y_m} \dot{Y_l} \bigg|_*, \tag{186}$$

which can be seen in Fig. 37. This block structure is achieved by separating the derivatives of interaction/reaction and diffusion terms in analogy to Eq. (182). If the reaction terms of a patch are independent of the concentrations in other patches we can ignore the derivatives.

$$\frac{\partial}{\partial X_{jb}} f_a(\boldsymbol{X_i}) = 0 \quad \forall i \neq j. \tag{187}$$

The derivative of a concentration function by a concentration within the same patch is identical to the derivative in the system without spatial component (Eq. (183)), therefore we get

$$\left.\frac{\partial}{\partial X_{ib}} f_a(\boldsymbol{X_i})\right|_* = P_{ab}\,. \tag{188}$$

The contribution of the local derivatives found in the full Jacobian can thus be combined in the matrix

$$\begin{pmatrix} \mathbf{P} & 0 & 0 & \cdots \\ 0 & \mathbf{P} & 0 & \cdots \\ 0 & 0 & \mathbf{P} & \cdots \\ \vdots & \vdots & \vdots & \ddots \end{pmatrix} \equiv \mathbf{I} \otimes \mathbf{P}\,,$$

where we use the identity matrix $\mathbf{I}$ of dimension $N \times N$ to reproduce the matrix $\mathbf{P}$ for each patch, while $\mathbf{P}$ has the dimension $M \times M$ as it carries the information of the species behaviour. The 0 entries are of the same dimension as $\mathbf{P}$.

Now that we have a convenient form for the species interactions we focus on the diffusion terms. For simple diffusion we get

$$\left.\frac{\partial}{\partial X_{jb}} \sum_k c_a L_{ik} X_{ka}\right|_* = c_a L_{ij} \left.\frac{\partial}{\partial X_{jb}} X_{ja}\right|_* \equiv (\mathbf{L} \otimes \mathbf{C})_{ia,jb} \tag{189}$$

with

$$\mathbf{C} = \begin{pmatrix} c_1 & 0 & 0 & \cdots \\ 0 & c_2 & 0 & \cdots \\ 0 & 0 & c_3 & \cdots \\ \vdots & \vdots & \vdots & \ddots \end{pmatrix}.$$

While this nicely shows the parallels to the reasoning for the continuous domain it is not necessary to assume simple diffusion. In particular for the model of a food web we would assume cases where species adapt their dispersal based on the concentration of other species, e.g. the predator seeks the prey and the prey avoids the predator. We thus can write the diffusion term of Eq. (182) as

$$-\sum_{j,b} c_{ab} L_{ij} X_{jb} \tag{190}$$

instead of $-\sum_j c_a L_{ij} X_{ja}$ which changes the coupling matrix $\mathbf{C}$ to

$$\mathbf{C} = \begin{pmatrix} c_{1,1} & c_{1,2} & c_{1,3} & \cdots \\ c_{2,1} & c_{2,2} & c_{2,3} & \cdots \\ c_{3,1} & c_{3,2} & c_{3,3} & \cdots \\ \vdots & \vdots & \vdots & \ddots \end{pmatrix}.$$

We can now use the block structure (as seen in Fig. 37) and the newly defined matrices $\mathbf{P}$ and $\mathbf{C}$ to write the Jacobian of the multi-patch and -species system as

$$\mathbf{J} = \mathbf{I} \otimes \mathbf{P} - \mathbf{L} \otimes \mathbf{C}. \tag{191}$$

This inherent structure of the Jacobian also manifests itself at the level of the eigenvector. Assume there is a vector

$$\boldsymbol{w} = v \otimes \boldsymbol{q} \tag{192}$$

where v is the eigenvector to the Laplace matrix

$$\mathbf{L}v = \kappa v \tag{193}$$

and $\boldsymbol{q}$ is a vector of dimension M which fulfils the eigenvalue equation

$$(\mathbf{P} - \kappa \mathbf{L})\boldsymbol{q} = \lambda \boldsymbol{q} \tag{194}$$

for an eigenvalue λ. We can now show that the vector $\boldsymbol{w}$ is an eigenvector to $\mathbf{J}$ for the eigenvalue λ. The proof is as follows.

$$\begin{aligned} \mathbf{J}\boldsymbol{w} &= (\mathbf{I} \otimes \mathbf{P} - \mathbf{L} \otimes \mathbf{C}) \cdot (v \otimes \boldsymbol{q}) \\ &= (\mathbf{I} \otimes \mathbf{P}) \cdot (v \otimes \boldsymbol{q}) - (\mathbf{L} \otimes \mathbf{C}) \cdot (v \otimes \boldsymbol{q}) \\ &= \mathbf{I}v \otimes \mathbf{P}\boldsymbol{q} - \mathbf{L}v \otimes \mathbf{C}\boldsymbol{q} \\ &= v \otimes \mathbf{P}\boldsymbol{q} - \kappa v \otimes \mathbf{C}\boldsymbol{q} \\ &= v \otimes (\mathbf{P} - \kappa \mathbf{C})\boldsymbol{q} \\ &= v \otimes \lambda \boldsymbol{q} = \lambda (v \otimes \boldsymbol{q}) = \lambda \boldsymbol{w}\,. \end{aligned} \tag{195}$$

Now there are obviously usually multiple eigenvalues κ for the Laplace matrix and just as many versions of Eq. (194). This means the full spectrum of the Jacobian of the network on network is only covered if we take the union of all eigenvalues of the combined matrix $(\mathbf{P} - \kappa \mathbf{L})$ for all κ.

$$\mathrm{Ev}(\mathbf{J}) = \bigcup_{n=1}^{N} \mathrm{Ev}(\mathbf{P} - \kappa_n \mathbf{C}), \tag{196}$$

This demonstrates how we can continue the analogy between continuous and discrete settings of the spatial domain even to the point of diffusion-driven instabilities as we can now define a diffusion-driven instability as any positive eigenvalue that emerges due to a change in κ. The eigenvectors and

	Continuous Space	Network
Laplacian Operator	Laplace Operator $\triangle$	Laplace Matrix -$\mathbf{L}$
Eigenmodes	$\triangle v_n = \kappa_n v_n$	$\mathbf{L} v_n = \kappa_n v_n$
Reaction diffusion system	$\dot{\boldsymbol{X}} = f(\boldsymbol{X}) + \mathbf{C} \triangle \boldsymbol{X}$	$\dot{\boldsymbol{X}}_i = f(\boldsymbol{X}_i) - L_{ij} \mathbf{C} \boldsymbol{X}_j$
Diffusive Instability	$\mathrm{Re}(\mathrm{Ev}(\mathbf{P} + \kappa_n \mathbf{C})) > 0$	$\mathrm{Re}(\mathrm{Ev}(\mathbf{P} - \kappa_n \mathbf{C})) > 0$

Figure 36: Analogy between diffusion in continuous space and in networks. To emphasize the similarity we have written the network reaction-diffusion system, Eq. (182), in matrix form and also allowed a coupling matrix $\mathbf{C}$ in the instability condition for the continuous space systems. While our derivation considered the simpler case where $\mathbf{C}$ is proportional to the identity matrix, such matrices appear in the case of cross diffusion where diffusion of one species depends on the concentration of other species (Baurmann et al., 2007). While the concentrations $\boldsymbol{X}$ are position dependent in continuous space, the state of the system on a network is captured by a discrete set of variables $\boldsymbol{X}_i$, with i being the node index. See Sec. 6.2 for more details.

eigenvalues of the Laplace operator are substituted by the eigenvectors and eigenvalues of the Laplace matrix and $\triangle$ is replaced by $-\mathbf{L}$ for the discrete spatial network but otherwise expressions remain the same (see Tab. 6.2 for a short comparison). We can therefore analyse the multilayer networks of spatially distributed food webs with dispersal or of comparable structure with the same methods that have already been extensively studied for multiple agents in continuous space (Baurmann et al., 2007).

6.3 Meta-Food Web Model

We apply the concepts of Sec. 6.2 to a meta-food web where the species of each local food web have identical densities on all patches and disperse across a discrete spatial network (see Fig. 37 for a schematic example of such a network and the section 6.5 for details on the local food web construction). We use the generalized modelling approach to define the dynamics of the system. In order to keep this reasonably brief, we skip over details of the process and description of all parameters. For a detailed derivation and an explanation of all parameters please read section 2.9.5 and 2.9.6.

Similar to the sections about simple two patches two species models we start with a very general description of possible interactions. We assume we have M patches of a spatial network that each are habitat to N ecological species:

$$\begin{aligned}\dot{X}_i^k &= G_i^k(X_i^k) - M_i^k(X_i^k) \\ &\quad + \epsilon_i F_i^k(X_1^k,\ldots,X_S^k) - \sum_j D_{ji}^k(X_1^k,\ldots,X_S^k) \\ &\quad + \sum_l \Big[E_i^{kl}(X_1^k,\ldots,X_S^k,X_1^l,\ldots,X_S^l) \\ &\qquad - E_i^{lk}(X_1^l,\ldots,X_S^l,X_1^k,\ldots,X_S^k) \Big]. \end{aligned} \tag{197}$$

The lower index i denotes a species and the upper index k denotes the patch. This description is in many ways analogous to the previous sections 4 and 5 with the difference that species can now feed on and be feed upon by multiple species and disperse between several patches. Alternatively, using the abbreviation $\boldsymbol{X^k} = \left[X_1^k,\ldots,X_S^k\right]$ we could write

$$\dot{X}_i^k = z_i^k(\boldsymbol{X^k}) + \sum_j \left(E_i^{kl}(\boldsymbol{X^k},\boldsymbol{X^l}) - E_i^{lk}(\boldsymbol{X^k},\boldsymbol{X^l}) \right) \tag{198}$$

which divides the equation into local interaction terms z_i^k and dispersal terms. We allow for different contributions of individual prey species to their predator which requires the introduction of new parameters. The total biomass available to a predator i is

$$T_i^k(\boldsymbol{X^k}) = \sum_j R_{ji}^k(X_i^k) \tag{199}$$

with $R_{ji}(X_i^k)$ as the individual contribution of species j to the total prey biomass. This only affects the local interactions:

$$\begin{aligned} z_i^k := \dot{X}_i^k =& G_i^k(X_i^k) - M_i^k(X_i^k) + \epsilon_i^k F_i^k(X_i^k, T_i^k(\boldsymbol{X^k})) \\ & - \sum_j \frac{R_{ij}^k(X_i^k)}{T_j^k(\boldsymbol{X^k})} F_j(X_j^k, T_i(\boldsymbol{X^k})) \end{aligned} \tag{200}$$

We can now compute the Jacobian for a meta-food web without any dispersal as z_i^k is describing exactly the dynamics for that case. We arrive at a block matrix structure for the local Jacobian $\mathbf{J}_P$

$$\mathbf{J}_P = \begin{pmatrix} \mathbf{P}^1 & \cdots & 0 \\ \vdots & \ddots & \vdots \\ 0 & \cdots & \mathbf{P}^N \end{pmatrix} \tag{201}$$

where each matrix $\mathbf{P}^k$ contains the derivations for the intra-patch dynamics of patch k. For the diagonal elements of $\mathbf{P}^k$ expressed in exponent and scale parameters we get

$$
\begin{aligned}
P_{ii}^k = & \\
\alpha_i^k \Bigg[& \quad \tilde{\nu}_i^k \tilde{\delta}_i^k \phi_i^k \\
& + \tilde{\nu}_i^k \delta_i^k \left(\gamma_i^k \chi_{ii}^k \lambda_{ii}^k + \psi_i^k \right) \\
& - \tilde{\rho}_i^k \tilde{\sigma}_i^k \mu_i^k \\
& - \tilde{\rho}_i^k \sigma_i^k \left(\beta_{ii}^k \psi_i^k + \sum_n \beta_{ni} \lambda_{ni} \left[\left(\gamma_n^k - 1 \right) \chi_{ni}^k + 1 \right] \right) \Bigg],
\end{aligned} \tag{202}
$$

and the non-diagonal elements

$$
\begin{aligned}
P_{ij}^k = & \\
\alpha_i^k \Bigg[& \quad \tilde{\nu}_i^k \delta_i^k \gamma_i^k \chi_{ij}^k \lambda_{ij}^k \\
& - \tilde{\rho}_i^k \sigma_i^k \left(\beta_{ji}^k \psi_j^k + \sum_n \beta_{ni}^k \lambda_{nj}^k \left(\gamma_n^k - 1 \right) \chi_{nj} \right) \Bigg].
\end{aligned} \tag{203}
$$

We can go through the same steps for the dispersal part of Eq. 198. Depending on the patch structure we get a Jacobian like

$$
\mathbf{J}_C = \begin{pmatrix}
\ddots & & & \\
& -\sum_m \mathbf{C}^{km} & \cdots & \mathbf{C}^{kl} \\
& \vdots & \ddots & \vdots \\
& \mathbf{C}^{lk} & \cdots & -\sum_m \mathbf{C}^{lm} \\
& & & \ddots
\end{pmatrix}, \tag{204}
$$

where each C^{km} is a matrix that contains the exponent parameters for the migration terms for the dispersal from patch m to patch k. For simple diffusion each C is a diagonal matrix but if there are dependencies of migration behaviour between species, called cross-diffusion, we have also non-diagonal elements.

We can now combine the two separate Jacobians and see that the Jacobian of the meta-food web with inclusion of dispersal has the form

$$
\mathbf{J} = \begin{pmatrix}
\ddots & & & \\
& \mathbf{P}^k - \sum_m \mathbf{C}^{km} & \cdots & \mathbf{C}^{kl} \\
& \vdots & \ddots & \vdots \\
& \mathbf{C}^{lk} & \cdots & \mathbf{P}^l - \sum_m \mathbf{C}^{lm} \\
& & & \ddots
\end{pmatrix}, \tag{205}
$$

which can be simplified to

$$\mathbf{J} = \begin{pmatrix} \ddots & & & \\ & \mathbf{P} - \sum_m \mathbf{C} & \cdots & \mathbf{C} \\ & \vdots & \ddots & \vdots \\ & \mathbf{C} & \cdots & \mathbf{P} - \sum_m \mathbf{C} \\ & & & \ddots \end{pmatrix} \tag{206}$$

under the assumption that we have homogeneous food webs and dispersal conditions on all patches. This type of steady state can be found in nature if one considers biomass per area instead of absolute biomass and often if the dispersal is not proportional to the patch size but rather to the number of links per spatial node.

The sum $\sum_m$ is equal to the number of patches m that patch k is connected to. This is the same as the degree d^k of patch k and we can write

$$\mathbf{J} = \begin{pmatrix} \ddots & & & \\ & \mathbf{P} - d^k\mathbf{C} & \cdots & \mathbf{C} \\ & \vdots & \ddots & \vdots \\ & \mathbf{C} & \cdots & \mathbf{P} - d^l\mathbf{C} \\ & & & \ddots \end{pmatrix}. \tag{207}$$

We now only need to remember that the Laplace matrix is the adjacency matrix minus the degree matrix (see Sec. 2.4.1) and it is easy to see that the Jacobian of the meta-food is

$$\mathbf{J} = \mathbf{I} \otimes \mathbf{P} - \mathbf{L} \otimes \mathbf{C}.$$

This equation is now completely identical to Eq. 191 which means we can use Eq. 194

$$(\mathbf{P} - \kappa\mathbf{L})\boldsymbol{q} = \lambda\boldsymbol{q} \tag{208}$$

to compute the eigenvalue sets of the Jacobian of the full meta-community for each Laplace matrix eigenvalue κ. All eigenvalues of the Jacobian are found in the union of these sets

$$\mathrm{Ev}(\mathbf{J}) = \bigcup_{n=1}^{N} \mathrm{Ev}(\mathbf{P} - \kappa_n\mathbf{C}), \tag{209}$$

which defines a master stability equation for the meta-community and we have

$$S(\kappa) = \mathrm{Re}\left(\lambda_{\max}(\kappa)\right). \tag{210}$$

as the master stability function (compare section 2.7 for details on the master stability equation) as it determines the stability of the system.

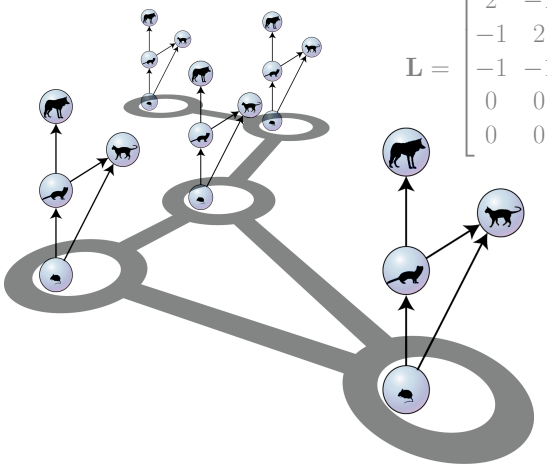

$$\mathbf{L} = \begin{bmatrix} 2 & -1 & -1 & 0 & 0 \\ -1 & 2 & -1 & 0 & 0 \\ -1 & -1 & 3 & -1 & 0 \\ 0 & 0 & -1 & 2 & -1 \\ 0 & 0 & 0 & -1 & 1 \end{bmatrix} \quad \mathbf{P} = \begin{bmatrix} P_{11} & P_{12} & P_{13} & 0 \\ P_{21} & P_{22} & P_{23} & P_{24} \\ P_{31} & P_{32} & P_{33} & 0 \\ 0 & P_{42} & 0 & P_{44} \end{bmatrix} \quad \mathbf{C} = \begin{bmatrix} C_{11} & 0 & 0 & 0 \\ 0 & C_{22} & 0 & 0 \\ 0 & 0 & C_{33} & 0 \\ 0 & 0 & 0 & C_{44} \end{bmatrix}$$

$$\mathbf{J} = \begin{bmatrix} \mathbf{P}-2\mathbf{C} & \mathbf{C} & \mathbf{C} & 0 & 0 \\ \mathbf{C} & \mathbf{P}-2\mathbf{C} & \mathbf{C} & 0 & 0 \\ \mathbf{C} & \mathbf{C} & \mathbf{P}-3\mathbf{C} & \mathbf{C} & 0 \\ 0 & 0 & \mathbf{C} & \mathbf{P}-2\mathbf{C} & \mathbf{C} \\ 0 & 0 & 0 & \mathbf{C} & \mathbf{P}-\mathbf{C} \end{bmatrix}$$

Figure 37: Example meta-food web with four species (blue bubbles and black arrows) on five patches (grey lines and circles). The stability of the system is described by the 20×20 Jacobian matrix **J**, which can be written as 5×5 matrix of 4×4 blocks. The blocks contain the intra-patch Jacobian matrix **P**, describing the dynamics within one patch, and the coupling matrix **C**, describing the dependence of migration rates on the population sizes, which is given here for a simple diffusion process. While the intra-patch Jacobian only appears on the diagonal of **J**, the coupling blocks **C** occur in a pattern given by the Laplacian matrix **L** that encodes the structure of the patch network and is shown here for a coupling strength of 1.

6.4 Master Stability Function

With help of the master stability function we can show for which spatial topologies we have stable leading eigenvalues and at what points we could observe diffusion-driven instabilities (DDIs).

The Eq. (196) completely separates the influences of the intra-patch dynamics from the dispersal between patches. All information about the spatial structure is carried by the eigenvalues κ_i and for each κ_i we get a completely independent set of eigenvalues of the Jacobian. We can now compute the leading eigenvalue for any κ using only the matrix **P**, which describes the local food web dynamics, and matrix **C**, which contains the dispersal behaviour of each species.

The stability of a concrete meta-food web can now be checked by computing the leading eigenvalues for all κ as given by the Laplacian matrix of that network and looking at the largest real part $\mathrm{Re}(\lambda_{\max}(\kappa))$. If all leading eigenvalues for each set of eigenvalues is below zero, then the system in its entirety is stable. If any κ falls within a range of the master stability function that is positive, then the system as whole is unstable. The ranges of the master stability function which have positive values are referred to as "forbidden" as they have to be avoided to maintain stability of the system.

As an example how such a master stability function might look and is affected by changes in the spatial network we refer to Fig. 38 and for a more complex master stability function to Fig. 39. The master stability function is different for each combination of **P** and **C** but only needs to be computed once for such a combination to give insights on stability for any spatial network. The eigenvalues κ of a Laplacian matrix can have any value equal or larger than zero but there is a always a zero eigenvalue as the Laplacian is rank deficient. For $\kappa = 0$ we look at the eigenvalues of **P** which is the local food web without any influence from dispersal. This means that the leading eigenvalue of the Jacobian of the isolated food web is always part of the set of for the spatially extended system. If the local food web is not stable then the homogeneous meta-food web cannot be stable either.

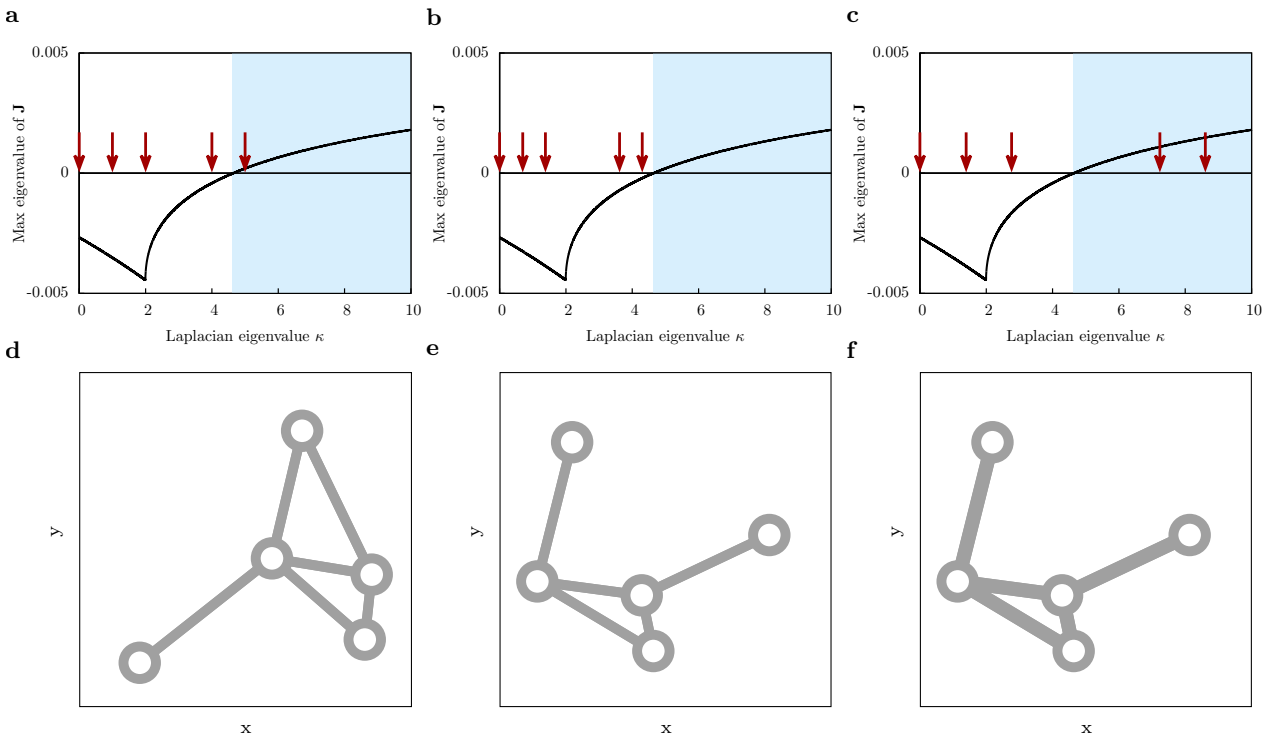

Figure 38: Master Stability Function (MSF) for meta-food webs (Brechtel et al., 2016). The graphs show MSFs (a-c) and spatial geometries (d-f) for the same local food web (that of Fig. 1) and coupling matrix **C** but for three different geometries (represented by circles, indicating patches, and lines, indicating migration links, in a two dimensional x,y landscape). The MSF (identical line in a-c) relates the Jacobian eigenvalue of the meta-food web to the Laplacian eigenvalue of the spacial network. The meta-food web is stable if none of the Laplacian eigenvalues (arrows) fall into ranges where the master stability function (line in a-c) is positive (blue shaded area). The food web under consideration is unstable on one geometry (a,d) but stable on another (b,e). Tightening the coupling (indicated by thicker lines in f) which is equivalent to multiplying the Laplace matrix with a factor can destabilize the stable system by stretching the Laplacian spectrum (cf. b,c). The same factor applied to the coupling matrix **C** would produce the same stability properties but instead of stretching the spectrum it would stretch the master stability function.

We numerically computed the master stability function for a variety of randomly generated food webs and coupling matrices.

Most master stability functions have relatively simple shapes, where the master stability function is either (i) negative at zero with a transition to unstable regions and then back to below zero, (ii) negative everywhere, or (iii) crosses from positive to negative values at a single $\kappa^* > 0$ (cf. Fig. 38). Multiple crossings are comparatively rare. The number of master stability function roots increases with larger food web sizes and connectivities.

The former two cases correspond to food webs that are unstable (iii) or stable (ii) irrespective of the geographical network, whereas the first case (i) is stable if all eigenvalues of the Laplacian are outside of the small unstable region. It is interesting to note that any prefactor to the Laplacian matrix **L** is indistinguishable from a prefactor to the coupling matrix **C**. This prefactor scales the master stability function proportionally. If we vary the overall coupling strength by applying such a prefactor we can

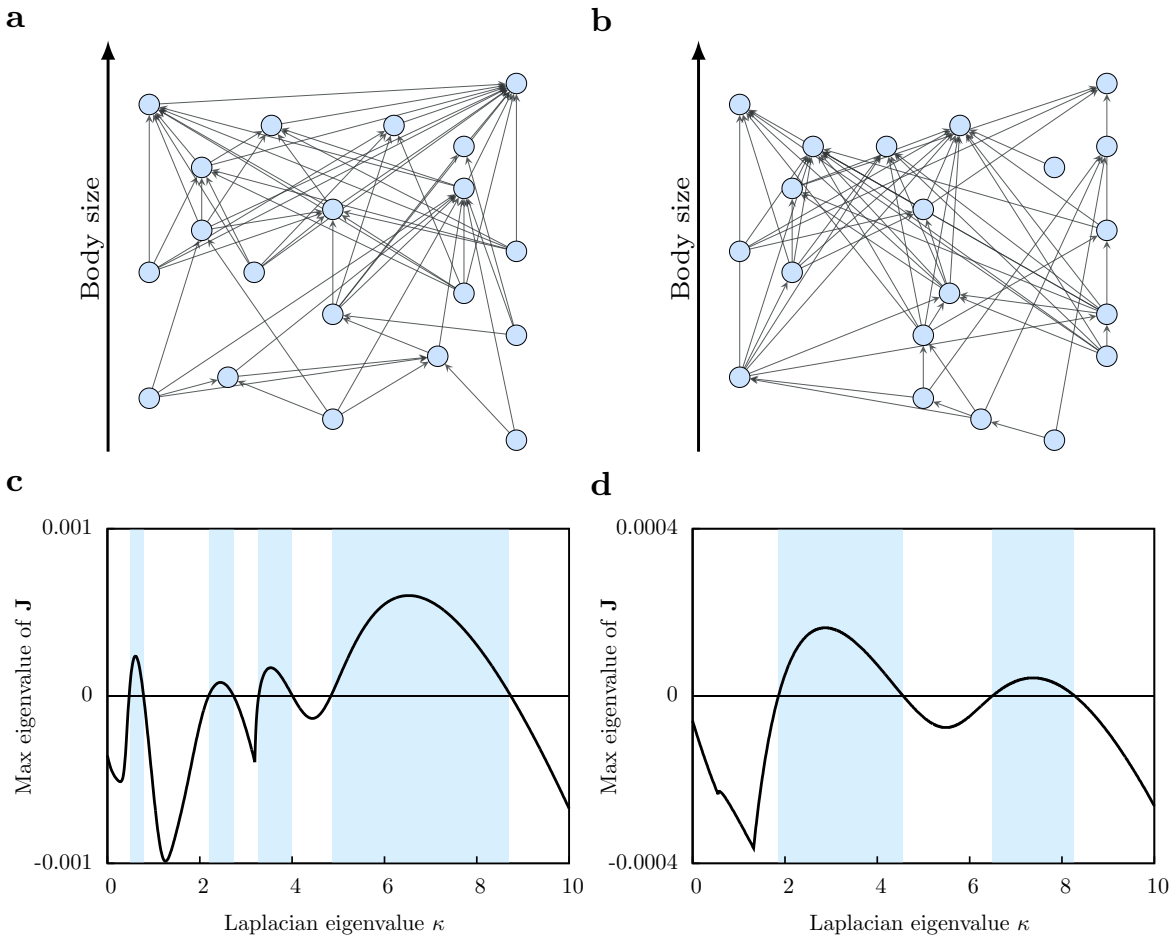

Figure 39: Complex Master Stability Functions (MSFs). Shown are two examples of food webs (a,b) of 20 species (blue bubbles) connected by predator-prey interactions (arrows). The coupling matrix **C** was constructed such that predators emigrate preferentially from patches with scarce prey and prey emigrates preferentially from patches with abundant predators. For c we have chosen an example were non-diagonal elements were rather large, roughly 17 times the size of diagonal elements, and for d we have rather small non-diagonal elements, about 0.17 times the size of the diagonal elements. The corresponding MSFs (c for a, d for b) have many forbidden (blue) ranges.

transition from stable to unstable regions (as can be seen Fig. 38). This would be analogous to diffusion-driven instabilities in continuous space as we are essentially increasing the diffusion coefficient.

As already shown in Sec. 6.2 the master stability equation is also applicable to non-diagonal coupling matrices **C**.

Such non-diagonal coupling is called cross-diffusion as the relationship between species influences the dispersal of each species in contrast to simple diffusion where diffusion only depends on the individual population. The simple assumption for cross-diffusion in food webs is that predators migrate with a higher rate from patches with low prey density (which can be interpreted as a search for prey) and prey species migrate faster from a patch if the predator density is high (they flee from predators). We use this naive concept for cross-diffusion in meta-food webs and get significantly more complex master stability functions (see Fig. 39). The form of the master stability function for cross-diffusion is sensitive to the size ratio between diagonal and non-diagonal elements. If the non-diagonal elements are too small we are looking at the same curves as for simple diffusion. If they are too large, we decrease complexity as well.

The non-diagonal elements in our examples seem to be in the range of roughly 0.1-20 times the size of the diagonal elements of the coupling matrix when they produce the maximum amount of roots. For such systems, we can see multiple switches between stable and unstable for increasing coupling strength and changing topology.

6.5 Niche Nets

We use niche nets for the local component of the meta-community. The basic construction schema of the niche webs has been explained in section 2.1.2. How to express a many species food web in generalized parameters can be found in Sec. 2.9. We use a β-distribution for the the feeding range r_i.

$$r_i = \left\{1-(1-x)^{\frac{2C}{1-2C}}\right\} \cdot n_i \tag{211}$$

with $n_i \in [0,1]$ as the niche value. Parameter C is the connectance of the food web and $x \in [0,1]$ is a random number. The feeding center c_i is chosen at random from the interval $[\frac{r_i}{2}, n-\frac{r_i}{2}]$ and any species with a niche value n_j within $[c_i-\frac{r}{2}, c_i+\frac{r}{2}]$ is a prey of species i. This choice of the feeding center and feeding range makes cannibalism impossible. This is a simplification of the original model (Williams and Martinez, 2000) which allowed for such links.

The niche value n_i is used to define the local biomass turnover per species

$$\alpha_i = 10^{-2\cdot n_i}, \tag{212}$$

as it is a proxy for body size which in turn is closely correlated to biomass turnover. We varied the generalized parameters for the food webs (see Tab. 10) as well as the number of species $(10, 20, 30)$ and the connectance of the food webs $(0.15, 0.20, 0.25)$. The correlations of different parameters for a generalized food web of this form have already been researched (Gross et al., 2009). The sensitivity of the predator to the prey density γ and the combined mortality and respiration exponent parameter μ are both stabilizing for high values. The sensitivity of the intrinsic growth rate of the basal species to their populations ϕ and the sensitivity of the functional response to changes in predator population ϕ are destabilizing for large exponents. This means the trends are similar to minimal predator-prey food webs though we no longer differentiate between mortality exponent parameters for predator and prey. We only varied ϕ and γ. It is also known from (Gross et al., 2009) that more species and higher food web connectance reduce the average stability.

We look at the percentage of stable webs for varying food web sizes and connectivities. We see in Tab. 11 that there are no stable webs for a parameter set I and II as can be explained by the relatively high value of ϕ. For set III and IV (see Tab. 12 and Tab. 13) we see a drop of stability towards higher connectivities and species numbers, as expected. Set III is stabler than set IV due to higher γ which means a stronger predation pressure response to prey population changes.

We already know from the previous section 6.4 about the master stability function for homogeneous food webs on many patches that dispersal cannot stabilize a meta-food web if the local community is unstable. Thus, we cannot get stable systems for parameter set I and II. We still consider these parameter sets as a comparison to the food webs that are capable of local stability to see if there are significant differences in master stability function curves and behaviour.

Table 10: The different niche net generalized parameters. For each set of parameters we took 10^4 food webs with 10, 20 and 30 species and connectances of 0.15, 0.20 and 0.25 (a total of nine ensembles per set of parameters).

Parameters Set	ϕ	γ	ψ	μ
Set I	1	0.95	1	1
Set II	1	0.75	1	1
Set III	0.5	0.95	1	1
Set IV	0.5	0.75	1	1

Table 11: Proportion of stable webs for parameter set I and II. In the left column we have the connectances and in the upper row the number of species of the food webs. All are completely unstable.

Conn./Size	10	20	30
0.15	0.0	0.0	0.0
0.20	0.0	0.0	0.0
0.25	0.0	0.0	0.0

Table 12: Proportion of stable webs for parameter set III. In the left column we have the connectances and in the upper row the number of species of the food webs.

Conn./Size	10	20	30
0.15	0.69	0.58	0.40
0.20	0.19	0.05	0.01
0.25	0.02	0.001	0.0

Table 13: Proportion of stable webs for parameter set IV. In the left column we have the connectances and in the upper row the number of species of the food webs.

Conn./Size	10	20	30
0.15	0.56	0.38	0.21
0.20	0.05	0.007	0.0007
0.25	0.002	0.0001	0.0

6.6 Eigenvalue Limits

The master stability function is the core element for the description of a multilayer network of the proposed form. While we can define the stability of a system with a particular spatial network using the master stability function, it would be interesting to see if we could define properties of the master stability function that would represent a tendency for stability of networks. Such a definition of stability for meta-communities would be independent of the spatial component and only depend on the matrix of local contributions, **P**, and the coupling matrix, **C**. Comparing stable and "forbidden" interval sizes of the master stability function comes to mind as a intuitive measure of stability but is only possible if we find a suitable range in which we evaluate the master stability function as we can compute the master stability function up to an arbitrary point. A proposal for such a range would be, for example, up to the last stability change. We (usually) cannot compute the stability changes analytically but using eigenvalue approximations like the Gershgorin circle theorem or the Brauer-Cassini ovals allows us to make estimations of the limits of the eigenvalues of the Jacobian. Under certain conditions it is possible to say that the sign of the master stability function cannot possibly change outside a certain range and thus the system cannot change its stability anymore.

We can get the eigenvalues of the Jacobian **J** of the meta-community with the combination matrix **P**-κ**C**. The elements of the combination matrix are

$$\mathbf{P}-\kappa\mathbf{C}=\begin{pmatrix} P_{ii}-\kappa C_{ii} & \cdots & P_{iN}-\kappa C_{iN} \\ \vdots & \ddots & \vdots \\ P_{Ni}-\kappa C_{Ni} & \cdots & P_{NN}-\kappa C_{NN} \end{pmatrix}. \tag{213}$$

We can use the Gershgorin theorem to compute boundaries of the eigenvalues of the combination matrix. To define the stability of the system we only need to know the real parts of the eigenvalues. All eigenvalues are within the Gershgorin disk $D(X,R)$ which lies in the complex plane and has a center at $X \in \mathbb{C}$ and a range of $R \in \mathbb{R}$. For a real combination matrix we know that the center X has no imaginary part and thus sits on the real axis of the complex plane at the value X. The largest real part of an eigenvalue is thus

$$\mathrm{Re}(\lambda_{\max}) = \mathrm{Re}(X) + R = X + R \tag{214}$$

The center X and range R can be written in terms of the matrix elements. The disk $D(X,R)$ then becomes $D\left(P_{ii}-\kappa C_{ii}, \sum_{i\neq j}^{N} |P_{ij}-\kappa C_{ij}|\right)$ or $D\left(P_{ii}-\kappa C_{ii}, \sum_{i\neq j}^{N} |P_{ji}-\kappa C_{ji}|\right)$ depending on whether we take the row or column sum for the approximation. For the sake of brevity we will omit the discs computed by using row sums as it is completely analogous to the computation with column sums. The maximum real part of the eigenvalue for column i that exists within that disk is

$$\lambda_{S,i} = P_{ii} - \kappa C_{ii} + \sum_{i\neq j}^{N} |P_{ij} - \kappa C_{ij}| \tag{215}$$

under the condition that no discs overlap. If discs overlap the eigenvalues can be situated anywhere within the connected discs and thus the largest $\lambda_{S,i}$ would be the limit for all eigenvalues associated with the overlapping discs. If the largest real part of all eigenvalues is below zero, we have a stable system. We also know that a system cannot be stable if there is a eigenvalue that lies within a Gershgorin disk that does not allow for eigenvalues with a below zero real part. The lower limit of the disk can be described by

$$\lambda_{I,i} = P_{ii} - \kappa C_{ii} - \sum_{i\neq j}^{N} |P_{ij} - \kappa C_{ij}|. \tag{216}$$

The eigenvalues depend on the Laplacian eigenvalue κ. The master stability function is usually depicted in the form of real part of leading eigenvalue over κ and therefore solve the largest real part of all eigenvalues for κ:

$$\kappa = \frac{P_{ii} - \sum_{i\neq j}^{N} \pm P_{ij}}{C_{ii} - \sum_{i\neq j}^{N} \pm C_{ij}}. \tag{217}$$

The signs of the $\mathbf{P}$ and $\mathbf{C}$ elements depend on the exact values. This formula does not necessarily have a feasible solution (say negative κ) and extraneous solutions have to be discarded. The value of κ for a disk that just reaches $\lambda_I = 0$ can be computed analogously to the equation (217).

A more graphical interpretation of the gersghorin disk may express the eigenvalue problem as such: If the radius of the gersghorin disk ($\sum_{i\neq j}^{N} |P_{ij,ji} - \kappa C_{ij,ji}|$) increases faster than the center of the disk ($P_{ii} - \kappa C_{ii}$) moves in a direction then we cannot establish a point at which we can guarantee the stability or instability of the system. This is the case when

$$C_{ii} < \sum_{i\neq j}^{N} |C_{ij,ji}| \tag{218}$$

as the local parameters covered by $\mathbf{P}$ are negligible for sufficiently large coupling strengths C_{ij} and/or κ.

The sign of the diagonal element C_{ii} gives the direction of the movement of the center of the disk. In most cases of migration we expect a positive value for the diagonal elements of the coupling matrix as we expect migration to increase with higher population densities.

An alternative to the Gershgorin discs as a way to approximate eigenvalue boundaries are the Brauer-Cassini ovals. While more ovals than discs need to be considered to get the limits of the eigenvalues, the boundaries are more precise.

The Cassini ovals for a complex $n \times n$ matrix $\mathbf{A} = [a_{i,j}]$ are defined as

$$|z - a_{i,i}| \cdot |z - a_{j,j}| \leq R_i \cdot R_j; \qquad z \in \mathbb{C}. \tag{219}$$

with R_i defined as the i-th column sum. We are only interested in the boundaries of the inequality and thus can write

$$|z - a_{i,i}| \cdot |z - a_{j,j}| = R_i \cdot R_j. \tag{220}$$

We can now solve the equation for z. There are four distinct solutions:

$$z_{\pm,\pm} = \frac{1}{2}\left(\pm\sqrt{a_{i,i}^2 - 2a_{i,i}a_{j,j} + a_{j,j}^2 \pm 4R_i \cdot R_j} + a_{i,i} + a_{j,j}\right) \tag{221}$$

The largest real value is obtained for $z_{+,+}$, where both plus-minus signs are plus. If $z_{+,+} = 0$ we know that all eigenvalues are at or below zero and thus the system should be stable for non-pathological cases. In our case $\mathbf{A}$ is the combination matrix $\mathbf{P} - \kappa\mathbf{C}$.

The limit value for the Laplace eigenvalue is always smaller or equal to the one computed with the Gershgorin discs. The trade-off is the slightly more costly computation of the boundaries.

6.7 Diffusive Case

We consider the case of purely diffusive migration; i.e. the coupling matrix has only diagonal elements. This allows to simplify the estimation of the eigenvalue limits and ensure that there is a sensible limit for the master stability function. The Gershgorin disk that contains a given eigenvalue λ_i can then be given as

$$D\left(P_{ii} - \kappa C_{ii}, \sum_{i\neq j}^{N} |P_{ij}|\right) \tag{222}$$

It is obvious that for sufficiently high κ any eigenvalue has to have a real part smaller than zero as the maximal possible real part $\lambda_{S,i}$ is defined as

$$\lambda_{S,i} = P_{ii} - \kappa C_{ii} + \sum_{i \neq j}^{N} |P_{ij}| \,. \tag{223}$$

If we solve this for κ and $\lambda_{S,i} = 0$ we get

$$\kappa\Big|_{\lambda_{S,i}=0} = \kappa_{S,i} = \frac{P_{ii} + \sum_{i \neq j}^{N} |P_{ij}|}{C_{ii}} \,. \tag{224}$$

For the case of diffusive dispersal and Cassini ovals we can substitute as follows into Eq. 221

$$a_{i,i} = P_{i,i} - \kappa C_{i,i} \tag{225}$$
$$a_{j,j} = P_{j,j} - \kappa C_{j,j} \tag{226}$$
$$R_i = \sum_{i \text{łeq} l} |P_{il}| \tag{227}$$
$$R_j = \sum_{j \leq l} |P_{jl}| \tag{228}$$
$$\tag{229}$$

and the equivalent to κ_S is then given by

$$\kappa_S = \left(C_{i,i}P_{j,j} + P_{i,i}C_{j,j} + \sqrt{(C_{i,i}P_{j,j} - P_{i,i}C_{j,j})^2 + 4C_{i,i}C_{j,j} \sum_{i \leq l} |P_{i,l}| \sum_{j \leq l} |P_{j,l}|} \right) / (2C_{i,i}C_{j,j}) \tag{230}$$

6.8 Cross-Diffusion

While it is in general not possible to compute a cut-off-point beyond which no more roots of the master stability function are found there are non-diagonal coupling matrices which allow for an easy estimate of κ_S. We consider the Gershgorin approximation for the upper limit of the eigenvalue

$$\lambda_{S,i} = P_{ii} - \kappa C_{ii} + \sum_{i \neq j}^{N} |P_{ij} - \kappa C_{ij}| \,.$$

We know derive a upper limit for the right hand term

$$\begin{aligned}\lambda_{S,i} &= P_{ii} - \kappa C_{ii} + \sum_{i\neq j}^{N} |P_{ij} - \kappa C_{ij}| \\ &< |P_{ii}| - \kappa C_{ii} + \sum_{i\neq j}^{N} (|P_{ij}| + |\kappa C_{ij}|) \\ &= (|P_{ii}| + \sum_{i\neq j}^{N} |P_{ij}|) - \kappa (C_{ii} - \sum_{i\neq j}^{N} |C_{ij}|).\end{aligned}$$

Under the assumption that

$$C_{ii} > \sum_{i\neq j}^{N} |C_{ij}|$$

we can now compute the upper limit for $\kappa_{S,i}$ of the form

$$\kappa_S < \frac{\sum_{i\neq j}^{N} C_{ii} - \sum_{i\neq j}^{N} |C_{ij}|}{\sum_{i\neq j}^{N} |P_{ii}| + \sum_{i\neq j}^{N} |P_{ij}|}.$$

This gives an simple criterion for the useful range for some types of cross-diffusion. The assumption that the diagonal element is larger than the sum of the non-diagonal elements means that the diffusive aspect of migration dominates the dispersal. Regrettably, for the case of large non-diagonal elements we cannot make any predictions even though this gives us the most complex and interesting master stability function curves.

For non-diffusive dispersal and Cassini ovals we have to consider Eq. 221. First we focus on the term

$$\begin{aligned}&\sqrt{a_{i,i}^2 - 2a_{i,i}a_{j,j} + a_{j,j}^2 + 4R_i^2 \cdot R_j^2} \\ =&\sqrt{\left((P_{i,i} - \kappa C_{i,i}) - (P_{j,j} - \kappa C_{j,j})\right) + 4\left(\sum_{i\leq l} |P_{il} - \kappa C_{il}|\right)^2 \left(\sum_{j\leq l} |P_{jl} - \kappa C_{jl}|\right)^2}.\end{aligned}$$

We see that for increasing κ we go towards positive infinity. For $\kappa C_{i,j} \gg P_{i,j}$ we can simplify the term to

$$\kappa\sqrt{\left(-C_{i,i} + C_{j,j}\right)^2 + 4\left(\sum_{i\leq l} |C_{il}|\right)^2 \left(\sum_{j\leq l} |C_{jl}|\right)^2}.$$

and now look at the full simplified equation

$$z_{\pm,\pm} = \frac{1}{2}\left(+\kappa\sqrt{\left(-C_{i,i} + C_{j,j}\right)^2 + 4\left(\sum_{i\leq l} |C_{il}|\right)^2 \left(\sum_{j\leq l} |C_{jl}|\right)^2} - \kappa(C_{i,i} + C_{j,j})\right). \tag{231}$$

It is now obvious that the real part will only have an upper boundary of zero for real positive κ if

$$\sqrt{\left(-C_{i,i}+C_{j,j}\right)^2+4\left(\sum_{i\leq l}|C_{il}|\right)^2\left(\sum_{j\leq l}|C_{jl}|\right)^2}<C_{i,i}+C_{j,j}. \tag{232}$$

This condition is fulfilled if we have similar diagonal elements and small off-diagonal elements.

6.9 Stability for Spatial Networks

We look at the value of κ_S. Any κ larger than κ_S must produce negative, that is to say stable, values for the master stability function. We do this for 10^4 niche nets for different parameter interval sets, connectivities and food web sizes (as can be seen in Tab. 10) and different coupling types (see Tab. 14). The coupling matrix has the general form

$$\mathbf{C}=\begin{pmatrix} c_{1,1} & c_{1,2} & c_{1,3} & \cdots \\ c_{2,1} & c_{2,2} & c_{2,3} & \cdots \\ c_{3,1} & c_{3,2} & c_{3,3} & \cdots \\ \vdots & \vdots & \vdots & \ddots \end{pmatrix}$$

but we only consider simple diffusive dispersal and therefore all elements $c_{i\neq j}$ are zero. We consider two types of diffusive dispersal. Dispersal type I assumes that large species migrate slower. This is the case for many types of passive migration; e.g. species that are carried by air or water currents. Dispersal of type II lets large species migrate faster. This is frequently the case for terrestrial species where the large species tend to have larger home ranges (Gaston and Blackburn, 1996) that are strongly correlated with dispersal ranges (Bowman et al., 2002).

In Fig. 40 we see the results for the approximation based upon the Gershgorin theorem. The κ_S values lie in drastically different ranges for different coupling types. This is a straightforward consequence of Eq. (224). For small $|C_{ii}|$ we have large quotients and for large $|C_{ii}|$ we get small values of κ_S. This makes sense on a intuitive level as well. If the influence of individual coupling links is weak it takes many links before a significant impact can be assured.

If the threshold κ_S falls below the second smallest eigenvalue of the Laplace matrix in question - the smallest always being zero - then any spatial mode is a stable mode. The second smallest eigenvalue is called the Fiedler eigenvalue or Fiedler value (see (Mohar, 1991)) and is bounded by

$$\lambda_F=\frac{4}{n\cdot D} \tag{233}$$

Table 14: The coupling types. We use purely diffusive dispersal, which means the coupling matrix has only diagonal elements. The diagonal values depend on the niche value n_i of the respective species i.

Coupling Type	Rules	Interpretation	
Type I	$10^{-4\cdot n_i}$	Large animals move slower	Species carried by air or water currents
Type II	10^{n_i}	Large animals migrate faster	Terrestrial species

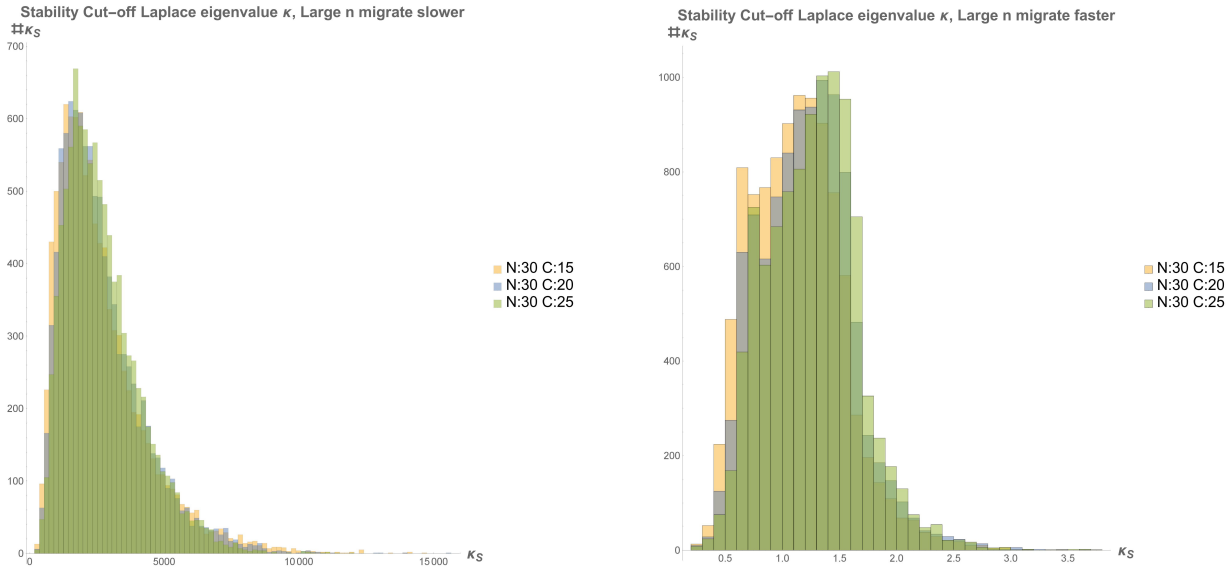

Figure 40: The histograms of the parameter κ_S computed with the Gershgorin theorem for a 30-species food web and different connectivities (0.15, 0.20 and 0.25). One the x-axis we see the κ_S values and on the y-axis the number of food webs with that value. The different colours represent different connectances with $C = 15, 20, 25$ meaning a connectance of $0.15, 0.20, 0.25$ respectively. On the left we see the coupling of type I and on the right coupling of type II. We can see that coupling type I produces significantly larger limits than coupling type II and has a significantly larger variance. Other food web sizes produce similar shapes and maximal κ_S though with slightly lower average κ_S for smaller food webs.

with n as the number of vertices and D as the maximal distance in steps between vertices. This means that the threshold, for which any discrete κ is in the stable range of the master stability function, is actually going towards zero for sufficiently large and connected spatial networks.

We compare these boundaries to the values of the Cassini oval approximation. For the Cassini ovals we always have tighter bounds than for the Gershgorin discs. This improvement is rather small for coupling type II where ranges are roughly halved but is remarkable for coupling type I where we have ranges with the Cassini ovals that are only at most about 150 compared to ranges for the Gershgorin discs of up to about $15,000$; which means the ranges can shrink in the most extreme cases to about 1% of the ones provided by the discs (see Fig. 41).

We look at the average percentage of stable regions compared to the total range as determined by the Gershgorin theorem. We do this for 10^4 niche webs and divide the full range for each master stability function into intervals of the size $\Delta\kappa = \frac{\kappa_S}{10000}$.

The relative size of the stable regions are above 90% for all parameter sets and coupling types. For coupling type I the unstable portion is below one percent at all times. For coupling type II we have slightly smaller stability values which decrease with higher species number and connectance. This means that the Gershgorin theorem seems to overestimate the interesting range of the master stability functions on a consistent basis for coupling type I and to some extend for coupling type II. There is little difference for primarily stable or unstable parameter sets.

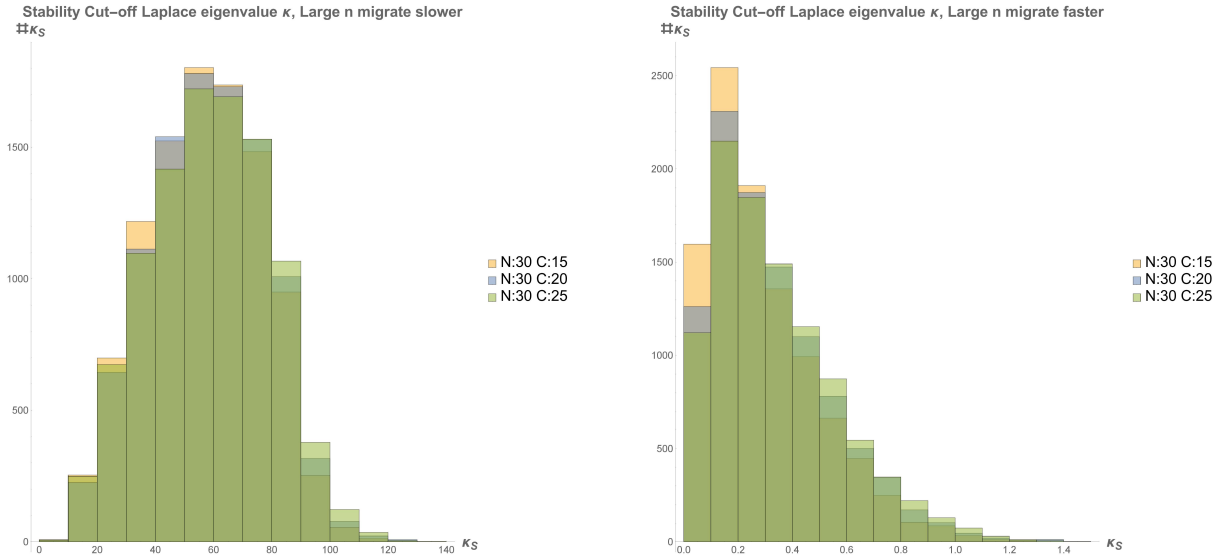

Figure 41: The histograms of the parameter κ_S for a 30-species food web and different connectivities (0.15, 0.20 and 0.25) for Cassini ovals. One the x-axis we see the κ_S values and on the y-axis the number of food webs with that value. The different colours represent different connectances with $C = 15, 20, 25$ meaning a connectance of $0.15, 0.20, 0.25$ respectively. On the left we see the coupling of type I and on the right coupling of type II. Compared to the limits value for the Gershgorin theorem we such far less variability for coupling type I, essentially removing any significant outliers. The limits for coupling type II are better as well but the benefit is less extreme with only a factor of about 1.5 to 2. Other food web sizes produce similar shapes and maximal κ_S with less differences between food webs sizes compared to the Gershgorin theorem.

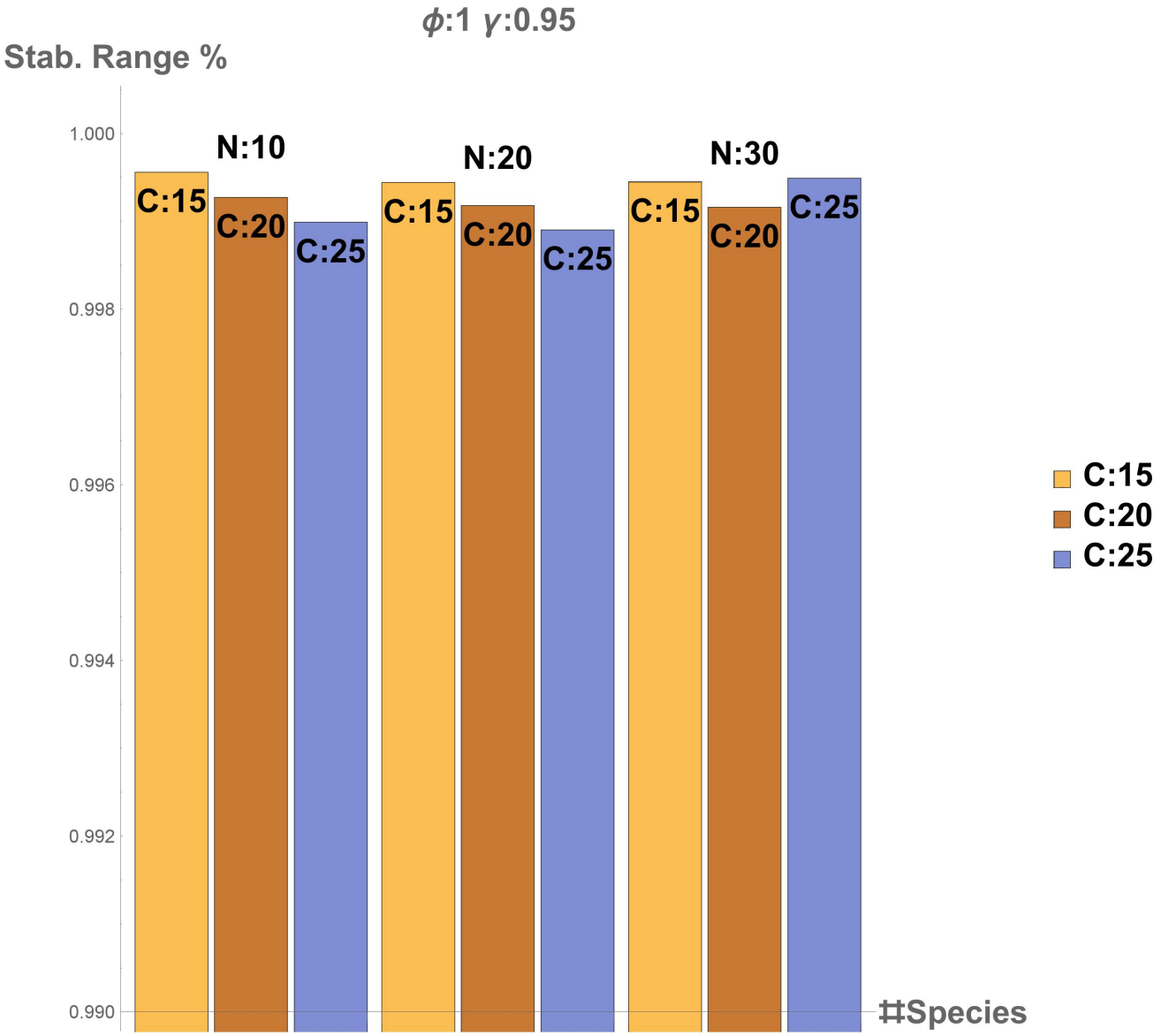

Figure 42: The percentage of stable range for coupling type I and parameter set I. The parameter N gives the number of species and the parameter C the connectance of the food web with $C = 15, 20, 25$ being equal to actual values of $0.15, 0.20, 0.25$. The stability is for all food web sizes and connectivities very close to one and we therefore start they y-axis at 0.99 to highlight the (small) differences. There seems to be no clear trend for any parameter (though low connectance has a slightly larger stable range) but since we look at tiny fractions of the total range, the resolution of the stable range is relatively low. The eigenvalue approximation with Gershgorin disks is too imprecise for this coupling type. The Cassini ovals would provide more accurate statements and perhaps reveal some trends. Other parameter sets behave similarly.

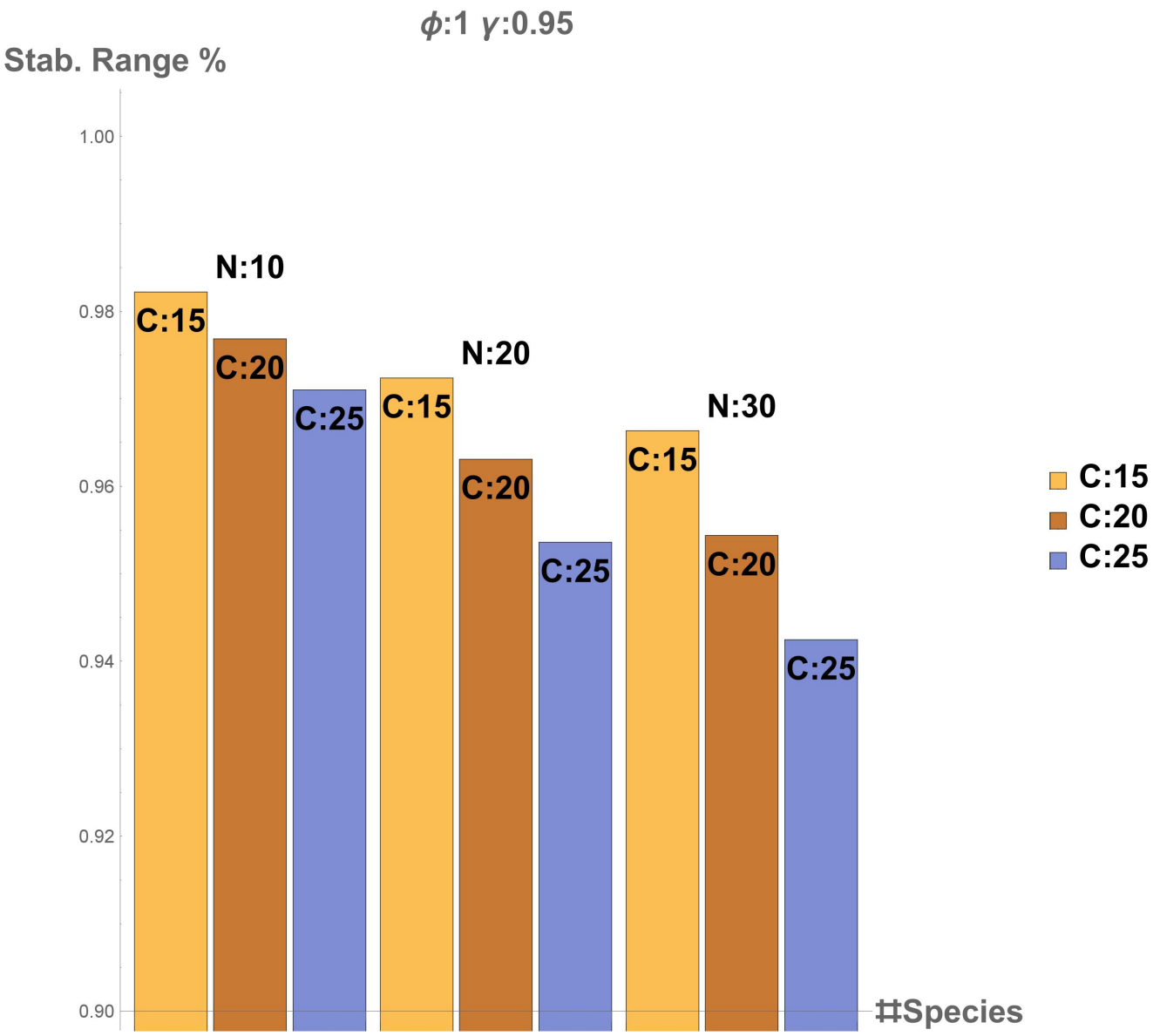

Figure 43: The percentage of stable range for coupling type II and parameter set I. The parameter N gives the number of species and the parameter C the connectance of the food web with $C = 15, 20, 25$ being equal to actual values of $0.15, 0.20, 0.25$. We start the y-axis at 0.90 to make the stability differences more visually striking. Larger food web sizes and connectivities produce larger "forbidden" ranges. The other parameter sets show comparable trends.

6.10 Bifurcations and Modes

As we have shown in Sec. 6.2, diffusive instabilities on networks are in many ways analogous to diffusive instabilities in the continuous space. The transition between a stable state and unstable state is classified by the type of bifurcation we encounter. We are interested in the type of bifurcations spatial change introduces on the network but we extend the analysis to the behaviour of modes on the system. The bifurcation parameter in question for spatial change would be the Laplace eigenvalue κ as it contains all spatial information. For every switch between stable and unstable regions of the master stability function we have a potential bifurcation, as a potentially stable web could be destabilized by slight changes of the eigenvalue and/or different coupling weights. This is of course only true if the system in question can be potentially stable which is only true (at least for the homogeneous case) if the local system is stable as all Laplace matrices have an eigenvalue of $\kappa = 0$. If we have an inherently unstable system the roots of the master stability function do not mark the position of bifurcations but rather changes of spatial modes. These modes can be defined analogously to different bifurcations. The behaviour of a bifurcation is defined by the mode that outgrows all other modes. Even when a mode does not grow unbounded we can use the same criteria towards the associated eigenvalues to define the behaviour that the system would have displayed if the mode was dominant. We thus call modes that would cause Hopf bifurcations by the name Hopf modes and those that would cause saddle-node bifurcations we call saddle-node modes. We compare properties of the system at the roots of the master stability function to find if there are inherent differences for locally unstable and stable systems and thus modes and bifurcations. In the following we find that spatial bifurcations are rare and thus most of our discussion of statistic results is not based upon spatial bifurcations but rather on spatial modes in systems that are dominated by their local structure. That spatial bifurcations exist for both simple and cross-diffusion can be seen in the examples of Fig. 38 and 39.

We took an ensemble of 10^4 niche nets of each parameter set (see Tab. 10 to 13), and computed the master stability function for both types of coupling considered. As we don't have a analytical expression for the master stability function curve we interpolate the curve from 10^4 points distributed evenly throughout the full range of κ_S as defined by the Gershgorin theorem for each individual master stability function.

It should be noted that we can have multiple roots for each master stability function and thus get several roots for one niche net-dispersal combination. As we have shown in the previous section "Food Webs on Many Patches" this is possible even for diffusive dispersal and relatively common for more complex coupling types. If a master stability function has an unstable local food web we must have at least one bifurcation. If the local food web is stable we need to see multiple roots as we have to cross the x-axis of the master stability function plot at least twice if we start in a stable region and become unstable at some point.

We start by looking at the mean number of roots per master stability function (see Fig. 44 and Fig. 45) for MSF with at least one root. For coupling type I we find that the average number of roots is close to 1 and between 1 and 2 for all cases which means that we seldom have complex master stability function curves with multiple roots. The mean number of roots per master stability function is lower for food web parameters with higher average stability. This might be counter-intuitive as we would expect values of two or higher if stable systems become unstable but must be on the stable side for high enough κ. The reason is that a system is seldom stable and becomes unstable at some point but rather that the MSF for the system remains in the stable region and only unstable local systems produce any roots to begin with. The number of roots per master stability function increases with connectance and species number which is only reasonable as more eigenvalues change with varying of κ and thus could provoke a stability change.

The variance of the number of roots per master stability function increases with food web size and connectance. Apparently there is no averaging effect that evens out the variance of the root number. As we have rather low numbers to begin with this might very well change for systems with inherently higher root numbers.

For coupling type II we have a near perfect average of one for all parameter combinations, food web sizes and connectivities. This strengthens the hypothesis that locally stable food webs almost never change stability if diffusive migration is added. The variance of the number of roots per master stability function is essentially zero for all cases for coupling type II. Multiple roots for a master stability function are extremely rare.

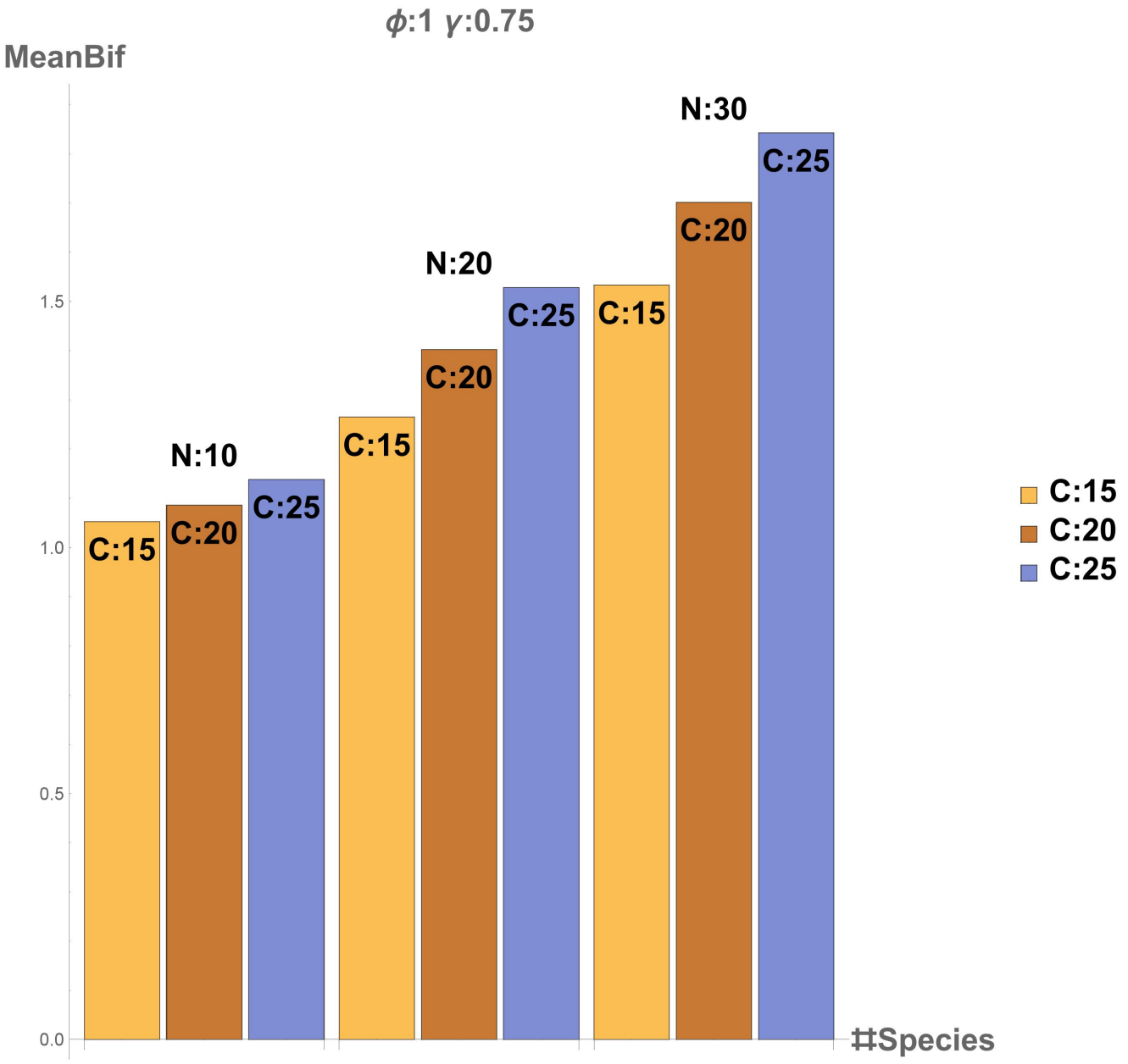

Figure 44: The average number of roots per master stability function if there is a root for coupling type I and parameter set II. The parameter N gives the number of species and the parameter C the connectance of the food web with $C = 15, 20, 25$ being equal to actual values of $0.15, 0.20, 0.25$. With increasing complexity in the form of more species or links between species the number or roots increases. This is intuitive for the species number as more species mean more eigenvalues that potentially could change their sign but is not trivial for increasing connectance. The variance of the root number increases with larger average root numbers. All trends apply to the other parameter sets as well.

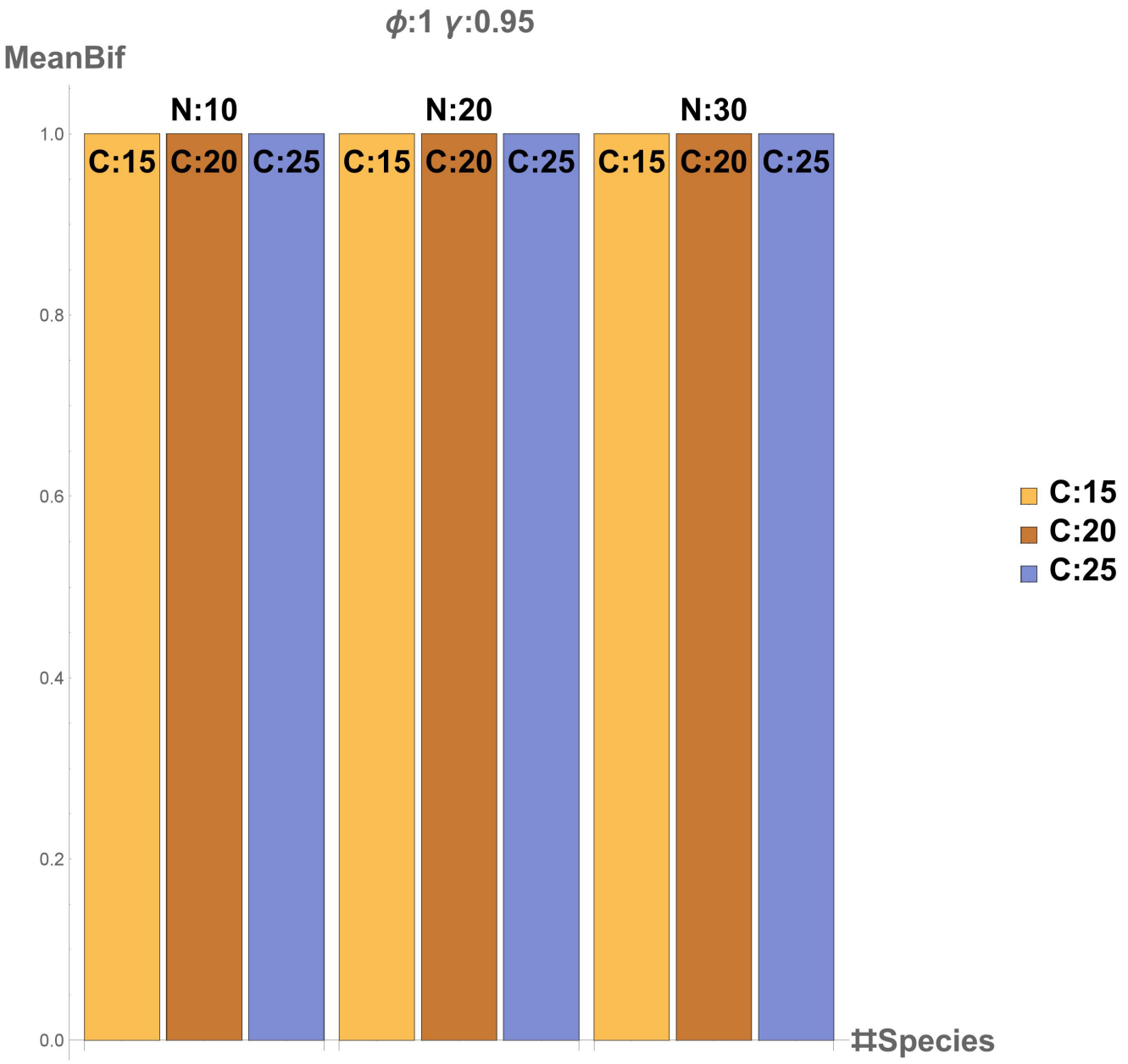

Figure 45: The average number of roots per master stability function if there is a root for coupling type II for parameter set I. The parameter N gives the number of species and the parameter C the connectance of the food web with $C = 15, 20, 25$ being equal to actual values of $0.15, 0.20, 0.25$. For this coupling type we see an average of one root per master stability function with barely any deviation for all parameter sets. The variance is zero for the parameter set I and nearly zero for all other sets.

Now that we have established the average number of roots per master stability function we would like to establish the behaviour of the system at the root. We look at the percentage of Hopf bifurcations or modes with Hopf-like behaviour at the point of master stability function roots compared to saddle-node bifurcations and modes. Actual bifurcations are quite rare as most locally stable systems have no root for the master stability function.

For coupling type I and primarily unstable webs we always find Hopf ratios of 50 percent or higher. Larger connectivities are reducing the ratio or keeping it roughly equal and larger food webs decrease the number of Hopf modes. For the stabler parameter sets III and IV we have lower Hopf ratios that increase with food web size but do not show a trend for different connectances.

For coupling type II we have overall higher ratios but in particular for the mostly unstable parameter sets we have ratios of close to one with very little change for different food web sizes or connectances. For the more stable sets we see an increase of the Hopf ratio with higher connectance and species number.

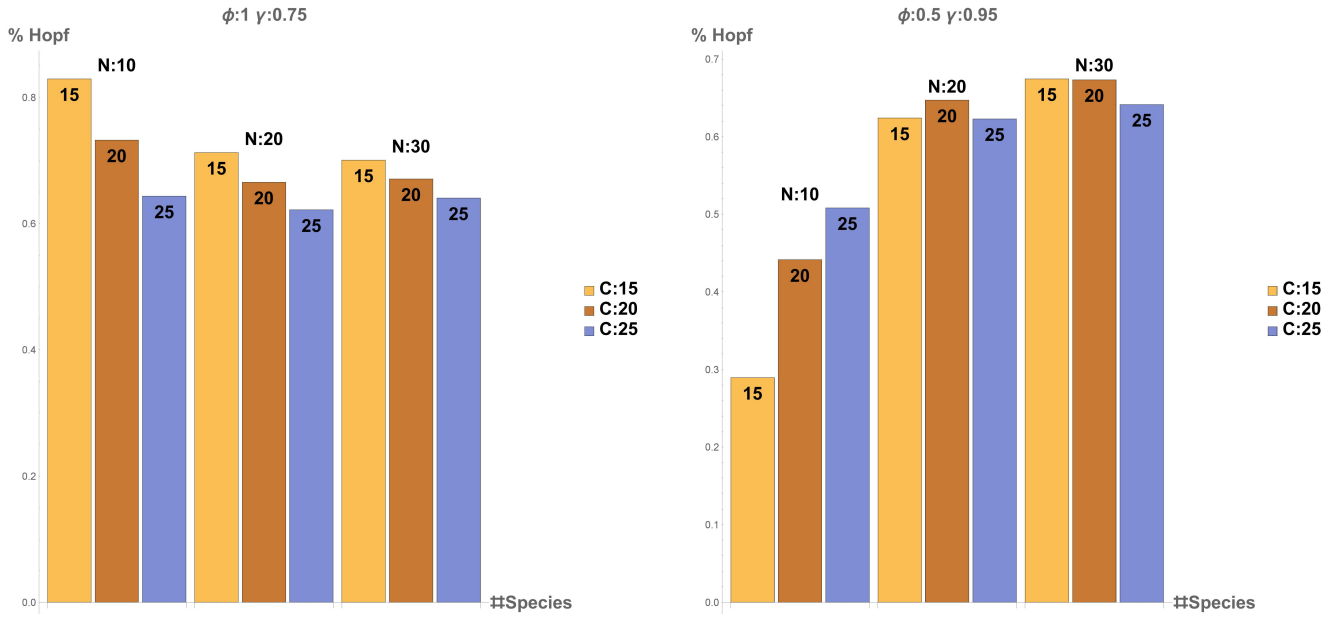

Figure 46: The proportion of Hopf bifurcations and Hopf-like modes of all roots for all local food webs of coupling type I for parameter set II (left) and III (right). The parameter N gives the number of species and the parameter C, marked with different colours, the connectance of the food web with $C = 15, 20, 25$ being equal to actual values of $0.15, 0.20, 0.25$. For the stabler parameter sets III and IV we find a trend of higher Hopf ratios for larger species numbers but not necessarily for higher connectance. For parameter sets I and II we find decreasing Hopf ratios for larger food webs and connectivities.

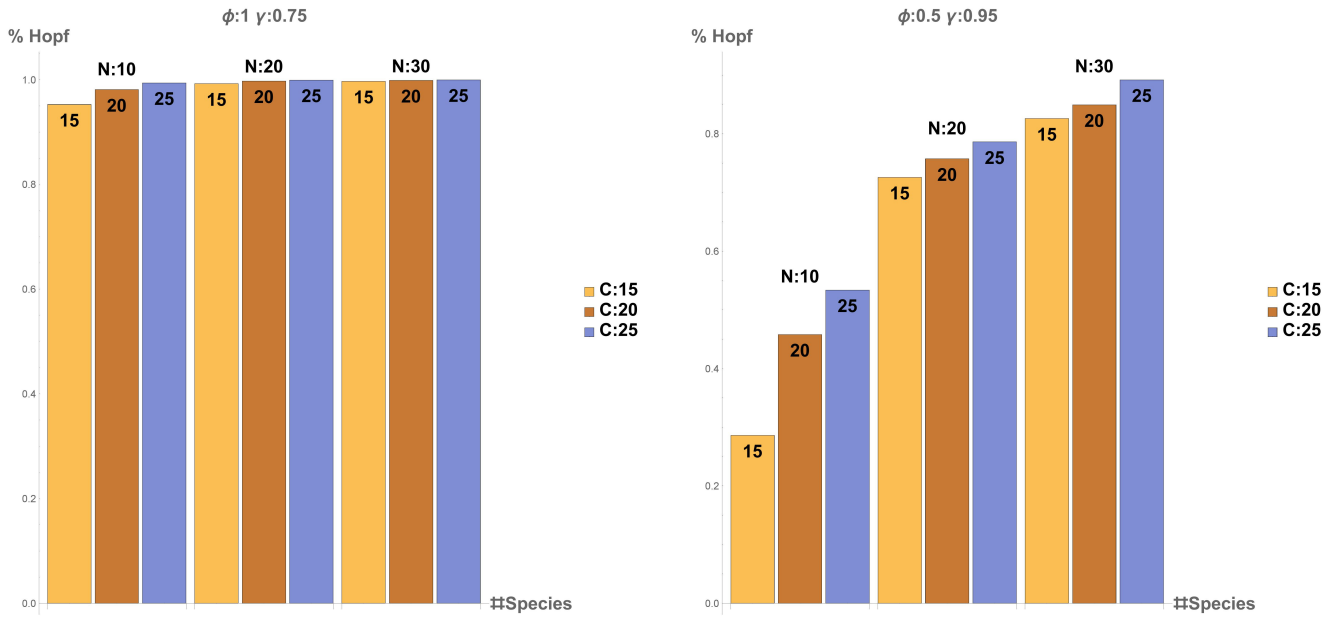

Figure 47: The proportion of Hopf bifurcations and Hopf-like modes of all roots for all local food webs of coupling type II for parameter set II (left) and III (right). The parameter N gives the number of species and the parameter C, marked with different colours, the connectance of the food web with $C = 15, 20, 25$ being equal to actual values of $0.15, 0.20, 0.25$. Here we see a clear development for parameter set III and IV to more oscillatory behaviour for larger food webs and connectivities up to Hopf ratios of nearly one. Interestingly, for parameter sets I and II we have ratios of nearly one for all combinations of food webs size and connectance.

There is a significant number of master stability functions with no roots, either because none happen at any point, which is the by far most frequent case, or the algorithm to find the root did not converge to an appropriate degree. If we start in the unstable region for the master stability function (as we do for parameter set I and II) we expect there to be a guaranteed stability change for the maximum range as we have diffusive dispersal which lowers the master stability function values for sufficiently large κ. This is confirmed by the simulations.

We see that for coupling type I about one to three percent of the completely unstable parameter sets have no bifurcation even though there should always be one. This can be explained by the failure of numerical convergence. The relatively large range limit for the last possible root position creates master stability functions with very small slopes. This can increase the difficulty for the algorithm to find the roots. Simply checking the master stability function at κ and κ_S shows that there has to be a bifurcation at some point.

For the parameter sets with higher average stability the ratio of webs with no bifurcation is essentially identical to average stability of the local food webs. Again, a locally stable web seldom has a bifurcation due to spatial structures.

For coupling type II we no longer have the same numerical problems as the κ_S values are significantly smaller on average and our interpolation points are closer together.

6.11 Order Parameter

We look at the eigenvector of the leading eigenvalue of the combination matrix at the roots of the master stability functions. This gives us the local dynamics at the point of bifurcation or for the emerging spatial mode.

We compute the order parameter of the eigenvector of the leading eigenvalue of the combination matrix at the root of the master stability function. This gives us a measure of the synchronization between species for the homogeneous niche nets on every patch which can be used as an indicator of robustness; with high synchronization being a common indicator for low robustness. This is NOT the order parameter for the spatially extended system, as the order parameter of the extended system has to be computed from the eigenvector of the leading eigenvalue of the full Jacobian. The eigenvectors of the full Jacobian are related to the eigenvectors of the combination matrix by the formula (compare Eq. (195))

$$\boldsymbol{w} = v \otimes \boldsymbol{q} \tag{234}$$

with $\boldsymbol{w}$ as the eigenvector of the Jacobian, v as the eigenvector of the Laplacian and $\boldsymbol{q}$ as the eigenvector of the combination matrix. As we only have $\boldsymbol{q}$ we miss the spatial component of the Laplacian which gives a prefactor to the species of each patch. The relationship between species on each individual patch is not affected by this but we cannot make any statement about the relationship between the patches. This depends on the exact spatial configuration and as multiple configurations can lead to the same κ and thus root for the master stability function we cannot compute the order parameter of the full Jacobian.

For the order parameter we find peaks for the saddle-node bifuraction/modes and a distribution for the Hopf bifuractions/modes. For saddle-node bifuractions/modes we can only get peaks for the order parameter r at

$$r = \frac{0}{n}, \frac{2}{n}, \ldots, \frac{n-2}{n}, \frac{n}{n}; \tag{235}$$

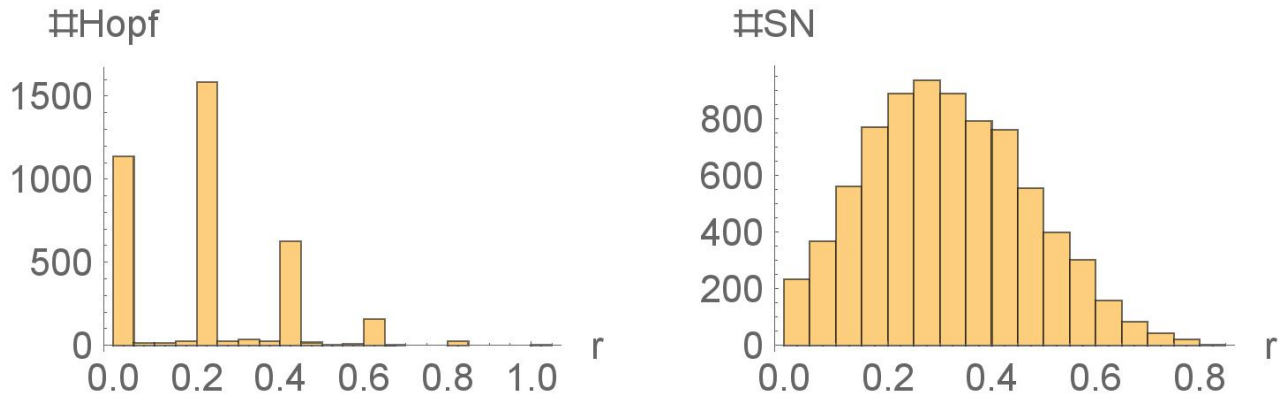

Figure 48: Sample histograms for the order parameter r for saddle-node (left) and Hopf like modes/bifurcations (right). On the left we see some background between the distinct peaks. These are modes that are falsely attributed as saddle-node due to numerical inaccuracy. The values are for the eigenvectors of parameter set I with ten species and connectance 0.15.

with n as the number of species. For an explanation for this we refer to Sec. 5 and the section "Phase difference between patches". For an example of the order parameter distribution see Fig. 48.

We look at the average order parameter for all roots for each parameter set and for saddle-node and Hopf dynamics respectively (see Fig. 49 and Fig. 50). The perhaps most remarkable characteristic of the order parameter here is the strong dependence on the coupling type. Despite different assumptions for the local dynamics we see essentially identical order parameters for all four parameter sets within a coupling type. Coupling type II has significantly higher values on average than type I. For increasing species and connectivities the order parameter increases for nearly all types of bifurcations with the exception of Hopf bifurcations and modes for small webs that use coupling matrices of type II. This overall trend would mean a likely decrease in robustness if we considered each patch in isolation. In combination with a potential RGG the meaning is less clear as the total order parameter for the entire system is determined in most cases by the spatial structure: The order parameter of the individual food web is interesting as high synchrony means significant fluctuations in biomass which could lead to extinction. If other patches compensate this fluctuations by contrasting dynamics the system in total could remain robust. The relationships of the inter-patch dynamics are captured by the order parameter of the Laplace matrix eigenvectors which can only be computed for concrete configuration. We try to find trends of the Laplace eigenvectors in the next section about localization; i.e. how many patches are affected by a perturbation.

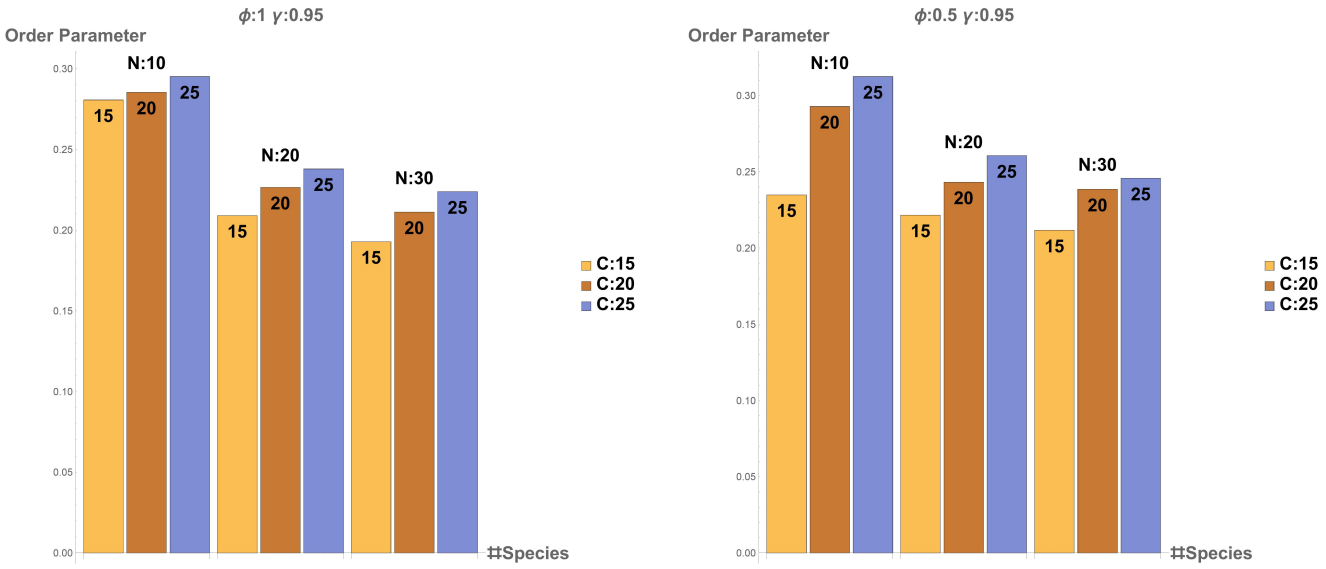

Figure 49: The order parameter of the eigenvector to the leading eigenvalue at the root of the master stability function for coupling type I. The parameter N gives the number of species and the parameter C, marked with different colours, the connectance of the food web with $C = 15, 20, 25$ being equal to actual values of $0.15, 0.20, 0.25$. For all parameters sets we see that the local food webs become less ordered with increasing size but more ordered with increasing connectance. The order parameter values and trends don't change noticeably if we look at Hopf- or saddle-node like behaviour independently.

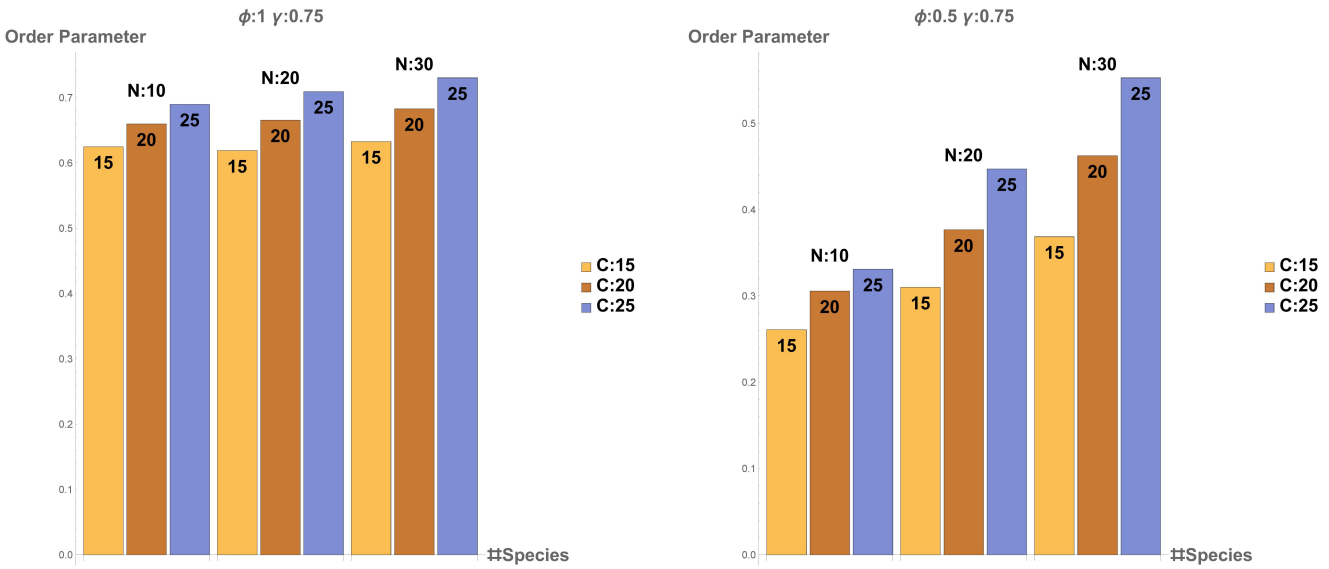

Figure 50: The order parameter of the eigenvector to the leading eigenvalue at the root of the master stability function for coupling type II. The parameter N gives the number of species and the parameter C, marked with different colours, the connectance of the food web with $C = 15, 20, 25$ being equal to actual values of $0.15, 0.20, 0.25$. For coupling type II we see an on average significantly higher order parameter for the unstable parameters sets I and II, a distinction which was not noticeable for coupling type I. Overall, we see that larger food webs and higher connectivities produce higher order parameters. This applies to Hopf-like bifurcations which make up the strong majority of bifurcations. Saddle-node-like behaviour is hard to quantify as such transitions are rare. The tentatively findings indicate the same order parameters as for Hopf-like dynamics.

6.12 Localization

Unlike the eigenvectors of the Laplacian in continuous space, eigenvectors of the Laplace matrix for discrete spatial structures tend to be rather complex. Any eigenvector entry is associated with a node of the network. For the networks-on-networks in question we know that the eigenvector of the Jacobian is a combination of the eigenvector of the Laplacian and an eigenvector which captures species behaviour. The eigenvalue associated with an eigenvector represents a perturbation. If for example the eigenvector had only one non-zero entry then the perturbation only affects one particular node. One can say that the particular eigenvalue and thus mode has only a localized effect on the system.

How strongly an eigenvector is localized can be computed by the participation number; a property closely related to the inverse participation ratio used in quantum mechanics (Kramer and MacKinnon, 1993). We consider a normalized eigenvector $\mathbf{q} = (q_1, \ldots, q_N)^\top$ of the Laplacian matrix of a system with N nodes. The participation number is given by

$$PN = \frac{1}{\sum_i^N |q_i|^4}. \tag{236}$$

For a system with only a single active node we get a score of $PN = 1$ and for a perfectly delocalized state we get a participation number of N which means all nodes are equally excited. The participation number is thus a rough measure for the number of involved nodes for an eigenmode.

Most eigenvectors of a Laplacian matrix for random geometric graphs are localised and only a minority results in changes on the full network scale (Cucuringu and Mahoney, 2011; Pastor-Satorras and Castellano, 2016; Nyberg et al., 2014) as can be seen in Fig. 51.

A system will, by definition, if it becomes unstable, diverge from the steady state in the direction of the eigenvector associated with the eigenvalue that has become positive in its real part. It is interesting to note that the final state reached after the instability often, though not always, mirrors the entries of the eigenvector; e.g. the heterogeneous steady state has biomass distributions that have the same relations as the eigenvector entries (Fig. 51).

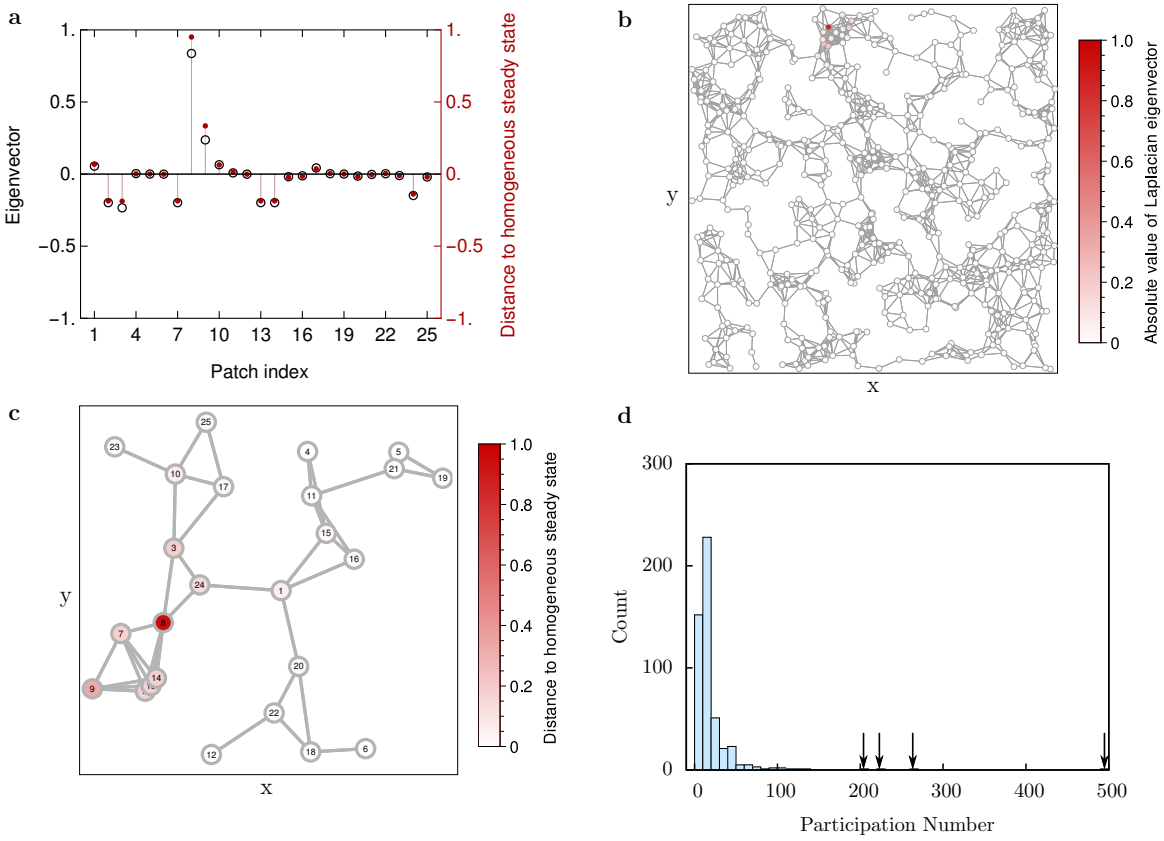

Figure 51: Localization of eigenvectors. The graphs shown a system where on a given topology (c) one eigenvalue of the Laplacian lies in one of the forbidden ranges where the master stability function of the food web is positive. Hence the system departs from the homogeneous steady state and approaches a non-homogeneous state. Color-coding the distance of the density of the apex predator population to the homogeneous value shows that the impact of the instability is confined to a relatively small area. In cases where the system approaches a state in the vicinity of the homogeneous state, the eigenvector corresponding to the destabilizing eigenvector is indicative of the pattern in the final state. A comparison (a) of the respective eigenvector (open circles) and the observed deviation from the homogeneous value in the final state (dots) shows good agreement in the example system (c), but similar accuracy cannot be guaranteed in general. The localization of many eigenvectors is a generic feature of geographical networks. For the 500-node example geometry in b the number of nodes on which eigenvectors have a significant amplitude can be quantified by the participation number or ratio. This reveals that the majority of eigenvectors only extend to relatively few nodes (histogram in d), while only 4 eigenvalues (arrows) have significant amplitude on a large fraction of the nodes. The example shown here is a case of real eigenvalues causing a Turing instability. When the leading eigenvalue is complex, the associated instability is a wave instability, i.e. a heterogeneous oscillation.

6.13 Conclusions

We have studied diffusion on multi-layer networks of a networks-on-networks subtype and created a master stability function approach that gives insight to the behaviour of such systems for any spatial network. This was done in analogy to diffusion in continuous space and allows quick investigation of the stability of discrete networks despite the often more complex eigenmodes compared to the continuous case.

While we use the master stability function to analyse meta-food webs we want to emphasize that this approach works equally well for any networks-on-networks system that fulfils the basic assumptions for a reaction-diffusion system. The agents on each node could alternatively be molecules in cells or bacteria in hosts. Even social interaction in terms of game theory would be possible.

The generalized meta-food webs we use incorporates the full spectrum of predator-prey species interaction with different time scales of interaction across trophic levels on non-linear dynamics. We show that simple diffusion can already produce pattern-forming bifurcations and how the master stability function can become increasingly complex for larger food webs with series of "forbidden" regions which allows for stabilizing and destabilizing influences of the spatial network and coupling. A spatially evolving network could pass through multiple phases of stability and instability this ways. This accentuates the need for the study of carefully chosen spatial networks as this can have significant effect on the results.

We considered if it is possible to have a measure of stability independent of actual topology. For simple diffusive dispersal and some forms of cross-diffusion we can give a boundary for the range of the master stability function worth exploring. The range encompasses all potential points of stability change for the given combination of local food web and coupling type. Such an approximation is not possible for all types of food webs and coupling but under certain conditions, i.e. if the sum of the non-diagonal elements in the coupling matrix are smaller than the diagonal elements, we can make predictions for non-diffusive dispersal as well. This would mean coupling types with strong diffusive qualities and small cross-species migration dependencies. We used two types of eigenvalue approximations – the Gershgorin discs and the Brauer-Cassini ovals – which both give limits for comparable situations. The Cassini ovals require slightly more initial computation time but can provide significantly better boundaries in some cases. Most system have forbidden regions and stability changes only for comparatively low values of the Laplacian eigenvalues. It is seldom necessary to look a the full range provided by the approximations.

We looked at the relationships between local community size, type and structure in combination with different coupling types to the type and frequency of emerging bifurcations. We computed an order parameter to measure the synchrony of the food web for the dominant spatial mode of the system at the roots of the master stability function.

The order parameter of the local food webs is strongly dependent on the coupling matrix and surprisingly little on the actual food web type and structure.

For dispersal that slows down with increased body size, coupling type I, we see a decrease of synchrony for larger food webs which indicates a higher robustness and an increase with higher connectance which should decrease robustness as well. For faster migration for larger species, coupling type II, we see an increase of the order parameter for larger and more densely linked local communities. In general we have more synchronous species behaviour for coupling type I than for coupling type II and also more for primarily unstable parameters sets than for mostly stable ones.

These statements are unfortunately limited to the synchrony of the local food web. The order parameter of the underlying geographic network must be taken into account to quantify the effect of this findings on the overall robustness of the multilayer network. Finding appropriate data on spatial net-

works as they occur in nature is paramount to combine these results and to make general statements on the robustness of networks networks.

But, assuming that random geometric graphs are comparable in their spectrum to real spatial networks, we can assume that most modes are rather localized. This means the population changes only have significant amplitudes on a small number of patches. This would indicate relatively small changes of total network biomass, at least in the early stages after a perturbation. First numerical experiments to see how the biomass distribution changes compared to predictions near the steady state indicate that it often keeps the same initial shape and character, e.g. Hopf bifurcations result in oscillations that endure beyond minimal deviations from the steady state and biomass densities mirror the initial eigenvector proportions.

The roots of the master stability functions show in most cases Hopf-like behaviour meaning that spatial modes and diffusion-driven instabilities have commonly oscillatory character and more so for larger food webs and higher connectance. This implies higher robustness in particular for systems with low synchrony as total biomass stays relatively constant.

7 Summary and Final Conlusions

We have used the generalized method to investigate meta-communities of varying complexity ranging from the smallest possible food web up to complex spatial and trophic structures.

We started with predator-prey interaction with no spatial element. We found that most commonly used models vary only in two generalized parameters and thus can be analysed analytically with little difficulty.

We then added dispersal by introducing a second patch but kept the steady states homogeneous; i.e. both patches have identical values at the steady state. Dispersal is at all times a destabilizing force if the isolated patch is considered the baseline but under certain circumstances more migration can improve stability compared to less migration. This is particularly the case with models that include adaptive migration of any form. All local bifurcation types – Hopf bifurcations, wave instabilities, saddle-node bifurcations and Turing instabilities – are possible in nearly all of the models despite the rather simple nature of the system. Simple pattern building due to dispersal is observed.

As the final step for a two patches two species model we allowed for differing steady state values for each patch and compared the new results with the homogeneous steady states. The number of total bifurcations resulting in oscillatory behaviour increased as well as the proportion of anti-synchronous oscillations. Heterogeneity could both benefit or hurt the linear stability of the steady states compared to the homogeneous system and it is hard to predict what will be the case. Adaptive dispersal types show larger changes in correlation of migration parameters with stability than models with diffusive migration. The increase in (anti-)oscillatory behaviour means in all likelihood that, despite the difficulty to predict effects of heterogeneity on the proportion of stable webs of a given model, the robustness as a separate measure of stability is increasing for all models. A number of models from recent research is analysed and we find good agreement between the results by generalized modelling and explicit modelling.

We considered more complex spatial networks with large niche nets under homogeneous steady state conditions. Meta-communities on discrete patches can be regarded as reaction/diffusion systems on networks and using this analogy we found a way to rewrite the dynamics of the system in the form of a master stability function. Locally stable niche nets can produce pattern-forming bifurcations with simple diffusive dispersal analogous to Turing bifurcations. Adaptive dispersal behaviour produces more complex master stability functions with numerous changes in stability for changing spatial conditions or coupling strengths. The concept of stability based only on the local dynamics and the coupling and thus the master stability function is discussed. We give a way to define stability for a system based on simple approximations of the eigenvalue limits. We discuss the benefits and drawbacks of two types of eigenvalue approximations; the Gershgorin discs and the Brauer-Cassini ovals. To quantify the properties of the system which can be defined by a master stability function, we use several parameter sets for niche webs and coupling types and investigate the dynamics of the systems at the roots of the master stability functions. If only a single eigenvalue of a system is in a forbidden region of the master stability function it can be used to extrapolate the behaviour of the entire meta-food web. This often holds true beyond small deviations from the homogeneous steady state and allows for a rough prediction of biomass distribution and behaviour as Hopf bifurcations produce cyclical populations dynamics and saddle-node bifurcations commonly lead to new heterogeneous steady states.

We test the alternative definition of stability for the simple case of diffusive migration and find that, while it does not fit particularly well for this case, it could be valuable for more complex migration rules that result in multiple roots in the master stability function. For simple diffusive dispersal the master stability functions do not produce any spatial bifurcations in the vast majority of cases. The maximal range computed by the Gershgorin theorem is usually significantly larger than needed as most roots are found at low κ values. The Cassini ovals, though slightly more complex to compute, perform significantly better and should be the go-to method for future attempts.

For coupling type I, which lets small species disperse faster than large species, there is a decrease in synchrony for larger food webs but an increase with connectance. The in-patch behaviour becomes increasingly synchronized with higher complexity (in the form of higher species number and connectance) of the local food web for coupling type II, which in contrast to type I has more dispersal for larger species. Mostly unstable parameters sets tend to have higher synchrony values compared to mostly stable sets. More synchronous systems are usually less robust but the results only apply to the synchronisation within a food web on a patch. We cannot include the relationship between patches as this depends on the exact spatial topology but we know that for random geometric graphs we should expect mostly localized modes. This implies relatively low biomass changes compared to the total biomass of the meta-community. We also find that most modes have oscillatory Hopf-like character, especially for larger and better connected food webs which is associated with higher robustness if the dynamics are not strongly synchronized. Both cyclical population fluctuations and modes that only affect few patches at a time are indicators of robust though not necessarily stable meta-communities as they prevent overly large fluctuations in biomass. Stability in the sense of linear stability of steady states decreases the more species there are and the higher the connectance is. This is true for homogeneous meta-communities of any spatial configuration because the whole system can only be stable if the isolated patch would be stable. It is also clear that the addition of patches for any spatial configuration creates new eigenvalues for the Laplacian matrix which could potentially destabilize the system but also shifts the eigenvalue spectrum depending on the links to other patches. For diffusive dispersal a more densely connected spatial network is in general stabilizing as it creates larger eigenvalues for the Laplace matrix. Larger networks with constant connectance are destabilizing as they fill same range in the master stability function with more eigenvalues that each could destabilize the system.

Looking at the entirety of our findings there is a trend towards lower stability of steady states for increasingly larger patch numbers; going from isolated patches to two patches to arbitrary many patches; and for more species involved; from a single predator-prey pair to food webs up to 30 species. This is in line with the original problem of ecology. The more complex a system is, the less stable it becomes. This holds true for the systems we analysed but this leaves us with the original question unanswered: How can complex systems in nature remain stable? Perhaps this question can be answered by looking at alternative definitions of stability. There are many indications that while linear stability is decreasing for most of the additions in complexity that robustness and persistence might increase. Adding a second patch connected by dispersal lowers stability but allows for a rescue effect (compare to (Plitzko and Drossel, 2015)) if a species goes extinct on one patch but survives on another and we see that the blow to stability by migration can be softened by using adaptive forms of dispersal. A heterogeneous system makes it more likely to have non-synchronous oscillatory population dynamics which stabilizes biomass and still provides a potential means for repopulation. For the combination of food webs on spatial networks we also see primarily limit cycles emerge after a perturbation and that most perturbations only affect few patches to a meaningful degree. All this hints at systems that can maintain biodiversity under external stress.

Of course, to use the generalized method – a method that is specifically built around the concept of linear stability – and take the results to make statements about other forms of stability is problematic. But this approach has allowed us to cover a variety of systems and find commonalities that otherwise might have been hidden. The generalized modelling approach is an excellent tool to gather insights with relatively little effort though it cannot provide the dynamics away from the steady states with any certainty. The formulation of the generalized method for periodic solutions by (Kuehn and Gross, 2011) might provide new insights as it could incorporate oscillations into the discussion about stability in a more meaningful manner. Ultimately, we will need to apply conventional methods as well to see if our predictions hold up and hopefully reveal a small slice of truth about the nature of real meta-communities.

It is the dilemma of scientific research that one is usually left with more questions than answers and that holds true for this thesis, too. We have made good progress in describing small meta-food webs in detail and have shown that the master stability function approach can be applied to large meta-communities but we lack a good approach for the construction of real spatial networks. Random geometric graphs are a sensible starting point but there is no solid data that would allow an appropriate selection of ranges or patch numbers for our meta-community model. This is a pity as we can easily compute properties for different topologies thanks to the master stability function but are limited to what could almost be considered platitudes. We need an ansatz that lets us know what kind of food web would exits on what kind of spatial network. Close collaboration with biologists and ecologist is certainly necessary to fill this gap in our description.

8 Dedication

Die finalen Worte der Doktorarbeit werde ich lieber in meiner Muttersprache verfassen. Wenn diese Danksagung etwas zu lang wird, dann sei es so. Die letzten Jahre in der AG Drossel waren eine schöne Zeit. Das lag, wie es meistens so ist, mehr an den Menschen als an der Arbeit, die man vollbrachte. Meine sehr geschätzte Doktormutter war stets zugänglich und verstand die besonderen Bedürfnisse eines haustiergeplagten Studenten. Es ist sicher nicht jeder Arbeitgeber so lenient, wenn man spontan aus tierärztlichen Gründen ein paar Tage Heimarbeit betreiben muss. Auf der Seite der Forschung muss ich hier meinen Dank auch an Thilo Gross aussprechen, der nicht einfach nur die zentrale Methode meiner Arbeit “entdeckt” hat, sondern sie mir auch bei mehreren Gelegenheiten erklärte. Außerdem hat er meinen und Andreas Brechtels Forscherdrang mit sichtlicher Freude gehegt und gelegentlich unfreiwillig gedämpft, wenn wieder einmal eine unser vermeintlich brillianten Ideen mit “Das hab ich schonmal gemacht. Das Paper liegt irgendwo rum. Nee, keine Zeit gehabt zum Publizieren...” niedergeschmettert wurde. Hätten wir alles veröffentlicht, was wir angedacht haben und Thilo schon längst in irgendeiner Schublade ausgearbeitet hatte, wären es wahrscheinlich dreimal so viele Paper geworden.

Meine Arbeitsgruppe war in jeder Besetzung und egal wieviel Zeit ich mit jedem einzelnen verbringen konnte ein Paradebeispiel von freundschaftlichem Umgang. Wir hatten und haben traditionell eine hohe Rate an Bachelor- und Masterstudenten (liebevoll Bätchis und Mastersklaven genannt) und auch die Reihe der Doktoranden hat sich komplett umgestellt in meiner Anwesenheit. Als Zwischengenerationskind muss ich mich daher bei alten und neuen Doktoranden bedanken. Die alte Riege hat mich freundlich aufgenommen und so gut es ging bei meinen Anfängen unterstützt. Besonderen Dank an:

- Sebastian Plitzko, der mir das erste Programm in die Hand drückte, mir das Admin-Passwort und die generalisierte Methode überreichte und dann sich viel zu schnell aus dem Staub machte (Kind, Arbeit und Haus(aus)bau sind annehmbare Ausreden).
- Korinna Allhoff, die allgemein ein toller Mensch ist und mir das Jonglieren ans Herz legte. Ich übte immer Jonglieren, wenn mich die GM oder das Programmieren frustriert haben. Ich lernte schnell.
- Marco Möller, der tatsächlich die meisten Admin-Sachen in meiner Anfangszeit gemacht hat, weil ich heillos überfordert war und er in jeder Hinsicht ein besser Mensch/Admin war und ist.

Nach dem Regimentwechsel kamen neue Gesichter, die mich plötzlich hier und da um Rat fragten, da ich innerhalb eines halben Jahres dann plötzlich dienstältester Promotionsstudent war. Da es aber alles helle Köpfe sind, ist das schon lange nicht mehr nötig und mittlerweile eher umgekehrt. Auch hier seien ein paar besonders hervorgehoben. Da wären:

- Andreas Brechtel, der mit mir Freud und Leid der generalisierten Methode geteilt hat. Da wir stets etwas inselartig mit unserem Thema waren, haben wir fast konstant zusammengearbeitet und uns viele seltsame Hobbies geteilt; von der Schwerathletik zum Kehlgesang.
- Michaela Hamm und Tatjana Thiel, die mit mir unzählige Kaffepausen verbracht haben und damit viel zu meiner geistigen Gesundheit beitrugen. Unser Versuch, die schwedische Sprache zu meistern, ist leider ein ruhendes Projekt, aber war in seiner Blüte sehr lustig. Potatis är bäst! Die beiden werfe ich hier einfach in einen Topf, da sie es so gewohnt sind.
- Elvira Bafong, die mir freundlich mein miserables Fränzösisch verziehen und mich mehrfach mit der besten kamerunischen Küche gemästet hat.
- Lara Becker, die als einziger Nicht-Doktorand hier einen Ehrenplatz hat. Herzlichen Dank für Hermann, den übergewichtigen Katzengötzen. Sein strenger aber gütiger Blick half bei vielen Programmierproblemen und allgemeinen Dürreperioden.

Natürlich gab es viele mehr, aber irgendwann muss Schluss sein. Ich hoffe, jedem in der Arbeitsgruppe ist klar, warum ich ihn oder sie zu schätzen weiß, auch wenn sie hier nicht namentlich aufgeführt sind.

Ich möchte mich nochmal besonders bei meinen Eltern und meiner Verlobten bedanken. Meine Eltern haben mir einen relativ einfachen Start ins Leben ermöglicht und damit viele Möglichkeiten gegeben, die anderen nicht weniger begabten verwehrt bleiben. Meine Verlobte hat mir allzeit den Rücken gestärkt und mein Leben in der stressigen Endphase (und natürlich auch sonst) in jeder Hinsicht erträglicher gemacht.

Den Korrekturlesern ein weiteres Lob, die da gewesen wären: Michaela Hamm, Tatjana Thiel, Andreas Brechtel, Elvira Pafong, Julian Geske, Sabrina Hanstein und mein lieber Vater. Danke für die Unterstützung.

Damit möchte ich die Danksagung abschließen und allen weiteren Generationen viel Erfolg im Leben und in der Forschung wünschen.

9 Curriculum Vitae

Philipp Fabian Gramlich, M.Sc.
geb. 06.10.1987, Schweinfurt
ledig

Schule

- 1994 – 1998 J. F. Kennedy–Schule, Grundschule, Münster
- 1998 – 2004 Schule auf der Aue, Gymnasialzweig, Münster
- 2005 – 2007 Alfred-Delp-Schule, Dieburg
  Hochschulreife (sehr gut)
- 9/2005 – 11/2005 “Saturday Morning Physics”
  (7-wöchiger Kurs zum Verständnis der modernen Physik)

Studium

- 10/2007 – 03/2011 Bachelorstudium, Fachbereich Physik, TU Darmstadt (gut),
  Abschlussarbeit: “7-Lithium NMR an Lithiumniobat”(sehr gut)
- 03/2011 – 09/2013 Masterstudium, Fachbereich Physik, TU Darmstadt (sehr gut)
  Abschlussarbeit: “Untersuchung von nicht-ionischen
  Mikroemulsionen mit Dynamischer Lichtstreuung” (sehr gut)
- 10/2012 – 03/2013 Tutor, FB Physik, TU Darmstadt
  “Festkörperphysik” (Prof. Dr. Stühn)
- 04/2013 – 09/2013 Tutor, FB Physik, TU Darmstadt
  “Kondensierte Materie” (Prof. Dr. Stühn)
- 05/2014 – Heute Promotionsstudium, FB Physik, TU Darmstadt

Beruf

- 12/2013 – 5/2014 Praktikum bei der ALV-Laser Vertriebgsgesellschaft m-b.H.,
  Statistische Modellierung
- 5/2014 – Heute Wissenschaftlicher Mitarbeiter, FB Physik, TU Darmstadt

List of Abbreviations and Nomenclature

Stability and Bifurcations	
PSW	Percentage of stable webs
HB	Hopf bifurcation
SN	Saddle-node bifurcation
WI	Wave instability
TI	Turing instability
MSF	Master stability function
Class nomenclature	
LV	Class based on Lotka-Volterra dynamics
RM	Class based on Rosenzweig-MacArthur dynamics
LG	Class with logistic growth term and Holling type I functional response
H.III	Class with Holling type III functional response
DeAngelis	Class based on Beddingtion-DeAngelis functional response
Stand	Class with particular wide parameter ranges to encompass all common models
Jan95	Class based on (Jansen, 1995)
Jan01	Class based on (Jansen, 2001)
Abrams	Class based on (Abrams and Ruokolainen, 2011)
Mchich	Class based on (Mchich et al., 2007)
ElAbdl	Class based on (Abdllaoui et al., 2007)
Huang	Class based on (Huang and Diekmann, 2001)
HuangR	Same as Huang but with reversed cross-species dispersal behaviour
Diff	Class with simple diffusion as migration term and RM intra-patch dynamics
Growth	Class that couples exponent parameters for functional response and primary production to the exponent parameters of dispersal behaviour
Growth2	Identical to Growth but with RM intra-patch dynamics
“Class”x	Same as “Class” but without any migration loss
“Class”y	Same as “Class” but no predator migration of any kind
“Class”z	Same as “Class” but loss and migration gain have identical values, i.e. migration outflow and inflow are matched

List of Tables

List of Publications

The following publications have evolved from my doctoral dissertation and represent large parts of this thesis.

Gramlich, Philipp, et al. "The influence of dispersal on a predator–prey system with two habitats." Journal of theoretical biology 398 (2016): 150-161.

Brechtel, Andreas, et al. "Master stability functions reveal diffusion-driven instabilities in multi-layer networks." arXiv preprint arXiv:1610.07635 (2016).

Gramlich, Philipp "The influence of heterogeneity on the stability of a predator-prey system on two habitats." arXiv (2017), *in progress*

References

Abbott, K. C. (2011). A dispersal-induced paradox: synchrony and stability in stochastic metapopulations. *Ecology letters*, 14(11):1158–1169.

Abdllaoui, A. E., Auger, P., Kooi, B. W., de la Parra, R. B., and Mchich, R. (2007). Effects of density-dependent migrations on stability of a two-patch predator–prey model. *Mathematical Biosciences*, 210(1):335 – 354.

Abrams, P. A. (2000). The impact of habitat selection on the spatial heterogeneity of resources in varying environments. *Ecology*, 81(10):2902–2913.

Abrams, P. A. and Ruokolainen, L. (2011). How does adaptive consumer movement affect population dynamics in consumer–resource metacommunities with homogeneous patches? *Journal of Theoretical Biology*, 277(1):99 – 110.

Addo-Bediako, A., Chown, S., and Gaston, K. (2002). Metabolic cold adaptation in insects: a large-scale perspective. *Functional Ecology*, 16(3):332–338.

Agency, U. (1965). Tiger bush plateau - aerial view. Wikipedia, the free encyclopedia. [Online;accessed July 5, 2017].

Amarasekare, P. (2008a). Spatial dynamics of foodwebs. *Annual Review of Ecology, Evolution, and Systematics*, 39:479–500.

Amarasekare, P. (2008b). Spatial dynamics of foodwebs. *Annual Review of Ecology, Evolution, and Systematics*, pages 479–500.

Amarasekare, P. and Nisbet, R. M. (2001). Spatial heterogeneity, source-sink dynamics, and the local coexistence of competing species. *The American Naturalist*, 158(6):572–584.

Andronov, A., Leontovich, E., Gordon, I., and Maier, A. (1971). Theory of dynamical systems on a plane. *Israel Program of Scientific Translations, Jerusalem*, page 50.

Arenas, A., Díaz-Guilera, A., Kurths, J., Moreno, Y., and Zhou, C. (2008). Synchronization in complex networks. *Phys. Rep.*, 469(3):93 – 153.

Armsworth, P. R. and Roughgarden, J. E. (2008). The structure of clines with fitness-dependent dispersal. *The American Naturalist*, 172(5):648–657.

Asllani, M., Busiello, D. M., Carletti, T., Fanelli, D., and Planchon, G. (2014). Turing patterns in multiplex networks. *Phys. Rev. E*, 90:042814.

Barrat, A., Barthelemy, M., and Vespignani, A. (2008). *Dynamical processes on complex networks*. Cambridge university press.

Barter, E. and Gross, T. (2016). Meta-food-chains as a many-layer epidemic process on networks. *Phys. Rev. E*, 93:022303.

Bascompte, J. and Solé, R. V. (1994). Spatially induced bifurcations in single-species population dynamics. *Journal of Animal Ecology*, pages 256–264.

Bashan, A., Berezin, Y., Buldyrev, S. V., and Havlin, S. (2013). The extreme vulnerability of interdependent spatially embedded networks. *Nature Phys.*, 9(10):667–672.

Baurmann, M., Gross, T., and Feudel, U. (2007). Instabilities in spatially extended predator–prey systems: spatio-temporal patterns in the neighborhood of turing–hopf bifurcations. *Journal of Theoretical Biology*, 245(2):220–229.

Bödeker, D. H. U. (2007). Turing bifurcation. Wikimedia Commons.

Beddington, J. R. (1975). Mutual interference between parasites or predators and its effect on searching efficiency. *The Journal of Animal Ecology*, pages 331–340.

Binzer, A., Guill, C., Brose, U., and Rall, B. C. (2012). The dynamics of food chains under climate change and nutrient enrichment. *Phil. Trans. R. Soc. B*, 367(1605):2935–2944.

Bjørnstad, O. N., Ims, R. A., and Lambin, X. (1999). Spatial population dynamics: analyzing patterns and processes of population synchrony. *Trends in Ecology & Evolution*, 14(11):427–432.

Black, A. J. and McKane, A. J. (2012). Stochastic formulation of ecological models and their applications. *Trends in ecology & evolution*, 27(6):337–345.

Blackburn, T. M. and Gaston, K. J. (1994). Animal body size distributions: patterns, mechanisms and implications. *Trends in Ecology & Evolution*, 9(12):471–474.

Blasius, B., Huppert, A., and Stone, L. (1999). Complex dynamics and phase synchronization in spatially extended ecological systems. *Nature*, 399(6734):354–359.

Bowman, J., Jaeger, J. A., and Fahrig, L. (2002). Dispersal distance of mammals is proportional to home range size. *Ecology*, 83(7):2049–2055.

Brauer, A. (1947). Limits for the characteristic roots of a matrix. ii. *Duke Math. J.*, 14(1):21–26.

Brechtel, A., Gramlich, P., Ritterskamp, D., Drossel, B., and Gross, T. (2016). Master stability functions reveal diffusion-driven instabilities in multi-layer networks. *arXiv preprint arXiv:1610.07635*.

Briggs, C. J. and Hoopes, M. F. (2004). Stabilizing effects in spatial parasitoid–host and predator–prey models: a review. *Theoretical population biology*, 65(3):299–315.

Brose, U., Cushing, L., Berlow, E. L., Jonsson, T., Banasek-Richter, C., Bersier, L.-F., Blanchard, J. L., Brey, T., Carpenter, S. R., Blandenier, M.-F. C., et al. (2005). Body sizes of consumers and their resources. *Ecology*, 86(9):2545–2545.

Brose, U., Jonsson, T., Berlow, E. L., Warren, P., Banasek-Richter, C., Bersier, L.-F., Blanchard, J. L., Brey, T., Carpenter, S. R., Blandenier, M.-F. C., et al. (2006). Consumer–resource body-size relationships in natural food webs. *Ecology*, 87(10):2411–2417.

Brown, J. H. and Kodric-Brown, A. (1977). Turnover rates in insular biogeography: effect of immigration on extinction. *Ecology*, 58(2):445–449.

Buldyrev, S. V., Parshani, R., Paul, G., Stanley, H. E., and Havlin, S. (2010). Catastrophic cascade of failures in interdependent networks. *Nature*, 464(7291):1025–1028.

Burt, W. H. (1943). Territoriality and home range concepts as applied to mammals. *Journal of mammalogy*, 24(3):346–352.

Cattin, M.-F., Bersier, L.-F., Banašek-Richter, C., Baltensperger, R., and Gabriel, J.-P. (2004). Phylogenetic constraints and adaptation explain food-web structure. *Nature*, 427(6977):835–839.

Chavez, M., Hwang, D.-U., and Boccaletti, S. (2007). Synchronization processes in complex networks. *The European Physical Journal-Special Topics*, 146(1):129–144.

Chiswick, C. (2012). Giant pufferfish skin pattern detail. Wikipedia, the free encyclopedia. [Online;accessed July 5, 2017].

Clarke, A. and Fraser, K. (2004). Why does metabolism scale with temperature? *Functional Ecology*, 18(2):243–251.

Cohen, J. E., Briand, F., and Newman, C. M. (2012). *Community food webs: data and theory*, volume 20. Springer Science & Business Media.

Cohen, J. E., Pimm, S. L., Yodzis, P., and Saldana, J. (1993). Body sizes of animal predators and animal prey in food webs. *Journal of animal ecology*, pages 67–78.

Cucuringu, M. and Mahoney, M. W. (2011). Localization on low-order eigenvectors of data matrices. *arXiv*, page 1109.1355.

Cushing, J. M. and Saleem, M. (1982). A predator prey model with age structure. *Journal of Mathematical Biology*, 14(2):231–250.

De Domenico, M., Solé-Ribalta, A., Cozzo, E., Kivelä, M., Moreno, Y., Porter, M. A., Gómez, S., and Arenas, A. (2014). Mathematical formulation of multilayer networks. *Physical Review X*, 3(4).

De Domenico, M., Sole-Ribalta, A., Omodei, E., Gomez, S., and Arenas, A. (2015). Ranking in interconnected multilayer networks reveals versatile nodes. *Nat. Commun.*, 6:6868.

de Ruiter, P. C., Neutel, A.-M., and Moore, J. C. (1995). Energetics, patterns of interaction strengths, and stability in real ecosystems. *Science*, 269(5228):1257.

DeAngelis, D. L., Goldstein, R., and O'neill, R. (1975). A model for tropic interaction. *Ecology*, 56(4):881–892.

del Genio, C. I., Gómez-Gardeñes, J., Bonamassa, I., and Boccaletti, S. (2016). Synchronization in networks with multiple interaction layers. *Science Advances*, 2:1–10.

Do, A.-L., Höfener, J., and Gross, T. (2012). Engineering mesoscale structures with distinct dynamical implications. *New Journal of Physics*, 14(11):115022.

Drossel, B. (2001). Biological evolution and statistical physics. *Advances in physics*, 50(2):209–295.

Drossel, B. and McKane, A. J. (2006). 10 modelling food webs. *Handbook of graphs and networks: From the genome to the internet*.

Drossel, B., McKane, A. J., and Quince, C. (2004). The impact of nonlinear functional responses on the long-term evolution of food web structure. *Journal of Theoretical Biology*, 229(4):539–548.

Dunne, J. A. (2006). The network structure of food webs. *Ecological networks: linking structure to dynamics in food webs*, pages 27–86.

Dunne, J. A., Williams, R. J., and Martinez, N. D. (2002). Network structure and biodiversity loss in food webs: robustness increases with connectance. *Ecology letters*, 5(4):558–567.

Dunne, J. A., Williams, R. J., and Martinez, N. D. (2004). Network structure and robustness of marine food webs. *Marine Ecology Progress Series*, 273:291–302.

Dunne, J. A., Williams, R. J., Martinez, N. D., Wood, R. A., and Erwin, D. H. (2008). Compilation and network analyses of cambrian food webs. *PLoS biology*, 6(4):e102.

Ehnes, R. B., Rall, B. C., and Brose, U. (2011). Phylogenetic grouping, curvature and metabolic scaling in terrestrial invertebrates. *Ecology Letters*, 14(10):993–1000.

Esa Ranta, V. K. and Lundberg, P. (1998). Population variability in space and time: The dynamics of synchronous population fluctuations. *Oikos*, 83:376–382.

Gaston, K. J. and Blackburn, T. M. (1996). Conservation implications of geographic range size-body size relationships. *Conservation Biology*, 10(2):638–646.

Gershgorin, S. A. (1931). Uber die Abgrenzung der Eigenwerte einer Matrix. . , (6):749–754.

Gillooly, J. F., Brown, J. H., West, G. B., Savage, V. M., and Charnov, E. L. (2001). Effects of size and temperature on metabolic rate. *Science*, 293(5538):2248–2251.

Gilpin, M. E. (1973). Do hares eat lynx? *The American Naturalist*, 107(957):727–730.

Goldwyn, E. E. and Hastings, A. (2008). When can dispersal synchronize populations? *Theoretical population biology*, 73(3):395–402.

Gramlich, P. (2017). The influence of heterogeneity on the stability of a predator-prey system on two habitats. *Journal of theoretical biology*. Submitted.

Gramlich, P., Plitzko, S., Rudolf, L., Drossel, B., and Gross, T. (2016). The influence of dispersal on a predator–prey system with two habitats. *Journal of Theoretical Biology*, 398:150 – 161.

Grenfell, B. and Harwood, J. (1997). (meta) population dynamics of infectious diseases. *Trends in ecology & evolution*, 12(10):395–399.

Grima, R. (2010). An effective rate equation approach to reaction kinetics in small volumes: Theory and application to biochemical reactions in nonequilibrium steady-state conditions. *The Journal of chemical physics*, 133(3):07B604.

Grimm, V. (1999). Ten years of individual-based modelling in ecology: what have we learned and what could we learn in the future? *Ecological modelling*, 115(2):129–148.

Grimm, V. and Wissel, C. (1997). Babel, or the ecological stability discussions: an inventory and analysis of terminology and a guide for avoiding confusion. *Oecologia*, 109(3):323–334.

Gross, T. and Feudel, U. (2006). Generalized models as a universal approach to the analysis of nonlinear dynamical systems. *Phys. Rev. E*, 73:016205.

Gross, T., Rudolf, L., Levin, S. A., and Dieckmann, U. (2009). Generalized models reveal stabilizing factors in food webs. *Science*, 325(5941):747–750.

Guckenheimer, J. (2007). Bifurcation. *Scholarpedia*, 2(6):1517. revision #91057.

Guill, C., Drossel, B., Just, W., and Carmack, E. (2011). A three-species model explaining cyclic dominance of pacific salmon. *Journal of theoretical biology*, 276(1):16–21.

Guo, J.-M. (2005). A new upper bound for the laplacian spectral radius of graphs. *Linear algebra and its applications*, 400:61–66.

Guttal, V. and Jayaprakash, C. (2008). Changing skewness: an early warning signal of regime shifts in ecosystems. *Ecology letters*, 11(5):450–460.

Hamm, M. and Drossel, B. (2017). Habitat heterogeneity hypothesis and edge effects in model metacommunities-marked manuscript. *Journal of Theoretical Biology*.

Hammock, J. R. (1971). Behavioral changes due to overpopulation in mice.

Hanski, I. A. and Gaggiotti, O. E. (2004). *Ecology, genetics and evolution of metapopulations*. Academic Press.

Hassell, M. and May, R. (1974). Aggregation of predators and insect parasites and its effect on stability. *The Journal of Animal Ecology*, pages 567–594.

Heckmann, L., Drossel, B., Brose, U., and Guill, C. (2012). Interactive effects of body-size structure and adaptive foraging on food-web stability. *Ecology letters*, 15(3):243–250.

Heino, M., Kaitala, V., Ranta, E., and Lindström, J. (1997). Synchronous dynamics and rates of extinction in spatially structured populations. *Proceedings of the Royal Society of London B: Biological Sciences*, 264(1381):481–486.

Hirt, M. R., Jetz, W., Rall, B. C., and Brose, U. (2017). A general scaling law reveals why the largest animals are not the fastest. *Nature Ecology & Evolution*, 1(August).

Hoegh-Guldberg, O. and Bruno, J. F. (2010). The impact of climate change on the world's marine ecosystems. *Science*, 328(5985):1523–1528.

Holland, M. D. and Hastings, A. (2008). Strong effect of dispersal network structure on ecological dynamics. *Nature*, 456(7223):792–794.

Holling, C. (1959). The components of predation as revealed by a study of small-mammal predation of the european pine sawfly. *The Canadian Entomologist*, 91(05):293–320.

Holmes, E. E., Lewis, M. A., Banks, J., and Veit, R. (1994). Partial differential equations in ecology: spatial interactions and population dynamics. *Ecology*, 75(1):17–29.

Holt, R. D. (1996). Food webs in space: an island biogeographic perspective. In *Food webs*, pages 313–323. Springer.

Hopf, E. (1942). Abzweigung einer periodischen Lösung von einer stationären Lösung eines Differentialsystems. *Ber. Math.-Phys. Kl Sächs. Akad. Wiss. Leipzig*, 94:1–22.

Huang, Y. and Diekmann, O. (2001). Predator migration in response to prey density: what are the consequences? *Journal of mathematical biology*, 43(6):561–581.

Hutchinson, G. E. (1959). Homage to santa rosalia or why are there so many kinds of animals? *The American Naturalist*, 93(870):145–159.

Hütt, M.-T., Kaiser, M., and Hilgetag, C. C. (2014). Perspective: network-guided pattern formation of neural dynamics. *Phil. Trans. R. Soc. B*, 369(1653):20130522.

Ives, A. R. and Carpenter, S. R. (2007). Stability and diversity of ecosystems. *science*, 317(5834):58–62.

Jansen, V. (1995). Regulation of predator-prey systems through spatial interactions a possible solution to the paradox of enrichment. *Oikos*, 74:384–390.

Jansen, V. A. (2001). The dynamics of two diffusively coupled predator–prey populations. *Theoretical Population Biology*, 59(2):119 – 131.

Jansen, V. A. and de Roos, A. M. (2000). The role of space in reducing predator-prey cycles. *The geometry of ecological interactions: simplifying spatial complexity*, pages 183–201.

Jansen, V. A. and Lloyd, A. L. (2000). Local stability analysis of spatially homogeneous solutions of multi-patch systems. *J. Math. Biol.*, 41(3):232–252.

Janzen, D. H. (1971). Seed predation by animals. *Annual review of ecology and systematics*, 2(1):465–492.

Jen, E. (2003). Stable or robust? What's the difference? *Complexity*, 8(3):12–18.

Jost, C., Demvulder, G., Vucetich, J. A., Peterson, R. ., and Arditi, R. (2005). The wolves of isle royale display scale-invariant satiation and ratio-dependent predation on moose. *Journal of Animal Ecology*, 74(5):809–816.

Kartascheff, B., Heckmann, L., Drossel, B., and Guill, C. (2010). Why allometric scaling enhances stability in food web models. *Theoretical Ecology*, 3(3):195–208.

Keeling, M. J. (1999). The effects of local spatial structure on epidemiological invasions. *Proceedings of the Royal Society of London B: Biological Sciences*, 266(1421):859–867.

Kisdi, E. (2010). Costly dispersal can destabilize the homogeneous equilibrium of a metapopulation. *Journal of Theoretical Biology*, 262(2):279 – 283.

Kitano, H. (2004). Biological robustness. *Nature Reviews Genetics*, 5(11):826–837.

Kleiber, M. (1932). Body size and metabolism. *ENE*, 1(9).

Koelle, K. and Vandermeer, J. (2005). Dispersal-induced desynchronization: from metapopulations to metacommunities. *Ecology Letters*, 8(2):167–175.

Koenig, W. D. and Knops, J. M. (2013). Large-scale spatial synchrony and cross-synchrony in acorn production by two california oaks. *Ecology*, 94(1):83–93.

Kouvaris, N. E., Hata, S., and Diaz-Guilera, A. (2015). Pattern formation in multiplex networks. *Sci. Rep.*, 5(10840):10840.

Kramer, B. and MacKinnon, A. (1993). Localization: theory and experiment. *Reports on Progress in Physics*, 56(12):1469.

Kuehn, C. and Gross, T. (2011). Nonlocal generalized models of predator-prey systems. *arXiv preprint arXiv:1105.3662*.

Kuznetsov, Y. A. (2006a). Andronov-Hopf bifurcation. *Scholarpedia*, 1(10):1858. revision #90964.

Kuznetsov, Y. A. (2006b). Saddle-node bifurcation. *Scholarpedia*, 1(10):1859. revision #151865.

Lade, S. J. and Gross, T. (2012). Early warning signals for critical transitions: a generalized modeling approach. *PLoS Comput Biol*, 8(2):e1002360.

Lafferty, K. D., Allesina, S., Arim, M., Briggs, C. J., De Leo, G., Dobson, A. P., Dunne, J. A., Johnson, P. T., Kuris, A. M., Marcogliese, D. J., et al. (2008). Parasites in food webs: the ultimate missing links. *Ecology letters*, 11(6):533–546.

Lafferty, K. D., Dobson, A. P., and Kuris, A. M. (2006). Parasites dominate food web links. *Proceedings of the National Academy of Sciences*, 103(30):11211–11216.

Lafferty, K. D. and Dunne, J. A. (2010). Stochastic ecological network occupancy (seno) models: a new tool for modeling ecological networks across spatial scales. *Theoretical Ecology*, 3(3):123–135.

Lauridsen, B., Edwards, F. K., Jones, J. I., Woodward, G., Blanchard, J., Figueroa, R. D., Warren, P. H., and Petchey, O. L. (2010). Individual-based food webs: species identity, body size and sampling effects. *Integrative ecology: from molecules to ecosystems*, 43:211.

Leibold, M. A., Holyoak, M., Mouquet, N., Amarasekare, P., Chase, J., Hoopes, M., Holt, R., Shurin, J., Law, R., Tilman, D., et al. (2004). The metacommunity concept: a framework for multi-scale community ecology. *Ecology letters*, 7(7):601–613.

Lenton, T. M. (2011). Early warning of climate tipping points. *Nature Climate Change*, 1(4):201–209.

Levins, R. (1969a). Some demographic and genetic consequences of environmental heterogeneity for biological control. *American Entomologist*, 15(3):237–240.

Levins, R. (1969b). Some Demographic and Genetic Consequences of Environmental Heterogeneity for Biological Control. *Bulletin of the Entomological Society of America*, 15(3):237–240.

Levins, R. (1974). Discussion paper: the qualitative analysis of partially specified systems. *Annals of the New York Academy of Sciences*, 231(1):123–138.

Leyva, I., Sevilla-Escoboza, R., Sendiña-Nadal, I., Gutiérrez, R., Buldú, J., and Boccaletti, S. (2017). Inter-layer synchronization in non-identical multi-layer networks. *Scientific Reports*, 7.

Li, Z.-z., Gao, M., Hui, C., Han, X.-z., and Shi, H. (2005). Impact of predator pursuit and prey evasion on synchrony and spatial patterns in metapopulation. *Ecological Modelling*, 185(2):245–254.

Liebhold, A., Koenig, W. D., and Bjørnstad, O. N. (2004). Spatial synchrony in population dynamics*. *Annual Review of Ecology, Evolution, and Systematics*, 35(1):467–490.

Liu, H., Lu, M., and Tian, F. (2004). On the laplacian spectral radius of a graph. *Linear algebra and its applications*, 376:135–141.

Lotka, A. J. (1910). Contribution to the theory of periodic reactions. *The Journal of Physical Chemistry*, 14(3):271–274.

Lotka, A. J. et al. (1925). Elements of physical biology.

Lou, Y. and Ni, W.-M. (1996). Diffusion, self-diffusion and cross-diffusion. *Journal of Differential Equations*, 131(1):79–131.

MacArthur, B. D., Sánchez-García, R. J., and Anderson, J. W. (2008). Symmetry in complex networks. *Discrete Applied Mathematics*, 156(18):3525–3531.

Marsden, J. E. and McCracken, M. (2012). *The Hopf bifurcation and its applications*, volume 19. Springer Science & Business Media.

Marshall, A. (1920). *Principles of Economics*. London: Macmillan and Co., Ltd.

May, R. M. (1972a). Limit cycles in predator-prey communities. *Science*, 177(4052):900–902.

May, R. M. (1972b). Will a large complex system be stable? *Nature*, 238(5364):413–414.

McCann, K. S. (2000). The diversity–stability debate. *Nature*, 405:229–233.

Mchich, R., Auger, P., and Poggiale, J.-C. (2007). Effect of predator density dependent dispersal of prey on stability of a predator–prey system. *Mathematical Biosciences*, 206(2):343 – 356. Arino Special Issue.

McKane, A. J. and Drossel, B. (2006). Models of food web evolution. *Ecological Networks: Linking Structure to Dynamics in Food Webs. Oxford University Press, Oxford*, pages 223–243.

Merris, R. (1998). Laplacian graph eigenvectors. *Linear Algebra Appl.*, 278(1-3):221–236.

Mieth, A. and Bork, H.-R. (2010). Humans, climate or introduced rats–which is to blame for the woodland destruction on prehistoric rapa nui (easter island)? *Journal of Archaeological Science*, 37(2):417–426.

Miller, G. H., Magee, J. W., Johnson, B. J., Fogel, M. L., Spooner, N. A., McCulloch, M. T., and Ayliffe, L. K. (1999). Pleistocene extinction of genyornis newtoni: human impact on australian megafauna. *Science*, 283(5399):205–208.

Mohar, B. (1991). The Laplacian Spectrum of Graphs. *Graph Theory, Combinatorics, and Applications, Vol. 2*, 2:871–898.

Moran, P. (1953). The statistical analysis of the canadian lynx cycle. *Australian Journal of Zoology*, 1(3):291–298.

Mougi, A. and Kondoh, M. (2016). Food-web complexity, meta-community complexity and community stability. *Sci. Rep.*, 6(April):24478.

Murray, J. (2011). *Mathematical Biology II: Spatial Models and Biomedical Applications*. Interdisciplinary Applied Mathematics. Springer New York.

Murray, J. D. (2002). Mathematical biology. i, volume 17 of interdisciplinary applied mathematics.

Neutel, A.-M., Heesterbeek, J. A., and de Ruiter, P. C. (2002). Stability in real food webs: weak links in long loops. *Science*, 296(5570):1120–1123.

Neutel, A.-M., Heesterbeek, J. A., Koppel, J. v. d., Hoenderboom, G., Vos, A., Kaldeway, C., Berendse, F., and De Ruiter, P. C. (2007). Reconciling complexity with stability in naturally assembling food webs. *Nature*, 449:559–603.

Newman, M. E. W., Watts, D. J., and Barabasi, L. (2006). *The Structure and Dynamics of Networks*. Princeton University Press, Princeton.

Nyberg, A., Gross, T., and Bassler, K. E. (2014). Mesoscopic structures and the Laplacian spectra of random geometric graphs. *J. Comp Netw.*, 3(4):543–551.

Oreskes, N. (2004). The scientific consensus on climate change. *Science*, 306(5702):1686–1686.

Parshani, R., Buldyrev, S. V., and Havlin, S. (2010). Interdependent networks: Reducing the coupling strength leads to a change from a first to second order percolation transition. *Phys. Rev. Lett.*, 105(4).

Pascual, M. and Dunne, J. A. (2005). *Ecological networks: linking structure to dynamics in food webs*. Oxford University Press.

Pastor-Satorras, R. and Castellano, C. (2016). Distinct types of eigenvector localization in networks. *Sci. Rep.*, 6:18847.

Pearson, K. (1895). Note on regression and inheritance in the case of two parents. *Proceedings of the Royal Society of London*, 58:240–242.

Pecl, G. T., Araújo, M. B., Bell, J. D., Blanchard, J., Bonebrake, T. C., Chen, I.-C., Clark, T. D., Colwell, R. K., Danielsen, F., Evengård, B., et al. (2017). Biodiversity redistribution under climate change: Impacts on ecosystems and human well-being. *Science*, 355(6332):eaai9214.

Pecora, L. M. and Carroll, T. L. (1998). Master stability functions for synchronized coupled systems. *Phys. Rev. Lett.*, 80:2109–2112.

Pikovsky, A., Kurths, J., and Rosenblum, M. (2001). *Synchronization*. Cambridge University Press, Cambridge.

Pillai, P., Gonzalez, A., and Loreau, M. (2011). Metacommunity theory explains the emergence of food web complexity. *Proceedings of the National Academy of Sciences*, 108(48):19293–19298.

Pillai, P., Loreau, M., and Gonzalez, A. (2010). A patch-dynamic framework for food web metacommunities. *Theoretical Ecology*, 3(4):223–237.

Pimm, S. L. (1982). Food webs. In *Food webs*, pages 1–11. Springer.

Plitzko, S. J. and Drossel, B. (2015). The effect of dispersal between patches on the stability of large trophic food webs. *Theoretical Ecology*, 8(2):233–244.

Plitzko, S. J., Drossel, B., and Guill, C. (2012). Complexity–stability relations in generalized food-web models with realistic parameters. *Journal of theoretical biology*, 306:7–14.

Poincaré, H. (1885). Sur l'équilibre d'une masse fluide animée d'un mouvement de rotation. *Acta mathematica*, 7(1):259–380.

Pongratz, J., Caldeira, K., Reick, C. H., and Claussen, M. (2011). Coupled climate–carbon simulations indicate minor global effects of wars and epidemics on atmospheric co2 between ad 800 and 1850. *The Holocene*, 21(5):843–851.

Riley, S., Eames, K., Isham, V., Mollison, D., and Trapman, P. (2015). Five challenges for spatial epidemic models. *Epidemics*, 10:68–71.

Ristl, K., Plitzko, S. J., and Drossel, B. (2014). Complex response of a food-web module to symmetric and asymmetric migration between several patches. *Journal of theoretical biology*, 354:54–59.

Rooney, N. and McCann, K. S. (2012). Integrating food web diversity, structure and stability. *Trends in ecology & evolution*, 27(1):40–46.

Rosenstock, T. S., Hastings, A., Koenig, W. D., Lyles, D. J., and Brown, P. H. (2011). Testing moran's theorem in an agroecosystem. *Oikos*, 120(9):1434–1440.

Rosenzweig, C., Karoly, D., Vicarelli, M., Neofotis, P., Wu, Q., Casassa, G., Menzel, A., Root, T. L., Estrella, N., Seguin, B., et al. (2008). Attributing physical and biological impacts to anthropogenic climate change. *Nature*, 453(7193):353.

Rosenzweig, M. L. and MacArthur, R. H. (1963). Graphical representation and stability conditions of predator-prey interactions. *American Naturalist*, pages 209–223.

Rossberg, A. G., Matsuda, H., Amemiya, T., and Itoh, K. (2005). An explanatory model for food-web structure and evolution. *Ecological Complexity*, 2(3):312–321.

Rowell, J. T. (2010). Tactical population movements and distributions for ideally motivated competitors. *The American Naturalist*, 176(5):638–650.

Ruiz-Baier, R. and Tian, C. (2013). Mathematical analysis and numerical simulation of pattern formation under cross-diffusion. *Nonlinear Analysis: Real World Applications*, 14(1):601–612.

Sæther, B.-E., Engen, S., Grøtan, V., Fiedler, W., Matthysen, E., Visser, M. E., Wright, J., Møller, A. P., Adriaensen, F., Van Balen, H., et al. (2007). The extended moran effect and large-scale synchronous fluctuations in the size of great tit and blue tit populations. *Journal of Animal Ecology*, 76(2):315–325.

Satake, A. and Koizumi, I. (2008). Population synchrony in ecological systems. *Population ecology*, 50(4):325–327.

Scheffer, M., Bascompte, J., Brock, W. A., Brovkin, V., Carpenter, S. R., Dakos, V., Held, H., Van Nes, E. H., Rietkerk, M., and Sugihara, G. (2009). Early-warning signals for critical transitions. *Nature*, 461(7260):53–59.

Schertzer, E., Staver, A., and Levin, S. (2015). Implications of the spatial dynamics of fire spread for the bistability of savanna and forest. *Journal of mathematical biology*, 70(1-2):329–341.

Segel, L. A. and Jackson, J. L. (1972). Dissipative structure: an explanation and an ecological example. *Journal of Theoretical Biology*, 37(3):545–559.

Sevilla-Escoboza, R., Sendiña-Nadal, I., Leyva, I., Gutiérrez, R., Buldú, J. M., and Boccaletti, S. (2016). Inter-layer synchronization in multiplex networks of identical layers. *Chaos*, 26(6):2–6.

Shigesada, N., Kawasaki, K., and Teramoto, E. (1979). Spatial segregation of interacting species. *Journal of Theoretical Biology*, 79(1):83–99.

Shu, J.-L., Hong, Y., and Wen-Ren, K. (2002). A sharp upper bound on the largest eigenvalue of the laplacian matrix of a graph. *Linear Algebra and its Applications*, 347(1):123 – 129.

Singh, A. and Gakkhar, S. (2010). Synchronization of chaos in a food web in ecological systems. *World Academy of Science, Engineering and Technology*, 70:94–98.

Skalski, G. T. and Gilliam, J. F. (2001). Functional responses with predator interference: viable alternatives to the holling type ii model. *Ecology*, 82(11):3083–3092.

Slack, N. G. (2010). *G. Evelyn Hutchinson and the invention of modern ecology*. Yale University Press.

Smith, H. (2008). The rosenzweig-macarthur predator-prey model. *School of Mathematical and Statistical Sciences, Arizona State University: Phoenix*.

Solow, A. R. and Beet, A. R. (1998). On lumping species in food webs. *Ecology*, 79(6):2013–2018.

Stigler, S. M. (1989). Francis galton's account of the invention of correlation. *Statistical Science*, pages 73–79.

Tang, L., Wu, X., Lü, J., Lu, J.-a., and D'Souza, R. M. (2016). Master stability functions for multiplex networks. *arXiv preprint arXiv:1611.09110*.

Taylor, S. M. (2011). Buffalo hunt: International trade and the virtual extinction of the north american bison. *The American Economic Review*, 101(7):3162–3195.

Thiel, T. and Drossel, B. (2017). Impact of stochastic migration on species diversity in meta food webs consisting of several patches. *Journal of Theoretical Biology*. Under review.

Thompson, J. N. (1998). Rapid evolution as an ecological process. *Trends in ecology & evolution*, 13(8):329–332.

Thompson, R. M., Brose, U., Dunne, J. A., Hall, R. O., Hladyz, S., Kitching, R. L., Martinez, N. D., Rantala, H., Romanuk, T. N., Stouffer, D. B., et al. (2012). Food webs: reconciling the structure and function of biodiversity. *Trends in ecology & evolution*, 27(12):689–697.

Tromeur, E., Rudolf, L., and Gross, T. (2013). Impact of dispersal on the stability of metapopulations. *arXiv preprint arXiv:1305.2769*.

Tromeur, E., Rudolf, L., and Gross, T. (2016). Impact of dispersal on the stability of metapopulations. *J. Theor. Biol.*, 392:1–11.

Turchin, P. (2003). *Complex population dynamics: a theoretical/empirical synthesis*, volume 35. Princeton University Press.

Turing, A. (1952). A theory of morphogenesis. *Phil. Trans. B*, 12.

Vasseur, D. A. and Fox, J. W. (2007). Environmental fluctuations can stabilize food web dynamics by increasing synchrony. *Ecology Letters*, 10(11):1066–1074.

Volterra, V. (1926). Fluctuations in the abundance of a species considered mathematically. *Nature*, 118(2972):558–560.

Volterra, V. (1927). *Variazioni e fluttuazioni del numero d'individui in specie animali conviventi*. C. Ferrari.

W Fox, J. (2006). Current food web models cannot explain the overall topological structure of observed food webs. *Oikos*, 115(1):97–109.

Walther, G.-R. (2010). Community and ecosystem responses to recent climate change. *Philosophical Transactions of the Royal Society of London B: Biological Sciences*, 365(1549):2019–2024.

Weier, B. (2005). Shark mauls horse. https://www.qt.com.au/news/apn-shark-mauls/83637/.

Williams, R. J. and Martinez, N. D. (2000). Simple rules yield complex food webs. *Nature*, 404(6774):180–183.

Xiao, Y. and Chen, L. (2001). Modeling and analysis of a predator–prey model with disease in the prey. *Mathematical Biosciences*, 171(1):59–82.

Yeakel, J., Moore, J., Guimarães, P., and Aguiar, M. (2014a). Synchronisation and stability in river metapopulation networks. *Ecology letters*, 17(3):273–283.

Yeakel, J. D., Moore, J. W., Guimarães, P. R., and de Aguiar, M. A. M. (2014b). Synchronisation and stability in river metapopulation networks. *Ecology Letters*, 17(3):273–283.

Yeakel, J. D., Pires, M. M., Rudolf, L., Dominy, N. J., Koch, P. L., Guimarães, P. R., and Gross, T. (2014c). Collapse of an ecological network in ancient egypt. *Proceedings of the National Academy of Sciences*, 111(40):14472–14477.

Yeakel, J. D., Stiefs, D., Novak, M., and Gross, T. (2011). Generalized modeling of ecological population dynamics. *Theoretical Ecology*, 4(2):179–194.

Zhang, X., Boccaletti, S., Guan, S., and Liu, Z. (2015). Explosive synchronization in adaptive and multilayer networks. *Physical Review Letters*, 114(3).